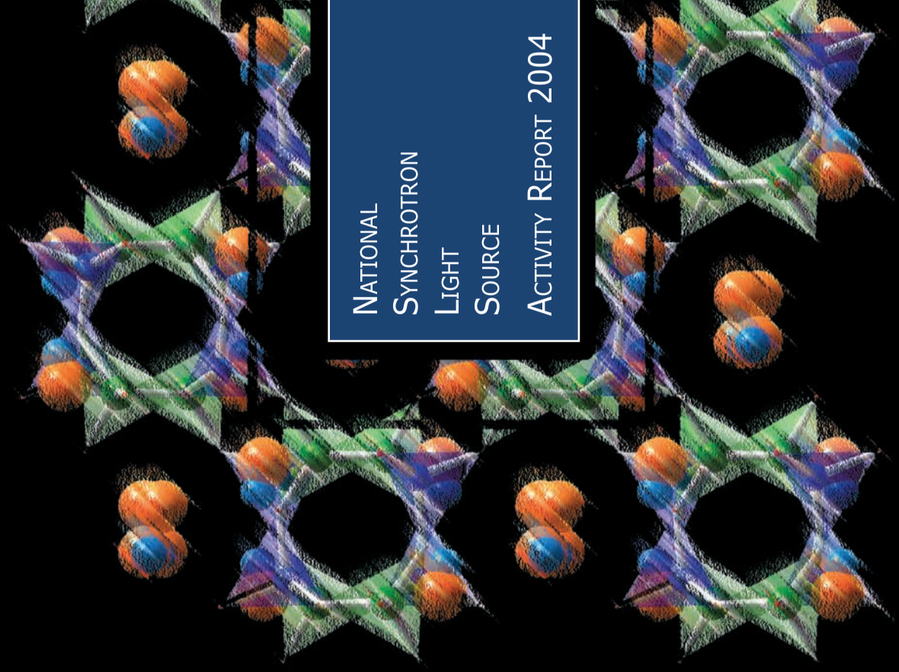

National Synchrotron Light Source Activity Report 2004

BNL 73577

National Synchrotron Light Source Activity Report 2004

BNL-73577-2005
UC400
(General Energy Research)

Printed in the United States of America
Available from
National Technical Information Service
U.S. Department of Commerce
5285 Port Royal Road
Springfield, VA 22161

Cover image from the Science Highlight by A.J. Celestian, J.B. Parise, C. Goodell, A. Tripathi, J. Hanson, "Time-Resolved Diffraction Studies of Ion Exchange: K^+ and Na^+ Exchange into Synthetic Aluminogermanate Molecular Sieve with the Gismondine Topology," page 2-54.

National Synchrotron Light Source
2004 Activity Report

Lisa M. Miller

managing editor

Laura Y. Mgrdichian

science editor

Nancye A. Wright, Stephen A. Giordano & Theresa A. Esposito

design & layout

The National Synchrotron Light Source Department is supported by the
Office of Basic Energy Sciences, United States Department of Energy, Washington, D.C.

Brookhaven National Laboratory, Brookhaven Science Associates, Inc., Upton, New York 11973
Under contract no. DE-AC02-98CH10886

BROOKHAVEN NATIONAL LABORATORY

nsls IR UV X

Office of Science U.S. DEPARTMENT OF ENERGY

Office of Basic Energy Sciences • Serving the Present, Shaping the Future •

Introduction

Science Highlights

Year in Review

NSLS Organization

Facility Report

Facts and Figures

Publications


NSLS
national synchrotron light source

Chairman's Introduction

Steven Dierker
Chairman, National Synchrotron Light Source

The NSLS remains a viable and productive facility, as can be seen by the rich and diverse science produced in 2004. In one of these exciting research projects published in Nature, researchers detected a rare "hole crystal" in a cuprate superconductor, which may provide insight into high-temperature superconductivity. In another Nature publication, the crystal structure of a segment of RNA was determined, opening a new window of knowledge into that crucial molecule. These are just a couple of the science highlights of 2004, and many others are displayed in the pages of this report. All told, more than 700 publications resulted from NSLS research this year, the facility hosted 2,299 users, and the number of experiments performed rose from 1,145 in 2003 to 1,374—clear indications that the NSLS continues to thrive.

As the NSLS accelerator complex enters its third decade of operations, it continues to perform very well. For 2004, the overall reliability of the VUV-IR ring was excellent at 99 percent. The reliability of the x-ray ring was just shy of 92 percent, primarily due to the need to replace the injection septum vacuum chamber, which developed a leak during the middle of the year. The Operations Division did a tremendous job of installing our spare chamber in minimal time, despite the complexity of the job and the inaccessibility of its location in the ring, as well as keeping downtime to a minimum throughout the rest of the year.

In order to continue to meet the needs of users, several key beamline upgrades took place this year that will enrich our scientific programs, including upgrades to beamlines U12IR, X1A, X13A, and X21. We are very excited about two brand-new beamlines that were commissioned in 2004: X29 and X27A. X29 is the new mini-gap undulator beamline designed for macromolecular crystallography, and it will meet the growing demand of NSLS users who perform research in that area. The establishment of an x-ray microprobe at beamline X27A, optimized for the environmental science community, is also very important, as it will help to satisfy the large over subscription rate for this technique at the NSLS. Two other important upgrades that were initiated this past year are the replacement of the X25 wiggler with an undulator and the construction of the X9 undulator beamline for small-angle scattering, with an emphasis on nanoscience research.

Another key activity that will benefit all users was the restoration of the x-ray ring lattice symmetry, which reduced the horizontal emittance and made the operational lattice more robust. Similarly, all users will benefit from the introduction of the PASS (Proposal Allocation Safety Scheduling) system this past year, which has greatly improved the process of proposal submission, review, allocation, and scheduling. This coming year we will work to add Rapid Access to the capabilities of PASS. Overall, the success of

these and the many other projects that space does not permit listing is a testament to the dedication, hard work, and skill of the NSLS staff.

Safety has always been an important issue at a large, complex scientific facility like the NSLS and in 2004 it received renewed attention. Safety is our highest priority and we spent a great deal of time reviewing and refining our safety practices and procedures. A new "Safety Highlights" web page was created for safety news, and a large number of safety meetings and discussions were held. These reviews and meetings generated many ideas on how the NSLS might improve its safety practices, and we are committed to putting these in place and improving our already very good safety program. We had no lost-time accidents in 2004, which is a notable accomplishment. Our goal is to be best in class and I'm confident that by working together we can achieve that status.

Several activities took place this past year to advance our proposal to replace the NSLS with a new National Synchrotron Light Source-II facility. These included a major workshop in support of the proposed facility in March, a mail review of our proposal outlining the scientific opportunities enabled by NSLS-II, and a technical review of the preconceptual design of the machine. The feedback from the reviews has been positive and indications are promising that NSLS-II will become a reality. The scientific opportunities enabled by NSLS-II are incredibly exciting and it is a critically needed addition to the nation's scientific infrastructure. It will ensure that we remain world leaders in synchrotron science for decades to come.

Notes from the UEC

Larry Shapiro
Columbia University

I'd like to take this opportunity to discuss the relatively difficult environment currently faced by the DOE synchrotron facilities, and our response to it. The problem has two primary origins. First is the budgetary environment, and second are rising concerns about safety that require attention from all of us. Both the UEC and the NSLS administration are taking concerted action on these issues, and I'd like to describe some of these efforts.

The short-term funding environment for science in the United States is highly tenuous. Even programs with such high public exposure as the Hubble space telescope are in danger of being cut, and we must be greatly concerned about the level of funding for the NSLS in the near future. It's difficult to know what to expect, but a continuation of tight budgets seems likely. This difficulty is further compounded by the expectation of cost increases, including a potential hike in electric power rates, and new DOE rules on infrastructure expenditures that may divert some funding away from operations. It's not yet clear where we'll be next year, but odds are we won't see much improvement in the near term.

The UEC has taken steps to help our political representatives understand the importance of the NSLS to the status of science in the Northeast, and NSLS-II to the continuation of great science here in the future. In anticipation of the budgetary process unfolding in Washington this month and next, I met with Long Island Congressman Tim Bishop to stress the importance of NSLS and ask for his active support. Congressman Bishop understands the importance of BNL to Long Island and New York, and understands that the NSLS is extremely important to the Lab. He will be a strong supporter in this year's budgetary process, and hopefully in those to come. The UEC has also started to arrange a trip to Washington, scheduled for April, in order to meet with legislators and legislative staff. This trip, as is the custom, will be made jointly with user representatives from the other DOE synchrotron facilities, and will attempt to underscore the national importance of synchrotron research.

Safety issues continue to demand attention at the NSLS and other facilities. An accident at SPEAR3, which caused serious injury to an electrician in mid-October, resulted in an extended shutdown of that facility. In the wake of this accident, safety measures at the NSLS may sometimes seem draconian, but increased attention to maintaining safe operations is absolutely necessary. The UEC, NSLS administration, and the NSLS Scientific Advisory Committee are committed to both augmenting safety guidelines and insuring that they are implemented fairly. Despite the challenges we face now, I think the community is effectively dealing with these issues, and I hope you share my confidence that the NSLS will continue in its long history of great scientific achievement.

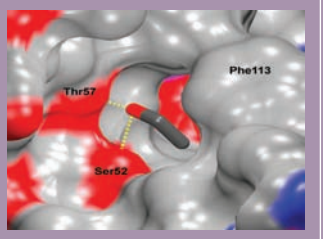
Phe113
Thr57
Ser52

Science at the NSLS

Laura Mgrdichian
NSLS SCIENCE WRITER

As the Information and Outreach Office wraps up 2004 with this report, so have I recently completed my first full year at the NSLS. I am happy to write that it's been a good year.

Being the NSLS science writer, as it turns out, is an education unto itself. Over the course of the year, we select about 50 scientific papers to appear on the NSLS homepage out of almost 700 hundred published by NSLS users in many journals. This means that, each month, I read numerous papers, spanning research in chemistry, soft and condensed matter physics, materials science, nanoscience, and the life sciences. As a result, I have learned about polymers, proteins, and minerals—to name just a few topics. I learn new things every week, in fact, and I feel fortunate to be immersed in such a diverse and rich scientific atmosphere.

However, choosing those 50 is one of the most difficult aspects of what I do, as each experiment at the NSLS helps to answer an interesting scientific question. How, for example, do certain catalysts affect the growth of carbon nanotubes? How does synchrotron light damage protein samples? What causes high-temperature superconductivity in certain materials?

Thus, while the pages beyond this introduction display only a small fraction of the science performed at the NSLS, they will show you how these and other fundamental questions are being answered. The "Science Highlights" are summaries of research papers and are written by users, for users; the "Feature Highlights," aimed at non-scientists, are written by me.

I thank the scientists I've worked with this year for helping me to understand their work and bring it to others, and I look forward to the year ahead.

Science Highlights

Feature Highlights

Chemical Sciences

CONDENSED MATTER PHYSICS

GEOLOGICAL AND ENVIRONMENTAL SCIENCES

LIFE SCIENCES

Soft Condensed Matter and Biophysics

NSLS Users Determine the Structure of a Protein "Gateway" in Cells

Scientists working at the Brookhaven National Laboratory have determined the structure of a tiny "gateway" protein on the surface of cells that allows other proteins to exit the cell. This structure, determined at the National Synchrotron Light Source (NSLS), is a significant scientific achievement that may provide insight into the complex mechanisms of several essential cellular functions. The structure is described in the January 1, 2004 issue of *Nature*.

These pore-like gateways are situated within the cell's protective, greasy outer "skin," called the membrane. The membrane contains thousands of pores, known as channels, which allow only certain substances, such as nutrients and energy sources, to enter and exit the cell. There are many types of channels, and each type is constructed to permit the passage of specific molecules.

The channel studied in this research is a protein-conducting channel. It permits "secretory proteins" to leave the cell by passing straight through the membrane and allows "membrane proteins" to integrate into the membrane so that parts of the protein appear on the outer side of the membrane. This passage system, called protein translocation, allows the proteins to perform many of an organism's essential functions: For example, secretory proteins, such as digestive enzymes and antibodies, leave the cell to help digest food and fight off disease, respectively, while membrane proteins are needed at the cell surface to fire off nerve signals or trigger the immune system.

Understanding precisely how the proteins traverse the channel – a question many scientists would like to answer – first requires determining the channel's intricate molecular structure. This task was successfully completed at the NSLS by a collaboration of scientists from Harvard Medical School, the Max Planck Institute of Biophysics in Frankfurt, Germany, and the University of Luebeck in Luebeck, Germany.

"The structure tells us much more than we ever hoped to be able to get out of it," said Tom Rapoport, a cell biologist at Harvard and the team's lead scientist. "We can now propose mechanisms for how the channel is opened, how other molecules are prevented from crossing the membrane, and other processes. The structure initiates a new era of more directed research into the mechanism of protein translocation."

At the NSLS, Rapoport and his colleagues slowly imaged and pieced together the components of the channel's overall structure. The final product is a huge step in the field of cell biology: a channel imaged to a degree of detail that had previously only been achieved for channels that transport much smaller molecules, such as water and ions.

The channel is shaped like an hourglass, but behaves quite differently, thanks to certain features. For example, the bottom region of the channel is separated from the top region by a molecular "plug" that swings open to allow the passage of outbound proteins and forms a barrier between the inside of the cell and the external aqueous environment. At the narrow "neck" connecting the top and bottom parts of the hourglass, the channel is lined by a gasket-like "pore ring" that forms a seal around exiting proteins. This keeps smaller molecules from sneaking in or out of the cell.

From left, William Clemons, Jr., Tom Rapoport, and Bert van den Berg

The channel also consists of a component that acts somewhat like two molecular "hands" clasped around a cup. By tightening or releasing their grip, the hands narrow or widen the pore, allowing it to admit a wide variety of proteins and shut away unwanted molecules. The hands can also unclasp at the point where their "fingertips" meet. This release mechanism permits proteins to slip sideways out of the channel and become integrated into the membrane.

Assembling this biological puzzle was a great challenge for the researchers. "This is the culmination of 25 years of work on the mechanism of protein translocation, and so it's rewarding to finally

see its three-dimensional structure," Rapoport said. "This is a dream for me."

The first step in that long process, selecting the organism that would produce the best sample to study, was a major hurdle. "We had to go through 10 different bacterial species," said Rapoport. "Finally, we found that a complex derived from an archaebacterium, a primitive organism, was the most stable. Altogether, it took us about five years."

A top view of the protein-conducting channel, looking down into it. The channel's "plug" is shown in green.

The researchers trapped the protein channel in a crystal form, a process that is like taking a three-dimensional "snapshot." Then, working at NSLS beamline X25 and Argonne National Laboratory, they studied the crystals using a technique known as x-ray crystallography: They placed the crystals in the path of an x-ray beam and recorded the pattern the rays created as they scattered and bounced off its molecules. Then, they used a computer to analyze the pattern and determine the structure of the protein in the crystal.

"The next big goal is to crystallize the channel in action," Rapoport concluded.

The other members of the research collaboration are Bert van den Berg, William Clemons, Jr., Yorgo Modis, and Stephen Harrison, all from Harvard Medical School; Ian Collinson, from the Max Planck Institute of Biophysics; and Enno Hartmann, from the University of Luebeck.

—Laura Mgrdichian

Tackling Water Pollution by Tracking Phosphorus in Soils

At the National Synchrotron Light Source (NSLS), scientists have determined how the element phosphorous, a plant fertilizer and surface water contaminant, adheres to two common soil minerals. This study will help to determine how phosphorus migrates from soils to water bodies and which types of soil are better at holding phosphorus – findings that may help to define future soil management policies and decrease the environmental impacts of phosphorous contamination.

The results appeared as the cover article in the March-April 2004 issue of the *Soil Science Society of America Journal*.

"Studying how soils hold phosphorus is necessary because soils are critical for food production and for removing environmental contaminants from water that flows into streams, rivers, lakes, and estuaries," explained Dean Hesterberg, a soil chemist from North Carolina State University who led the study. "However, soils are made up of very complex mixtures of minerals, and it is difficult to determine exactly how plant nutrients and contaminants bind in the soil."

"Therefore, preventing water pollution by managing soil phosphorous levels is often based on indirect approaches that measure how easily a portion of phosphorus can be pulled out of the soil, rather than on an understanding of how the phosphorus is chemically bound in the soil. Knowing the latter helps in more accurately predicting how environmental changes affect phosphorus release."

Phosphorus is commonly added to soils as fertilizers for agricultural crop production. "Phosphorus becomes an environmental concern when it is applied to soils in excessive amounts, as sometimes occurs when waste materials, such as animal waste, are used to fertilize crop soils," Hesterberg said. If the amount of phosphorus added to soils exceeds the plants' needs and the soil's holding capacity, he explained, then excess phosphorus migrates to rivers and lakes via runoff waters, and abnormally stimulates the growth of aquatic plants. The boom in plant growth depletes the waters' oxygen content, endangering fish and other aquatic plants, and deteriorating water quality.

"This work was important because it showed that we can use x-rays to obtain more exact information on how phosphorus binds to different minerals that occur together, and to better understand how each mineral contributes to holding phosphorus in soils," he said. "This is necessary for developing better ways to manage many different soils so that phosphorus movement to waterways is minimized, and we can better evaluate how much phosphorus can be added to soils without causing environmental problems."

Phosphorus occurs at different concentrations in different types of soil, but soils rich in iron (iron oxide) and aluminum (aluminum oxide) minerals can hold more phosphorous. In this research, two such minerals, iron oxide-based ferrihydrite and aluminum oxide-based boehmite, were investigated to determine how phosphorus (in the form of phosphate, a phosphorus compound) is adhered, or "adsorbed," onto them, and to understand how phosphorus is distributed between both types of minerals in soils.

Clockwise (From left, top): Nidhi Khare, Dean Hesterberg, Shan-Li Wang, and Suzanne Beauchemin

Working at NSLS beamline X19A, the scientists tracked how much phosphate was held by each mineral. They determined how phosphate adsorbed onto ferrihydrite and boehmite by shining x-rays at soil samples containing just ferrihydrite, just boehmite, and mixtures of both. By looking at the unique patterns created as the x-rays emerged from each sample, the scientists were able to determine how much phosphate had adsorbed onto each mineral in the mixture based on data for the individual minerals.

The results show that, at low phosphate concentrations,

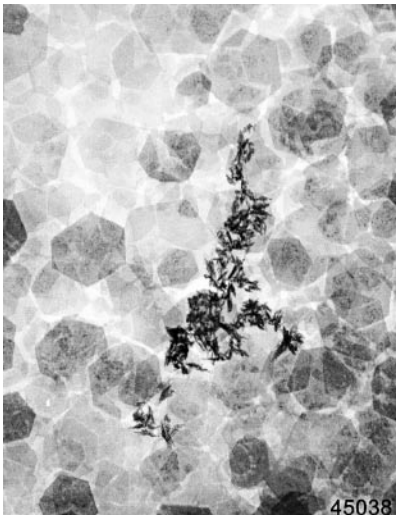

Transmission electron microscope image (50,000X magnification) of a mixture of iron- and aluminum-oxide minerals: hexagonal gibbsite [α-$Al(OH)_3$] platelets and aggregated, lathe-shaped goethite (α-FeOOH) particles. Iron and Al-oxides are considered the most important minerals for retaining phosphate in soils, but their relative importance as they coexist in soils is unclear.

ferrihydrite holds phosphate more strongly than boehmite. The researchers also found that at intermediate concentrations, each of these minerals adsorbs phosphate about equally well. This information will help determine how phosphate dissolves and migrates within different soils, which may contribute to the development of soil management policies aimed at minimizing the effect of phosphorus on the environment.

The other researchers who participated in this study are Dr. Nidhi Khare, a former Ph.D. student in Hesterberg's lab and the lead author, now a post-doctoral researcher at the University of Wyoming; Dr. Suzanne Beauchemin, from Natural Resources Canada; and Dr. Shan-Li Wang, now an Assistant Professor at National Chung Hsing University in Taichung, Taiwan.

This research was funded by the U.S. Department of Agriculture's National Research Initiative (Soils and Soil Biology Program) and the North Carolina Agricultural Research Service.

—Laura Mgrdichian

Evidence of Ancient Water on an Asteroid

May help lead to new information on the formation of Earth

Working in part at the National Synchrotron Light Source (NSLS), scientists have discovered evidence of ancient water on a large asteroid previously thought to lack water. The findings indicate that water was most likely deposited *onto* the asteroid, suggesting it came from an outside source, such as a collision with an icy comet. The discovery may give scientists new insight into the rules governing the mobility and availability of water in the solar system at the time Earth was formed.

The results appear in the March 15, 2004 issue of *Earth and Planetary Science Letters*.

The scientists learned about the asteroid, named 4 Vesta, which orbits the Sun in our solar system, by studying a meteorite that is believed to have once been part of it, due to the two bodies' very similar chemical compositions. The meteorite, called Serra de Magé, fell to Earth in 1923. When analyzing Serra de Magé, the researchers discovered a sign that water had once been present: threads, or "veinlets," of quartz, a mineral that is often deposited onto rocks by liquid water solutions. The appearance and condition of the veinlets suggested that water existed on the meteorite long ago, and could only have been deposited before Serra de Magé broke away from 4 Vesta.

Allan Treiman, a geologist from the Lunar and Planetary Institute and the study's lead scientist, explained, "The veinlets are quite old – 4.5 billion years – so they formed when the solar system was quite young. Because Vesta is now so dry, our best guess is that the veinlets' water came from an outside source, such as comets or water-rich meteorites that hit Vesta."

According to Treiman, this hypothesis has some important potential implications. "Scientists have theorized water delivery by comets for the early solar system, especially for how the Earth got enough water to make our oceans. However, gathering evidence for or against this theory has been difficult, because few Earth rocks (or Moon rocks) are old enough. But this ancient meteorite from Vesta appears to show that it received water somehow, which suggests that water could have been delivered to Earth in a similar way."

To analyze Serra de Magé, the researchers bombarded it with x-rays at NSLS beamline X26A. In this method, called x-ray micro-diffraction, the x-rays entered the sample, scattered off its molecules, and emerged from the sample in a distinct pattern. A camera created an image of the diffracted x-rays, and, from this, the scientists were able to determine what materials make up the sample based on known diffraction patterns of many different substances. This is how they identified the quartz veinlets.

4 Vesta is the third-largest asteroid in the Main Asteroid Belt – the ring of cosmic debris that orbits the Sun outside Mars' orbit and inside Jupiter's. The asteroid is 320 miles in diameter, or about as wide as the state of Iowa, and is roughly spherical in shape. Its chemical composition is unique: Unlike other large asteroids, Vesta appears to have once contained a hot molten center, as Earth does. This finding contradicts conventional ideas that asteroids are cold, rocky remnants of the early days of planet formation. Studying Vesta may help scientists learn how Earth formed, as the asteroid has other characteristics similar to terrestrial planets, such as evidence of ancient lava eruptions. Its surface is pocked with impact craters – which is most likely how Serra de Magé was knocked loose.

Allan Treiman

In the future, Treiman and his colleagues plan to study other meteorites from 4 Vesta and look for similar quartz veinlets. They will also study them for more definitive signs of water on the asteroid, such as actual water – very small droplets trapped in the quartz – or water-bearing minerals. Another approach is to look for excess hydrogen in Serra de Magé as compared to meteorites without quartz veinlets, which would indicate that water, a hydrogen-oxygen compound, may have been present. This could be done using the infrared rays produced at the NSLS vacuum ultra-violet (VUV) ring.

The collaboration that performed this research also includes Antonio Lanzirotti,

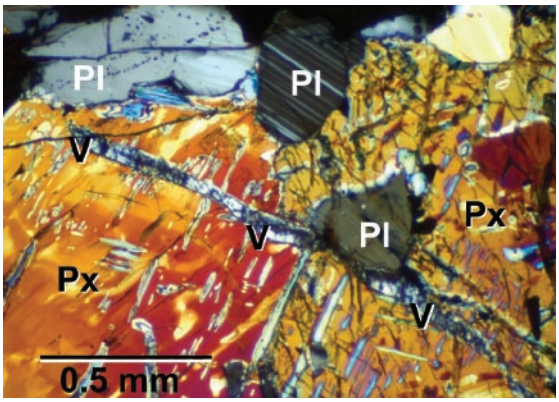

The largest quartz veinlet in the meteorite (V), surrounded by the minerals pyroxene (Px) and plagioclase (Pl).

of the University of Chicago's Consortium for Advanced Radiation Sources at Brookhaven National Laboratory and Dimitrios Xirouchakis, of the National Aeronautic and Space Administration's (NASA) Johnson Space Center.

The work is funded by NASA, the Lunar and Planetary Institute, and the U.S. Department of Energy's (DOE) Geosciences Research program within the Office of Basic Energy Sciences in DOE's Office of Science.

—Laura Mgrdichian

New Brookhaven Laser Facility Captures Molecules in Action

Scientists at Brookhaven National Laboratory have released results from the first experiment at Brookhaven's Deep Ultraviolet Free Electron Laser (DUV-FEL), a facility that produces powerful ultraviolet laser light for research applications. The researchers investigated how gas molecules break apart when they are highly energized by the laser light – research that may offer insight into many fundamental chemical and physical processes that are based on molecule-light interactions, such as photosynthesis, radiation damage, and ozone formation.

"This experiment has helped us to understand the specifics of what happens when we excite molecules with energetic ultraviolet light," said Brookhaven chemist Arthur Suits, the experiment's lead scientist. The results are described in the February 27, 2004 issue of *Physical Review Letters*.

"We also learn, more generally, how electrons rearrange in molecules in response to the light, the nature of chemical bonds, and the dynamics of bond-breaking processes," he said.

The gas used in this experiment is called methyl fluoride. Each molecule can be thought of as the sum of two parts: a negatively charged fluorine atom, or fluorine ion, and a positively charged methyl ion containing three hydrogen atoms bonded to one carbon atom. When Suits and his group aimed the ultraviolet beam from the DUV-FEL at a beam of methyl fluoride gas, the gas molecules each absorbed a single energetic photon, or tiny "packet," of light, which caused them to separate, or dissociate, into their positive and negative fragments, called ion pairs.

This dissociation is a special case, Suits explained. When a molecule absorbs a great deal of energy, normally it will spit out an electron and become a positive ion. But sometimes, molecules can temporarily exist in "superexcited" states, absorbing enough energy to ionize, but without doing so. Instead, they can dissociate into fragments. By studying the parts, scientists can gain information about the whole molecule and the details of the bond-breaking process.

In this experiment, Suits and his collaborators used a technique called "ion pair imaging" to learn about methyl fluoride's reaction to the light. After breaking the molecules into ion pairs, they tracked the motion of the fluorine ions by causing them to strike a screen that records each ion's impact location. The resulting pattern gives the scientists information about the speed and trajectory of the fluorine ions. By working backward, they can learn about the properties of the entire methyl fluoride molecule and its interaction with the light.

Wen Li (left) and Arthur Suits

"Methyl fluoride was a good test case to use in the first FEL experiment, but we hope to study other dissociation processes," said Suits. "We have yet to take full advantage of the DUV-FEL's many unique features and capabilities, which will help us learn more about how electrons move in molecules as chemical bonds are changed and broken."

Understanding the DUV-FEL

The DUV-FEL is located at the National Synchrotron Light Source (NSLS), which produces light by accelerating electrons in a circular path at very high speeds, but it does not work the same way. Instead, the electrons are first accelerated in a straight line down a linear accelerator (linac). They then pass through a "wiggler," a device that uses a series of permanent magnets to force them to "wiggle" in a wavy path. This wiggling motion causes the electrons to emit light.

At this point, the electrons need a little help in order to produce light with the qualities DUV-FEL scientists need to perform their experiments – a steady wavelength and frequency, and very short pulses. Thus, as they traverse the wiggler, the electrons are simultaneously coupled with light from a "seed laser." The seed laser light gives the electrons a boost by regulating their motion so that they emit more concentrated, laser-like light. Next, the electrons enter a "bunch compressor" device, where they are

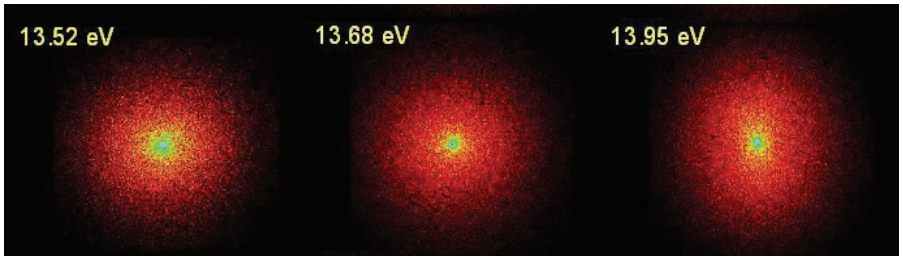

Images of fluorine ions from the ion pair dissociation of methyl fluoride. The images show the changing anisotropy of the ions with increasing excitation energy (eV = electron volts).

grouped into tiny clusters. Finally, the electrons are sent into a second, longer wiggler, where they emit light pulses that can be used for experiments."

"The DUV-FEL is a very intense source of high-energy light pulses," Suits said. "But the FEL light has other unique properties. It is very coherent, or steady, and each pulse lasts less than one trillionth of a second. These short, intense 'flashes' allow us to make very rapid 'snapshots' of brief molecular processes, such as chemical reactions, using the light. These are the kinds of experiments we hope to perform in the future."

The research was funded by the Office of Basic Energy Sciences in the Department of Energy's Office of Science, the National Science Foundation, and the Robert A. Welch Foundation.

—Laura Mgrdichian

Scientists Create and Manipulate Nanoscale "Water Wires"

Scientists working at the National Synchrotron Light Source (NSLS) have caused tiny strands of water, each less than one nanometer (a billionth of a meter) in width, to form inside a common mineral. These nanoscale "water wires" give the scientists a new opportunity to study the properties of very small quantities of water, such as that found inside cells, which behave differently than water at the macro-scale.

Tom Vogt

The results are published in the March 17, 2004 issue of *Nano Letters*. Brookhaven physicist Tom Vogt led the research, performed with collaborators Yongjai Lee of Brookhaven Lab; Joe Hriljac of the University of Birmingham, United Kingdom; and C. Dave Martin and John B. Parise, both of Stony Brook University.

"Water in cells is distinct from bulk water as we know it," explained Vogt. "For instance, it can take the form of long chains of single water molecules, which we call 'water wires' or 'water polymers.' But scientists know very little about water in this form."

They do know, however, that water wires are responsible for proton transport across cell membranes, which is one step in the fundamental process by which most organisms produce energy. Scientists understand how proton conduction occurs in bulk water, but not yet in water at the nanoscale. Studying water wires may shed light on the mechanism.

"In order to understand the biological role of water wires, we must relate their structure to the properties they display, such as their stability and how they transport protons," Vogt said. "Confining very small amounts of water inside minerals and glasses is a good way to model and thus learn about water polymers."

Lee and Martin placed a sample of the mineral natrolite (**Figure 1**) inside a diamond anvil cell, a device that applies very high pressure to a sample using the polished faces of two diamonds. In this case, the pressure was applied after the researchers first surrounded the natrolite sample with a water/alcohol solution. As the high pressure altered the natrolite structure, it also forced water molecules into its empty spaces – a process called pressure-induced hydration. Like tennis balls inserted into a canister, the water molecules nestled one-by-one within the structural framework, forming water wires.

As pressure was continually applied, it nudged the oxygen atoms in adjacent water molecules closer together than oxygen atoms in bulk water. This suggests that the wires may be good proton conductors, since protons travel in water by "hopping" from one molecule to the next, choosing the path of least water-to-water distance.

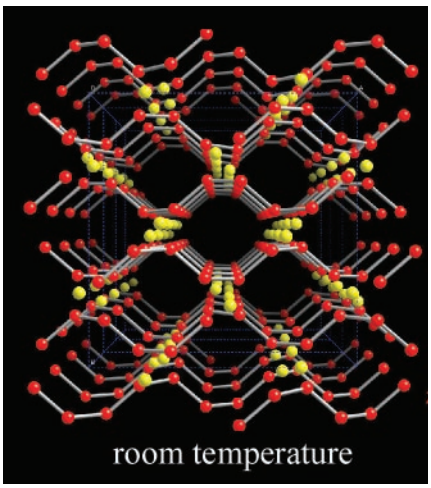

Figure 1. The orientation of the waterwires (water molecules are shown as red balls) as they exist within the natrolite structure at room temperature. The yellow balls represent sodium ions.

Next, Vogt and his group heated the sample to 200 degrees Celsius (**Figure 2**). Under pressure *and* heat, the natrolite structure expanded non-uniformly, i.e. more in one direction than the other. As a result, some water molecules moved closer together while others moved farther apart. This shifted the direction of the shortest water-to-water distance, creating a new preferred hopping route for protons. Because the direction of proton hopping is what defines the water wires, this shift also changed the wires' orientation.

Understanding proton transport at the nanoscale in water wires could be useful in the development of applications such as hydrogen fuel cell technology, which also involves proton transport. It may also help scientists better understand biological processes that depend on proton transport, such the production of adenosine triphosphate, the compound that provides the energy for many cellular functions.

The scientists followed the natrolite's structural changes at NSLS beamline

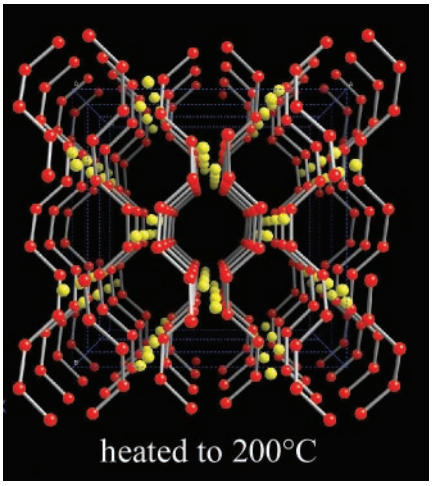

Figure 2. The waterwires within the natrolite structure, heated to 200 degrees Celsius. Upon heating, the wires change direction.

X7A. They focused a beam of x-rays at the sample as they increased the diamond anvil cell pressure. The x-rays entered the sample, bounced off its atoms, and emerged in a distinct pattern, creating a "signature" of the sample. By analyzing its changing signature, the scientists tracked the sample's changing structure.

This research was funded by a grant from Brookhaven's Laboratory Directed Research and Development (LDRD) program.

—Laura Mgrdichian

Unlocking the Secrets of Titanium, a "Key" that Assists Hydrogen Storage

New research may lead to better catalysts for hydrogen fuel cells

Scientists at Brookhaven National Laboratory and the New Jersey Institute of Technology have taken steps toward understanding how a titanium compound reacts with a hydrogen-storage material to catalyze the release and re-absorption of hydrogen. Their results, appearing in the July 19, 2004, issue of *Applied Physics Letters*, may help scientists learn how similar catalysts work, improve their performance, and possibly develop more efficient storage materials for hydrogen fuel cells.

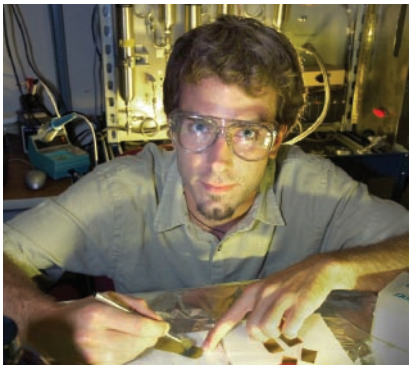

Jason Graetz

In the late 1990s, scientists discovered that adding, or "doping," a small amount of titanium to sodium aluminum hydride, a hydrogen storage compound (also known as sodium alanate), allows it to reversibly release and re-absorb hydrogen. In a sense, the titanium acts like a molecular "key" that facilitates hydrogen absorption and allows the reaction to proceed more rapidly. Until now, however, the nature of that reaction was not well understood.

"We found that the titanium resides on the surface of sodium alanate as a titanium aluminum compound called titanium aluminide, rather than entering the bulk material and replacing other atoms or occupying empty spots within the lattice," said the study's lead author, Brookhaven physicist Jason Graetz.

Graetz and his collaborators first prepared two titanium-doped samples by mixing titanium chloride and sodium alanate using a planetary mill, a device that grinds substances together using marble-sized metal spheres. They then prepared two samples from each doped sample (for a total of six): a dehydrided sample (containing no absorbed hydrogen) and a hydrided sample. By working with both types, the researchers were able to study the titanium's properties before and after hydrogen absorption. This gave them one more way to determine the titanium's role in the reaction.

The group probed the samples with high-energy x-rays at the National Synchrotron Light Source (NSLS) beamline X19A. Because every substance absorbs x-rays differently, having a unique "signature," the researchers were able to compare the six sample signatures to those of different titanium compounds and pure titanium. From this, they determined that the titanium chloride reacted with sodium alanate to form titanium aluminide.

"Our finding is the first step toward an even more interesting discovery: determining exactly how titanium aluminide helps the hydride release and re-absorb hydrogen," Graetz said. "Understanding that mechanism may help us identify better catalysts for the sodium alanate system and help us find dopants for new compounds that are currently impractical energy-storage materials, due to the high temperatures and pressures required to release and re-absorb hydrogen."

Sodium alanate is one of several metal-based hydrogen storage materials, called metal hydrides, being investigated for use in hydrogen fuel cells. A fuel cell works like a battery: Hydrogen atoms enter the negative terminal and split into their constituent particles, protons and electrons. The protons pass through the cell to the positive terminal, while the electrons leave the cell as a stream of electric current. The electrons then re-enter the cell at the positive terminal and reunite with the protons and oxygen to form water molecules.

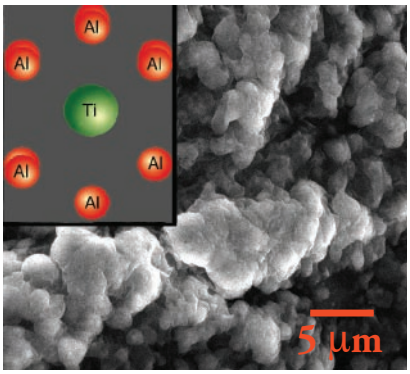

Scanning electron microscope image of Ti-doped sodium aluminum hydride.

The known hydrides are impractical for fuel cells because they are quite heavy and have relatively low storage capacities (less than five percent hydrogen by weight). However, they have more potential than compressed hydrogen gas or liquid hydrogen, which pose explosion and freezing risks. These forms of hydrogen must be stored in tanks under very high pressure or at temperatures cold enough to liquefy the oxygen in air.

This research was funded by a Brookhaven Laboratory Directed Research and Development grant and the National Science Foundation.

—Laura Mgrdichian

NSLS Users Help Decode RNA

Working at the National Synchrotron Light Source (NSLS), scientists from Yale University have determined the crystal structure of a section of ribonucleic acid (RNA), the molecule in cells that uses the information contained in deoxyribonucleic acid (DNA) to synthesize proteins. The work, described in the July 1, 2004 issue of *Nature*, illuminates a piece of RNA never seen before, and may lead to many discoveries, ranging from new information on how proteins behave to new ways to prevent or treat genetic disorders.

Scott Strobel

"The structure contains a number of features that have not been seen before in any structurally-determined macromolecule," said Scott Strobel, the lead author of the paper. "This is very exciting, since there is substantially less known about RNA than protein."

The structure contains an RNA segment called an "intron" flanked by two additional segments called "exons." Exons are the information-carrying pieces of RNA, while introns do not carry information. The process of putting exons together and removing introns is called RNA splicing, and it is a process performed on almost all RNA molecules before they are used by cells.

Until now, however, knowledge of how splicing occurs, and what the splicing site looks like, was limited. Usually, RNA splicing is performed by a large RNA-protein complex called the spliceosome, but, in some RNA molecules, the introns can self-splice by removing themselves without the help of proteins. Strobel and his group crystallized an RNA molecule of this type to learn more about the splicing process.

"We determined the crystal structure of one of these self-splicing introns that includes both of the exons that are about to be joined, or ligated, together," Strobel said. "This configuration displays a splicing intermediate step, where one of the exons has been severed from the intron and is about to be ligated to the second exon, which results in the release of the intron."

Self-splicing, essentially a chemical reaction in which the intron is the catalyst, is the same reaction as that catalyzed by the spliceosome. Although self-splicing involves a much simpler mechanism than that carried out by the spliceosome, this self-splicing "snapshot" is useful because it is likely to reveal how the spliceosome removes introns during exon ligation. This, in turn, may have implications for human health and medicine, since splicing defects are responsible for many genetic disorders.

The crystal structure of the RNA section, with the exons (red) attached to the intron (orange, blue, and green). The intron catalyzes a reaction in which the red segments are joined together and the blue segment is released.

Using the structure, Strobel and his colleagues were also able to closely study the splicing site, or "active" site. They discovered that the site contains two metal ions, whose role is to promote the splicing reaction. This is very similar to the metal ions found within the active sites of the protein enzymes that catalyze the formation of RNA and DNA chains. Thus, studying the behavior of these ions may explain how these protein enzymes "learned" to perform their function.

The RNA structure was determined at NSLS beamline X25 using a technique called macromolecular crystallography, which uses intense x-rays to "see" the molecular structure of different materials. The x-rays are scattered, or diffracted, by atoms in the crystal, forming a unique pattern on a detector screen when they emerge from the sample. By analyzing this pattern, the researchers were able to determine the location of each atom in their RNA crystal.

Strobel and his group plan to continue their research by investigating how the metal ions in the active site promote the splicing reaction. They would also like to learn more about how the intron is rearranged during splicing. This research was funded by the National Science Foundation and the National Institutes of Health.

—Laura Mgrdichian

New Physics Law Unifies Several Superconducting Compounds

A research group led by a scientist at Brookhaven National Laboratory has discovered a simple relationship that mathematically links the properties of a class of high-temperature superconductors, materials that, below a certain temperature, conduct electricity with no resistance. This new, unexpected law applies to superconductors with very different structures and compositions, and may provide clues to understanding the mechanism of high-temperature superconductivity. It is discussed in the July 29, 2004 issue of *Nature*.

"Because this law unifies many different materials, it may allow us to predict the behavior of other superconductors, giving us deeper insight into how these systems work," said Brookhaven Lab physicist Christopher Homes, who led the research.

Homes focused on several members of a class of high-temperature superconductors known as cuprates, which are characterized by layers of copper oxide. He found a relationship between three of each cuprate's physical properties: direct current, or dc, conductivity (how much direct current it conducts); critical temperature (the temperature below which it superconducts); and the "superfluid density" in the superconducting state. This last property refers to how many current carriers — electrons or "holes" (which are spaces in the electron sea that act positively charged) — are in the superconductor.

The new law, called a scaling relation, states that the superfluid density is proportional to the dc conductivity multiplied by the critical temperature. When the researchers plotted this relationship on a graph for each material and compared the shape of these plots, they observed that the overall result is a straight line.

"The interpretation of this result and exactly what it says about the nature of the superconductivity in these materials is a source of ongoing debate," Homes said, "but it should provide insight into the origins of superconductivity in these materials, or even give us a way to predict the behavior of other superconductors."

The scaling relation applies regardless of each cuprate's crystal structure, doping level (the amount of other elements, such as calcium or strontium, added to improve their performance), and type of disorder (how the crystal lattices are distorted by impurities). The relation also works regardless of the direction in which the properties are measured — parallel to the copper oxide planes or perpendicular to them. This is significant because, in a cuprate, the electric current only runs parallel to the copper oxide planes. Perpendicular to the planes, the cuprate acts much like an insulator, with very little current flowing.

"The fact that this scaling law makes a connection between the superconductivity in both directions, where the properties are very different, was surprising," said Homes.

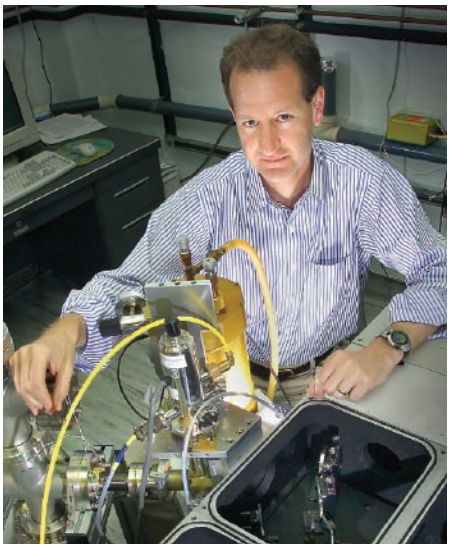

Christopher Homes

Homes and his group studied each material using a wide range of light, from microwaves to ultraviolet rays. In some cases, they worked at the National Synchrotron Light Source infrared beamline U10A. They measured how much light is reflected away from each sample, a value called absolute reflectance. From this measurement, they calculated the properties used to determine the scaling relation.

"The beauty of this technique is that this simple measurement allows both the conductivity and the superfluid density to be measured without touching the material," Homes said. "It is amazing what you can learn about a material just by looking at how it reflects light."

Homes also applied the scaling law to two conventional superconductors, the metals lead and niobium, using known measurements from literature. He and his group will continue this research by studying certain other conventional superconductors, to see if they obey the scaling law.

This research is the result of a collaboration between researchers at Brookhaven Lab, the University of British Columbia, the Central Research

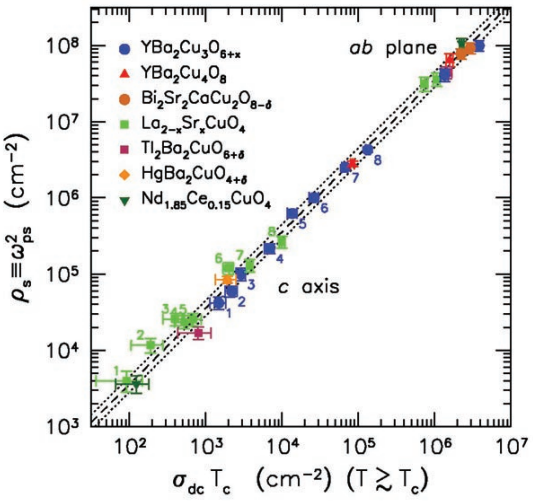

The log-log plot of the superfluid density (y-axis) versus the product of the dc conductivity (measured just above the transition temperature) and the critical temperature (x-axis) for a variety of cuprates, using data taken perpendicular to the copper-oxide planes. Within error (dotted lines), all the data for the cuprates are described by the dashed line.

Institute of Electric Power Industry (Japan), Stanford University, the Stanford Synchrotron Radiation Laboratory, the University of California at San Diego, and McMaster University.

The research was funded by the Office of Basic Energy Sciences within the U.S. Department of Energy's Office of Science, the National Science Foundation, the Natural Sciences and Engineering Research Council of Canada, and the Canadian Institute for Advanced Research.

—Laura Mgrdichian

First Glimpse of DNA Binding to Viral Enzyme

May serve as new target for antiviral drugs

Scientists at Brookhaven National Laboratory and the Albert Einstein College of Medicine have produced the first molecular-scale images of DNA binding to an adenovirus enzyme — a step they believe is essential for the virus to cause infection. The images, which appear on the cover of the October 2004 issue of *Molecular and Cellular Proteomics*, show how binding to DNA may stimulate the enzyme and are already being used to design new antiviral drugs to block this interaction.

"We were quite surprised to see that DNA actually stimulated the activity of the enzyme," said Brookhaven biologist Walter Mangel, a co-author on the paper. "If we can block this interaction, we should be able to prevent the virus from replicating, and thereby thwart infection."

Adenoviruses cause respiratory, gastrointestinal, and eye infections, including highly contagious viral pink eye. Some adenovirus eye infections lead to blindness. Respiratory epidemics of adenovirus are often prevalent on army bases. In patients with compromised immune systems, such as those infected with human immunodeficiency virus (HIV), an opportunistic adenovirus infection can be deadly.

During infection, adenovirus makes an enzyme called a protease, which cleaves or degrades viral "scaffolding" proteins to complete the maturation of newly synthesized virus particles. Mangel and others have been working to understand all the steps necessary for this enzyme's function, looking for new ways to stop its action and, therefore, block an adenovirus infection.

The scientists didn't expect the viral DNA to bind to the protease, but they figured they should look just to rule out such an interaction. "It was something we had to do, to make sure they did not interact," Mangel said. The discovery that the viral DNA interacts with the protease was unprecedented and led them to characterize the interaction in detail. The scientists now believe that inside the virus particle the protease uses the DNA as a guide wire, sliding along the genetic material to remove the internal "scaffolding" proteins, all located near the DNA.

The team used a technique called synchrotron x-ray footprinting, which was pioneered by paper co-author Mark Chance and his colleagues at the Albert Einstein College of Medicine to show where DNA binds on the adenovirus protease.

"Synchrotron footprinting is a technique recently developed at Einstein that allows structural information on the contacting surfaces of biological molecules to be precisely mapped. These contact points are regions providing critical communication in the cell," Chance explained. "In this study, the footprinting approach provided information on the DNA binding region of the adenovirus protease that has not been solved by other techniques and can be used in drug design."

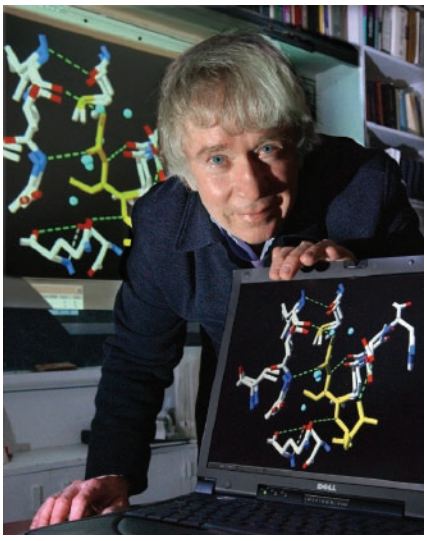

Walter Mangel

At the National Synchrotron Light Source, beamline X28C Einstein's Sayan Gupta, the study's lead author, bombarded different solutions of the adenovirus protease and DNA with x-rays and characterized the changes that occurred on the surface of the protein. With this technique, the team was able to deduce the location of the DNA binding site based upon the changes in accessible surface area.

"There is extensive contact between the enzyme and the DNA," Gupta said. "The DNA wraps around more than half the enzyme molecule. It appears like a strap, holding two parts of the protease together."

Since the DNA binding site is quite long, there are numerous locations along it that could be used as targets for drugs to block the interaction and act as

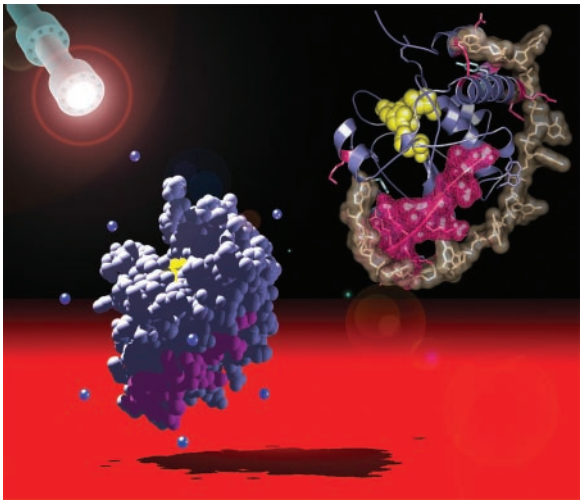

Two views of the adenovirus protease, an enzyme required for viral replication. DNA, depicted by the white "sticks," is shown binding to the enzyme on the right. Drugs that prevent the DNA from binding should prevent the virus from replicating and stop an infection.

antiviral agents, Mangel said. The scientists have already begun looking for such drugs and hope to have the National Institutes of Health test some of them for anti-viral activity within a year.

This work was funded by the Office of Biological and Environmental Research within the U.S. Department of Energy's Office of Science, the Biotechnology Resource Centers Program of the National Institute of Biomedical Imaging and Bioengineering of the National Institutes of Health, and by the National Institute of Allergy and Infectious Diseases of the National Institutes of Health.

—Karen McNulty Walsh

Under Pressure, Zirconium is a "Glass" Act

By working in part at the National Synchrotron Light Source (NSLS), scientists from Los Alamos National Laboratory have produced a new glass material by squeezing the metal zirconium under very high pressures. This glass may be stronger and more resilient than traditional glasses, and has the potential to be a better material for medical, sports, and electronics products. The research is published in the July 15, 2004, issue of *Nature*.

"This is the first time that this type of glass has been formed from a single element or pure metal," said Jianzhong Zhang, one of the two scientists who performed the research. "Moreover, because of its single-element nature and high stability at extreme temperatures, this zirconium glass has many exciting, potential applications."

Jianzhong Zhang (courtesy of Los Alamos National Laboratory)

Unlike conventional metals and metal alloys, which are made of tiny crystalline grains and are thus prone to breakage, metallic glasses made from a single element have a uniform, non-granular structure. These "bulk" glasses have many desirable properties, such as a high resistance to breaking, shattering, and distortion. In this way, bulk metallic glasses behave like a plastic yet are much stronger than other metal materials. These characteristics make them attractive engineering materials, for example.

At the NSLS and Argonne National Laboratory (ANL), Zhang and Zhao created the glass by placing a crystalline sample of pure zirconium in a device that subjected it to extreme conditions – up to 80,000 times atmospheric pressure and 1,300 degrees Fahrenheit. These factors caused the zirconium atoms in the crystal to change their positions and bond to each other differently, producing a material that is still made of zirconium, but takes on a different form: glass. As opposed to other pressure production methods, which produce microscopic samples, this method creates millimeter-sized samples of bulk glass and can even create inch-sized pieces large enough to be used in industry.

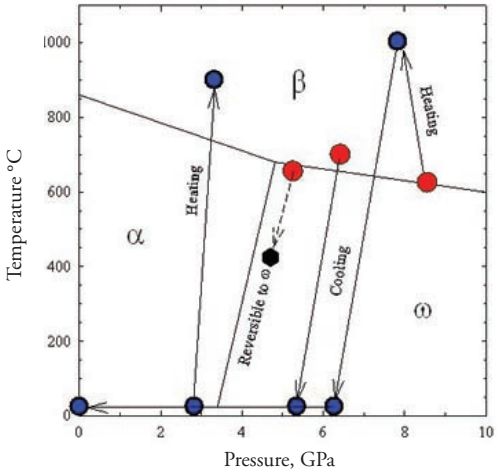

Glass-forming conditions and stability of amorphous zirconium. Circles in red refer to pressures and temperatures at which crystalline zirconium metal transformed into an amorphous phase upon heating. Arrows indicate the selected experimental P-T paths along which no precipitation of any crystalline phase was observed after the formation of amorphous zirconium. Circles in blue refer to a portion of data collected along the paths. The hexagon symbol corresponds to the conditions where the reversed transformation from glass to ω phase was observed upon cooling.

Bulk metallic glasses are being used in an increasing number of practical applications, such as to make electronics components, jewelry, and sports equipment. Scientists believed that bulk metallic glasses can only be alloys. But alloy glasses are not as stable as glasses made from pure metals, and are conventionally produced by melting the alloy metal and rapidly cooling it in water.

This research has dispelled these conventions. "We've broken new ground by showing that metallic glasses do not have to be alloys, and can be produced using an alternate method," said Yusheng Zhao, Zhang's colleague and the paper's co-author.

Zhang and Zhao used x-rays at NSLS beamline X17B2 and ANL to watch how the zirconium changed from a metal to a glass as the pressure and temperature increased. When shined at the sample, the x-rays acted like tiny probes. They bounced off the zirconium atoms and then exited the sample, forming a pattern recorded by a detector. When analyzed, the pattern yielded information about how the structure of the zirconium crystal changed as it was squeezed and heated.

In ongoing follow-up research, Zhang and Zhao will work with commercial-grade zirconium, which is not as pure and, therefore, is less expensive. They want to create a similar glass, but have found that even higher temperatures and pressures are required, and yield a glass

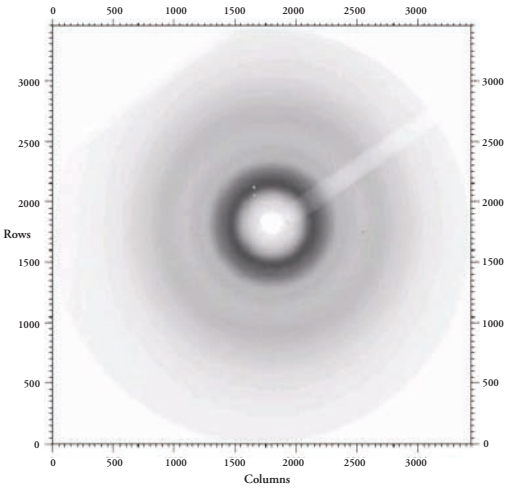

An x-ray scattering image recorded in a CCD detector for a zirconium specimen recovered at ambient conditions. The pattern is characteristic of an amorphous phase and does not reveal any diffraction lines of crystalline zirconium metal.

with lesser quality than that produced using pure zirconium. The researchers hope to remedy this with future experiments.

This work is funded by the Office of Basic Energy Sciences within the U.S. Department of Energy's Office of Science and a Laboratory Directed Research and Development grant from Los Alamos National Laboratory.

—Laura Mgrdichian

Research on "Holes" May Unearth Causes of Superconductivity

Working at the National Synchrotron Light Source (NSLS), scientists have uncovered another possible clue to the causes of high-temperature superconductivity, a phenomenon in which the electrical resistance of a material disappears below a certain temperature. In a superconducting compound, they found evidence of a rarely seen arrangement of "holes" – locations where electrons are absent. The results appear in the October 28, 2004, issue of *Nature*.

The researchers were studying a compound made of strontium, copper, and oxygen (which they've dubbed SCO) that is one of the "cuprates," a family of compounds that contain copper oxide. In SCO, the scientists found evidence of a "hole crystal" – a rigid, ordered arrangement of holes. Holes are positively charged and, like electrons, may interact with each other to produce a superconducting current.

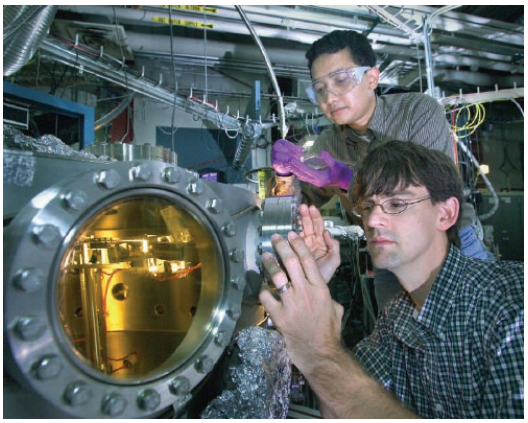

Peter Abbamonte (bottom) and student researcher Andrivo Rusydi

"A hole crystal is a very unusual phenomenon," said NSLS physicist Peter Abbamonte, the study's lead researcher. "Its existence is a direct result of the correlations between holes, which are believed to produce superconductivity in other cuprates."

SCO consists of one layer of strontium atoms sandwiched by two sheets of different copper oxides. In one sheet, the copper-oxide molecules form long, parallel chains. The other copper-oxide layer, which contains the hole crystal, has a ladder structure, resembling chains that are linked horizontally.

A hole crystal is just one type of arrangement of electric charge in a material. These arrangements are important because some researchers believe that superconductivity is the result of a particular arrangement, or occurs when a superconductor approaches a boundary between two arrangements. In other cuprates, for example, scientists are studying a charge arrangement in which ribbons of holes and magnetic regions form alternating "stripes."

"We believe the hole crystal and stripes may be linked," said Abbamonte. "Specifically, the hole crystal in SCO may be a 'low-dimensional' precursor to stripes, meaning it exists only along the copper-oxide ladders, rather than in an entire copper-oxide plane."

He and his collaborators studied SCO using x-rays. They placed an SCO sample in the path of an x-ray beam, varied the wavelength of the beam, and watched how the x-rays reflected away from the sample.

At a particular energy, the sample reflected back the x-rays very intensely. The research group discovered that this reflection was caused by the holes, which led them to determine that the holes formed an ordered lattice since randomly placed holes could not have produced such a strong reflection.

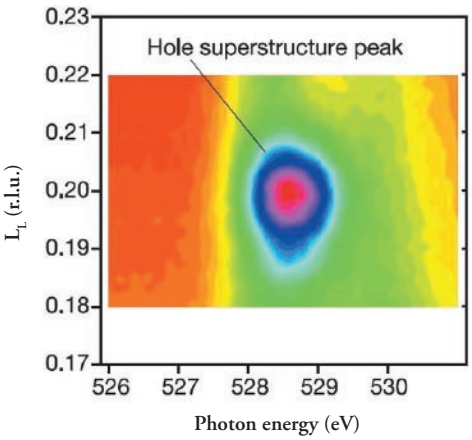

The peak intensity and ladder position (L_L) of the hole crystal reflection.

Abbamonte and his collaborators plan to continue this research by varying the chemical composition of SCO to see if it changes the hole crystal. They will also examine another cuprate to see if its stripes are related to the crystal.

"Clearly, more research needs to be done to study these phases and their possible link to superconductivity," said Abbamonte.

The research was funded by the Office of Basic Energy Sciences within the U.S. Department of Energy's Office of Science, the National Science Foundation, Bell Laboratories, the Dutch Science Foundation, and the Netherlands Organization for Fundamental Research on Matter.

—Laura Mgrdichian

A Brain Cell Gateway

New protein structure may lead to therapies for neural conditions

At the National Synchrotron Light Source (NSLS), scientists from Columbia University have determined the crystal structure of a cell membrane protein that transports glutamate, a chemical essential for normal human brain development and function, in and out of brain cells. This structure has helped them explain how glutamate enters and exits brain cells, which may help researchers develop treatments for neural conditions based on glutamate dysfunction, such as Alzheimer's disease and depression.

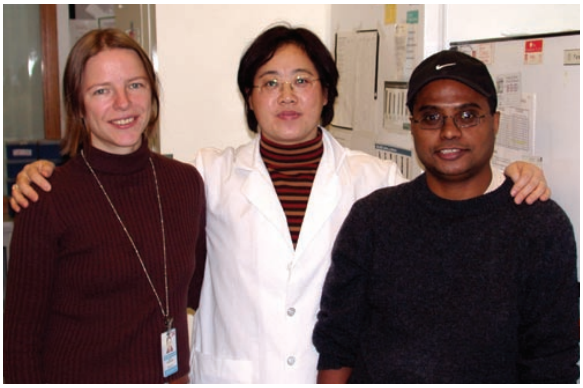

Columbia Researchers Olga Boudker, Yan Jin, and Dinesh Yernool

"Until now, there was no information on the three-dimensional structure of a glutamate transport protein or the mechanisms it uses," said Columbia biochemist Eric Gouaux, who led the study. "This structure gives us a very good idea of how the transporter functions."

Glutamate is one of the most important signaling molecules that is transmitted between brain cells, or neurons. These chemical "messengers," called neurotransmitters, enter and exit a neuron by crossing the membrane, a cell's outer skin, via a transporter protein situated within the membrane.

To understand how these transporters function, scientists must first determine their three-dimensional structures. The researchers determined that the glutamate transport protein's structure – the first-ever structure of a neurotransmitter transporter – is bowl-shaped. The bowl, which is filled with a watery solution, is nestled into the membrane such that the basin dips about midway into the membrane and the rim rises just above it.

The bowl's major structural elements are three wedge-shaped segments. The wide ends of each wedge form the rim of the bowl, while the pointy ends meet to form the basin. Each wedge has an intricate sub-structure, composed of multiple helix-shaped protein strands, called "alpha-helices," that are folded and twisted together. These include two helical, hairpin-shaped substructures (hairpins 1 and 2) that are key players in the transport mechanism.

Hairpin 1 is located at the bottom of the basin. Positioned approximately vertical, it spans the thickness of the bowl such that its curved end points up. Hairpin 2 is closer to the rim of the bowl and is connected to hairpin 1 horizontally, with the two curved ends touching, forming a hinge with an inverted "L" shape. Additionally, a large portion of hairpin 2's surface area touches the solution inside the basin.

Gouaux and his team think that hairpin 1 can unhinge from hairpin 2 and swing away from it, like a gate. When glutamate from a neighboring neuron enters the basin and diffuses down through the solution, the gate opens and the glutamate molecule slips through. Together, the three gateways – one in each wedge – make up the glutamate passage system.

"We now have a much better idea of how glutamate is transported into a cell, which gives us more information on how neurons communicate," said Gouaux. "In turn, we may be able to use this information to help find treatments for neural diseases and conditions that are based on glitches in glutamate transport."

The structure of the cell membrane protein, from a view parallel to the cell membrane.

The researchers made these findings at NSLS beamlines X4A, X6A, X25, and X26C. Using a method called protein crystallography, they scattered x-rays off a crystal sample of the transport protein. The scattered x-rays were collected by a detector and then analyzed by a computer, yielding a three-dimensional model of the protein. This research is funded by the Howard Hughes Medical Institute and the National Institutes of Health.

—Laura Mgrdichian

The Structure and Unusual Hydration/Dehydration Behavior of the New Aluminophosphate SSZ-51

A. Burton, R. Morris, L.M. Bull, and S.I. Zones

School of Chemistry, University of St Andrews and ChevronTexaco Energy Research and Technology Company

The aluminophosphate SSZ-51 is a novel molecular "sieve" prepared using 4-(dimethylamino) pyridine as a structure-directing agent in aluminophosphate gels containing fluoride. We studied the calcination and dehydration behaviors of SSZ-51 using powder x-ray diffraction at beamline X7A. We found that the as-made structure changes only slightly when heated to 300°C. However, at 400°C, there are dramatic changes in both the peak diffraction positions and intensities as the organic structure-directing agent and the fluoride are removed from the structure. As water is adsorbed, reversible structural changes occur within the framework of SSZ-51.

The aluminophosphate mineral SSZ-51 is a novel molecular "sieve" prepared using 4-(dimethylamino) pyridine as a structure-directing agent in aluminophosphate gels containing fluoride. The SSZ-51 unit cell is monoclinic, with a = 21.759, b = 13.821, c = 14.224 Å, and β = 98.85°. The structure of SSZ-51 (**Figure 1**) is closely related to the silicoaluminophosphate SAPO-40. Both structures possess intersecting 12- and 8-ring channels.

The powder diffraction pattern of SSZ-51 changes dramatically after calcination, which removes the occluded organic template and fluoride ions (**Figure 2**). Except for the low-angle 110 and 200 peaks, the diffraction pattern of the calcined material shows little resemblance to the as-made form, suggesting perhaps that the material is decomposing during calcination. However, it was quite puzzling that SSZ-51 possessed an appreciable microporosity, and that adsorption measurements were consistent with the presence of 12- and 8-rings in the calcined structure. We therefore decided to collect variable temperature powder diffraction data at beamline X7A on the as-made sample, to monitor structural changes as SSZ-51 was heated in air.

The sample was placed in a glass capillary and heated in open air in 100°C increments up to 800°C. After completing the initial series of experiments to remove the organic component, the material was placed over a beaker containing water. After hydrating for a day, the sample was loaded into another capillary and data were again collected in 100°C increments.

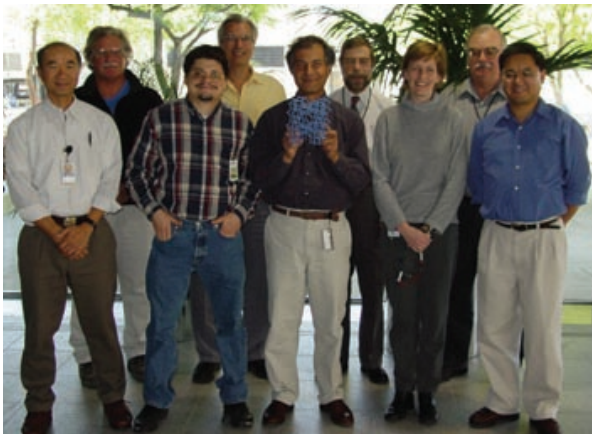

Authors (left to right) (front) Ignatius Chan, Allen Burton, Saleh Elomari, Lucy Bull, and Cong-Yan Chen; (back) Stacey Zones, Steven Vittoratos, Charlie Wilson, and Chuck Kibby

Figure 3 shows the effect of temperature on the powder diffraction pattern of the as-made sample of SSZ-51. As the material is heated to 300°C, there are only slight changes in the x-ray

BEAMLINE X7A

Funding
The Royal Society; National Science Foundation; U.S Department of Energy – Division of Materials Sciences, Division of Chemistry

Publication
R.E. Morris, A. Burton, L.M. Bull, and S.I. Zones, "SSZ-51-A New Aluminophosphate Zeotype: Synthesis, Crystal Structure, NMR, and Dehydration Properties," *Chem. Mater.*, **16**(**15**), 2844-2851 (2004).

Contact information
Russell E. Morris
School of Chemistry, University of St. Andrews

Email: rem1@st-and.ac.uk

diffraction (XRD) pattern. However, at 400°C there are dramatic changes in both the peak positions and intensities as the organic structure-directing agent and the fluoride are removed from the structure. The shifts are readily apparent in the positions of the 110, 200, and 310 reflections. This XRD pattern can be indexed by a C-centered monoclinic cell with lattice parameters of a = 22.471, b = 13.735, c = 14.052, and β = 98.5°. While the other lattice parameters show little change, the a lattice parameter increases by 3.3%. This change seems mostly due to the relaxation of the framework as the fluoride bonds with the framework are broken.

After 400°C, there is little variation in the pattern. At 800°C the XRD pattern shows some disparity near 9.43 and 11.98 °2θ, likely due to structural changes in the berlinite impurity, which exhibits a phase transition near 600°C.

We were surprised that the material survived calcination to 800°C. We then thought that the changes we initially observed in the XRD pattern might be due to adsorption of water rather than to thermal instability. If we allowed the sample to hydrate for a day, would we then obtain the grotesque XRD pattern we observed in our calcined samples? If so, could we reheat the sample and recover a nice "crystalline" diffraction pattern? **Figure 4** shows that the answer to both questions is "Yes." In fact, at 100°C, most of the expected reflections from the unit cell are distinctly visible.

So how do we explain these reversible structural changes induced by water? It appears the adsorbed water removes the long-range order from the otherwise crystalline structure. Water is known to coordinate with aluminum atoms in the frameworks of aluminophosphate zeotypes to produce octahedrally coordinated aluminum species. In some cases water may even hydrolyze the framework bonds to destroy the structure. If the water molecules do not bond to each crystallographically equivalent aluminum atom in the same manner, the long-range symmetry of the structure is lost and a diffraction pattern is obtained with features similar to the one at the bottom of **Figure 2**.

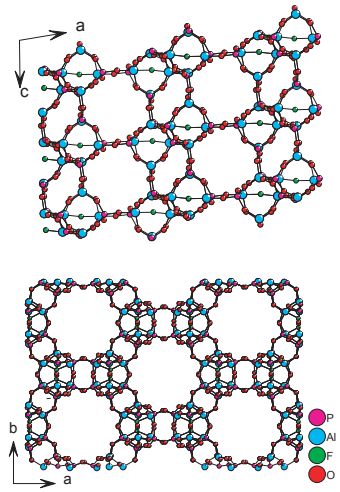

Figure 1. Structure of the novel aluminophosphate SSZ-51.

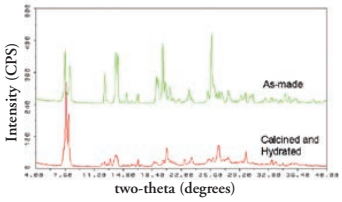

Figure 2. XRD (CuKa) patterns of SSZ-51 taken before and after calcination.

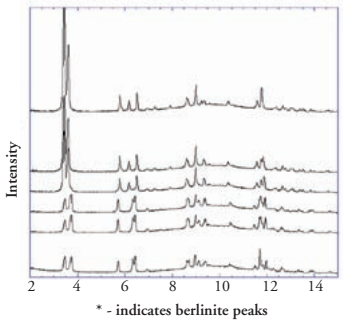

Figure 3. Calcination of the as-made form of SSZ-51.

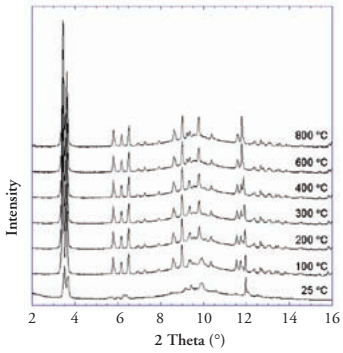

Figure 4. Dehydration of calcined SSZ-51.

Effects of Shear Flow on Interfacial Ordering in Liquids: X-ray Studies

C. Yu, G. Evmenenko, J. Kmetko, and P. Dutta

Northwestern University, Department of Physics and Astronomy

We have directly observed shear-induced structural changes in two interfacial liquids using x-ray reflectivity. The liquids are tetrakis (2-ethylhexoxy) silane (TEHOS) and polydimethylsiloxane (PDMS). Both are insulating, nonpolar liquids, but TEHOS molecules are spherical (non-entangling), while PDMS molecules are linear (entangling). The static interfacial structure of TEHOS, approximately three layers at the interface, was gradually destroyed as the shear rate increased. PDMS, which has no observable interfacial layers when unsheared, developed approximately four layers at the interface at the shear rate of about 10^4 units/second (s^{-1}), applied for 1.5 minutes. We suggest possible correlations between our observations and unusual shear responses reported by other researchers.

Classical hydrodynamics assumes isotropic, continuous media, but this assumption is likely to fail near interfaces, and there is considerable evidence that it does fail. Many experiments have showed a non-classical shear response in interfacial liquids, but the relation between this response and structural changes in the interfacial liquid is not clear. We have directly observed structural changes in interfacial liquids under shear. We used the liquids tetrakis(2-ethylhexoxy)silane (TEHOS) and polydimehylsiloxane (PDMS) in this study. These materials are chemically similar (both are insulating, nonpolar, nonreactive van der Waals liquids), but the molecules are geometrically very different (TEHOS is spherical and PDMS is spaghetti-like).

Surface Force Apparatus (SFA) experiments on nanoscopic round-molecule liquids confined between two smooth solid surfaces have showed shear thinning (reduction of shear viscosity) above a threshold shear rate about 10^8 times smaller than that for bulk liquids. The reduction follows a power law. Computer simulations indicate that shear thinning occurs only in the interfacial region. While our experiments used much thicker liquid films than the SFA experiments, we applied the same shear rates and looked at the structure in the interfacial region. For this purpose we fabricated a shearing apparatus that maintains micrometer-thick liquid films while rotational shear is applied (**Figure 1**).

When no shear is applied, TEHOS is known to develop layers (density oscillations) near hard surfaces. Our shear-dependent x-ray reflectivity data show that these density oscillations are gradually lost above a threshold shear rate, as indicated by the loss of scattering peak height. The relaxation time of the interfacial TEHOS, 0.01 s, can be estimated from the inverse of the threshold shear rate. However, we observed that the disrupted diffraction peak did not significantly redevelop for at least a few hours. We attribute this discrepancy to

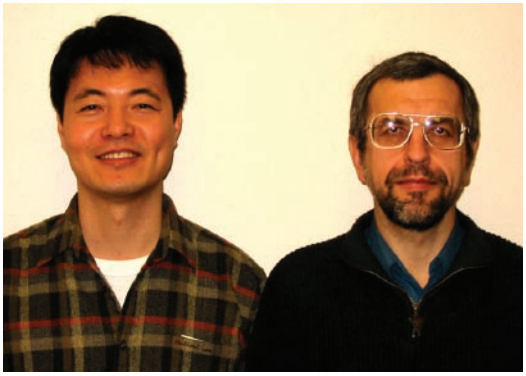

Authors (left to right)
Chungjong Yu and Guennady Evmenenko

BEAMLINE X18A

Funding
National Science Foundation

Publication
C.J. Yu, G. Evmenenko, J. Kmetko, and P. Dutta,"Effects of Shear Flow on Interfacial Ordering in Liquids: X-ray Studies," *Langmuir,* **19**, 9558 (2003).

Contact information
Pulak Dutta
Department of Physics & Astronomy, Northwestern University

Email: pdutta@northwestern.edu

the fact that the shear rate we quote is based on the bulk viscosity of TEHOS, while near the interface a far higher viscosity is likely to exist. The anomalous increase of viscosity at the solid-liquid interfaces has been observed experimentally and is supported by computer simulations.

A very different behavior was observed for PDMS. Unsheared PDMS has a featureless reflectivity pattern (no layering). After shear of $10^4\ s^{-1}$ was applied for 1.5 minutes, a peak developed corresponding to a spacing equal to the backbone diameter of PDMS. This ordering persisted after the shear was no longer being applied, returning to the unsheared state in approximately three hours. The peak is probably a consequence of the disentanglement of PDMS molecules (**Figure 2**).

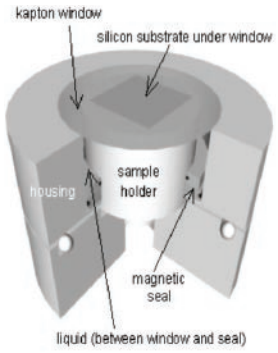

Figure 1. Schematic diagram of the experimental setup. The outer housing and attached kapton window are rotated to apply shear.

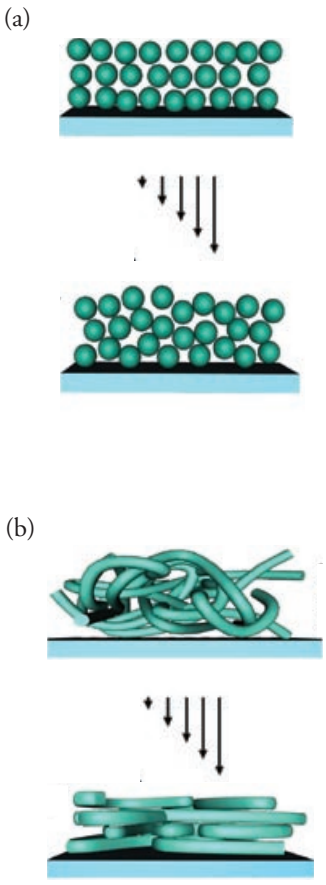

Figure 2. Schematic representation of the effect of shear stress near an interface on (a) TEHOS and (b) PDMS

Chemistry of SO_2 on $Ce_{1-x}Zr_xO_2$ Nanoparticles and $Ce_{1-x}Zr_xO_2$(111) Surfaces

J.A. Rodriguez[1], X. Wang[1], G. Liu[1], J. Hanson[1], J. Hrbek[1], C.H.F. Peden[2], A. Iglesias-Juez[3], and M. Fernández-García[3]

[1]Brookhaven National Laboratory; [2]Pacific Northwest National Laboratory; [3]Instituto de Catálisis y Petroleoquímica, Spain

A major effort in environmental cleanup is controlling the emission of toxic pollutants produced during the combustion of fuels in factories, power plants, and automotive engines. Cerium oxide (CeO_2) -based materials are utilized as catalysts for the destruction of one of these pollutants, sulfur dioxide (SO_2), and are also used to prevent acid rain. High-resolution photoemission, time-resolved x-ray diffraction (TR-XRD), and x-ray absorption near-edge spectroscopy (XANES) were used to investigate the chemistry of SO_2 on cerium oxide zirconium ($Ce_{1-x}Zr_xO_2$) nanoparticles and $Ce_{1-x}Zr_xO_2$(111) surfaces ($x \leq 0.5$). Sulfur K-edge XANES spectra pointed to sulfate (SO_4) as the main product of the adsorption of SO_2 on these mixed-metal oxides. Full SO_2 dissociation was seen on the nanoparticles, but not on the $Ce_{1-x}Zr_xO_2$(111) surfaces. The metal cations at corner or edge sites of the $Ce_{1-x}Zr_xO_2$ nanoparticles probably play a very important role in interactions with the SO_2 molecules.

The $Ce_{1-x}Zr_xO_2$ system is one of the most studied mixed-metal oxides in the literature. Typically, the Ce and Zr cations are randomly distributed in a fluorite-type structure. The focus has been on examining possible correlations between the CeO_2:ZrO_2 interactions and differences in the behavior of $Ce_{1-x}Zr_xO_2$ and CeO_2. Oxide nanostructures can have special chemical properties due to size-induced structural distortions and the presence of corner sites and oxygen vacancies. Recent studies have shown that $Ce_{1-x}Zr_xO_2$ nanoparticles can be prepared by a novel microemulsion method that leads to materials with highly homogenous chemical compositions (i.e. Ce, Zr distribution) and a narrow distribution of particle sizes. Following this approach, we synthesized nanoparticles with sizes between 4 and 7 nm. We investigated their reactivity, and the reactivity of $Ce_{1-x}Zr_xO_2$(111) surfaces, towards SO_2.

Figure 1 shows the structure of an ideal $Ce_{1-x}Zr_xO_2$(111) surface ($x < 0.4$). The top layer consists of O atoms, but within this layer there are holes that expose the Ce or Zr cations in the second layer. This well-defined surface allows the detailed study of O↔SO_2 and Ce,Zr↔ SO_2 interactions. For the $Ce_{1-x}Zr_xO_2$ nanoparticles, the results of transmission electron microscopy show rough surfaces that can be O-or cation-terminated and have a high density of edge or corner sites. These different structural properties affect the chemical reactivity of these mixed-metal oxides.

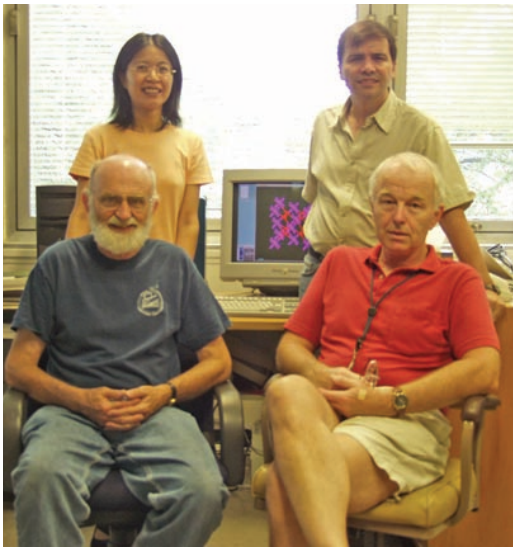

Authors (left to right)
(standing) Xiaqin Wang and Jose A. Rodriguez
(sitting) Jon Hanson and Jan Hrbek

The top of **Figure 2** shows S K-edge XANES spectra for the ad-

BEAMLINES
U7A, X7B, X19A

Funding
U.S. Department of Energy; Interministerial Committee on Science and Technology (Cicyt, Spain)

Publication
G. Liu et al, "Adsorption and Reaction of SO_2 on Model $Ce_{1-x}Zr_xO_2$(111) Catalysts," *J. Phys. Chem. B*, **108**, 2931 (2004).

Contact information
José A. Rodriguez
Chemistry Department, Brookhaven National Laboratory

Email: rodrigez@bnl.gov

sorption of SO_2 on $CeO_2(111)$ and $Ce_{0.7}Zr_{0.3}O_2(111)$ surfaces at room temperature. A comparison to the corresponding peak positions for sulfates and sulfites indicates that SO_4 is the main species formed on the oxide surfaces, with a minor concentration of SO_3 ($SO_{2,gas} + nO_{lattice} \rightarrow SO_{3,ads}$ or $SO_{4,ads}$). The cations in the second layer have all of their O neighbors (eight in total), and interact very weakly with an adsorbed SO_2 molecule. One must introduce O vacancies in $CeO_2(111)$ and $Ce_{0.7}Zr_{0.3}O_2(111)$ to see the interaction of SO_2 with the metal cations and the subsequent dissociation of the molecule.

Figure 2 also shows S K-edge XANES spectra taken after exposing nanoparticles of CeO_2, $Ce_{0.66}Zr_{0.33}O_2$ and $Ce_{0.66}Ca_{0.33}O_{2-y}$ to SO_2 at 25°C. Again, we found that SO_4 is the main sulfur-containing species present on the oxides, but, in addition, we saw features at photon energies between 2470 and 2472 eV that denote the existence of metal-S bonds as a consequence of full SO_2 dissociation. Thus, the nanoparticles have metal cations at corner or edge sites that can interact well with the SO_2 molecule. In addition, there may be O vacancies in the surface of the $Ce_{0.66}Zr_{0.33}O_2$ and $Ce_{0.66}Ca_{0.33}O_{2-y}$ nanoparticles that facilitate S-O bond cleavage.

Figure 3 shows the effect of temperature on the SO_4 signal for the CeO_2 and $Ce_{1-x}Zr_xO_2$ systems in **Figure 2**. As the temperature is raised, SO_4 decomposes. The SO_4 adsorbed on the nanoparticles is somewhat more stable than that present on the (111) surfaces. For both types of systems, the presence of Zr seems to induce an increase in the thermal stability of the adsorbed sulfate.

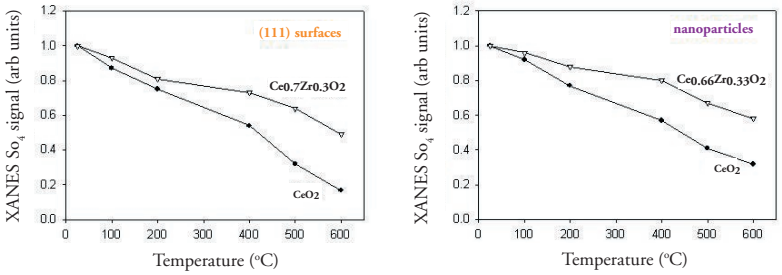

Figure 3. Effect of temperature on the XANES signal for the SO_4 formed on the CeO_2 and $Ce_{1-x}Zr_xO_2$ systems shown in Figure 2. The top panel shows the results for the (111) surfaces, while the bottom panel contains the corresponding results for the nanoparticles.

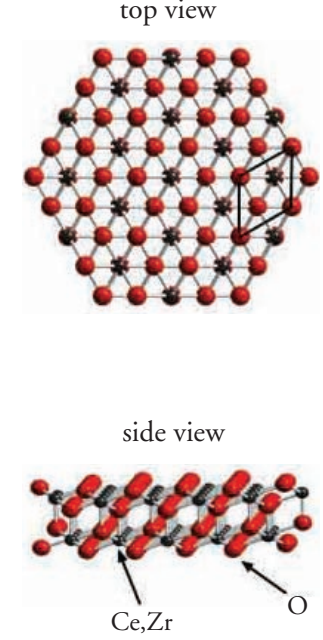

Figure 1. Top and side views of an oxygen-terminated $Ce_{1-x}Zr_xO_2(111)$ surface ($x < 0.4$). The large spheres represent O atoms, and the small spheres correspond to Ce or Zr atoms in a solid solution.

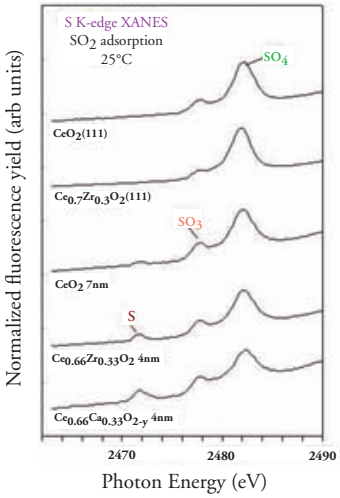

Figure 2. S K-edge spectra taken after dosing SO_2 to $CeO_2(111)$ and $Ce_{0.7}Zr_{0.3}O_2(111)$ surfaces, and nanoparticles of CeO_2, $Ce_{0.66}O_{0.33}O_2$ and $Ce_{0.66}Ca_{0.33}O_{2-y}$. The samples were exposed to 0.1 Torr of SO_2 for five minutes at 25°C.

Peering Into the Self-Assembly of Surfactant Templated Thin-Film Silica Mesophases

D.A. Doshi[1,£], A. Gibaud[2,3], V. Goletto[4], M. Lu[1,*], H. Gerung[1], B. Ocko[5], S.M. Han[1], and C.J. Brinker[1,2]

[1]Department of Chemical and Nuclear Engineering and Center for Micro-Engineered Materials, University of New Mexico; [2]Sandia National Laboratories; [3]Université du Maine, Faculté des Sciences, France; [4]Chimie de la Matière Condensée, Université Pierre et Marie Curie, France; [5]Department of Physics, Brookhaven National Laboratory; [£]Currently at Los Alamos National Laboratories; [*]Currently at Intel Corporation, Portland Technology Development

In this study, time-resolved grazing incidence small angle x-ray scattering (GISAXS) was combined with gravimetric analysis and infrared spectroscopy to structurally and compositionally characterize in situ the evaporation-induced self-assembly (EISA) of a homogeneous silica/surfactant/solvent solution into a highly ordered surfactant-templated mesostructure. Using detergent-like molecules of cetyl trimethyl ammonium bromide (CTAB) as the structure-directing agents, a two-dimensional hexagonal thin film with cylinder axes oriented parallel to the substrate surface forms from an incipient lamellar (layered) mesophase through a correlated micellar intermediate. A comparison with the corresponding CTAB/water/alcohol system (prepared without silica) shows that the hydrophilic and non-volatile silicic acid components actively participate in self-assembly and, along with the presence of solid-liquid and liquid-vapor interfaces, significantly influence the self-assembly pathway.

It is now recognized that self-assembly is a powerful synthetic approach to the fabrication of nanostructures with feature sizes smaller than achievable with state-of-the-art lithography, and with a complexity approaching that of biological systems. For example, recent research has shown that silica/surfactant self-assembly can direct the formation of porous and composite thin film mesostructures characterized by precise periodic arrangements of inorganic and organic constituents on the scale of one to 50 nanometers in size. Despite the potential utility of these films for a diverse range of applications, such as sensors, membranes, catalysts, waveguides, lasers, nano-fluidic systems, and low dielectric constant insulators, the mechanism of thin film self-assembly remains largely unexplored. Understanding and ultimately controlling self-assembly is critical in order for it to transition from largely a laboratory practice to a reliable 'tool' for nanofabrication.

In this study we used time-resolved GISAXS combined with gravimetric analysis to structurally and compositionally characterize *in situ* the EISA process. Solutions were dispensed onto a silicon substrate positioned horizontally on the platform of a weighing balance that was confined within a cell, allowing controlled solvent evaporation. The liquid spectrometer at beamline X22B allowed the x-rays to impinge upon the surface at grazing incidence, and the scattering was continuously collected onto a charge-coupled device camera. *In situ* stress and attenuated total reflection-Fourier transform infrared spectroscopy (ATR-FTIR) measurements, performed using

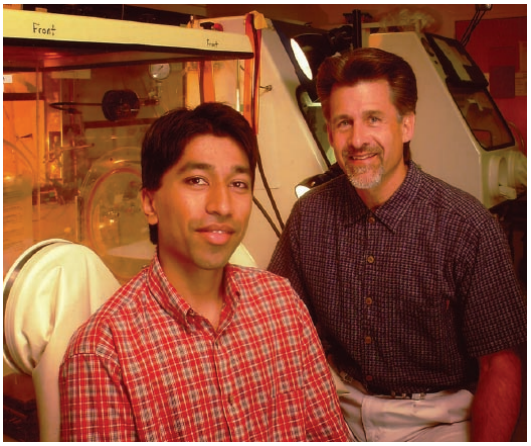

Authors (left to right)
Dhaval Doshi and Jeffrey Brinker

BEAMLINES
X22B, X22A

Funding
University of New Mexico; National Science Foundation; French ACI "Nanostructure"; Department of Energy's Office of Basic Energy Sciences;Air Force Office of Scientific Research; A Laboratory Directed Research and Development (LDRD) grant from Sandia National Laboratories

Publication
D.A. Doshi, A. Gibaud, V. Goletto, M.C. Lu, H. Gerung, B. Ocko, S.M. Han, SM, and C.J. Brinker, "Peering Into the Self-Assembly of Surfactant Templated Thin-Film Silica Mesophases," *J. Am. Chem. Soc.*, **125**(**38**), 11646-11655 (2003).

Contact information
C.J. Brinker
Advanced Materials Laboratory

Email: cjbrink@sandia.gov

the identical horizontal geometry and x-ray reflectivity analysis of the final self-assembled films, enabled further structural interpretation of the GISAXS results, providing greater insight into the self-assembly pathway.

Figure 1 shows the temporal evolution of starting weight percentage for the 0.12 sample (where 0.12 is the CTAB-to-Si molar ratio), along with that calculated for the surfactant, CTAB. The self-assembly pathway comprises four successive stages: (I) isotropic, (II) lamellar, (III) correlated micellar, and (IV) hexagonal, where each is characterized quantitatively by the *d*-spacing observed normal to the substrate, and, for the hexagonal phase, the in-plane spacing a_{fcr} (where fcr is the face-centered rectangular lattice representation of the hexagonal lattice). **Figure 2** maps the evaporation-induced compositional trajectories of the three CTAB/silica systems onto the bulk water/ethanol/CTAB phase diagram. Also plotted is the trajectory for the sample prepared without silica (WS). Selected corresponding GISAXS patterns obtained after the specified times, *t* (seconds), are presented.

The formation of the lamellar phase (Region II in **Figure 1**, inset **b** in **Figure 2**) is completely unexpected from the bulk phase diagram and is not observed in the WS system. Based on orientation, we attribute its appearance to the local enrichment of the sol (the silica/surfactant/solvent solution) at the liquid-vapor interface. We also observe a continuous reorganization of both the mesostructure and the lattice dimension within Regions II-IV (**Figure 1**) that results from the reorganization of the surfactant molecules within the lamellar or micellar structures due to ethanol evaporation. For all samples of CTAB and the other surfactant systems that were studied, we find that the presence or absence of hydrophilic silica species dramatically influences mesophase development. Generally, without silica, the evaporation of solutions like WS results in a crystalline surfactant product without forming the mesophase(s) anticipated from the bulk phase diagram. This apparent kinetic effect presumably results from the evaporation of water. We suppose that such kinetic barriers are avoided for silica-containing systems because the silicic acid species serve as non-volatile fluids that are as hydrophilic as water.

As a result of this study, we now recognize the opportunity to controllably interrupt EISA to derive novel intermediate sandwich-like structures or fine-tune the *d*-spacing and its associated properties, such as surface area, refractive index, and dielectric constant.

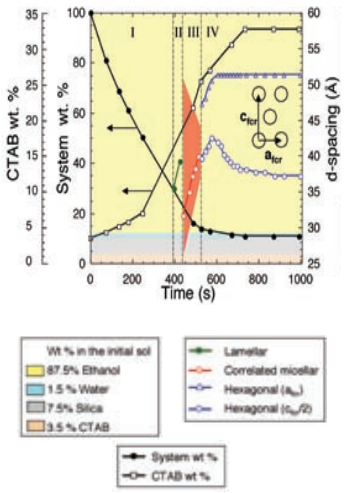

Figure 1. The temporal evolution of structure and composition for the 0.12 sample.

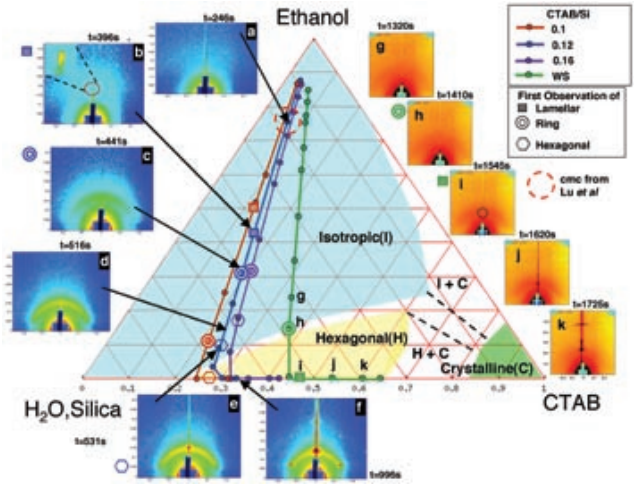

Figure 2. Bulk and thin-film ternary phase diagram. The evaporation-induced compositional trajectories of the three CTAB/silica systems (0.10, 0.12, and 0.16) and the WS systems are mapped onto the bulk water/ethanol/CTAB phase diagram, considering the hydrophilic silicic acid precursors to be equivalent to water. For the 0.12 sample (a) corresponds to the isotropic phase, (b) the lamellar, (c & d) the correlated micellar, and (e & f) the hexagonal. For the WS sample, (g) corresponds to isotropic, (h) correlated micellar, (i & j) lamellar and correlated micellar, and (k) to crystalline CTAB.

Structures and Properties of Supramolecular Assembled Fullerenol/Poly(dimethylsiloxane) Nanocomposites

S. Zhou[1], J. Ouyang[1], and S.H. Goh[2]

[1]Department of Chemistry, The College of Staten Island and the Graduate Center, The City University of New York; [2]Department of Chemistry, National University of Singapore

We prepared supramolecular assembled fullerenol/poly (dimethylsiloxane) nanocomposites by solution-casting the complexes of fullerenol and poly (dimethylsiloxane) (PDMS-di-NH_2) at different molar ratios. The results from our small-angle x-ray scattering (SAXS) study of the nanocomposites indicate that nanodomains of fullerenol aggregates are confined homogeneously in the PDMS matrix and grow in size when fullerenol molecules are gradually added. This novel structural feature, together with the unique molecular properties of fullerenol, gives these nanocomposites superior thermal and thermal mechanical stability, excellent elastic response, and attractive dielectric properties — i.e., one can enhance the permittivity but dramatically decrease the loss factor of the materials.

Fullerene-based nanomaterials are popular research targets due to their unique electrical and optical properties. However, the low solubility of fullerenes in polar media and the difficulty of controlling their aggregation states have prevented these materials from being fabricated into novel materials for advanced applications. One strategy for overcoming these obstacles is to modify fullerenes, such as C_{60}, and incorporate them into polymer matrixes. Poly(dimethylsiloxane) (PDMS-di-NH_2) is an ideal polymer candidate to host C_{60} due to its many useful properties, such as its flexibility, low glass transition temperature, very low surface energy, good thermal stability, and biocompatibility. Making novel materials that combine the outstanding properties of C_{60} fullerene and PDMS is thus desirable.

Recently, we prepared a series of freestanding C_{60}-containing PDMS nanocomposite films via the strong hydrogen bonding interactions between the hydroxyl (-OH) groups of fullerenol and the terminal NH_2 groups of PDMS. **Figure 1** shows the small-angle x-ray scattering (SAXS) profiles of pure PDMS-di-NH_2 and the fullerenol/PDMS nanocomposite films formed at different molar ratios of OH/NH_2. While the bulk PDMS-di-NH_2 has no scattering peaks, the fullerenol/PDMS composites exhibit a single scattering peak, as a result of the homogeneous embedding of fullerenol domains in the PDMS matrix. The gradual addition of fullerenol into the nanocomposites not only sharpens and intensifies the peaks, but also shifts the peak positions to lower *q* values, indicating a gradual increase in the inter-distances of fullerenol nanodomains. In our design, the fullerenol molecules are constrained by the end-functionalized PDMS chains, which means that the distance between neighboring fullerenol nanodomain surfaces should be equivalent to the PDMS chain length. Therefore, the increase in the inter-distances of fullerenol nanodomains could only be explained by an increase in the size of individual fullerenol nanodomains.

Figure 2 depicts the formation and expansion process of fullerenol nanodomains in fullerenol/PDMS

Authors (left to right)
Shuiqin Zhou and Jianying Ouyang

BEAMLINE X27C

Funding
National Science Foundation
Division of Chemistry,
Organic and Macromolecules

Publication
J. Ouyang, S. Zhou, F. Wang, and S. Hong Goh, "Structures and Properties of Supramolecular Assembled Fullerenol/Poly(dimethylsiloxane) Nanocomposites," *J. Phys. Phys. Chem. B*, **108**(**19**), 5937-5943 (2004).

Contact information
Shuiqin Zhou
Department of Chemistry,
The College of Staten Island
and Graduate Center, The
City University of New York

Email: Zhoush@mail.csi.cuny.edu

nanocomposites upon a gradual addition of fullerenol molecules. This three-dimensional network structure, with fullerenol nanodomains homogeneously confined in the PDMS matrix, gives the material superior thermal and thermal mechanical stability, a strongly suppressed crystalline phase, and excellent elastic mechanical properties. More importantly, the controllable size of these fullerenol nanodomains enables us to adjust the dielectric constants of the nanocomposite films. **Figure 3** shows the temperature dependence of dielectric permittivity (ε') and loss factor (ε") of PDMS-di-NH_2 and the fullerenol/PDMS composite film, formed at a molar ratio of OH/NH_2 = 2:1 under several frequencies. The strong interactions between fullerenol and PDMS-di-NH_2 can severely restrain the dipole mobility, resulting in very low ε' and ε" values. On the other hand, the unrestricted, highly polar fullerenol molecules possess very high ε' values due to their direct current conductivity. For relatively large fullerenol nanodomains, only those OH groups located on the domain surface were linked with the PDMS chains. Thus, the unrestricted interior fullerenol molecules could enhance the ε' value for the nanocomposites, which explains the higher ε' value of the nanocomposite film than that of PDMS-di-NH_2 (**Figure 3A**). This unique dielectric property of Fol/PDMS-di-NH_2 nanocomposites has the potential to lead to novel materials with high ε' values and much lower ε" values.

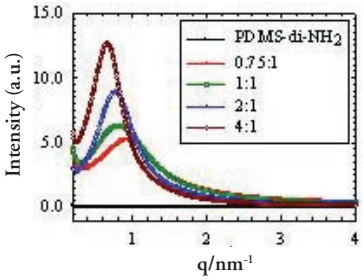

Figure 1. SAXS profiles of pure PDMS-di-NH_2 and fullerenol/PDMS nanocomposite films formed at different molar ratios of OH/NH_2 groups.

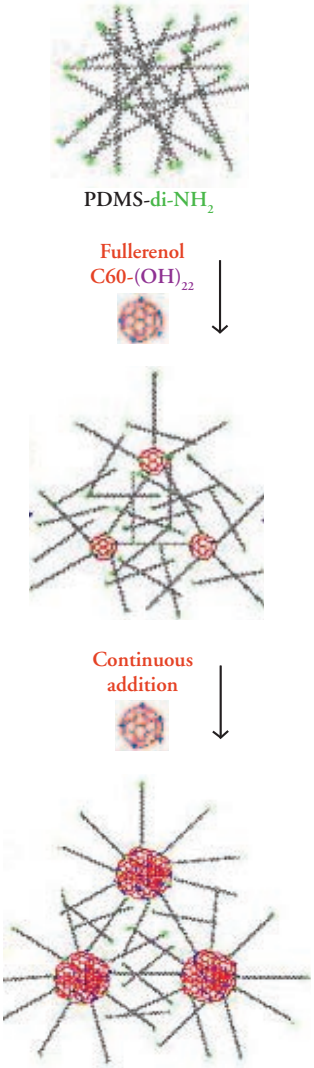

Figure 2. Structural model for the formation of fullerenol/PDMS nanocomposites and the expansion of fullerenol nanodomains upon the continuous addition of fullerenol molecules.

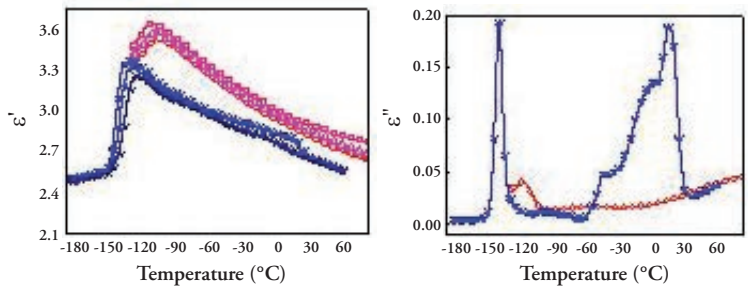

Figure 3. Temperature dependence of ε' and ε" of PDMS-di-NH_2 (star symbols) and fullerenol/PDMS composite film formed at a molar ratio of OH/NH_2 = 2:1 (solid symbols). ε'= 0.3 kHz (square), 3 kHz (up triangle), and 30 kHz (circle). ε"= 0.3 kHz.

Vapor Phase Self-Assembly of Electrooptic Thin Films Via Triple Hydrogen Bonds

P. Zhu[1], H. Kang[1], A. Facchetti[1], G. Evmenenko[2], P. Dutta[2], and T.J. Marks[1]

[1]Department of Chemistry and [2]Department of Physics and Astronomy, Northwestern University

Microstructural acentricity – the alignment of molecular dipole moments in a material – is one of the basic requirements for creating electrooptic (EO) materials useful for high-speed optical telecommunications. A new molecular chromophore, DTPT (5-{4-[2-(4,6-diamino-[1,3,5]triazin-2-yl)-vinyl]-benzylidene}-pyrimidine-2,4,6-trione), was designed and synthesized to create a precursor for the vapor phase growth of a high-response organic EO film. Triple H-bonding interactions between neighboring molecules direct self-assembled chromophore alignment in a head-to-tail orientation using a straightforward vapor-phase thin-film deposition process. Angle-dependent Second Harmonic Generation (SHG) interference patterns and the quadratic dependence of the output light intensity on the film's thickness demonstrate high, reproducible film quality and uniformity. Synchrotron x-ray diffraction (XRD) demonstrates long-range order in the film and yields a molecular tilt angle in good agreement with polarized SHG data. This shows that out-plane ordering of chromophore molecules – i.e. ordering perpendicular to the substrate – has been achieved.

Organic EO materials represent a promising direction in the quest to develop novel technologies for increased optical data network speed, capacity, and bandwith. Achieving microstructural acentricity is a key, yet synthetically daunting challenge for developing such materials. To date, the principle EO active films that have been developed are electric-field poled polymers, Langmuir-Blodgett films, and covalent self-assembled superlattices (SASs) formed layer by layer. In addition to advantages, each approach also poses challenges – ranging from the inherent thermodynamic instability of poled polymers, to the inefficiency of SAS growth techniques, to the fragility of amphiphilic (having both water-loving and water-hating components) lattices enforced principally by van der Waals interactions.

We reported an alternative, vapor phase approach that utilizes robust patterns of directed triple H-bonds to assemble microstructurally acentric, EO-active films in an expedited growth process. This approach utilizes specifically designed intermolecular longitudinal triple H-bonding interactions to align chromophore molecules head-to-tail and preferentially perpendicular to the substrate, forming thin solid films from the vapor phase. Out-plane non-centrosymmetric microstructures are thereby achieved in smooth, optically clear, thermally robust films, which can be grown in hours. Theoretical work shows that such head-to-tail orientations also produce intermolecular cooperative effects, which substantially enhance the effective molecular hyperpolarizability of the films. The chromophore DTPT (5-{4-[2-(4,6-diamino-[1,3,5]triazin-2-yl)-vinyl]-benzylidene}-pyrimidine-2,4,6-trione), containing H-bond + electron donor and H-bond + electron acceptor modules,

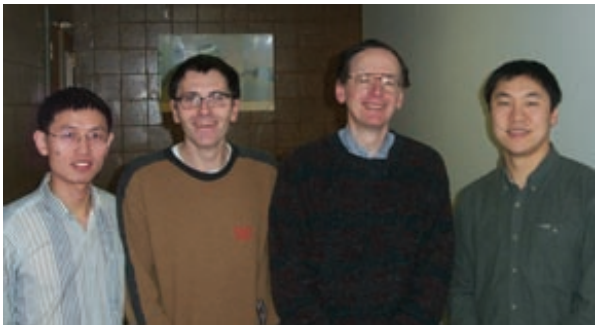

Authors (left to right)
Peiwang Zhu, Antonio Facchetti, Tobin J. Marks, and Hu Kang

BEAMLINE X23B

Funding
Defense Advanced Research Projects Agency/Office of Naval Research; National Science Foundation's Materials Research Science and Engineering Centers

Publication
P. Zhu, H. Kang, A. Facchetti, G. Evmenenko, P. Dutta, and T.J. Marks, "Vapor Phase Self-Assembly of ElectroOptic Thin Films Via Triple Hydrogen Bonds", *J. Am. Chem. Soc.*, **125**(**38**), 11496 (2003).

Contact information
Tobin J. Marks
Department of Chemistry, Northwestern University

Email: t-marks@northwestern.edu

was synthesized and characterized using conventional analytical/spectroscopic techniques. The pyrimidine-2,4,6-trione and 4,6-diamino-1,3,5,-trizine-2-yl moieties of DTPT form longitudinally directed donor-acceptor triple H-bonds between neighboring molecules (**Figure 1**).

In this process, a melamine template was first anchored to a glass or Si (100) substrate. A Denton Vacuum DV-502 deposition apparatus (10^{-5} ~ 10^{-6} Torr) was then used to fabricate films at 100 °C at a growth rate of 0.5 – 2.0 Å/s. The film growth rate and thickness was monitored with a quartz crystal sensor. The resulting films are optically transparent (α ~ 10 cm^{-1} at 640 – 1800 nm) and smooth, as measured using atomic force microscopy (AFM) (rms roughness = 1.7 nm over a 25 μm^2 area for a 1.22 µm-thick film). Polarized transmission SHG measurements were carried out at λ_o = 1064 nm. Angle-dependent interference patterns for glass substrates coated on both sides (**Figure 2a**, inset) demonstrate that identical film quality and uniformity on both sides of the substrate is achieved. The quadratic dependence of the 532 nm light output intensity ($I^{2\omega}$) on film thickness (**Figure 2a**) further demonstrates the uniformity of the chromophore orientation. Calibrating the data (**Figure 2a**, inset) vs. quartz yields nonlinear optical coefficients of d_{33} = 0.15 pm/V (picometers per volt) and d_{31} = 0.25 pm/V. Using standard assumptions, the SHG analysis yields an average chromophore tilt angle of ~61.3° with respect to the substrate normal.

Synchrotron XRD techniques were employed to probe film microstructural regularity. The data reveal a specular (mirror-like) feature at 0.69 $Å^{-1}$, which corresponds to a repeat distance of 9.1 Å (**Figure 2b**). Molecular modeling shows that the repeat distance between DTPT molecules in a H-bonded chain is ~16.8 Å, which, combined with the XRD data, yields a molecular tilt angle relative to the substrate normal of ~57° (**Figure 2b**, inset). This result is in good agreement with the tilt angle derived from SHG data and shows that out-plane ordering of chromophore molecules has been achieved. Importantly, these results demonstrate that appropriately designed molecule precursors can be used in gas phase film growth processes to produce smooth, robust, EO-active films with high microstructural acentricity.

Figure 1. Scheme for DTPT self-assembly.

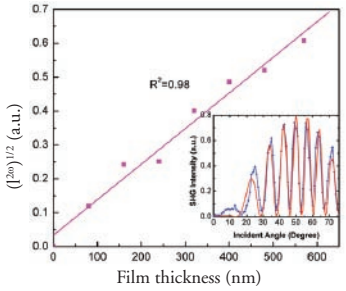

Figure 2a. Square-root of second harmonic generation response $(I^{2\omega})^{1/2}$ as a function of DTPT film thickness. Inset: $I^{2\omega}$ as a function of fundamental beam incident angle. The dashed line is drawn as a guide to the eye. The solid line is the fitting result.

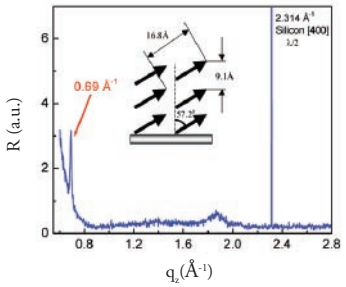

Figure 2b. Specular synchrotron x-ray diffraction pattern for a DTPT film grown on a template-functionalized Si(100) substrate. Inset: Proposed molecular alignment in film.

Growth of Controlled Diameter Single-Walled Carbon Nanotubes

D. Ciuparu, Y. Chen, S. Lim, G.L. Haller, and L. Pfefferle
Department of Chemical Engineering, Yale University

The electronic properties of single-walled carbon nanotubes (SWNTs) depend on their diameter and the chiral angle along which a single graphene sheet is rolled in a cylinder. The selective growth of SWNTs of predetermined diameters allows the synthesis of SWNTs with uniform electronic properties, which are required for electronic applications. We have shown that SWNTs can be produced with a narrow distribution of diameters centered at different discrete values. The average size of the cobalt (Co) clusters used as catalysts for SWNT growth has been determined by extended x-ray absorption fine structure (EXAFS) spectroscopy at beamline X23A2.

Catalytic processes that provide more than 90% selectivity to single-walled carbon nanotubes (SWNTs) have been developed, but catalysts that allow the engineered control of the mean diameter of SWNTs are not available. Since the properties of SWNTs depend on the tube diameter, a catalyst that selectively produces a given, preselected size is technologically important. Here we demonstrate that the cobalt-based catalyst Co-MCM-41 (where MCM stands for "mobil crystalline material") can be used to control the cluster size of cobalt metal in the pores. This, in turn, catalytically produces SWNTs with a narrow distribution of diameters (± 0.05 nm) in the 0.5 to 0.8 nm range.

We chose Co as the catalytic material because it has been demonstrated to be a selective catalyst for SWNTs, especially when stabilized against total reduction. We hypothesized that if Co were isomorphously substituted for silicon (Si) in MCM-41, the MCM-41 matrix would stabilize the Co against total reduction and sintering. Since catalyst metal particle size has been hypothesized to control tube diameter, we studied whether catalyst pore size could be used to control Co cluster size and, thus, SWNT diameter. Four catalysts with pore diameters of about 1.9, 2.2, 2.6, and 2.9 nm (as determined by the classical Barrett-Joyner-Halenda method) were prepared hydrothermally using C10, C12, C14, and C16 organic templates, where 10, 12, 14, and 16 denote the number of carbon atoms in the alkyl chain of the template. The diameters of the SWNTs (synthesized by the disproportionation of carbon monoxide, i.e. the Boudouard reaction) were estimated from the nitrogen adsorption isotherms and high-resolution transmission electron microscope (TEM) imaging, with the former occurring after hydrofluoric acid purification and the latter occurring before the removal of the SWNTs from the catalysts. These estimates were consistent with data from UV-visual/near-infrared absorption spectroscopy, multiple excitation wavelength Raman, and fluorescence (the last two techniques were only used for the C16 template).

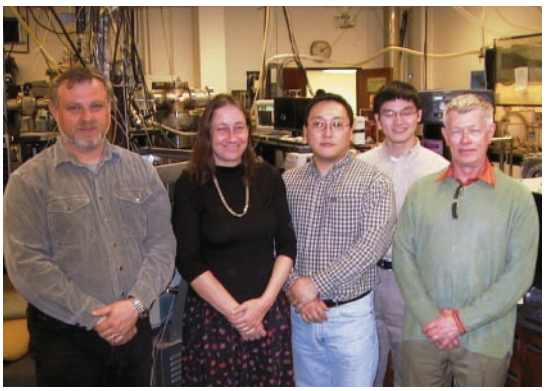

Authors (left to right)
Dragos Ciuparu, Lisa Pfefferle, Sangyun Lim, Yuan Chen, and Gary Haller

In **Figure 1** the average SWNT diameter, determined from ni-

BEAMLINE X23A2

Funding
Defense Advanced Research Projects Agency; Defense Sciences Office Department of Energy; Office of Basic Energy Sciences

Publication
D. Ciuparu et al., "Uniform-Diameter Single-Walled Carbon Nanotubes Catalytically Grown in Cobalt-Incorporated MCM-41," *J. Phys. Chem. B,* **108**(**2**), 503-507 (2004).

Contact information
Dragos Ciuparu
Department of Chemical Engineering, Yale University

Email: dragos.ciuparu@yale.edu

trogen isotherms, is plotted against the Co-MCM-41 pore size (also determined from nitrogen desorption isotherms) and compared with the inner diameter of the SWNT, which was estimated from TEM. A remarkable linear correlation between the synthesized SWNT and the Co-MCM-41 pore size is observed. It is apparent, however, that the SWNT diameter control is not a result of simple geometric or mechanical constraint by the pore walls.

We hypothesize that the actual sites for SWNT growth are Co metal clusters, which is consistent with previously proposed growth mechanisms, and that the diameters of the SWNTs are controlled by the Co metal cluster size. The metal cluster size, in turn, is determined by the stability of the Co^{2+} ions in the MCM-41 silica wall. Controlling the cluster size is done using the metal precursor as a cation constituent of the MCM-41 pore wall, which stabilizes the metal against reduction and migration/sintering during catalyst preparation. The smaller the pore diameter of the Co-MCM-41, the more resistant is the Co^{2+} against reduction, and the smaller is the Co metal cluster that is formed. We have confirmed this hypothesis using the temperature-programmed reduction method. We used EXAFS to measure the Co cluster size in variable-diameter Co-MCMC-41 samples exposed to the Boudouard reaction under identical conditions. The EXAFS results indicate increased Co cluster sizes in MCM-41 with larger pore diameters, as shown in **Figure 2**.

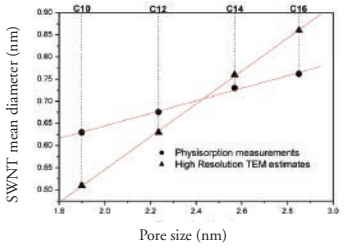

Figure 1. SWNT diameters determined by nitrogen physisorption and HR-TEM for samples produced using catalysts with different pore sizes.

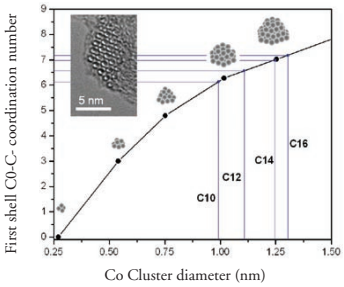

Figure 2. Size of metallic Co clusters determined from Co-Co coordination number estimated determined by fitting the EXAFS spectra recorded for Co-MCM-41 samples reacted with CO under identical conditions. The cluster sizes were calculated assuming a (111) truncated hemispherical cuboctahedron model for the cobalt clusters. The TEM image inset shows a SWNT bundle in a closed hexagonal packing characteristic only for uniform diameter nanotubes.

Structural Characterization of Self-Assembled Monolayer Films of (α–Quarterthiophene) Phosphonate Bonded to the Silicon Native Oxide Surface

E.L. Hanson, J. Schwartz, B. Nickel, N. Koch, and M.F. Danisman

Department of Chemistry, Princeton University

Electron transport across an interface might be controllable by chemically bonding monolayer films to a substrate surface; one possible application is in organic field effect transistors (OFETs), which necessitate a film that is dense and ordered. α-Quarterthiophene-2-phosphonate (4TP) has a band gap comparable to α-sexithiophene, which has been examined as a semiconducting layer in OFETs. A self-assembled monolayer (SAM) film of 4TP was grown on SiO_2/Si. Atomic force microscopy (AFM) showed a comprehensive film with no pinholes over large areas. Film thickness measurements were made by section analysis. An x-ray reflectivity study confirmed this measurement, which was calculated to be 1.8 nm, indicating that the 4TP units are nearly perpendicular to the surface. The profile for 4TP/SiO_2/Si is not as abrupt as that for clean SiO_2/Si, indicating some microscopic disorder within the 4TP film.

Electron transport across or at interfaces might be controllable by chemically bonding monolayers to a substrate surface, which themselves could be modified to further enhance device function. One such possible application of surface-bound monolayers is for organic field effect transistors (OFETs), for use in "next generation" electronic devices. An interesting observation for OFETs is that most of the charge transport occurs through the first few electroactive organic monolayers. We were therefore interested in determining if such films might be prepared from phosphonate derivatives of oligoaromatic species via self assembly on the native oxide surface of silicon (SiO_2/Si). α-Quarterthiophene-2-phosphonate (4TP) would be an attractive example of an oligoaromatic phosphonate for use in such a film, since this material would be easy to process and quarterthiophene (4T) has a band gap comparable to α–sexithiophene, which has been examined previously as a semiconducting layer in OFETs.

α-Quarterthiophene-2-phosphonic acid (4TPA) was prepared from 4T and was used to grow a self-assembled monolayer (SAM) film on SiO_2/Si using our "T-BAG" (Tethering By Aggregation And Growth) method. Atomic force microscopy (AFM) showed a comprehensive monolayer on the surface (**Figure 1a**). The absence of pinholes in large (20 μm x 20 μm, **Figure 1b**) sections revealed the high degree of homogeneity in the SAM. Film thickness measurements therefore had to be made by section analysis (**Figure 1c**), based on the 4TP/SiO_2/Si film edge; this indicated the thickness to be 2.0 ± 0.2 nm. Because the estimated length

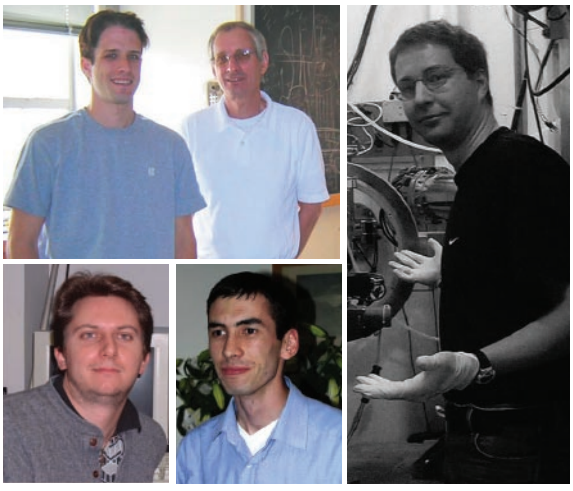

Authors (left to right)
(Top) Eric L. Hanson, Jeffrey Schwartz, (bottom) Norbert Koch, Mehmet Fatih Danisman, and (far right) Bert Nickel

BEAMLINE X10B

Funding
National Science Foundation

Publication
E. Hanson, J. Schwartz, B.Nickel, N. Koch, and M. Danisman, "Bonding Self-Assembled, Compact Organophosphonate Monolayers to the Native Oxide Surface of Silicon," *J. Am. Chem. Soc.*, **125**, 16074-16080 (2003).

Contact information
Jeffrey Schwartz
Department of Chemistry, Princeton University

Email: jschwartz@princeton.edu

of 4TP is approximately 1.9 nm, this measurement suggests only a small deviation, if any, of the 4T moiety from vertical. The surface loading of the 4TP SAM was measured using quartz crystal microgravimetry (QCM) to be 0.66 ± 0.03 nmol/cm^2. This corresponds to a molecular cross-sectional area of 25.1 ± 0.4 Å^2/molecule, which is in the range reported for crystalline 4T (23.4-25.6 Å^2/molecule).

An x-ray study was undertaken using beamline X10B. Measurements were performed in reflectivity mode (ν-2ν), resulting in a momentum transfer, q_z, along the surface normal ($q_z = 4\pi/\lambda \sin \nu$). Analyses of films of 4TP bonded to chemically reoxidized Si (HNO_3 oxidation of H-terminated Si; rms roughness 0.21 nm) were performed in air, and both rinsed and unrinsed samples of 4TP/SiO_2/Si were used. Data were analyzed using dynamical scattering theory. Various parameterizations for electron density profiles (n) were used to model the reflectivity from the organic layer.

X-ray reflectivities were measured for 4TP/SiO_2/Si after the film was prepared, thermally set on the surface (**Figure 2a**; o) (both before and after rinsing to remove any multiplayer material)(**Figure 2a**; ■), and were plotted against the momentum transfer, q_z. Intensities were multiplied by q^4 to compensate for overall decay. As shown in **Figure 2a**, measurements made for the 4TP-covered surface before rinsing show intensity variations in the range $q_z \approx 0.1$ Å^{-1}. These data indicate a structural feature in direct space on the order of about $2\pi/0.1$ = 70 Å, indicative of multilayer formation. Reflectivity data from this multilayered structure could not be modeled. In contrast, reflectivity data obtained after rinsing (**Figure 2b**; ■) were well-modeled; the solid line in **Figure 2b** represents a best fit based on the inset electron density profile (normalized to the density of SiO_2). The striped area in this profile is due to the organic film, which is calculated to be 1.8 nm thick. Furthermore, the profile shape for 4TP/SiO_2/Si indicates some microscopic disorder exists within the 4TP film.

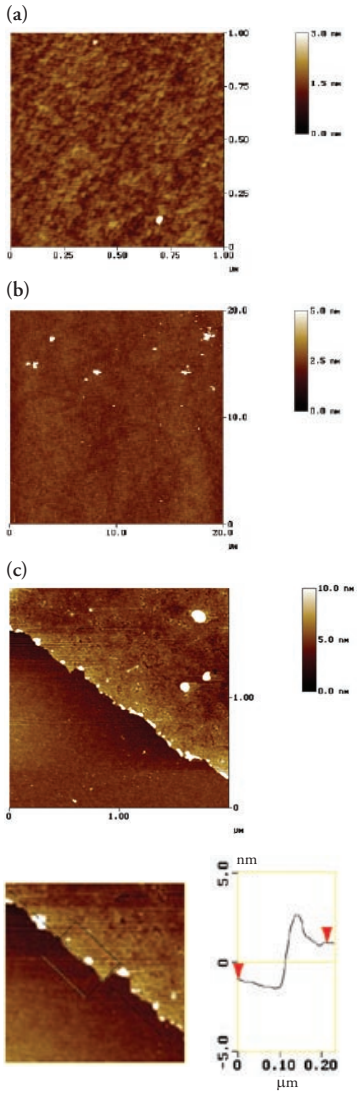

Figure 1. Both (a) and (b), Atomic Force Microscopic (AFM) images of 4TP/SiO_2/Si, and (c) section analysis of a film edge.

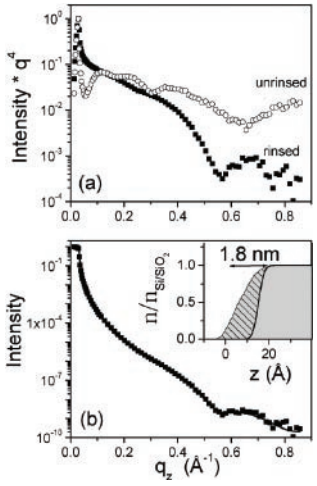

Figure 2. (a) X-ray reflectivity of unrinsed vs. rinsed 4TP/SiO_2/Si and (b) profile of rinsed 4TP/SiO_2/Si.

XAS Study of Au Supported on TiO_2: Influence of Oxidation State and Particle Size on the Catalytic Activity

V. Schwartz, D.R. Mullins, W. Yan, B. Chen, S. Dai, and S.H. Overbury

Chemical Sciences Division, Oak Ridge National Laboratory

We investigated the effect of synthesis, pre-treatment, and reaction conditions on the structure, activity, and oxidation state of Au clusters supported on nanocrystalline and mesoporous TiO_2. X-ray absorption spectroscopy was applied to correlate the particle size and oxidation state with several parameters, such as the pH of the precursor solution, Au loading, pre-treatment, and support structure. Catalytic CO oxidation activity data were obtained and correlated with the particle size, indicating a decrease of activity with particle growth. In-situ studies of Au supported on different allotropic forms of TiO_2 revealed that the high activity state corresponds to Au in a fully reduced state.

Catalysis by small gold particles has been the object of considerable attention in the past few years. The reactivity of gold (Au) was found to be tunable for many important reactions, such as CO oxidation, through the control of particle size and the selection of support materials. It is generally accepted that the Au particle structure and the consequent catalytic properties depend on the support used, Au loading, the synthesis method, and pre-treatment conditions. Among various supports, reducible oxides, such as TiO_2, are perhaps the most popular due to the expected strong metal-support interaction phenomena they exhibit. Our goal was to vary many of these factors and characterize the gold supported on titania, during preparation and the working state, using x-ray absorption spectroscopy (XAFS). We scrutinized Au supported on different allotropic nanocrystalline forms of titania and on mesoporous titania material. The XAFS data at the Au L_{III}-edge were collected at beamline X18B in transmission and fluorescence mode using a channel cut Si (111) monochromator.

The effect of Au loading on the particle size and reducibility of Au clusters was studied using mesoporous TiO_2 as a support. The most important observation was that lower Au loadings resulted in bigger Au aggregates with lower reducibility. The x-ray absorption near-edge structure (XANES) provided information regarding changes in the Au oxidation state during in-situ pre-treatment and reaction conditions. Varying the titania crystalline structure does not seem to affect the redox behavior of the Au clusters. For instance, during the study of Au supported on anatase, a gradual reduction of the Au precursor was clearly observed when the reaction mixture, 1% CO/air, was present at room temperature (**Figure 1a**), even though the concentration of oxygen is 20 times higher than the reductant. Once fully reduced in H_2, no re-oxidation occurs under reaction conditions, even after flowing air at higher temperatures (**Figure 1b**).

Authors
David Mullins and Viviane Schwartz

BEAMLINE X18B

Funding
U.S. Department of Energy Office of Basic Energy Sciences

Publication
V. Schwartz, D.R. Mullins, W. Yan, B. Chen, S. Dai, and S.H. Overbury, "XAS Study of Au Supported on TiO_2: Influence of Oxidation State and Particle Size on Catalytic Activity," *J. Phys. Chem. B,* **108**, 15782-15790 (2004).

Contact information
Viviane Schwartz
Surface Science and Catalysis Group, Chemical Sciences Division, Oak Ridge National Laboratory

Email:schwartzv@ornl.gov

These observations imply that reaction conditions also drive the sample irreversibly towards the fully reduced state. Furthermore, a comparison of lightoff curves after exposing a single sample to a sequence of pretreatment steps demonstrated that Au is in a highly active state, in the form of Au^0, after treatment in H_2 at 150°C. This indicates that oxidized Au is not necessary for high activity.

A comparison of the activity for CO oxidation and the mean particle size determined by extended x-ray absorption fine structure (EXAFS) is provided in **Figure 2**. The activity is described using T_{50}, the temperature at which the conversion reaches 50%. The particle size is estimated using the hemispherical cuboctahedron model given the Au-Au first shell coordination number, which is obtained directly from the EXAFS. By these measures, we see that there is a correlation between the Au particle size in the range studied and the activity. Data are given for each sample following the treatment in H_2 at 150°C and following treatment in O_2 at 300°C. Although the catalytic activities of Au supported on these different allotropic forms of titania are comparable after low temperature treatments, the stability of the Au-catalysts at higher temperatures is dependent upon the TiO_2 structure-type. Au on brookite exhibited no significant particle agglomeration and was the most active catalyst after treatment at 300°C.

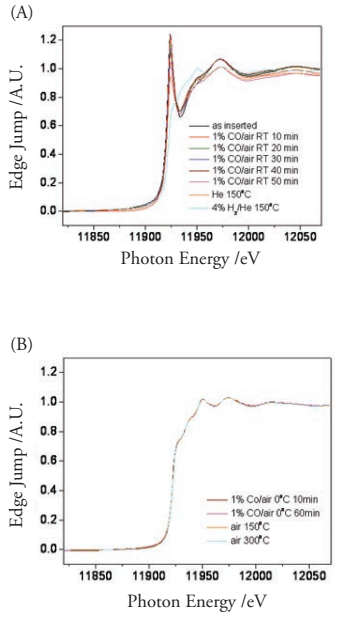

Figures 1A and 1B. XANES of the Au supported on anatase after different pretreatment protocols.

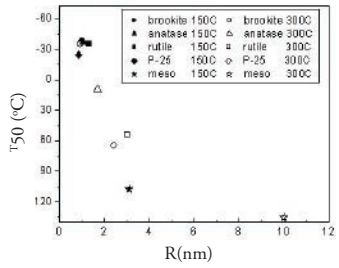

Figure 2. Relationship between activity on CO oxidation and particle size.

High Anisotropy CoPtCrB Magnetic Recording Media

M.F. Toney[1], E.E. Marinero[2], M.F. Doerner[3], and P.M. Rice[4]

[1]Stanford Synchrotron Radiation Laboratory, Stanford Linear Accelerator Center; [2]Hitachi San Jose Research Center; [3]Hitachi Global Storage Technologies; [4]IBM Almaden Research Center

Scientists from the Stanford Synchrotron Radiation Laboratory, Hitachi Global Storage Technologies, and the IBM Almaden Research Center have used x-ray diffraction (XRD) at the National Synchrotron Light Source to understand the microstructure of advanced magnetic recording media and to relate this physical structure to the magnetic properties of the media. The studies were conducted on thin film CoPtCrB media with platinum (Pt) concentrations varying from 10 to 43 percent. We find that the magnetic anisotropy and coercivity of the media, which determine the media's stability and the strength of the field needed to flip the media's magnetization, increase as Pt concentration increases to about 30 percent, plateau, and then decrease for concentrations greater than 40 percent Pt. The x-ray diffraction data show that, with increasing Pt, a face-centered cubic (fcc) cobalt (Co)-alloy phase is progressively formed at the expense of the hexagonal close-packed (hcp) Co-alloy, and that this fraction becomes significant for Pt concentrations greater than 35 percent. The formation of the fcc phase likely causes the behavior in the anisotropy.

The development of thermally stable, small-grain recording media is pivotal to achieving magnetic recording densities beyond 200 Gbits/in^2, in accordance with consumer demands for better and better recording devices. This requires media with high magnetic anisotropy (which determines its stability) and coercivity (field-flipping strength). There are several alternative materials under investigation that provide adequately high anisotropy, including chemically-ordered alloys, such as FePt and CoPt, and rare-earth transition-metal alloys. Another way to achieve this goal is to increase the magnetocrystalline anisotropy of current state-of-the-art CoPtCrB alloys. The anisotropy is enhanced by substituting Pt atoms for the Co atoms in the hexagonal-close packed (hcp) structure. This approach is advantageous because it only requires a relatively small change in the disk manufacturing process.

The disk structures consisted of a glass or nickel-phosphorus substrate, followed by thin films of a seedlayer, a chromium (Cr)-based underlayer, the CoPtCrB media, and a protective carbon coating. The media films were 10 to 20 nanometers thick, with 10 to 43 percent Pt, 15 to 17 percent Cr, and nine to 11 percent boron (B). **Figures 1a** and **b** show, respectively, the magnetic anisotropy (Hk) and coercivity (Hc) as a function of Pt concentration. Large Hk and Hc are needed for stable media. As is evident, Hk increases




Authors (left to right)
(top) Mike Toney and Mary Doerner
(bottom) Philip Rice and Ernesto Marinero

BEAMLINES
X20C, X20A

Funding
U.S. Department of Energy
Office of Science

Publications
M.F. Toney, E.E. Marinero, M.F. Doerner, P.M. Rice, "High Anisotropy CoPtCrB Magnetic Recording Media," *J. Appl. Phys.*, **94**, 4018 (2003).

M.F. Doerner et al., "Demonstration of 35 Gbit/in^2 Media on a Glass Substrate," *IEEE Trans. Magn.*, **37**, 1052 (2001).

Contact information
Mike Toney
Stanford Synchrotron Radiation Laboratory, SLAC

Email:mftoney@slac.stanford.edu

nearly linearly up to about 30 percent Pt, then plateaus, and finally drops above about 40 percent Pt; Hc follows a similar trend. The thermal decay rate of our CoPtCrB media decreases with increasing Pt (from about 15 percent per decade to about one percent per decade), which is consistent with the increase in Hk.

To understand the structural origins of this behavior, x-ray diffraction measurements were done to determine the lattice parameters, the film texture, the stacking fault densities and the fraction of fcc regions in the media. An example of diffraction scans that pass through the fcc(200) and hcp(10$\bar{1}$1) peaks are shown in **Figure 2** for media with 10, 17, 36, and 41 percent Pt. As is evident, the intensity of the fcc(200) peak, and hence the amount of fcc CoPtCrB alloy, increases significantly with increasing Pt concentration. However, since x-ray diffraction is performed over the entire volume of the media, we cannot determine if the fcc regions form isolated grains or are inter-granular.

The fcc concentration was quantified from the integrated intensity of the fcc(200) peak to that of the hcp(10$\bar{1}$1) peak. This is shown in **Figure 1c**. From these data, it is apparent that the fcc fraction is approximately linear until about 35 percent Pt. Above this Pt concentration, the fcc fraction increases more quickly. The fcc phase of Co has a much lower magnetic anisotropy than the hcp phase, suggesting that the increasing presence of the fcc phase with increasing Pt causes the plateau, and then the drop, in Hk that is shown in **Figure 1**.

Interestingly, for all Pt concentrations studied, both the growth and deformation fault densities (specific defects in the way atoms stack in an fcc crystal) do not show a significant trend with increasing Pt concentration, except, perhaps, for a slight increase in the growth faults above about 35 percent Pt. This lack of an increase in fault density with increasing Pt concentration is rather surprising, since high fault concentrations are found in Co-alloys near the fcc-hcp transition region.

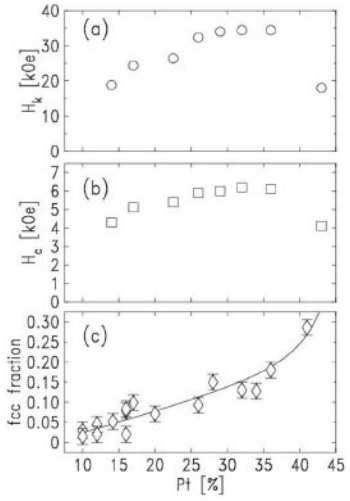

Figure 1. Anisotropy field (Hk), coercivity (Hc), and fcc concentration as a function of Pt concentration in (a), (b), and (c), respectively. Present media have Hc ≈ 4 kilo-Oersteds (kOe) and Hk ≈ 20 kOe, while Hk for pure, bulk Co is 6.4 kOe.

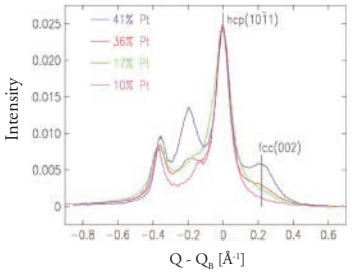

Figure 2. Radial diffraction scans for several media with varying Pt concentration. These diffraction scans pass through the fcc(200) and hcp (10$\bar{1}$1) peaks. To facilitate comparison, the intensity is plotted relative to the position of the hcp peak (QB), the background scattering has been subtracted, and the intensities have been normalized to the peak intensity of the hcp(10$\bar{1}$1) peak. The peak near Q-QB = -0.2 Å^{-1} is the media fcc(111) diffraction peak overlapping the under/seed layer (110) diffraction peak, while the peak near -0.4 Å^{-1} corresponds to hcp(10$\bar{1}$0).

Orbital and Spin Correlations in a Manganite Probed With Soft X-ray Resonant Diffraction

K.J. Thomas[1], J.P. Hill[1], S. Grenier[1,2], Y.-J. Kim[1], P. Abbamonte[3], L. Venema[4], A. Rusydi[3], Y. Tomioka[5], Y. Tokura[5,6,7], D.F. McMorrow[8,9], G. Sawatzky[10], and M. van Veenendaal[11,12]

[1]Department of Physics, Brookhaven National Laboratory; [2]Department of Physics and Astronomy, Rutgers University; [3]National Synchrotron Light Source, Brookhaven National Laboratory; [4]Materials Science Centre, University of Groningen, Netherlands; [5]Correlated Electron Research Center, National Institute of Advanced Industrial Science and Technology, Tsukuba, Japan; [6]Department of Applied Physics, University of Tokyo; [7]Spin Superstructure Project, ERATO, Japan Science and Technology Corporation, Tsukuma, Japan; [8]London Centre for Nanotechnology, London, UK; [9]Department of Physics and Astronomy, University College London, London, UK; [10]University of British Colombia, Vancouver, Canada; [11]Northern Illinois University; [12]Argonne National Laboratory

Soft x-ray resonant diffraction was used to directly probe spin and orbital correlations in a near-half doped manganite. The diffraction was performed at the manganese (Mn) L_{II} and L_{III} absorption edges, providing a sensitive spectroscopy method for studying the Mn 3d states in the spin and orbitally ordered phases. These measurements suggest that the established "checkerboard" model for charge ordering of the Mn^{3+} and Mn^{4+} ions is too simplistic, and reveal a surprising discrepancy between the orbital and magnetic correlation lengths.

In doped manganites of the form $RE_{1-x}A_xMnO_3$ (where *RE* is a rare earth and *A* is a divalent element), the magnetic coupling between Mn sites depends on the overlap of the Mn 3*d* electron orbitals. Therefore, a complex behavior arises in these materials when the direction of the highest occupied Mn 3*d* orbital is itself a degree of freedom. For example, the Mn 3*d* orbitals can undergo long-range order, usually in association with cooperative distortions of the oxygen octahedra that surround the Mn sites. Understanding how the orbital physics drives the overall ground state necessitates a direct probe of both orbital and magnetic order.

We used resonant x-ray diffraction to directly probe the magnetic and orbital order in the near half-doped manganite $Pr_{0.6}Ca_{0.4}MnO_3$, for which the proposed spin, charge, and orbital ground state is shown in **Figure 1**. The incident energy at a magnetic, (½ 0 0), or orbital, (0 ½ 0), Bragg peak was tuned through the Mn L_{II} and L_{III} atomic absorption edges (~ 650 eV). At the L-edges, core Mn $p_{1/2}$ and $p_{3/2}$ electrons are resonantly excited into unoccupied 3*d* levels, which enhances the Mn sites' contribution to the diffracted intensity. The strength of the $2p \rightarrow 3d$ resonance at a Mn site depends on the local charge distribution of the occupied 3*d* orbitals. This leads to a large contrast between the resonant scattering factors on sites 1 and 2 (**Figure 1**) and a large enhancement of the orbital (0 ½ 0) Bragg peak. The resonance matrix element also depends on the direction of the spin in the 3*d* levels, resulting in magnetic resonant scattering at the antiferromagnetic Bragg peak, (½ 0 0). The magnetic enhancement at the L-edges is truly enormous – off resonance, the magnetic scattering is too weak to be

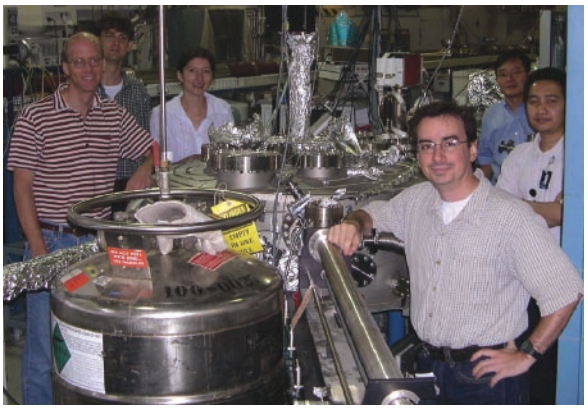

Authors (clockwise from left) John Hill, Peter Abbamonte, Jessica Thomas, Young-June Kim, Andrivo Rusydi, and Stephane Grenier

BEAMLINE X1B

Funding
Department of Energy, Division of Materials Science; The Netherlands Organization for Scientific Research (NWO) Spinoza program

Publication
K.J. Thomas, J.P. Hill, S. Grenier, Y-J. Kim, P. Abbamonte, L. Venema, A. Rusydi, Y. Tomioka, Y. Tokura, D. F. McMorrow, G. Sawatzky, and M. van Veendendaal, "Soft X-ray Resonant Diffraction Study of Magnetic and Orbital Correlations in a Manganite Near Half-Doping," *Phys. Rev. Letts.*, **92**, 237204 (2004).

Contact information
Jessica Thomas
Department of Physics,
X-ray Scattering Group,
Brookhaven National Laboratory

Email:jessica@bnl.gov

observed in these materials – and thus provides a unique opportunity to directly compare the orbital and magnetic correlations in a manganite.

Figure 2a shows the orbital and magnetic resonant line shapes (energy scans at fixed Q). The features in the line shapes are the different excited states in the *3d* band, which are probed with increasing incident energy. The 3 eV shift in spectral weight and the large difference in intensity between the orbital and magnetic spectra suggests that the checkerboard charge-ordered picture in **Figure 1** is too simple. Furthermore, longitudinal scans through the orbital and magnetic Bragg peaks show that the orbital peak is approximately two times wider than the magnetic peak (**Figure 2b**). This suggests that the orbital correlations are shorter-ranged than the magnetic correlations, a result that appears at odds with orbitally driven magnetic order.

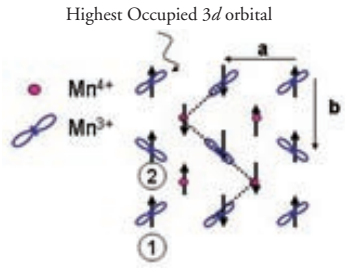

Figure 1. Schematic of the ground state exhibiting charge-orbital-magnetic order in $Pr_{0.6}Ca_{0.4}MnO_3$, showing only the Mn sites in the Mn-O plane. In $Pr_{0.6}Ca_{0.4}MnO_3$, the charge order is modeled as a checkerboard of Mn^{3+} and Mn^{4+} ions and only the Mn^{3+} ions have the orbital degree of freedom. (The symmetry of the highest occupied electron orbital is indicated by a blue lobe). The orbital zig-zag chains couple the Mn sites ferromagnetically along the chain and antiferromagnetically between the chains. The orbital order doubles the unit cell along b, leading to (0 ½ 0) type reflections, while the spin order doubles the unit cell along a, leading to (½ 0 0) reflections.

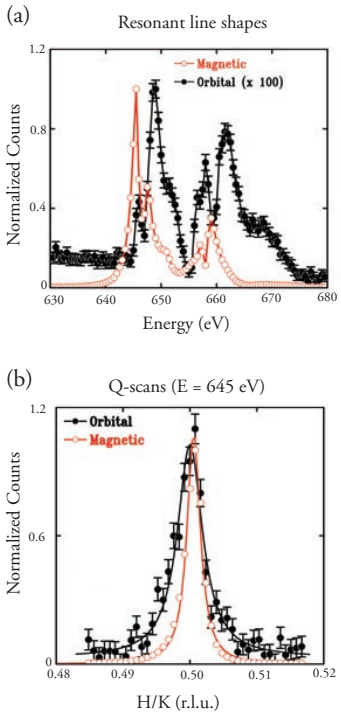

Figure 2. (a) Resonant diffraction line shapes at fixed Q at the orbital (0 ½ 0) position (black curve) and the magnetic (½ 0 0) (red curve). Note that the magnetic resonant line shape is peaked ~ 3 eV below the orbital line shape. (b) Longitudinal Q scans through the magnetic and orbital Bragg peaks, at the same energy.

Melting Point Enhancement of a Self-Assembled Monolayer Induced by a Van-Der-Waals-Bound Capping Layer

F. Schreiber[1,2], M.C. Gerstenberg[2], H. Dosch[1], and G. Scoles[2]

[1]Max Planck Institut für Metallforschung and Institut für Theoretische und Angewandte Physik at the Universität Stuttgart; [2]Princeton Materials Institute, Princeton University

Using in-situ surface x-ray diffraction, the temperature dependence and thermal stability of a self-assembled monolayer (SAM) of decanethiol, sandwiched between the Au(111) substrate and a van-der-Waals-bound capping layer of PTCDA (3,4,9,10-perylenetetracarboxylic dianhydride), are measured. While the bare SAM on Au(111) undergoes a melting transition at 100°C, this transition temperature is raised to 115°C if the SAM is capped by PTCDA. Possible mechanisms and implications of this capping-layer-mediated melting point enhancement are discussed.

Phase transitions in reduced geometry are a very fundamental issue in condensed matter science, and even the seemingly simple case of hard discs in two dimensions continues to be a matter of discussion. A particularly interesting situation arises if a thin film is subject to interactions on both the bottom and top interfaces.

For phase transitions in complex low-dimensional organic materials, the internal degrees of freedom of the molecules, which are an important characteristic of organics, have to be considered and a very rich phase behavior, as seen, for example, in Langmuir films (on liquid surfaces), can be found. Among the well-defined, crystalline two-dimensional organic thin films chemisorbed on a solid substrate, self-assembled monolayers (SAMs) are probably the best characterized systems, and the phase behavior of the archetypal SAM system (alkanethiols on Au(111)) as a function of coverage and temperature has been thoroughly studied.

Here we present the case of rather soft boundary conditions for an organic monolayer, namely a SAM of decanethiol on Au(111) capped by a van-der-Waals-bound crystalline multilayer of PTCDA, a model compound for organic molecular beam deposition (**Figure 1**).

The SAM melting curve is obtained from the area under a Bragg reflection as a function of temperature, T. Compared to the uncapped SAM, we found that the melting temperature of the PTCDA-capped SAM is enhanced by about 15°C, while the character of the transition appears unaltered (**Figure 2**). Note that PTCDA remains solid to well above 200°C – i.e., at the SAM melting T it is still a solid capping layer.

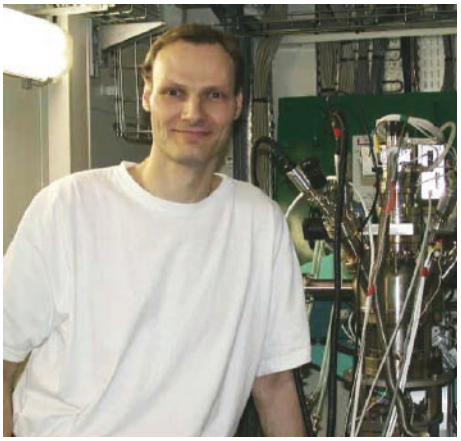

Frank Schreiber

Since the PTCDA layer is only coupled to the SAM itself, it cannot directly exert a significant pressure on the SAM. Therefore, we believe that the mechanism for the melting point enhancement observed here is different from a pressure-induced scenario. We note that the system studied here does not correspond to a confined-melting phenomenon in

BEAMLINE X10B

Funding
Deutsche Forschungsgemeinschaft (DFG); Max-Planck-Gesellschaft; Air Force Office of Scientific Research; National Science Foundation

Publication
F. Schreiber, M.C. Gerstenberg, H. Dosch, and G. Scoles, "Melting Point Enhancement of a Self-Assembled Monolayer Induced by a Van-Der-Waals-Bound Capping Layer," *Langmuir (Letters)*, **19**, 10004 (2003).

Contact information
Frank Schreiber
Physical and Theoretical Chemistry Laboratory, University of Oxford

Email:frank.schreiber@chem.ox.ac.uk

the conventional sense of a hard confinement, since the capping layer is connected only to the SAM and thus is not at a fixed height above the substrate. In fact, one way for the SAM to gain space and thus reduce its density during the phase transition is to reduce the tilt angle of the chains, and thereby increase the effective chain-to-chain distance in the plane. The exact need for this extra volume is not known, but it is clear that the capping layer would not impose serious restrictions on this change of the SAM's effective height, due to the weak interaction of the capping layer with the substrate over this distance. Nevertheless, one should expect that the PTCDA layer at least tends to reduce the fluctuations along the surface normal, which may have an impact on the phase transition.

In addition, the capping layer can have an effect on the lateral interactions within the SAM, in that it tends to "clamp" the chain termina to certain positions in the corrugated potential of the flat-lying PTCDA molecules and, thereby, effectively stabilizes a certain chain-to-chain distance. In this context, it is important to note that PTCDA grows with a well-defined epitaxial relationship, implying that the lateral variation of the PTCDA-SAM interaction potential does not average out. While it is difficult to quantify these interactions, the impact of the capping layer on the fluctuations both along the normal and on the (indirect) in-plane interaction appear to be plausible mechanisms for the melting point enhancement.

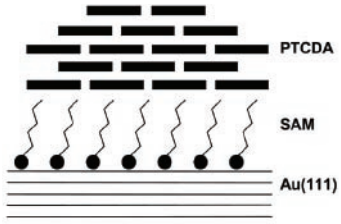

Figure 1. Schematic of the layered structure of the sample (Au(111) substrate / SAM / PTCDA).

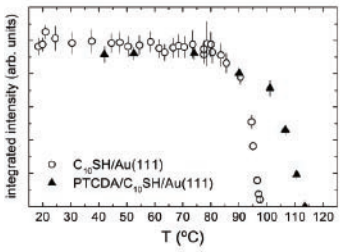

Figure 2. Melting curve as determined from the temperature dependence of the Bragg intensity (integral of the hexagonal in-plane reflection) of the SAM with and without the PTCDA capping layer. For the capped SAM, the melting temperature is enhanced by ~ 15 K.

Measurement of Ti, Ta and Sc Off-Center Displacements in Relaxor Ferroelectric PST-PT

A.I. Frenkel[1], D.M. Pease[2], J. Giniewicz[3], E.A. Stern[4], D.L. Brewe[4,5], M. Daniel[2], and J.Budnick[2]

[1]Yeshiva University; [2]University of Connecticut; [3]Indiana University of Pennsylvania; [4]University of Washington; [5]Advanced Photon Source, Argonne National Laboratory

We probed titanium (Ti), tantalum (Ta), and scandium (Sc) environments in the (1-x)Pb(Sc,Ta)O_3 – $xPbTiO_3$ relaxor ferroelectric (PST-PT), which displays variable order–disorder, relaxor, a mixed phase region, and normal ferroelectric behaviors as x is increased. The abrupt structural phase transition from rhombohedral to tetragonal is observed by x-ray diffraction at x = 0.45. According to x-ray absorption fine structure (XAFS) studies, the structure around Ta, Sc, or Ti atoms changes differently with x and there are no abrupt changes at any concentration. No displacements of Ta or Sc atoms from their oxygen octahedron centers were observed. But surprisingly, we find that Ti is displaced along the (111) direction for x = 0.05. However, it gradually changes direction from (111) to (001) as x increases. We suggest that PST-PT consists of mixed regions, some characterized by a (111) Ti displacement and others by a (001) displacement. The displacement averaged over all regions becomes more weighted toward (001) as x increases.

Relaxor ferroelectrics display a diffuse temperature dependence of their polarization-related macroscopic properties. The origin of this behavior lies in the interactions of polarized entities at the nanoscale. Relaxors typically belong to a class of "oxygen-octahedra compounds," in which six oxygen ions surround a particular transition metal ion, such as Ti, Ta, or Sc (**Figure 1**). The unique characteristics of the relaxor ferroelectric (1-*x*) $Pb(Sc_{1/2}Ta_{1/2})O_3 - x\ PbTiO_3$ (PST-PT) are revealed when one traverses a variety of compositions, *x*. A variety of thermally "adjustable" states of structural ordering, Curie temperatures, and material properties are accessible for these materials. PST-PT is attractive for device applications, and also as a model to explore the nature of relaxor ferroelectrics.

The structure determined by x-ray diffraction (XRD) was rhombohedral for low *x* values, but abruptly becomes tetragonal for $x = 0.45$. The Ta L_3-edge XAFS data of the same samples were measured at beamline X11A. The Sc and Ti K-edges were measured at the Pacific Northwest Consortium - Collaborative Access Team beamlines at the Advanced Photon Source.

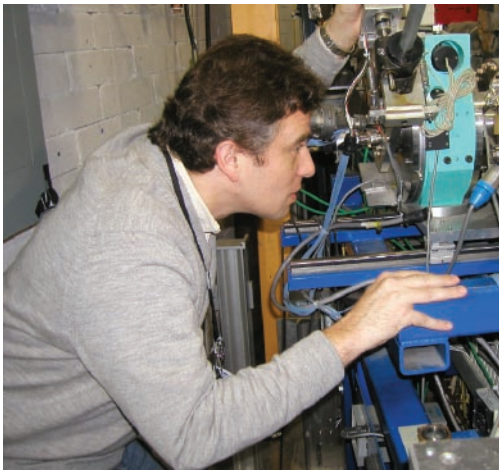

Anatoly Frenkel

At low *x* values, an energy dispersive detector is required to separate Ti K_α fluorescence photons from the Sc K_α photons that dominate the fluorescence background. We used a log-spiral of revolution analyzer designed by Doug Pease and Joe Budnick, recently improved by the addition of the annular ion chamber, designed by Ed Stern. We know of no other detector setup that could

BEAMLINE X11A

Funding
U.S. Department of Energy

Publication
A.I. Frenkel et al., "Concentration-Dependent Short Range Order in Relaxor Ferroelectric (1-*x*)Pb(Sc,Ta)O_3 - $xPbTiO_3$," *Phys. Rev. B,* **70**, 014106 (2004).

Contact information
Anatoly I. Frenkel
Physics Department
Yeshiva University

Email:Anatoly.Frenkel@yu.edu

successfully separate the dilute Ti fluorescence from the otherwise overwhelming Sc fluorescence photons without saturating the detector, and with much more intensity than any other crystal monochromator.

Ti K-edge x-ray absorption near-edge structure (XANES) data of all the samples (**Figure 2**, left) have a feature "A" located in the region corresponding to the dipole-forbidden 1s-3d transition. In order to contribute to the XANES data, the *p*-character of the final state of the photoelectron has to be added in the solid. That may occur due to, for example, hybridization between Ti 3*d* and O 2*p* orbitals that is enhanced if Ti is displaced away from the inversion symmetry center. The presence of a large peak "A" is, therefore, a signature of the off-center displacements of Ti atoms. The area under the peak can be used to quantify the off-center displacement *d* of the Ti atom ($A \propto d^2$). In the Ti K-edge XANES data of all the samples (**Figure 2**, left), the intensity of the signal in this region is much larger than in the reference cubic $EuTiO_3$ system. For all $x < 1$, we obtained $d \sim 0.23(2)$ Å. We found that this large Ti atom displacement is in marked contrast with Ta and Sc atom behaviors, where no measurable displacement from the oxygen octahedron centers (**Figure 1A**) was found by their EXAFS or XANES (**Figure 2**, left (inset)) analyses.

The EXAFS analysis (**Figure 2**, right) revealed that Ti atoms were displaced along the (111) cubic direction from $x = 0.05$ (**Figure 1B**). However, this displacement gradually changes direction from (111) to (001) as *x* increases (**Figure 1C**).

These results allow two interpretations. First, the Ti atom displacement direction changes gradually from (111) to (001) as *x* increases, going through the intermediate orientations. The second interpretation, supported by Maaskant and Bersuker (MB) theory, allows no intermediate orientation between the (111) and (001) directions. In the framework of the MB model, we propose that the PST-PT system consists of mixed regions, some having (111) Ti displacement and others having (001) displacement. The displacement averaged over all regions becomes more weighted toward (001) as *x* increases.

Our work resulted in the atomic-level scenario of the structural transformations in PST-PT. We found that the changes in the local structure could not be simply interpolated from the average structure data: The independent, element-specific measurements were required to elucidate the structure around each atomic species. Our results give the first experimental observation of the 111-displacement direction of a Ti atom in the ferroelectric perovskite system.

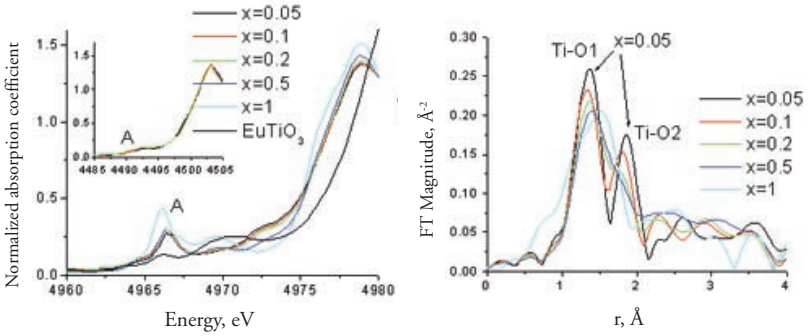

Figure 2. Left: XANES spectra of Ti K-edge in $(PST)_{1-x}(PT)_x$ samples. Feature A denotes the energy region of the dipole-forbidden 1s-3d transition. (A) The inset shows the featureless 1s-3d transition region in Sc K-edge XANES. Right: the Ti K-edge EXAFS: Fourier transform magnitudes of $k\chi(k)$ in $(PST)_{1-x}(PT)_x$ samples. Shown by arrows are groups of Ti-O distances that correspond to either (111) or (001) displacement of the Ti atom from the center of the TiO_6 octahedron, depicted schematically in Figure 1 (B) or (C), respectively.

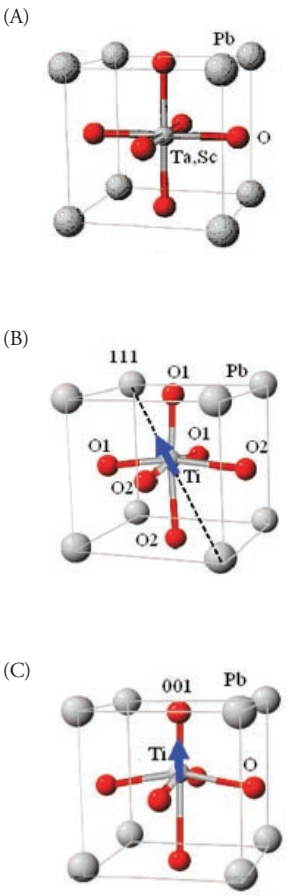

Figure 1. Perovskite pseudo-cubic ABO_3 unit cell (A=Pb, B=Ta, Sc,Ti). (A) The Ta and Sc atoms were shown to be approximately in the cell center. Arrow shows different directions of Ti atom displacements obtained by XAFS for (B) x=0.05 and (C) x=1.

Time-Resolved Diffraction Studies of Ion Exchange: K^+ and Na^+ Exchange into Synthetic Aluminogermanate Molecular Sieve with the Gismondine Topology

A.J. Celestian[1], J.B. Parise[1,2], C. Goodell[1], A. Tripathi[3], and J. Hanson[4]

[1]Stony Brook University, Department of Geosciences; [2]Stony Brook University, Department of Chemistry; [3]Texas A&M, Department of Chemistry; [4]Brookhaven National Laboratory, Department of Chemistry

Time-resolved in situ x-ray diffraction was used to determine how ions are exchanged in the potassium (K^+) and sodium (Na^+) forms of the aluminogermanate molecular "sieve" (AlGe-GIS) with the topology of the gismondine (GIS) family of zeolite minerals. The AlGe-GIS structure is of particular interest due to its highly flexible framework and its use in industrial processes. This study illustrates the ion site-selective exchange pathways that are created during the substitution process and also determines possible ion exchange mechanisms. Bond valence calculations indicated that the preferred charge-balancing cation in the GIS structure is K^+, due to its larger framework bonding coordination. Experiments were conducted at beamline X7B.

Zeolites are nanoporous minerals built from a fully corner-shared framework of tetrahedra. In the gismondine (GIS) family of zeolites, the synthetic aluminogermanate (AlGe-GIS) framework is composed of aluminum (Al^{3+}) and germanium (Ge^{4+}) ions, resulting in a net negative (-1) charge for every Al^{3+} ion in the framework. Therefore, extra-framework cations must be incorporated to charge-balance the structure and maintain electro-neutrality (**Figures 1** and **2**). These extra-framework cations are found in the large channels of the zeolitic framework and can be substituted for other cations. Due to the size, shape, and composition of the zeolitic channels, these materials behave as molecular "sieves" that selectively absorb and desorb cations – a property often used in environmental and industrial applications.

The information obtained from time-resolved *in situ* x-ray diffraction measurements enables us to directly follow the ion exchange process. The exchange of potassium ions (K^+) into Na-AlGe-GIS proceeded to 90% (± 1%) completion within the time frame of the experiment (**Figures 3** and **4**). During the first 10% of K^+ substitution, K^+ only entered the [-101] channel (**Figures 1** and **4**) of the Na-AlGe-GIS structure. After 10%, exchange site-specific substitution could no longer be followed. In the reverse exchange (Na^+ into K-AlGe-GIS; data not shown), a gradual growth of the Na-AlGe-GIS phase was observed and stopped after approximately 10% substitution (**Figure 4**) in the time frame of the experiment. Site-specific ion exchange was not observed during the substitution of Na^+ into K-AlGe-GIS.

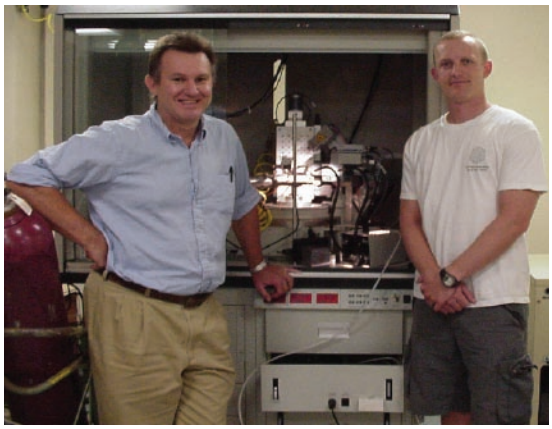

Authors (left to right)
John Parise and Aaron Celestian

The affinity of the GIS framework for the K^+ ion can be explained through bond valence analysis. In K-AlGe-GIS, K conducts most of its bond valence electrons to the O^{2-} framework

BEAMLINE X7B

Funding
National Science Foundation Division of Materials Research

Publication
A.J. Celestian, J.B. Parise, C. Goodell, A. Tripathi, and J. Hanson, "Time Resolved Diffraction Studies of Ion Exchange: K^+ and Na^+ Exchange into (Al, Ge) Gismondine (GIS) $Na_{24}Al_{24}Ge_{24}O_{96}$•$40H_2O$ and $K_8Al_8Ge_8O_{32}$•$8H_2O$," *Chem. of Mat.*, **16**(**11**), 2244-2254 (2004).

Contact information
Aaron J. Celestian
Center for Environmental and Molecular Sciences, Department of Geosciences, Stony Brook University

Email: aaron.celestian@stonybrook.edu

(approximately 51% of its total valence), thus achieving direct framework charge balancing. In Na-AlGe-GIS, Na^+ conducts most of its bond valence electrons through interstitial water molecules (approximately 71% of its total valence). This effectively reduces the amount of direct charge balancing that Na^+ can accomplish and results in a less stable bonding configuration relative to the K^+ bonding environment.

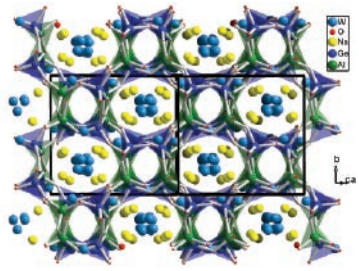

Figure 1. Crystal structure of Na-AlGe-GIS $Na_{24}Al_{24}Ge_{24}O_{96}$•40 H_2O in the C2/c space group. The 8-member ring channel is filled with Na^+ (yellow) and water molecules (blue). Unit cell drawn in black. View is down the [-1 0 1] direction.

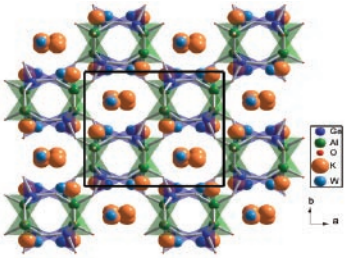

Figure 2. Crystal structure of K-AlGe-GIS $K_8Al_8Ge_8O_{32}$•8H_2O in the I 2/a space group. The 8-member ring channels are filled with K^+ (orange) and water molecules (blue). The unit cell is drawn in black. View is down [0 0 1].

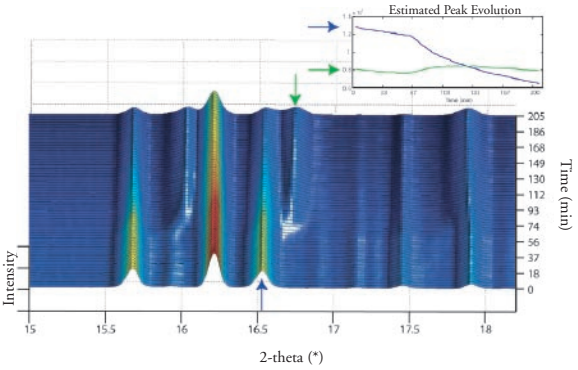

Figure 3. In situ time resolved diffraction patterns (selected 2-theta range shown for clarity). Each diffraction pattern is collected for 60 sec with 2.5 min between each pattern. The onset of ion exchange is seen approximately 60 min from the start of the experiment. New peak growth at 2-theta 16° and 16.75° indicate the K-AlGe-GIS phase forming. Top right insert shows the Iterative Targeted Transformation Factor Analysis (ITTFA), which follows peak position and intensity over all the diffraction patterns. ITTFA serves as an indicator of when subtle changes in the diffraction patterns occur and identifies those patterns for subsequent structure refinements.

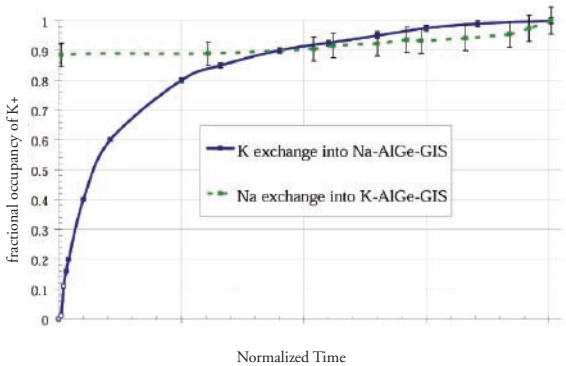

Figure 4. Plot of K^+ occupancy as a function of time during forward and reverse ion exchanges in AlGe-GIS. Open circles represent structure refinements where site-specific occupancies were refined. Time is normalized due to different experimental time frames.

Localization and Speciation of Chromium in Subterranean Clover Using XRF, XANES, and EPR Spectroscopy

J.A. Howe[1], R.H. Loeppert[1], V.J. DeRose[2], D.B. Hunter[3], and P.M. Bertsch[3]

[1]Department of Soil and Crop Sciences, Texas A&M University; [2]Department of Chemistry, Texas A&M University; [3]Advanced Analytical Center for Environmental Sciences, Savannah River Ecology Laboratory, University of Georgia

Scientists from Texas A&M University and the University of Georgia have used x-ray absorption near edge spectroscopy (XANES) and synchrotron x-ray fluorescence (SXRF) microprobe spectroscopy at beamline X26A, as well as electron paramagnetic resonance (EPR) spectroscopy, to investigate the absorption, localization, and transport of chromium (Cr) in plants. These studies have shown that the reduction of Cr(VI) to Cr(III) and the immobilization or compartmentalization of Cr are important detoxification mechanisms used by the plant.

The industrial use and release of chromium compounds into the environment has led to the contamination of water and soil, and therefore to associated environmental and health concerns. In soils, Cr occurs predominately in the +3 and +6 oxidation states. The more soluble and more toxic +6 state presents the greater environmental concern. In efforts to remediate soils contaminated with low levels of Cr(VI), the use of plants to extract or immobilize the metal (phytoremediation) has been proposed. But before phytoremediation can be performed effectively and safely, it is necessary to understand the mechanisms of Cr uptake, translocation, tolerance, and bonding by plants, and the conditions under which Cr is absorbed and/or immobilized.

Nondestructive techniques, such as electron paramagnetic resonance (EPR) spectroscopy, x-ray absorption near edge spectroscopy (XANES), and synchrotron x-ray fluorescence (SXRF) microprobe spectroscopy, are useful for the chemical investigation of Cr, to minimize changes in the metal's chemistry that might occur with destructive techniques. The objectives of this study were to localize Cr in the leaf using SXRF microprobe spectroscopy, determine the oxidation state of Cr in the plant using EPR and XANES, and evaluate possible modes of Cr complexation in the plant using EPR. These analyses were performed on subterranean clover plants exposed to various concentrations of inorganic Cr(III), Cr(VI), and Cr(III)-organic complexes.

Authors (left to right)
Vickie DeRose, Julie Howe, and Richard Loeppert

Localization of the translocated Cr in leaves using SXRF microprobe spectroscopy indicated two distinct Cr accumulation patterns. At the low Cr(VI) treatment concentration (0.04 mM), Cr accumulated primarily at leaf margins with some slight accumulation in the veins (**Figure 1A**). This result corresponded

BEAMLINE X26A

Funding
U.S. Department of Energy, Environmental Remediation Sciences Division in the Office of Biological and Environmental Research; U.S. Department of Energy and the University Research Alliance, formerly the Amarillo National Research Center

Publication
J.A. Howe, R.H. Loeppert, V.J. DeRose, D.B. Hunter, and P.M. Bertsch, "Localization and Speciation of Chromium in Subterranean Clover using XRF, XANES, and EPR Spectroscopy," *Environ. Sci. Technol.*, **37**, 4091 (2003).

Contact information
Richard H. Loeppert
Soil and Crop Sciences Department, Texas A&M University

Email: r-loeppert@tamu.edu

with visual observations of red pigmentation at the leaf margin. At the high Cr(VI) treatment concentration (1.6 mM), Cr accumulation was observed in or around the veins (**Figure 1B**). This accumulation corresponded to regions of brown coloration and tissue damage along the leaf veins. The high Cr(VI) concentration resulted in the death of the plants within seven to 10 days.

The oxidation state of Cr in the plant was determined using both EPR and XANES. This combination of techniques was used because the +6 oxidation state is not detectable using EPR, but is easily identifiable as a pre-edge peak in the Cr K-edge XANES spectrum. In plants grown with the low Cr(VI) treatment concentration and with various Cr(III) treatments (i.e., $CrCl_3$, Cr(III)-EDTA, Cr(III)-citrate, and Cr(III)-oxalate), the Cr in the plant was only observed in the +3 oxidation state. Furthermore, the EPR spectra indicated the occurrence of Cr(III)-organic complexes, except in the case of the plants grown in $CrCl_3$ and the low Cr(VI) treatment. The EPR spectra from these two treatments indicated the presence of a precipitated $Cr(OH)_3$ phase in or on the roots. EPR spectra of both the roots and shoots of plants grown in a high Cr(VI) treatment concentration revealed distinct Cr(V) signals and additional signals of Cr(III)-organic complexes in the leaf. Using XANES, Cr(VI) was only positively identified in the roots of plants grown with the high Cr(VI) treatment concentration (**Figure 2**). Successive scans revealed the rapid disappearance of this peak, indicating the rapid reduction of Cr(VI) (**Figure 2F, 2G**).

Results from this study provide information on how plants tolerate Cr(VI). This tolerance must involve the complete reduction of highly toxic Cr(VI), Cr(V), or Cr(IV) to the considerably less toxic Cr(III), and either the immobilization or compartmentalization of Cr(III). Three processes of immobilization and compartmentalization were identified: (i) the precipitation of a Cr(III) hydroxide phase at the root, (ii) the complexation of Cr(III) and its probable storage as Cr(III)-organic complexes, and (iii) the transport of Cr(III)-organic complexes to the leaf margins, where the Cr is less disruptive to plant metabolic processes.

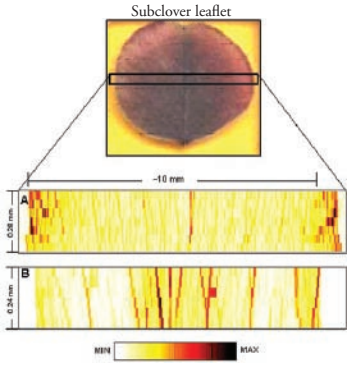

Figure 1. SXRF microprobe images of the relative Cr concentrations in transects of subclover leaves grown in (A) 0.04 mM Cr(VI) for 21 days and (B) 1.6 mM Cr(VI) for 4 days. The rectangle on the subclover leaflet at the top of the figure indicates the approximate location of the transect.

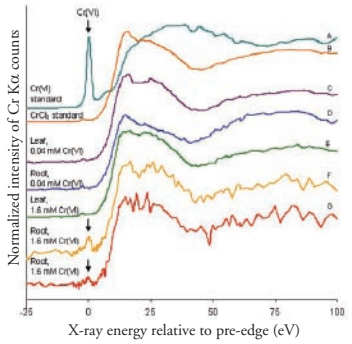

Figure 2. XANES Cr K-edge spectra of 5% (w/w) standards of (A) Cr(VI) and (B) Cr(III), fresh subclover (C) leaf and (D) root tissue grown with 0.04 mmol L^{-1} Cr(VI), fresh subclover (E) leaf and (F, G) root tissue grown with 1.6 mM Cr(VI). Spectra F and G are successive scans at the same position on the root indicating the rapid reduction of Cr(VI).

Quantifying Hazardous Species in Particulate Matter Derived from Fossil-Fuel Combustion

F.E Huggins[1], G.P. Huffman[1], W.P. Linak[2], and C.A. Miller[2]

[1]Consortium for Fossil Fuel Science, Department of Chemical and Materials Engineering, University of Kentucky; [2]National Risk Management Research Laboratory, U.S. EPA

X-ray absorption fine structure (XAFS) spectroscopy at beamlines X18B and X19A was used to investigate and assess the hazards posed to human health from the presence of potentially toxic species in airborne particulate matter (PM) released during the combustion of fossil fuels. XAFS spectroscopy was combined with a leaching protocol and used to quantify the oxidation states of As and Cr in PM from coal combustion and the presence of Ni sulfides in PM from residual oil combustion. Such speciation information is needed in order to assess the potential bioavailability and health hazards posed by metals and other species in airborne PM.

In 1997 the U.S. Environmental Protection Agency (U.S. EPA) promulgated new regulations regarding exposure to fine airborne particulate matter, based on the results of several major epidemiological studies that demonstrated an association between the amount of fine particulate matter (PM) in the ambient atmosphere and various respiratory and cardiovascular health problems in humans. The new regulations propose keeping existing limits on emissions of particulate matter less than 10 μm in size (PM_{10}) and including new limits on finer PM, viz., the fraction less than 2.5 μm in size ($PM_{2.5}$). The additional regulations place increased emphasis on particle emissions from combustion processes that typically generate very fine particles (0.01 – 2.5 μm) in comparison to mechanical processes based on comminution and fracture processes, which tend to generate coarser particles, usually greater than 2.5 μm in size. Major combustion processes thought to contribute significantly to ambient $PM_{2.5}$ include fossil-fuel (e.g. coal, residual oil) combustion for electrical power generation, biomass combustion (e.g. crop-clearing fires, forest fires, wood-stove combustion), and internal combustion engines powered by liquid (diesel, gasoline) fuels.

Although the link between the $PM_{2.5}$ content of the atmosphere and adverse health effects is well established, the actual mechanism of injury is still poorly understood and a multitude of different theories are being pursued. Another important research area is how to determine the relative proportions of different source contributions to the ambient $PM_{2.5}$ fraction.

Authors (left to right)
(top) Frank Huggins and Jerry Huffman
(bottom) Bill Linak and Andy Miller

BEAMLINES
X18B, X19A

Funding
National Science Foundation

Publication
F.E. Huggins, G.P. Huffman, W.P. Linak, and C.A. Miller, "Quantifying Hazardous Species in Particulate Matter Derived from Fossil-Fuel Combustion," *Environ. Sci. and Tech.*, **38**, 1836-1842 (2004).

Contact information
Frank E. Huggins
Research Professor, CME/
CFFS University of Kentucky

Email: fhuggins@engr.uky.edu

In this work, we used XAFS spectroscopy at beamlines X18B and X19A to investigate the speciation of hazardous metals in $PM_{2.5}$ derived from the combustion of coal and residual oil. Coal and residual oil samples were combusted in large laboratory-scale combustion units at the U.S. EPA's National Risk Management Research Laboratory, and two fractions of PM – a coarse $PM_{2.5+}$ fraction and a fine $PM_{2.5}$ fraction – were separated using a cyclone with a cut-point of 2.5 µm. The PM samples were then subjected to leaching in deionized water and hydrochloric acid, and both bulk samples and residues from the leaching experiments were investigated by XAFS spectroscopy. The combination of XAFS spectroscopy and leaching studies not only provides the means for quantifying the presence of various toxic species in PM samples, but can also provide important information regarding the solubility, and hence potential bioavailability, of such species. For coal combustion, the oxidation states of As and Cr in PM are important issues, whereas, for residual oil combustion, it is important to be able to establish the presence or absence of nickel sulfides. Our results show that the toxic species are distributed unequally among PM samples from different sources. For example, in coal PM, the toxic oxidation state of Cr, viz. Cr(VI), comprises between 10% and 40% of the total Cr in $PM_{2.5}$ derived from low-sulfur, lower-rank coals from the western United States. However, it is not usually detected (<5% of the total Cr) in $PM_{2.5}$ from the combustion of higher sulfur coals from the eastern United States. In PM from residual oil combustion, nickel sulfides were more prevalent in coarse $PM_{2.5+}$ than in fine $PM_{2.5}$ fractions (**Figure 1**). Similar information regarding the occurrence of individual hazardous species in PM samples collected for epidemiological or toxicological studies should be of significance for testing specific mechanisms of injury arising from exposure to PM.

The study summarized here is just one aspect of a large NSF-supported effort, involving groups at the Universities of Kentucky, Missouri and Utah in collaboration with groups at U.S. EPA, Ford Motor Company, EPRI, the Lovelace Respiratory Research Institute, etc., that is designed to provide detailed characterization of PM derived from combustion of fossil fuels in both stationary and mobile combustion processes.

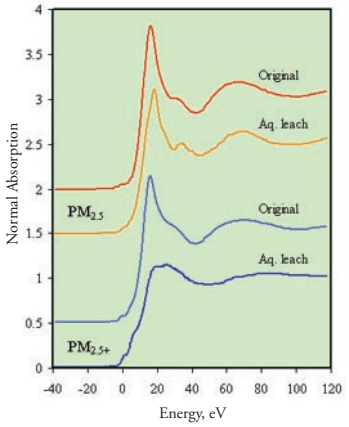

Figure 1. Ni XANES spectra for fine ($PM_{2.5}$) and coarse ($PM_{2.5+}$) particulate matter fractions from combustion of a low-sulfur No. 6 residual oil and for the residues obtained from them by aqueous leaching. The spectra are dominated by nickel sulfate in the original, as-received state, but, as a result of aqueous leaching, the Ni spectra have dramatically changed and indicate that the insoluble Ni is predominantly present as a nickel-bearing spinel in the $PM_{2.5}$ leaching residue and as a nickel sulfide in the coarse $PM_{2.5+}$ leaching residue. The zero-point of energy corresponds to 8333 eV.

Arsenic Speciation and Reactivity in Poultry Litter

Y. Arai[1], A. Lanzirotti[2], S. Sutton[2,3], J.A. Davis[1], and D.L. Sparks[4]

[1]U.S. Geological Survey, Water Resource Division; [2]Consortium for Advanced Radiation Sources, University of Chicago; [3]Department of Geophysical Sciences, University of Chicago; [4]Department of Plant and Soil Sciences, University of Delaware

Recent U.S. government action to lower the Maximum Concentration Levels of total arsenic (As) in drinking water (currently 10 parts per billion) has raised serious concerns about the agricultural use of As-containing biosolids such as poultry litter (PL). Microfocused (μ) synchrotron x-ray fluorescence (SXRF) and μ-x-ray absorption near edge structure spectroscopic (XANES) analyses showed that As(III and V) was always concentrated in abundant needle-shaped microscopic particles (approximately 20 μm x 850 μm) that are associated with Ca, Cu, and Fe, and to a lesser extent with S, Cl, and Zn. Post-edge XANES features of litter particles are dissimilar to those of the organo As(V) compound in poultry feed (i.e. roxarsone), suggesting possible degradation/transformation of roxarsone in the litter and/or in poultry digestive tracts. Our research results raise concerns about long-term PL amendment effects on As contamination in surrounding soil-water environments.

In the last four decades, the poultry industry has become one of the major livestock operations in the middle Atlantic states of the U.S. While PL has been recycled on agricultural lands as an N amendment, much of the trace metal(loid) input (total annual As inputs between 20 and 50 metric tons) into the environments has been neglected. The origin of As in PL is an organo-As(V) compound (3-nitro-4-hydroxyphenylarsonic acid (roxarsone)) for coccidiosis control in the poultry feed (approximately 25 - 50 mg of roxarsone is mixed per kilogram of feed). Feed spillage and digested materials have increased the mean total As concentration in PL to 14 - 76 mg kg^{-1}. At present, annual total metal(loid) inputs on agricultural lands via PL amendments are not specifically regulated at either the state or federal levels, and continuous PL amendment effects on As contamination in Atlantic coastal plain soil/water environments remain virtually unknown. To better understand the reactivity of As from PL to surface and ground water, the As solid-state speciation in the PL was investigated using SXRF and μ-XANES at beamline X26A and the Advanced Photon Source.

A photomicrograph of one of 17 As-rich particles (approximately 20 x 850 μm) found in an approximately 200 mm^2 area (**Figure 1**) shows the distinctive elongated particle morphology. The XRF analyses at the center of this particle (indicated by a black open square) show that elevated As levels are associated with Ca, Fe, and Cu, and to a lesser extent with Zn, Ti, Cl, and S (**Figure 1**). A total of 17 similar particles were found in nearly half of the thin section (about 200 mm^2). Elemental maps (**Figure 2**) generated from the region in the white open square in **Figure 1** also show that the distribution of As is highly associated with Cl and Cu. Assuming no significant changes in the sample thickness and the density of the particle, the flux-normalized fluorescence counts in

Yuji Arai

BEAMLINE X26A

Funding
National Science Foundation
U.S. Department of Energy

Publication
Y. Arai, A. Lanzirotti, S. Sutton, J.A. Davis, and D. L. Sparks, "Arsenic Speciation and Reactivity in Poultry Litter," *Environ. Sci. & Tech.*, **37**, 4083–4090 (2003).

Contact information
Yuji Arai
U.S. Geological Survey,
Water Resource Division

Email: yarai@usgs.gov

Figure 2 can be correlated to relative elemental concentrations for each element. It is possible that the formation of mixed metal-As, As-S precipitates, and/or As sorption complexes on metal oxide precipitates were occurring in the litter and/or during poultry digestion. Our preliminary microfocused x-ray diffraction analyses at the NSLS showed no distinctive diffraction patterns on these particles, indicating the amorphous nature of the As-containing particles. The μ-XANES measurements were performed on the particle in **Figure 1** (i.e. particle A in **Figure 3b**) and several additional As-containing particles (only particles B and C are shown in **Figure 3a** and **3b**). They all produce similar XRF spectra as particle A (data not shown). Wide whiteline peaks are consistently observed in particles A-C (**Figure 3a** and **3b**), indicating the presence of mixed As(III and V) oxidation states in these particles. Although the absorption energy position at ≈11871 eV might indicate the presence of the orpiment-like As(III)-sulfide species, the exact As(V) species are difficult to elucidate based on the absorption edge LC fit, since the energy positions for different As(V) standards closely occur within 0.8 eV (**Figure 3a**). Post-edge XANES features of the particles (indicated by a dotted circle in **Figure 3b**) are dissimilar to those of the organo-As(V) compound in poultry feed, suggesting possible degradation/transformation of roxarsone in the litter and/or in poultry digestive tracts.

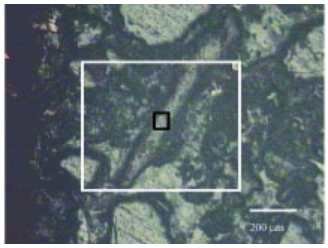

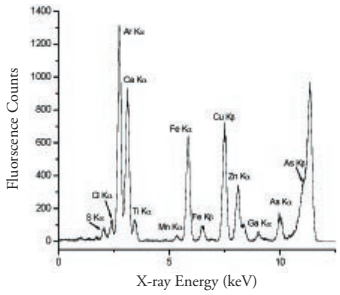

Figure 1. A photographic image of a thin section of poultry litter and a synchrotron-based microfocused x-ray fluorescence spectrum of an arsenic-rich particle inside the black open square region. The white open square (approximately 600 x 600 μm) indicates the selected area for microfocused x-ray fluorescence maps shown in Figure 2.

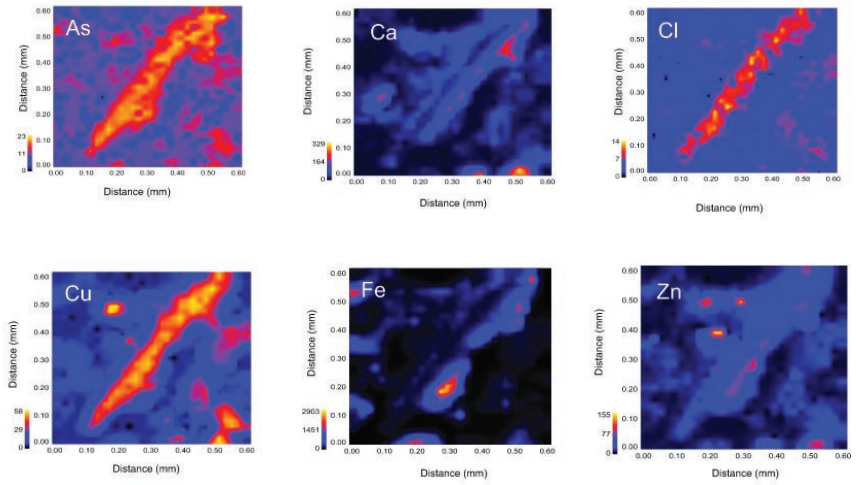

Figure 2. Synchrotron-based microfocused x-ray fluorescence maps (600 x 600 μm) of the white open square area in the photographic image in Figure 1. Flux-normalized fluorescence counts / 20 sec are shown for each element.

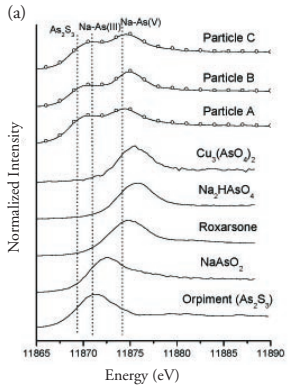

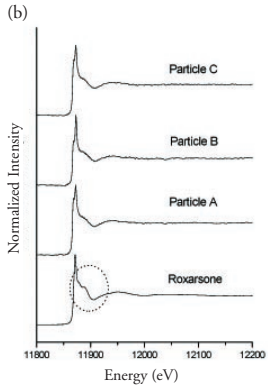

Figure 3 (to right). (a) Short-range normalized XANES spectra of As reference materials (sodium arsenate (Na_2HAsO_4), sodium m-arsenite ($NaAsO_2$), $Cu_3(AsO_4)_2 \cdot 27H_2O$, orpiment ($As_2S_3$), and roxarsone) and As-rich particles in poultry litter are shown. The open circles overlying the sample spectra are the best fit from the linear combinations of model compounds. Spectra contribution (%) of roxarsone and As_2S_3 are 54 and 46 for particle A, 64 and 36 for particle B, and 53 and 47 for particle C, respectively. Three vertical dashed lines are at the absorption edge energy positions of orpiment (As_2S_3 ≈11869 eV), sodium m-arsenite (Na-As(III)≈11871 eV), and sodium arsenate salt (Na-As(V)≈11874 eV), respectively. (b) Long-range normalized XANES spectra are shown for roxarsone and As-rich particles A, B, and C.

Natural Occurrence and Synthesis of Two New Post-Spinel Polymorphs of Chromite

M. Chen[1], J. Shu[2], H-k. Mao[2], X. Xie[1], and R.J. Hemley[2]

[1]Guangzhou Institute of Geochemistry, Chinese Academy of Sciences, China; [2]Geophysical Laboratory, Carnegie Institution of Washington

Chromite is a common accessory mineral occurring in most meteorites and in many mantle rocks. A high-pressure polymorph of chromite, the first natural sample with the calcium ferrite structure, has been discovered in the shock veins of the Suizhou meteorite. Synchrotron x-ray diffraction analyses reveal the sample has an orthorhombic $CaFe_2O_4$-type (CF) structure. The unit-cell parameters are a = 8.954(7) Å, b = 2.986(2) Å, c = 9.891(7) Å, and V (volume) = 264.5(4) Å^3 (Z, the number of molecules per unit cell, = 4), with space group Pnma. The new phase has a density of 5.62 g/cm^3, which is 9.4 % denser than the chromite-spinel phase. Laser-heated diamond anvil cell experiments were performed to establish that chromite-spinel transforms to CF at 12.5 GPa and then to the recently-discovered $CaTi_2O_4$-type (CT) structure above 20 GPa. With the ubiquitous presence of chromite, the CF and CT phases may be among the more important index minerals for tracking the natural transition sequence and P-T conditions in mantle rocks, shock-metamorphosed terrestrial rocks, and meteorites.

Chromite is a common accessory mineral that is a member of the spinel group of minerals, a group of oxides that have very similar structures. Chromite occurs in most meteorites and in many mantle rocks. The experimentally calibrated CF and CT polymorphs of chromite could therefore be ideal pressure gauges, not only for shock-metamorphosed terrestrial rocks and meteorites, but also for mantle rocks covering the important pressure range throughout the transition zone.

Spinel structure is the most important type of structure occurring in minerals in Earth's mantle. $CaFe_2O_4$-type (CF) and $CaTi_2O_4$-type (CT) structures were proposed as the top candidates for "post-spinel" transitions in the deep mantle (**Figure 1**). However, no dense post-spinel polymorphs have been discovered in nature. A preliminary examination of the shock-metamorphosed Suizhou meteorite has recently revealed a CT polymorph of chromite $(Fe,Mg)(Cr,Al)_2O_4$. This study reports another new CF-type polymorph of chromite in the same meteorite.

Synthesis experiments were performed at pressures from 7.5 to 25 GPa at a temperature of 2000°C, using laser-heated diamond anvil cells. Our experiments indicate that chromite-spinel transforms to the CF structure above 12.5 GPa, and to the CT structure above 20 GPa (**Figure 2**). The x-ray diffraction pattern of the quenched CF polymorph was indexed to give lattice parameters *a* = 8.955(7)Å, *b* = 2.985(2)Å, *c* = 9.909(7)Å, *V* = 264.9(4)Å^3 (Z=4), density (ρ) = 5.61 g/cm^3, and space group *Pnma*. For the CT polymorph, the parameters are *a* = 9.467(5) Å, *b* = 9.550(7) Å, *c* = 2.905(2) Å, *V* = 262.6(4) Å^3 (Z=4), ρ = 5.65g/cm^3, and space group *Cmcm*. The densities of synthetic CF and

Ming Chen

BEAMLINE X17C

Funding
Chinese Academy of Sciences; National Science Foundation of China; National Science Foundation (U.S.); U.S. Department of Energy

Publication
M. Chen, J. Shu, H.K, Mao, X. Xie, and R.J. Hemley, "Natural Occurrence and Synthesis of Two New Post-Spinel Polymorphs of Chromite," *Proc. Nat. Acad. Sci. USA*, **100** (**25**), 14651-14654 (2003).

Contact information
Dr. Ming Chen
Guangzhou Institute of Geochemistry, Chinese Academy of Sciences, China

Email: mchen@gig.ac.cn

CT polymorphs are 9.4 % and 10.1 % denser, respectively, than that of chromite.

Some chromite grains in the Suizhou meteorite covered a shock-induced pressure gradient. These grains show three zones of distinct densities corresponding to the pressure gradient - a CT phase zone close to the shock vein, a chromite zone relatively apart from the vein, and a lamella-rich (layered) zone between the CT phase zone and the chromite zone (**Figure 3**). These three zones have a uniform chromite chemical composition. We used a synchrotron x-ray beam to probe the shock chromite grain *in situ* in the thin section mount of the meteorite, and confirmed that a zone in contact with the shock vein, ranging from 20 to 30 μm in width, had transformed into a fine-grained polycrystalline aggregate with a CT-type structure identical to the CT phase that was synthesized experimentally. We also confirmed that the clear zone at the low-pressure end has the usual chromite-spinel structure.

We focused the x-ray microprobe on the lamella-like zone between the CT and spinel zones and obtained distinct diffraction patterns for the CT phase, which are consistent with a mixture of the CF and spinel phases, and a trace amount of the CT phase, with the fraction of spinel decreasing toward the shocked vein and the CT phase increasing toward the shocked vein. The x-ray patterns collected from different orientations of the sample show that the lamellae-like slices are polycrystalline in nature. X-ray reflections from the CF phase were indexed to an orthorhombic cell with parameters a = 8.954(7) Å, b = 2.986(2) Å, c = 9.891(7) Å, and V = 264.5(4) Å^3 (Z=4). The structure is identical to the synthetic CF phase in our high-pressure experiment. The calculated density of the natural CF phase is ρ = 5.62 g/cm^3, which is 9.4 % denser than that of the chromite-spinel phase. This is the first natural occurrence of a dense $FeCr_2O_4$ polymorph displaying the CF structure.

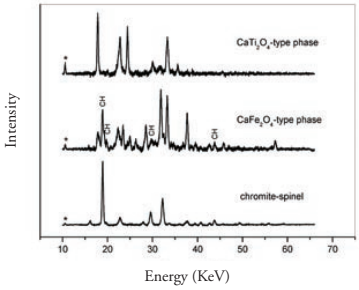

Figure 2. X-ray diffraction patterns from the natural chromite-spinel, synthesized $CaFe_2O_4$-type, and $CaTi_2O_4$-type phases. The peaks labeled with 'CH' from the residue of the starting material, chromite-spinel. * = escape peaks.

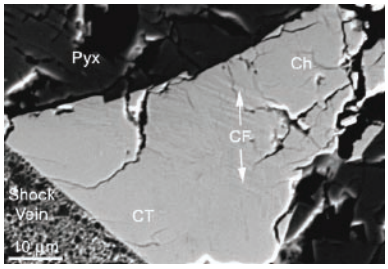

Figure 3. Back-scattered electron images (BSE) of shock-metamorphosed chromite-spinel grains in the Suizhou meteorite. A chromite grain was transformed to a $CaTi_2O_4$-type phase zone (CT) contacting with the shock vein, and partially to a $CaFe_2O_4$-type phase zone (CF) between the CT phase zone and the chromite zone (Ch) apart from the shock vein. The CF phase occurs as lamella-like slices associating with a chromite matrix, and two to three sets of slices are observed. On the image, both the CT and CF phases are brighter than chromite. Pyx = pyroxene.

(a)

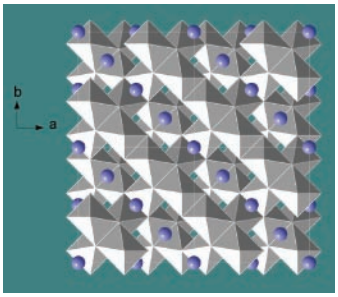

(b)

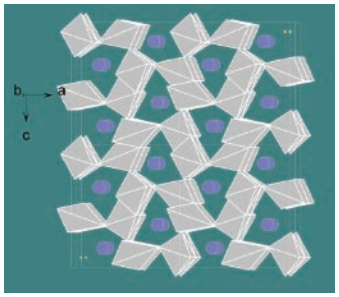

(c)

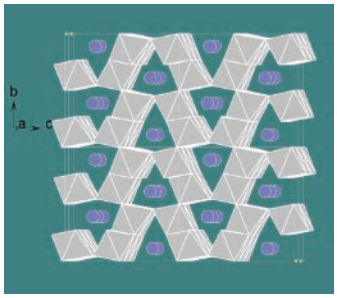

Figure 1. Schematic view of the (A) spinel, (B) $CaFe_2O_4$, and (C) $CaTi_2O_4$ type structures. The spinel structure has octahedral and tetrahedral sites. In the CF and CT structures, a compact three-dimensional network is formed by edge- and corner-sharing octahedra, with hollow channels parallel to the b axis (CF structure) and the a axis (CT structure), respectively, where the large Ca cations are located. These two structures contain dodecahedral and octahedral sites; the difference between the two structures lies in slight modifications of the polyhedral linkage. There are two types of FeO_6 octahedral sites in the CF structure, and one type of FeO_6 octahedral site in the CT structure.

The Origin of Organic Matter in the Solar System: Evidence from the Interplanetary Dust Particles

G.J. Flynn[1], L.P. Keller[2], M. Feser[3], S. Wirick[3], and C. Jacobsen[3]

[1]Department of Physics, SUNY-Plattsburgh; [2]NASA Johnson Space Center; [3]Department of Physics, Stony Brook University

Researchers from SUNY-Plattsburgh, the NASA Johnson Space Center, and Stony Brook University measured the types and abundances of organic matter in interplanetary dust particles, originating from asteroids and comets, that NASA research aircraft collected from the Earth's atmosphere. They found the same amount and types of organic matter in both anhydrous and hydrated interplanetary dust particles. This suggests that aqueous processing, long believed to have played an important role in the production of organic matter, was much less important, and that most of the pre-biotic organic matter in the Solar System formed at about the same time as the first dust that condensed from the Solar Nebula. It is also possible that this matter formed even earlier, in circumstellar or interstellar space.

Extraterrestrial materials, including asteroids, comets, and grains in interstellar space, contain organic compounds that may have been important starting materials for the origin of life. How this pre-biotic organic matter formed is not known, but a wide variety of processes, ranging from catalyzed reactions on the surfaces of grains to reactions involving liquid water, have been proposed. If this organic matter was produced by the aqueous alteration of elemental carbon, which is believed to happen on wet asteroids, then we would expect to see organic matter occurring preferentially in interplanetary materials that exhibit evidence of aqueous activity, such as the presence of hydrated silicates. If the organic matter were produced either during the nebula phase of Solar System evolution or in the interstellar medium, we would expect this organic matter to be incorporated into the dust as it formed, so that it would be present in the anhydrous interplanetary materials as well. Earlier studies of meteorites showed abundant organic matter in the hydrated meteorites, but mostly amorphous carbon, with little or no organic matter, in the anhydrous meteorites. This suggested aqueous activity was important in the production of the pre-biotic organic matter. However, all the anhydrous, carbon-rich meteorites show significant depletions of the moderately volatile elements in a pattern that indicates these meteorites were once exposed to temperatures as high as 1200 degrees Celsius, hot enough to destroy any organic matter initially present. To make a proper comparison, we were forced to examine interplanetary dust particles (IDPs) like the one shown in **Figure 1**, which are fragments from asteroids and comets, approximately 10 micrometers in size, that NASA collects from the Earth's stratosphere. These particles are so small that we required the high sensitivity of the synchrotron-based instruments at the National Synchrotron Light Source to perform the analyses. We mapped the carbon distribution in approximately 100 nanometer (nm) thick slices of seven anhydrous and four hydrated IDPs, determining the carbon abundance, and we performed carbon x-ray absorption near-edge structure (XANES) and infrared spectroscopy, both of

George Flynn

BEAMLINES
X1A, U10B

Funding
NASA Exobiology Research Program

Publication
G.J. Flynn, L.P. Keller, M. Feser, S. Wirick, and C. Jacobsen, "The Origin of Organic Matter in the Solar System: Evidence from the Interplanetary Dust Particles," *Geochim. et Cosmochim. Acta*, **67**(**24**), 4791-4806 (2003).

Contact information
George J. Flynn
Department of Physics, SUNY-Plattsburgh

Email: george.flynn@plattsburgh.edu

which identify specific carbon functional groups. The carbon-XANES spectra of the hydrated and anhydrous IDPs (**Figure 2**) are very similar, with strong absorptions at about 285 electron volts (eV), identifying C=C, and at about 288.5 eV, identifying C=O. The infrared spectra of the hydrated and anhydrous IDPs are also very similar (**Figure 3**), with the pair of features near the 2926 and 2854 cm^{-1} wavelengths identifying aliphatic CH_2, and the feature near 2960 cm^{-1} identifying aliphatic CH_3 (where 'aliphatic' refers to organic compounds containing short-chain arrangements of carbon atoms). In some anhydrous IDPs the individual mineral grains are coated with this carbonaceous material, apparently the "glue" holding the aggregate particle together. We found that organic matter is present in similar types and abundances in both the anhydrous and the hydrated IDPs, indicating that the bulk of the pre-biotic organic matter in the Solar System did not form by aqueous processing. Instead, this organic matter had already formed at the time that primitive, anhydrous dust was being assembled. The hydrated meteorite, Murchison, has a higher ratio of aliphatic CH_3 to CH_2 (indicating a shorter mean aliphatic chain length) and Murchison also contains more aromatic C-H (the broad absorption at approximately 3050 cm^{-1} in **Figure 3**) than either type of IDP, consistent with Murchison being more thermally processed than the hydrated IDPs.

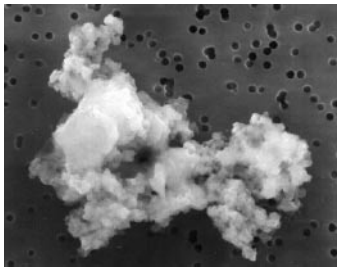

Figure 1. Scanning electron microscope image of an approximately 10 micrometer-diameter interplanetary dust particle, showing many small grains that aggregated to form the particle. (NASA photo)

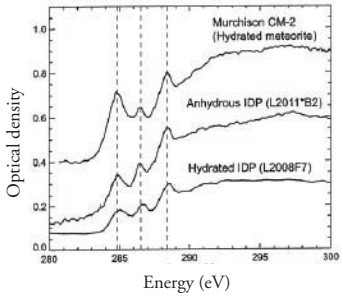

Figure 2. Carbon XANES spectra of typical anhydrous and hydrated IDPs and the organic residue extracted from the Murchison hydrated meteorite.

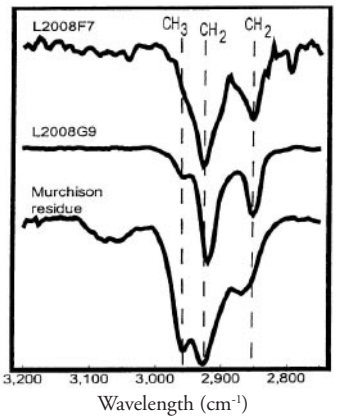

Figure 3. Infrared spectra of typical anhydrous and hydrated IDPs and the organic residue extracted from the Murchison hydrated meteorite.

X-ray Structure Analysis of a Designed Oligomeric Miniprotein Reveals a Discrete Quaternary Architecture

M.H. Ali[1], E. Peisach[2], K.N. Allen[2], and B. Imperiali[1]

[1]Department of Chemistry, Massachusetts Institute of Technology; [2]Department of Physiology and Biophysics, Boston University School of Medicine

Oligomerization, or noncovalent association, is a fundamental strategy for determining protein structural and functional complexity in nature. In this research, miniproteins adopting a defined oligomeric state were designed to study the advantages of protein oligomerization. Peptide 1 is a discretely folded, mixed α/β, homo-oligomeric miniprotein motif with only 21 amino acids. The x-ray crystal structure of peptide 1 at 1.2 Å resolution reveals that it associates as a tetramer (a four-unit oligomer), in which α and β components form a tightly-packed and well-defined hydrophobic core. The miniprotein is thermally stable and shares many of the characteristics of larger proteins.

Miniproteins are short peptide sequences that adopt a discrete protein-like fold in aqueous solution. Therefore, they are valuable minimal models for studying natural proteins. Oligomeric miniproteins, in particular, are good model systems for quaternary structure formation in proteins. Moreover, they are appropriate platforms for determining whether more complex oligomeric structures might ultimately support function.

A homo-oligomeric ββα miniprotein was derived from a monomeric precursor by a strategy inspired by "domain swapping," an important evolutionary mechanism for protein oligomerization. The monomeric ββα motif includes intramolecular interactions between α and β secondary structural elements, where α is a helix and ββ is a hairpin. We introduced a bias towards oligomerization by shortening the length of the hinge region between the α and β elements, thereby precluding intermonomer interactions. A fluorescence-screening assay yielded a homo-oligomeric miniprotein composed of 21 amino acids, with eight residues in the β hairpin and 12 residues in the α helix. Biophysical studies revealed that this miniprotein forms a defined oligomer in solution and has many of the features of larger proteins, including cooperative folding and a solvent-protected core. However, the exact nature of the miniprotein structure and the forces contributing to the native-protein-like stability remained unknown. We thus set out to determine the crystal structure of peptide 1, a more stable analog of the original homo-oligomer.

Authors (left to right)
(top) Mayssam H. Ali and Barbara Imperiali
(bottom) Karen N. Allen and Ezra Peisach

BEAMLINE X12C

Funding
National Science Foundation
National Institutes of Health

Publication
M.H. Ali, E. Peisach, K.N. Allen, and B. Imperiali, "X-ray Structure Analysis of a Designed oligomeric miniprotein reveals a discrete quaternary architecture," *Proc. Natl. Acad. Sci., USA*, **101**(33), 12183-8 (2004).

Contact information
Prof. Karen Allen
Department of Physiology and Biophysics, Boston University School of Medicine

Email: allen@med-xtal.bu.edu

The nature of oligomerization in peptide 1 was revealed by the 1.2 Å x-ray crystal structure, determined using multi-wavelength anomalous diffraction (MAD) phasing. The tetramer consists of four monomers arranged in an antiparallel topology (**Figure 1**), with each monomer flanked by two others oriented in the opposite direction. The tetramer possesses approximate four-fold symmetry: Each monomer is slightly closer to one neighbor than the other. The well-defined central hydrophobic core of the tetramer is formed by residues from one monomer in proximity to core residues from the other three monomers. Those residues on the periphery of the hydrophobic interface interact with residues of the antiparallel monomer nearest them, while the polar residues are solvent-exposed.

Each tetramer is enveloped by a sheath of waters of crystallization with a demarcated water-exclusion zone in the central core region, indicating that no waters can pass into this hydrophobic core. The tetrameric structure is highly protein-like in terms of the degree of complexity and the tight packing of side chains. In fact, the relationships between surface area, volume, and molecular weight fit well to a series of empirical relationships for monomeric and oligomeric proteins of varying sizes. The hydrophobic core is defined by five palindromic layers (**Figure 2**) composed of residues from the α-helix and the β-sheet. The packing "register" between monomers might be determined by the conformationally restricted aromatic residues of the core or the interactions made by the hairpin region. The tight packing of the hydrophobic core accounts for the cooperative unfolding and high melting temperatures of peptide 1. This packing is remarkable in light of the very short linear sequence. Overall, this "miniprotein" structure provides a view of the forces that contribute to oligomerization and a model for understanding quaternary structure in large natural proteins.

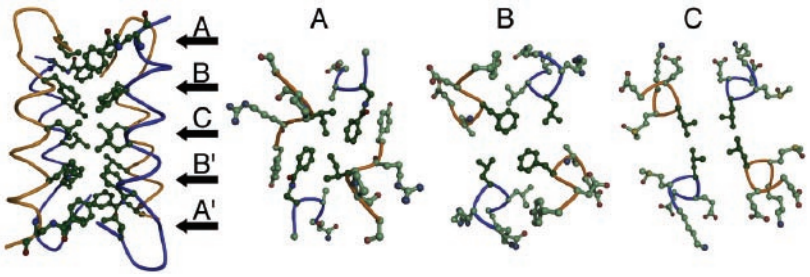

Figure 2. The hydrophobic core of tetrameric peptide 1. At left, a side view of the tetramer, highlighting the positions of the five palindromic core layers. At right are cross-sectional slices through layers A (Ile-3/DapBz-20), B (Phe-8/Leu-16), and C (Leu-12/Leu-12). Residues comprising the core are in bold.

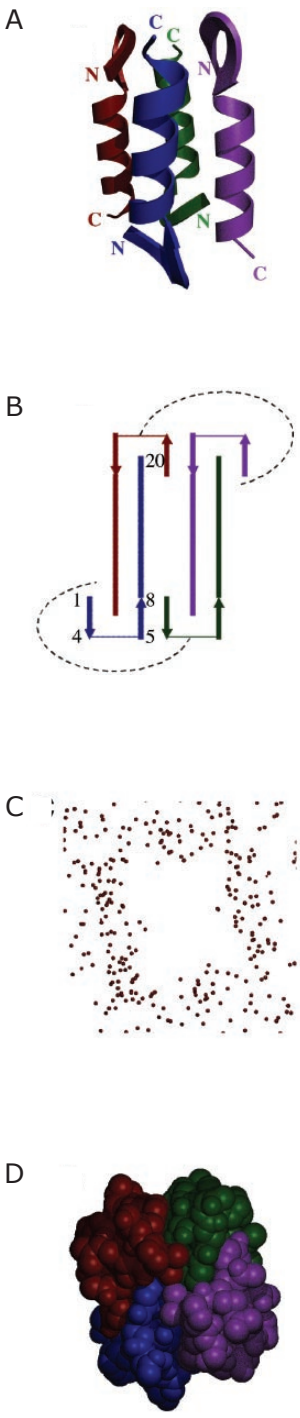

Figure 1. Tetrameric structure of peptide 1. (A) Ribbon diagram of tetramer, side view. (B) Topology diagram. Dashed line indicates inter-monomer interaction. (C) Crystallographic waters, with void in the shape of the tetramer. (D) CPK model of peptide 1 indicating space occupied by tetramer.

Structure of the ClpB Molecular Chaperone

S. Lee, M.E. Sowa, and T.F. Tsai

Verna and Marrs McLean Department of Biochemistry and Molecular Biology, Baylor College of Medicine

Molecular chaperones are cellular proteins that assist other proteins in the folding and assembly of higher order structures without being components of these final structures. ClpB is an essential protein of the bacterial heat-shock response, but unlike other chaperones, has the remarkable ability to rescue proteins from an aggregated state. The 3.0 angstrom (Å) resolution crystal structure of ClpB reveals that the ClpB middle region forms an 85 Å-long, mobile coiled-coil structure, which resembles the shape of a two-bladed propeller. The conformation and motion of this coiled-coil are critical for ClpB's chaperone function. The coiled-coil is located on the outside of the ClpB hexamer, where it can interact with aggregated proteins. This suggests that the long coiled-coil may function as a "molecular crowbar" that mediates protein disaggregation.

Bacterial ClpB is a molecular chaperone that requires adenosine triphosphate (ATP) for function. Members of the ClpB family form large ring structures and contain two ATP-binding domains. Moreover, ClpB has a longer middle region, known as the ClpB-linker, and, unlike other Clp proteins, does not direct the degradation of its substrate proteins. Instead, ClpB has the remarkable ability to rescue stress-damaged proteins from an aggregated state.

Despite the wealth of biochemical and genetic data, the mechanism by which ClpB disaggregates stress-damaged proteins has remained elusive. To investigate this structure-function relationship, we have determined the 3.0 Å-resolution crystal structure of ClpB bound to adenosine 5'-(β,γ-imido)triphosphate (AMPPNP), an ATP analog. We have also determined the structure of the physiological assembly at approximately 21 Å resolution using electron cryomicroscopy (cryo-EM). Our crystal structure reveals that ClpB consists of five domains (**Figure 1A**). The most remarkable structural feature is its 85 Å-long coiled-coil that consists of the ClpB-linker. There are three independent representations of ClpB in the asymmetric unit of our crystal. The three molecules are arranged in a manner that gives rise to a helical assembly (**Figure 2A**), which extends throughout the crystal and forms a hexameric ring structure when viewed in projection (**Figure 2B**). Interestingly, each ClpB molecule adopts a different conformation even though they are in the same nucleotide-bound state. This suggests that ClpB is a dynamic molecule that can undergo large conformational rearrangements. Using a combination of structure-based targeted mutagenesis and biochemical experiments, we have further demonstrated that the conformation and motion of the long coiled-coil are critical for chaperone activity.

The structure of the functional ring assembly was determined using cryo-EM and single-particle reconstruction techniques

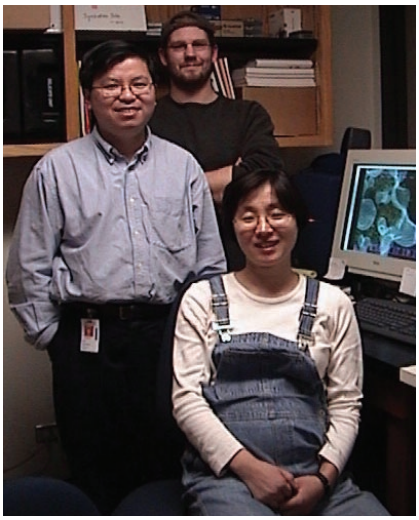

Authors (left to right)
Francis T.F. Tsai, Mathew E. Sowa, and Sukyeong Lee

BEAMLINE X25

Funding
Baylor College of Medicine
American Heart Association
Robert A. Welch Foundation

Publications
J.S. Lee, M.E. Sowa, Y. Watanabe, P.B. Sigler, W. Chiu, M. Yoshida, and F.T.F. Tsai, "The Structure of ClpB: A Molecular Chaperone that Rescues Proteins from an Aggregated State," *Cell*, **115**, 229-240 (2003a)

S. Lee, M. Hisayoshi, M. Yoshida, and F.T.F. Tsai, "Crystallization and Preliminary X-ray Crystallographic Analysis of the Hsp100 Chaperone ClpB from *Thermus Thermophilus*," *Acta Crystallogr.*, **D59**, 2334-2336 (2003b).

Contact information
Dr. Francis T.F. Tsai
Department of Biochemistry & Molecular Biology, Baylor College of Medicine

Email: ftsai@bcm.tmc.edu

of ClpB-AMPPNP complexes. Our three-dimensional reconstruction shows that ClpB is a hexamer and that both of its ATP-binding domains are required for hexamer formation in the AMPPNP-bound state (**Figure 1B**). An atomic model of the ClpB hexamer was generated by fitting the crystal structure of ClpB into the cryo-EM density map (**Figure 1B**). Our model reveals that the ClpB-linker is located on the outside of the hexamer, where it can interact with large aggregated substrate proteins. Taken together, our structural and biochemical studies support a mechanism in which the long coiled-coils function as "molecular crowbars" that pull apart large aggregates, thereby mediating protein disaggregation.

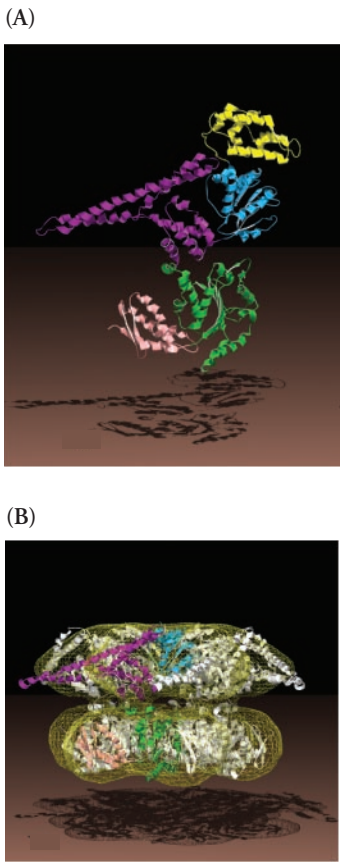

Figure 1. (A) Ribbon drawing of the ClpB monomer. The N-terminal domain is colored in yellow, the D1-large domain or NBD1 in cyan, the D1-small domain in purple, the D2-large domain or NBD2 in green, and the D2-small domain in pink. The bound AMPPNP molecules have been omitted for clarity. (B) Single-particle reconstruction of the ClpB hexamer. The cryo-EM map is contoured as a yellow mesh, with the atomic coordinates of an N-terminal domain truncated ClpB hexamer docked in. The N-terminal domains and part of the ClpB-linker are not visible in the reconstruction because they are mobile.

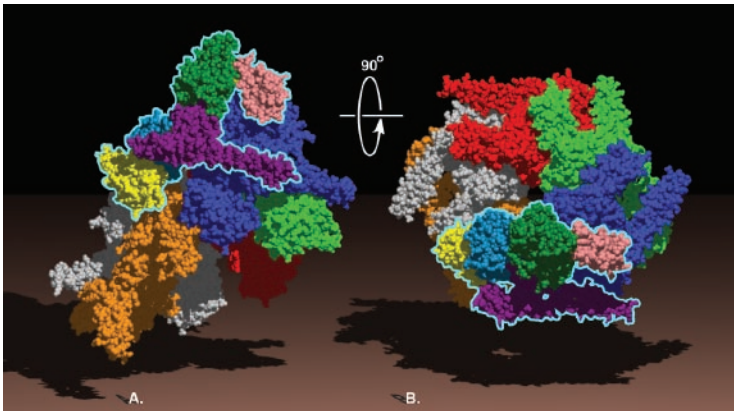

Figure 2. Molecular arrangement of six ClpB molecules as seen in our crystal structure. The figure illustrates the molecular contents of two asymmetric units, which are related by a crystallographic two-fold screw axis. Each ClpB monomer is colored differently. To depict the relative orientation of ClpB in our crystal, one of the six molecules has been highlighted and color-coded as shown in Figure 1A.

Crystal Structure of Human α-Tocopherol Transfer Protein Bound to its Ligand: Implications for Ataxia with Vitamin E Deficiency

K.C. Min[1,2,3], R.A. Kovall[3], and W.A. Hendrickson[1,3]

[1]Howard Hughes Medical Institute, [2]Department of Neurology, and [3]Department of Biochemistry and Molecular Biophysics, Columbia University

Human α-tocopherol transfer protein (ATTP) plays a central role in vitamin E homeostasis, preventing the degradation of α-tocopherol (α-T), a lipophilic molecule, by routing it for secretion by hepatocytes (liver cells). Mutations in the gene that encodes ATTP have been shown to cause a severe deficiency in α-T, which results in a progressive neurodegenerative spinocerebellar ataxia, a disorder of neurons primarily in the brainstem and spinal cord, known as ataxia with vitamin E deficiency (AVED). We have determined the high-resolution crystal structure of human ATTP with (2R, 4'R, 8'R)-α-T in the binding pocket. One mutation associated with human disease is located directly in the binding pocket, likely disrupting binding to α-T.

Ataxia with Vitamin E Deficiency (AVED) is a recessively inherited condition in which afflicted individuals develop problems with balance, typically starting in the late teen years. As the disease progresses, many individuals are limited to a wheelchair, lose sensation in their hands and feet, and have difficulties with slurred speech. Some develop retinitis pigmentosa, a blinding condition caused by the degeneration of the retina. Mutations in α-tocopherol transfer protein (ATTP) have been shown to cause AVED.

ATTP exists in the fluid portion of a cell's cytoplasm and is expressed mainly in the liver. The heterologous expression of ATTP in cell culture confers its ability to secrete α-T by a non-Golgi pathway, preventing the degradation of α-T. Patients with AVED absorb α-T from their diets normally, but have nearly immeasurable steady-state plasma levels due to the defective incorporation of α-T for transport with very low density lipoprotein. A transgenic mouse in which the ATTP gene was deleted replicated the phenotype of the human disease.

There are eight forms of vitamin E (including α-δ tocopherol and α-δ tocotrienol), which differ in two structural features: the degree of methylation (decreasing from α-T to δ-T) of the chroman ring and saturation of the phytyl tail. All forms are potent lipophilic antioxidants, but α-T is the most biologically potent due to the action of ATTP. Of the eight possible stereoisomers, i.e. variations, of α-T, only (2*R*, 4′*R*, 8′*R*)-α-T occurs naturally. Synthetic vitamin E supplements are racemic mixtures, but ATTP is sensitive to stereochemistry and particularly so at the C2 stereocenter.

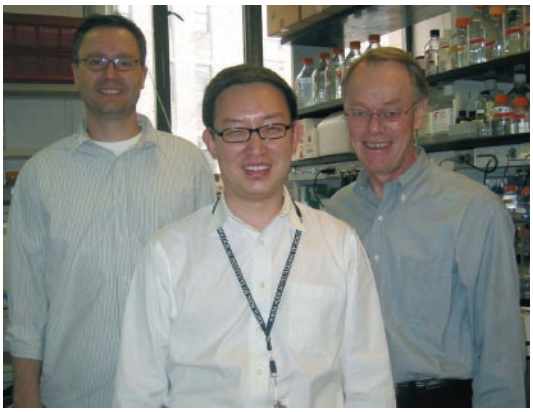

Authors (left to right)
R.A. Kovall, K.C. Min, and W.A. Hendrickson

The high-resolution 1.5Å structure of ATTP in a complex with (2*R*, 4′*R*, 8′*R*)-α-T was determined from multiwavelength anomalous diffraction (MAD) data measured at beamline X4A using a selenomethionyl recom-

BEAMLINE X4A

Funding
Howard Hughes Medical Institute; Leukemia and Lymphoma Society; National Institutes of Health

Publication
K.C. Min, R.A. Kovall, and W.A. Hendrickson, "Crystal Structure of Human Alpha-Tocopherol Transfer Protein Bound to its Ligand: Implications for Ataxia with Vitamin E Deficiency," *Proc. Natl. Acad. Sci. USA*., **100**(**25**), 14713-8 (2003).

Contact information
Wayne A. Hendrickson, Howard Hughes Medical Institute, Columbia University

Email: wayne@convex.hhmi.columbia.edu

binant protein crystal. The structure of ATTP is composed of two domains: an N-terminal all-helical domain and a C-terminal domain, which at its core is composed of a βαβαβαβ fold and contains the binding pocket for α-T (**Figure 1**). The most striking feature of the structure is the buried, solvent-inaccessible binding pocket, which would require significant conformational changes to release α-T. Most of the interactions between ATTP and α-T are through van der Waals contacts, although there are three well-ordered water molecules that appear to form a hydrogen bonding network with the hydroxyl group of α-T (**Figure 2A**).

In ATTP, a number of missense mutations – which occur when one DNA base pair is substituted for another – have been associated with AVED. One mutation, L183P – a change from one amino acid, leucine, to another, proline – was found to map directly to the binding pocket (**Figure 2A**). The sidechain of L183 has extensive van der Waals contacts with α-T, and a change to proline at this position would not only be expected to disrupt these interactions, but would also affect the residues in the nearby α-helix that also form contacts with α-T. When expressed in *E. coli*, the L183P mutant was insoluble and could not be further characterized.

Three other missense mutations, R59W (arginine-to-tryptophan), R192H (arginine-to-histidine), and R221W, involve a change in positively charged residues, which help to form a prominent positively charged surface on ATTP (**Figure 2B**). Although the function of this region is not understood, it seems unlikely to affect binding to α-T directly. We have proposed that it may represent a site of protein-protein or protein-lipid interaction that regulates the release of α-T from the binding pocket of ATTP. Interestingly, a similar mutation (R233W) in a related protein, cellular retinaldehyde binding protein, causes a hereditary retinopathy, suggesting that this region of the protein may have a conserved function across multiple members of this family of lipophilic transfer proteins.

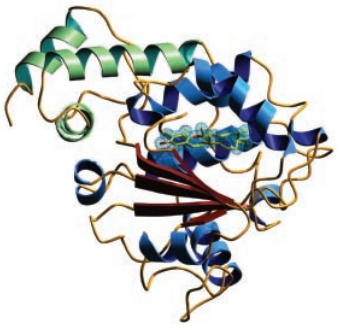

Figure 1. Ribbon diagram of ATTP viewed down the β-sheet. α-T is colored in yellow. The N-terminal domain helices are indicated in green, and the C-terminal domain's helices are in blue and its strands in red. The electron density that covers α-T is drawn as a blue mesh at 1σ.

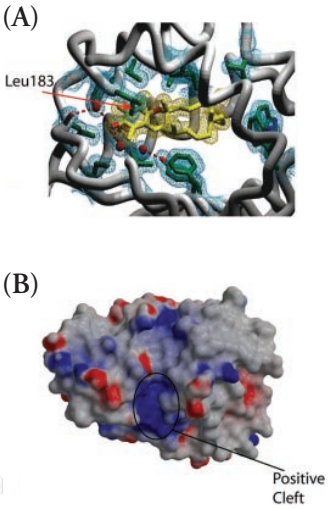

Figure 2. (A) Close-up view of the ligand binding pocket. Side chains (in green) that form van der Waals contacts with α-T (in yellow) or participate in hydrogen-bonding networks in the ligand-binding pocket are shown. Three well-ordered water molecules located in the binding pocket are shown as red spheres. The protein backbone is shown as a worm model, excluding residues 216-220 and 249-275 for clarity. Electron densities that cover the residues of interest, α-T, and three water molecules are drawn as mesh at 1σ. Dashed red lines indicate hydrogen bonds. (B) Electrostatic potential surface map of ATTP. A positively charged cleft indicates where a number of disease-causing mutations are located.

The Mutant Proteins of a Neurodegenerative Disorder

J. Stine Elam[1], A.B. Taylor[1], R. Strange[2], S. Antonyuk[2], P.A. Doucette[3], J.A. Rodriguez[3], S.S. Hasnain[2], L.J. Hayward[4], J. Selverstone Valentine[3], T.O. Yeates[3], and P.J. Hart[1]

[1]Department of Biochemistry and the X-ray Crystallography Core Laboratory, The University of Texas, Health Science Center at San Antonio; [2]CCLRC Daresbury Laboratory; [3]Department of Chemistry and Biochemistry, University of California; [4]Department of Neurology, University of Massachusetts Medical School

Mutations in copper-zinc superoxide dismutase (SOD1) proteins cause the neurodegenerative disorder familial amyotrophic lateral sclerosis (FALS). In human spinal cord neurons and in transgenic mice expressing these proteins, proteinaceous inclusions (aggregates) containing pathogenic SOD1 are observed. These aggregates are believed to interfere with a variety of cellular processes, eventually leading to motor neuron death. We discovered that several metal-deficient, pathogenic SOD1 proteins can undergo conformational changes that do not occur in non-pathogenic (native) SOD1. This promotes a "gain-of-interaction" between the molecules, causing them to "stick" to each other. In turn, this leads to the formation of extensive helical and linear, or "amyloid-like," arrays of SOD1. Such non-native protein-protein interactions, leading to larger, or "higher order," SOD1 assemblies, could thus represent a toxic property that is common to mutants of SOD1 linked to FALS.

Amyotrophic lateral sclerosis (ALS, also known as Lou Gehrig's disease or motor neuron disease) is a neurodegenerative condition characterized by the loss of motor neurons in the spinal cord and brain. The disorder results in paralysis, leading to the death of the afflicted individual within two to five years of diagnosis. A subset of ALS cases are familial (FALS), and most of these are associated with dominantly inherited mutations in copper-zinc superoxide dismutase (SOD1). SOD1 is an antioxidant enzyme that is 32 kilodaltons (kDa) in size (where one Da is equal to one atomic mass unit), and is homodimeric, meaning it consists of two identical molecules. Initial hypotheses suggested that SOD1-linked FALS comes from extensive oxidative damage in the neurons, arising from diminished SOD1 activity. However, mice without SOD1 appear normal and live to adulthood without developing motor neuron disease. In contrast, transgenic mice expressing human FALS SOD1 mutants become paralyzed, even though they possess normal levels of SOD1 activity from their own endogenous SOD1. Together, these observations strongly suggest that pathogenic SOD1 molecules act by gaining the ability to kill other cells (becoming "cytotoxic") and not by losing their enzymatic function.

There has been increasing support for the concept that this "toxic gain of function" of pathogenic SOD1 is due to the propensity of these proteins to misfold and aggregate. This is supported by the manifestation of aggregates containing pathogenic SOD1 in human spinal cord neurons and in transgenic mice expressing these proteins. These pathogenic SOD1 aggregates (or their soluble precursors) could play a role in pathogenesis, either by occupying the neurons' heat

Authors (left to right)
Nick Criscimagna, Stephen Holloway, P. John Hart, Jennifer Stine Elam, Lisa Whitson, Alex Taylor, and Ahmad Galaleldeen

BEAMLINE X8C

Funding
National Institutes of Health's National Institute of Neurological Disorders and Stroke (NIH-NINDS); Robert A. Welch Foundation; Amyotrophic Lateral Sclerosis (ALS) Association; the Council for the Central Laboratory of the Research Councils (CCLRC) Daresbury Laboratory

Publication
J.S. Elam, A.B. Taylor, R. Strange, S. Antonyuk, P.A. Doucette, J.A. Rodriguez, S.S. Hasnain, L.J. Hayward, J.S. Valentine, T.O. Yeates, and P.J. Hart, "Amyloid-Like Filaments and Water-Filled Nanotubes Formed by SOD1 Mutants Linked to Familial ALS," *Nat. Struct. Biol.*, **10**, 461-467 (2003).

Contact information
P. John Hart, Ph.D.
Associate Professor of Biochemistry, Director of the X-ray Crystallography Core Laboratory ,The University of Texas Health Science Center at San Antonio

Email: pjhart@biochem.uthscsa.edu

shock proteins and preventing them from doing their jobs, which leaves the neuron vulnerable, and/or interfering with the way the neurons transport materials along their length (or along their axons) and get rid of unwanted proteins. However, the molecular basis underlying the formation of pathogenic SOD1 oligomers has remained undefined.

To partially address this issue, we determined the crystal structures of the pathogenic SOD1 mutants H46R and S134N, which are members of a larger class of "metal-binding region mutants." As the name suggests, members of this class of pathogenic SOD1 cannot properly bind either copper or zinc, or both. In the absence of the proper complement of these metal ions, structural features normally involved in metal binding, called loop elements, undergo conformational changes that allow H46R and S134N to polymerize into two types of higher-order filamentous arrays. **Figure 1** shows that both metal-free H46R and metal-deficient S134N (which crystallize in different crystal systems) form nearly identical linear, amyloid-like fibers. A variation on this theme can be seen in **Figure 2(D)**, which shows that copper-free, but zinc-loaded H46R engages in slightly different pathogenic SOD1-SOD1 interactions, leading to the formation of helical, rather than linear, filamentous arrays. From the perspective in **Figure 2(D)**, the interactions (which occur in the red patches) form a donut shape. Thus, propagating them leads to hollow, water-filled nanotubes. Importantly, when native SOD1 dimers are structurally aligned with the pathogenic SOD1 dimers in these linear and helical arrays, it is obvious that the native variety cannot participate in filamentous assembly. This is due to clashes and unfavorable electrostatic interactions between the loop elements described above.

In summary, the filamentous arrangement of mutant, metal-deficient SOD1 proteins provides justification for a specific and testable hypothesis that links various pathogenic SOD1 mutations to protein aggregation, thereby making it possible to draw a parallel between ALS and other established amyloid diseases.

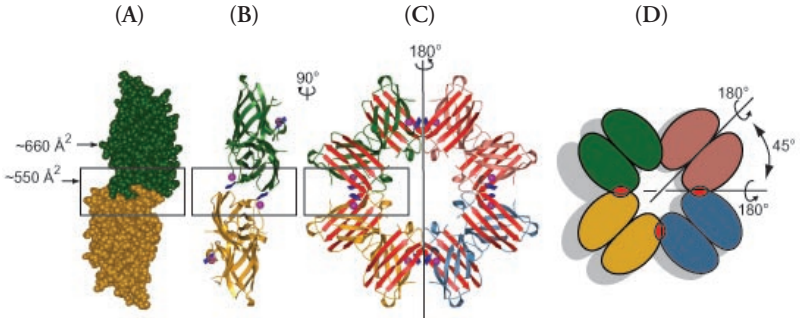

Figure 2. The gain-of-interaction in zinc-loaded H46R (Zn-H46R) SOD1, giving rise to water-filled helical nanotubes. The GOI interface between Zn-H46R dimers is boxed, and buries approximately 550 Å² of solvent-accessible surface area per polypeptide. (A) and (B) One-half of the helical Zn-H46R filament is represented by two dimers, shown from top to bottom in green and gold, respectively. Image B is related to the left half of image (C) by a rotation of 90 degrees. (C) The approximate location of the crystallographic two-fold axis, which runs along the diagonal in the tetragonal unit cell, is indicated by a black line without arrows and a 180-degree rotation symbol. Applying this two-fold operator generates one complete turn of the helical filament. One-half of each SOD1 β-barrel is shown in red. Residues of the zinc loop undergo a conformational change and form a short β-strand (shown in blue) that reciprocally adds to this sheet in neighboring Zn-H46R dimers, stabilizing the GOI interface. Zinc ions are shown as magenta spheres. (D) A schematic representation of SOD1 dimers in the helical filaments in the same orientation as in image (C). The GOI interfaces are represented by red patches.

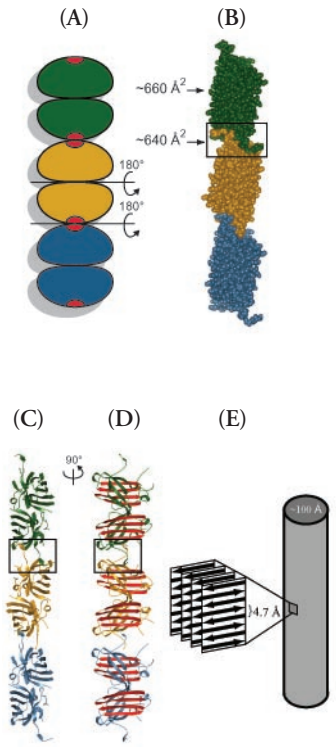

Figure 1. The gain-of-interaction (GOI) interfaces in pathogenic SOD1 give rise to cross-β fibers (or filaments) in two different crystal systems. Two orthogonal views of the linear, amyloid-like apo-H46R filament are represented by three dimers, shown from top to bottom in green, gold, and blue, respectively. Because the overall architecture and GOI interfaces in the S134N filament and the metal-free H46R filament are nearly identical, both filaments are represented by the single filament shown in this panel. The GOI interface is boxed, and buries approximately 640 square angstroms (Å²) of solvent-accessible surface area per polypeptide. (A) A schematic representation of SOD1 dimers in the amyloid-like filaments (in the same orientation as in image (D). The GOI interfaces are represented by red patches. (B) and (C) Space filling and ribbon representations of the filaments, respectively. These are rotated 90° relative to the images in (A) and (D). In (B), the naturally occurring interface between SOD1 monomers is also indicated and buries approximately 660 Å² of solvent-accessible surface area per polypeptide. (D) One-half of each SOD1 β-barrel, shown in red. (E) The long axes of the red strands run perpendicular to the long axis of the filament, an architecture similar to the "cross-β" structure observed in amyloid fibrils.

The Crystal Structure of Biotin Synthase, an *S*-Adenosylmethionine-Dependent Radical Enzyme

F. Berkovitch[1], Y. Nicolet[1], J.T. Wan[2], J.T. Jarrett[2], and C.L. Drennan[1]

[1]Department of Chemistry, Massachusetts Institute of Technology; [2]Johnson Research Foundation and Department of Biochemistry and Biophysics, University of Pennsylvania

The crystal structure of biotin synthase addresses how "AdoMet radical" enzymes, also called "Radical SAM" enzymes, use an Fe_4S_4 cluster and S-adenosyl-L-methionine to generate organic radicals. Biotin synthase catalyzes the radical-mediated insertion of sulfur into dethiobiotin (DTB) to form biotin (vitamin B_8). The structure places the substrates, i.e. DTB and AdoMet, between the Fe_4S_4 cluster (essential for radical generation) and the Fe_2S_2 cluster (postulated to be the source of sulfur), with both clusters in unprecedented coordination environments.

Biotin is an essential vitamin that plays a ubiquitous role in human growth and metabolism. Biotin deficiency results in skin lesions, abnormal fat distribution, neurological symptoms, and immunodeficiency. A low biotin level has also been correlated to an increased incidence of type II diabetes mellitus. Biotin is a valuable commercial commodity, used as an additive in food, health, and cosmetic products, and as a research tool in the biochemical sciences.

We recently reported the crystal structure of *E. coli* Biotin Synthase (BioB), which belongs to the emerging "AdoMet radical" or "radical SAM" enzyme superfamily. The superfamily is characterized by the presence of a conserved CX_3CX_2C motif, ("C" is the amino acid cysteine and "X" is any amino acid), and the requirement of a 4Fe-4S cluster and *S*-adenosyl-L-methionine (AdoMet or SAM) to perform carbon-based radical chemistry. Enzymes that utilize radical chemistry are able to catalyze challenging and unusual reactions, but are difficult to work with because of their aberrant reactivity and oxygen sensitivity. We were able to grow crystals of BioB in an anaerobic chamber and, over a 17-month period, obtained crystals of high-enough quality to solve the structure of this fascinating protein (**Figure 1**).

BioB activates DTB, a biotin precursor, for sulfur (S) insertion between two non-activated carbon atoms, forming biotin (**Figure 2**). The molecular basis for this remarkable chemistry lies in a novel reactivity of AdoMet in the presence of unique Fe-S clusters. BioB is a homodimer (i.e. formed by two identical molecules), with one active site per protomer and no interactions between the two active sites. Each protomer adopts a common protein structure known as the "TIM barrel," and contains two Fe-S clusters, both of which have unprecedented coordination environments. At the C-terminal end of the TIM barrel, a 4Fe-4S cluster is coordinated by the three cysteines of the CX_3CX_2C motif, and a unique Fe of this cluster is coordinated by the amino and carboxyl groups of AdoMet. Buried deep in the center of the TIM barrel, a 2Fe-2S cluster is coordinated by three cysteines and one arginine, each of which is absolutely conserved. DTB is

Fred Berkovitch

BEAMLINE X25

Funding
National Institutes of Health; Searle Scholars Program; Cecil and Ida Green Career Development Fund; Lester Wolfe Predoctoral Fellowship; Cellular, Biochemical, and Molecular Sciences training grant; U.S. Department of Energy; National Institute of General Medical Sciences

Publication
F. Berkovitch, Y. Nicolet, J.T. Wan, J.T. Jarrett, and C.L. Drennan, "The Crystal Structure of Biotin Synthase, an *S*-Adenosylmethionine-Dependent Radical Enzyme," *Science,* **303**, 76-79 (2004).

Contact information
Catherine Drennan
Department of Chemistry, Massachusetts Institute of Technology

Email: cdrennan@mit.edu

bound between AdoMet and the 2Fe-2S cluster (**Figure 3**).

The coordination of the 4Fe-4S cluster by AdoMet ensures efficient electron transfer from the cluster to the cofactor. The donation of one electron by the 4Fe-4S cluster to AdoMet results in reductive cleavage of the carbon-sulfur bond, generating the high-energy 5'-deoxyadenosyl radical (Ado•), an intermediate that has historically been associated with adenosylcobalamin (AdoCbl)-dependent radical enzymes. Ado• removes hydrogen atoms from DTB, preparing it for sulfur insertion. The unique 2Fe-2S cluster is proposed to be the S donor in the BioB reaction, and the close linear arrangement of AdoMet, DTB, and the 2Fe-2S cluster supports this hypothesis. It is possible that the arginine ligand plays a role in the reaction mechanism, or helps stabilize the 2Fe-2S cluster after sulfur insertion.

The structures of BioB and diol dehydratase, an AdoCbl-dependent radical enzyme, show remarkable similarities. Both deploy the TIM barrel fold to bind their radical-generating cofactors. Moreover, the active sites of BioB and diol dehydratase show that the positions of the substrate, cofactors, essential metals, and secondary structural elements coincide. These structural similarities point to the evolutionary relationship between the AdoMet-dependent and AdoCbl-dependent radical enzymes.

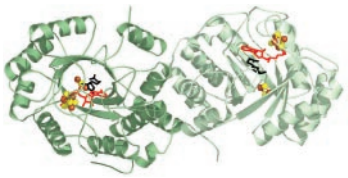

Figure 1. The BioB dimer. BioB is a homodimer, composed of two TIM barrel protomers (colored different shades of green). The 4Fe-4S cluster, which is present in all AdoMet radical proteins, is located at the C-terminal end of the cluster. AdoMet (red sticks) coordinates a unique Fe of this cluster. The substrate, DTB (black sticks), is located between AdoMet and a 2Fe-2S cluster, which is buried in the core of the barrel and is proposed to be the S donor in the BioB reaction. Fe and S atoms are represented by brown and yellow spheres, respectively.

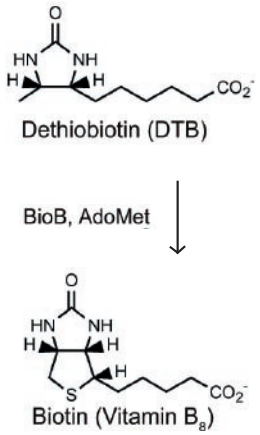

Figure 2. Reaction of BioB

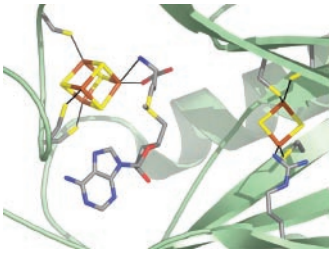

Figure 3. The unique Fe-S clusters of BioB. The 4Fe-4S cluster is shown, coordinated by the CX_3CX_2C motif and by the amino and carboxyl groups of AdoMet. The 2Fe-2S cluster is coordinated by three cysteines and one arginine. All ligands to both clusters are absolutely conserved.

Structure of a Specific Alcohol-Binding Site Defined by the Odorant Binding Protein LUSH from Drosophila Melanogaster

S.W. Kruse[1], R. Zhao[2], D.P. Smith[3], and D.N.M. Jones[1,4]

Departments of [1]Pharmacology, [2]Biochemistry and Molecular Genetics, and the [4]Program in Biomolecular Structure, University of Colorado Health Sciences Center; [3]Department of Pharmacology and Center for Basic Neuroscience, University of Texas Southwestern Medical Center

LUSH is a non-enzymatic alcohol-binding protein that is required for a normal chemosensory response to alcohols, such as ethanol in the fruit fly Drosophila melanogaster. We have recently solved the structures of LUSH in complex with ethanol, n-propanol, and n-butanol to 1.49 angstroms (Å), 1.45Å, and 1.25Å, respectively. From these structures we have identified a set of inter-molecular interactions that act in concert with each other and may help to increase the binding affinity of alcohol to the protein, and thereby defines a specific alcohol-binding site. We propose that this structure may represent a general alcohol-binding motif that is believed to exist in a number of alcohol-sensitive ion channels in mammalian cells.

There is substantial evidence that many of the biochemical effects of alcohol are linked to changes in the structure and dynamics of a number of receptors in the central nervous system, including the gamma-amino butyric acid (GABA) and nicotinic acetylcholine (nAChR) receptors. Alcohol appears to bind to these receptors at specific sites, but the details of this interaction remain unclear because of the lack of structural information about these membrane-associated proteins. Our goal is to determine the molecular architecture of specific alcohol-binding sites through structural studies of a model protein, LUSH, from the fruit fly Drosophila melanogaster. In insects, odorant binding proteins are key components of the insect sensory system and bind to odor molecules from various sources, including those from food or other insects. LUSH is an odorant binding protein that is required for the normal behavioral response to alcohols. Adult flies have an active avoidance mechanism that responds to high concentrations of short chain alcohols, but this mechanism is defective in flies that lack the lush gene. LUSH was given its name because fruit flies without the corresponding gene are attracted to alcohol.

From the high-resolution structures of LUSH determined by Miyazawa et al., we identified a structural motif that may provide a high-affinity alcohol-binding site. An essential part of this study was the availability of the "Mail-in Data Collection" program at the NSLS. Since we work in a laboratory that traditionally uses nuclear magnetic resonance (NMR) spectroscopy to analyze protein structures, this service gave our group rapid access to synchrotron beam time, which would have otherwise been difficult to obtain through a conventional application. In addition, we received expert assistance from NSLS staff, in particular Dr. Howard Robinson. LUSH protein labeled with

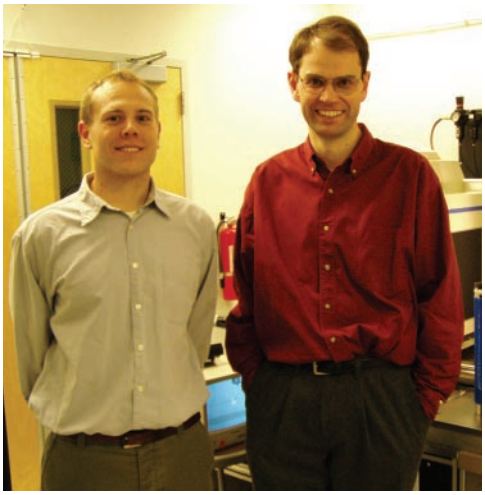

Authors (left to right)
Schoen Kruse and David Jones

BEAMLINE X12C

Funding
National Institutes of Health (National Institute on Alcohol Abuse and Alcoholism); American Heart Association

Publication
S.W. Kruse, R. Zhao, S.P. Smith, and D.N.M. Jones, "Structure of a Specific Alcohol-Binding Site Defined by the Odorant Binding Protein LUSH from *Drosophila melanogaster*," *Nat. Struct. Biol.*, **9**, 694-700 (2003).

Contact information
David N.M. Jones
University of Colorado Health Sciences Center

Email: David.Jones@uchsc.edu

seleno-methionine was crystallized at the University of Colorado Health Sciences Center and sent to the NSLS for data collection. As a result, we were able to solve the structure in a matter of weeks, rather than several months.

The structure of LUSH consists of six α-helices and a short segment of a 3_{10}-helix that surround a central cavity that is hydrophobic (does not like aqueous environments) and contains the alcohol-binding site. The hydroxyl group of the alcohol forms hydrogen bonds (H-bonds) to two amino acids in LUSH, serine (Ser52) and threonine (Thr57), at one end of this cavity (**Figure 1**). The structure was solved in the presence of 30 to 50 millimolar (mM) alcohol, and under these conditions we only observe the one alcohol-binding site, suggesting that the chemistry within this site may have evolved to specifically bind alcohols. We hypothesize that this is a result of the side-chain hydroxyl of Ser52 making an H-bond to the main-chain oxygen of Thr48, another amino acid, increasing the ability of the side chain of Ser52 to accept a H-bond from the alcohol. The positioning of Thr57 as a H-bond donor to the alcohol may simultaneously make the alcohol a better H-bond donor to Ser52.

The recent structure of the nAChR from the Torpedo Ray suggests the possibility that serine and threonine residues could be positioned within the protein interior to make a set of concerted interactions with alcohol in a manner analogous to that seen in LUSH. If so, then as the acetylcholine receptor is the archetypal model for several receptors implicated in the effects of alcohol consumption. We suggest that the alcohol-binding site defined in LUSH may represent a general model for alcohol binding in other proteins. We are now testing the role that individual amino acids play in binding alcohol by solving the structure of proteins that have undergone amino acid substitutions. We believe these structures will provide further insights into the nature of alcohol-binding sites.

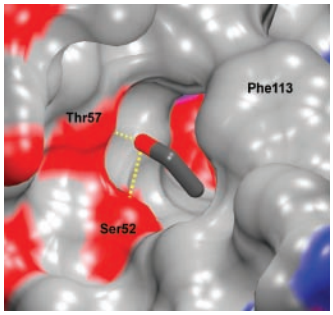

Figure 1. A surface representation of key residues in the LUSH alcohol-binding pocket. The pocket is lined with hydrophobic residues with the exception of Thr57 and Ser52, which form concerted hydrogen bonds with the alcohol. Ethanol is shown in a stick representation. The hydrogen bonds between the alcohol and the hydroxyl groups of Thr57 and Ser52 are shown as yellow dotted lines.

Crystal Structure of LeuA from Mycobacterium Tuberculosis, a Key Enzyme in Leucine Biosynthesis

N. Koon[1,2], C.J. Squire[1,2], and E.N. Baker[1,2,3]

[1]Centre for Molecular Biodiscovery; [2]School of Biological Sciences; and [3]Department of Chemistry, University of Auckland

The leucine biosynthetic pathway is essential for the growth of Mycobacterium tuberculosis, and is a potential target for the design of new anti-tuberculosis drugs. We have used multiwavelength anomalous diffraction (MAD) phasing to determine the high-resolution crystal structure of α-isopropylmalate synthase, the product of the leuA gene. The structure reveals a tightly associated dimer comprised of an $(\alpha/\beta)_8$ barrel catalytic domain joined by flexibly-hinged linker domains to a C-terminal regulatory domain. The structure shows how the substrate, the leucine precursor α-ketoisovalerate, binds to an essential zinc atom in the catalytic domain, and a potential mechanism of feedback inhibition by leucine binding in the regulatory domain.

Tuberculosis (TB) is responsible for more deaths worldwide than any other infectious disease – more than two million each year, with an estimated one third of the world's population infected. The problem is compounded by the length of current treatments and by the ability of *Mycobacterium tuberculosis*, the causative agent, to survive in a dormant state inside activated macrophages in the lung for long periods of time, emerging many years later as active infections. Multi-drug resistance is also a growing problem. The genome sequence of *M. tuberculosis*, completed in 1998, has stimulated new approaches, including the formation of the TB Structural Genomics Consortium. Our goals, as part of this consortium, are to determine the three-dimensional structures of proteins that are potential new targets for TB drug development or that will help to understand TB biology.

The biosynthetic pathways for the branched-chain amino acids leucine, isoleucine and valine (i.e. the series of enzyme reactions that produce these amino acids) are essential for the survival of the TB organism. These pathways are not present in humans, indicating that inhibitors targeted against enzymes from them could be useful as anti-TB drugs. We chose the enzyme α-isopropylmalate synthase (α-IPMS), the product of the *leuA* gene, for structural analysis. This enzyme catalyzes the first step in leucine biosynthesis, in which an acetyl group is transferred from acetyl-coenzymeA to the substrate α-ketoisovalerate (α-KIV), the leucine precursor. The enzyme was known to be dimeric (2 x 70 kDa), metal ion-dependent, and subject to feedback inhibition by the end product leucine, but its three-dimensional structure was unknown.

The structure was solved using multiwavelength anomalous diffraction (MAD) data from a selenomethionine-substituted α-IPMS crystal, which was frozen and sent from New Zealand to beamline X8C (FedEx crystallography) for data collection. The data quality was such that 70% of the 1288 residues in the dimer could be

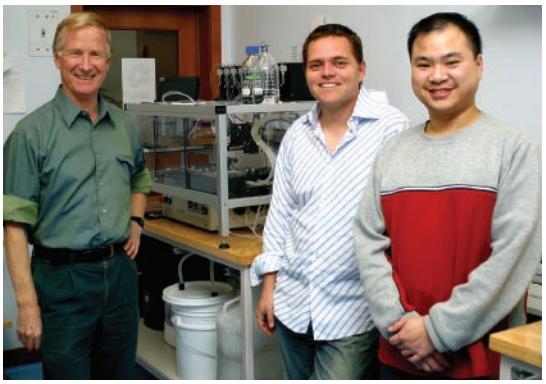

Authors (left to right)
Ted Baker, Chris Squire, and Nayden Koon

BEAMLINE X8C

Funding
Health Research Council of New Zealand

Publication
N. Koon, C. J. Squire, and E. N. Baker, "Crystal Structure of LeuA from Mycobacterium Tuberculosis, a Key Enzyme in Leucine Biosynthesis," *Proc. Natl. Acad. Sci. USA*, **101**, 8295-8300 (2004).

Contact information
Edward N. Baker
School of Biological Sciences, University of Auckland, New Zealand

Email: ted.baker@auckland.ac.nz

immediately traced and autobuilt. The structure was then completed and refined at 2.0 Å resolution. A spherical peak for a bound metal ion, marking the active site of each monomer, was identified by a fluorescence scan as zinc. We also subsequently prepared complexes with α-KIV (substrate) and leucine (feedback inhibitor).

The α-IPMS monomer is folded into three domains (**Figure 1**), an $(\alpha/\beta)_8$ barrel catalytic domain, a helical linker domain, and a C-terminal domain of novel fold. Two α-IPMS monomers form a domain-swapped dimer in which the linker domain of one monomer sits over the catalytic domain of the other. This domain swapping makes the active site almost completely enclosed, except for a tunnel that allows the entry of substrates. In the crystal structure, the substrate α-KIV is bound to the zinc (**Figure 2A),** and although acetyl-CoA is not present, two water molecules mark where the acetyl group would sit, adjacent to α-KIV. With this information we can propose a catalytic mechanism for α-IPMS, based on that of malate synthase, an enzyme that is evolutionarily unrelated but carries out a very similar reaction on a very similar substrate.

Several features make the α-IPMS structure suitable for drug development: the zinc ion as a template for inhibitor binding and surrounding invariant side chains inside the enclosed active site cavity. The structure also reveals an intriguing mechanism for feedback inhibition. Leucine binds in the regulatory C-terminal domain (**Figure 2B)** 70 Å away from the nearest active site, but this binding must be signalled via the flexible linker domain, which inserts two key residues into the active site.

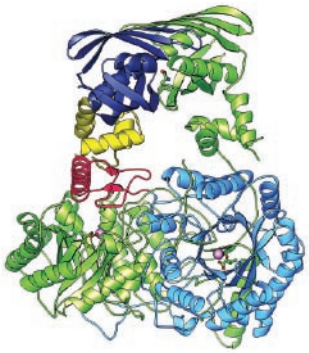

Figure 1. Ribbon diagram of the LeuA dimer. One monomer is in green. The other is colored to show the three domains: the N-terminal catalytic domain (light blue), the central linker domain (shown as red and yellow subdomains), and the C-terminal regulatory domain (dark blue). The active site of each monomer is shown by the zinc atom (magenta sphere) and bound α-KIV substrate. Each active site is covered by helix α10 from the other monomer of the dimer. A leucine molecule is shown bound in the regulatory domain.

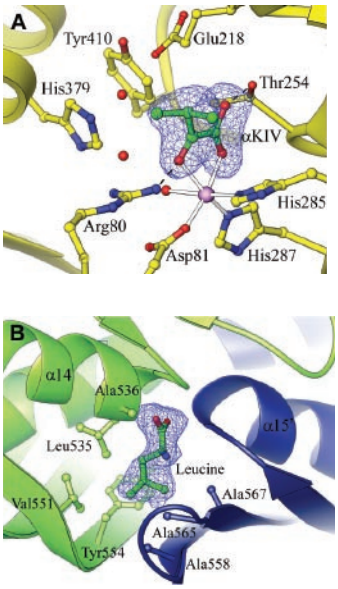

Figure 2. Close-up of the ligand binding sites. (A) The α-KIV substrate (shown in its electron density as a blue mesh), bound to zinc. Two water molecules (small red spheres) mark where the acetyl group of acetyl-CoA would bind. The side chains of His379 and Tyr410 are from helix α10 of the other monomer, which covers the active site. (B) A leucine molecule bound in the regulatory domain with its carboxyl group between two helices.

Structural Basis of the α_1–β Subunit Interaction of Voltage-Gated Ca^{2+} Channels

Y.-h. Chen, M.-h. Li, Y. Zhang, L.-l. He, Y. Yamada, A. Fitzmaurice, Y. Shen, H. Zhang, L. Tong, and J. Yang

Department of Biological Sciences, Columbia University

High voltage-activated (HVA) Ca^{2+} channels in cell membranes control diverse biological processes, such as muscle contraction and hormone release. They are composed of α_1, α_2-δ, β, and sometimes γ, subunits. The proper expression and function of HVA Ca^{2+} channels are critically dependent on the β subunit, which binds directly to the α interaction domain (AID) in α_1, presumably through the β interaction domain (BID). We have solved the crystal structure of the conserved core region of β_3, alone and in complex with AID, and of β_4 alone. The structures show that the β core contains two common protein-interacting domains (an Src homology 3 (SH3) domain and a guanylate kinase (GK) domain) and that AID does not bind to BID. These represent the first crystal structures of a Ca^{2+} channel subunit or domain and suggest that β may be a multifunctional protein.

There are four subfamilies of Ca^{2+} channel β subunits (β_1-β_4). Each β subunit contains five regions, with the three middle regions forming a core that can perform most functions of full-length β. The crystal structure of the β_3 core in complex with a 49-amino acid segment of α_1, which contains the 18-amino acid α interaction domain (AID) (at 2.6 Å-resolution), shows that the three regions comprising the β core are: an Src homology 3 (SH3) domain, a guanylate kinase (GK) domain, and a "HOOK" region that connects them (**Figure 1A**). The SH3 and GK domains interact intramolecularly. The AID forms an α-helix and binds to a hydrophobic (water-fearing) groove in the GK domain. The interactions between AID and β are extensive, involving hydrophobic interactions, hydrogen bonds, and an ion pair (**Figure 1B**). These interactions form the basis for the high-affinity binding between α_1 and β. Most of the amino acids involved in the interactions are conserved in both subunits. The structure also reveals that the β interaction domain (BID) spans all three regions of the SH3-HOOK-GK motif and is thus crucial for the intramolecular interaction between the SH3 and GK domains, as well as their structural integrity. But, it is not directly involved in binding AID (**Figure 1A**).

The overall structure of the unliganded (unbound) β_3 core is very similar to that of the β_3 core bound to AID, indicating that AID binding does not change the β subunit structure. Also, as predicted by the high amino acid similarity, the structure of the β_4 core is nearly identical to that of the β_3 core.

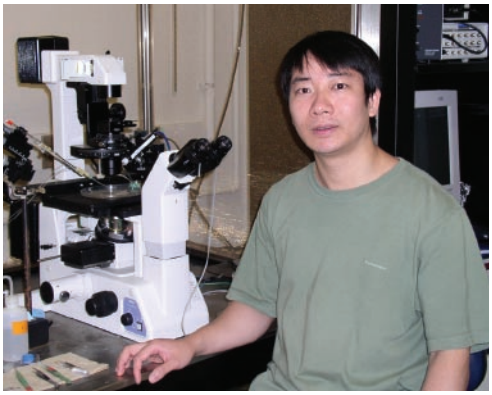

Yu-hang Chen

The β subunit SH3 domain (β-SH3) is structurally similar to canonical SH3 domains, but, unlike the continuous configuration of the latter, β-SH3 is split, with a separate, flexible HOOK region inserted between the first four β strands and the last one. Furthermore, although β-SH3

BEAMLINE X4A

Funding
National Institutes of Health; The McKnight Foundation; The EJLB Foundation; The American Heart Association

Publication
Y-h. Chen, M-h. Li, Y. Zhang, L-l. He, Y. Yamada, A. Fitzmaurice, Y. Shen, H. Zhang, L. Tong, and J. Yang. "Structural Basis of the α_1–β Interaction of Voltage-Gated Ca^{2+} Channels," *Nature,* **429**, 675-680 (2004).

Contact information
Prof. Jian Yang
Department of Biological Sciences, Columbia University

Email: Jy160@columbia.edu

possesses several amino acids critical for binding PXXP motifs (molecules that typically bind to SH3 domains), it is unlikely to interact with PXXP-containing proteins because the binding site is shielded by part of the HOOK. Likewise, although the overall structure of the β subunit GK domain (β-GK) is similar to that of the yeast GK domain, it is catalytically inactive. Thus, the function of the β subunit SH and GK domains remains to be determined.

Interestingly, the SH3-HOOK-GK motif is also a common structural signature of a family of proteins called membrane-associated guanylate kinase homologs (MAGUKs). Many members of this family, including PSD95, are concentrated at the boundaries between neurons, or "synapses," as are HVA Ca^{2+} channels, and play a central role in clustering and organizing both pre- and post-synaptic ion channels and neurotransmitter receptors. Electrophysiological studies indicate that the PSD95 SH3-HOOK-GK and PSD95_GK do not interact with HVA Ca^{2+} channels (**Figure 2A**). A comparison of the structure of PSD95_GK and β_GK clearly reveals why: The AID-binding pocket is completely blocked in PDS95_GK (**Figure 2B**). Our study thus provides a structural basis for the specificity of Ca^{2+} channel β subunits and MAGUK proteins.

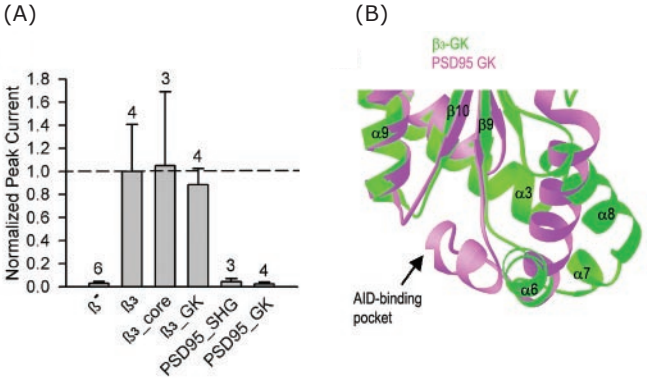

Figure 2. Structural and functional comparisons of β with PSD95. (**A**) Whole-oocyte current measured in oocytes injected with Cav2.1 (α_1) and α_2-δ only (β^-) or together with the indicated construct. β_3_GK represents amino acids M177-G366 of β_3; PSD95_SHG represents the SH3-HOOK-GK motif (amino acids G473-L767) of PSD95; and PSD95_GK represents the GK domain (amino acids H575-S755) of PSD95. The current was normalized using the mean current obtained with wild-type β_3. (**B**) Superposition of the GK domain of unliganded β_3 (green) and PSD95 (1KJW, pink). Only the region around the AID binding site is shown. Secondary structures are labeled only for β_3.

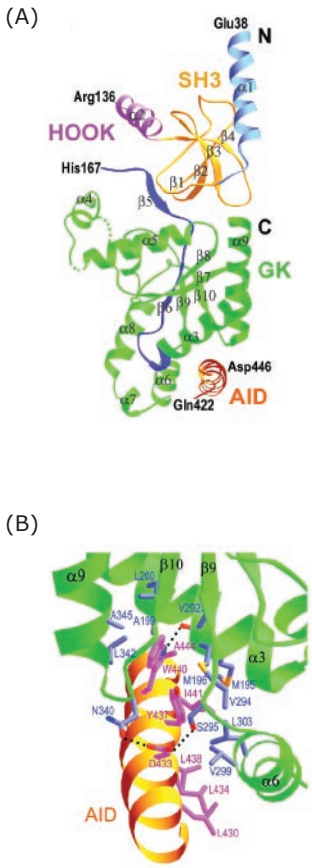

Figure 1. Crystal structure of the β_3 core in complex with its α_1 binding partner (AID). (**A**) The β_3 core can be divided into three regions: an SH3-domain (gold), a HOOK region (purple), and a GK domain (green). The AID and BID are colored in orange and blue, respectively. (**B**) Close-up of the interface between β_3 and AID. Most residues involved in the interactions are shown.

Structure of Mammalian Protein Geranylgeranyltransferase Type-I

T.S. Reid, J.S. Taylor, K.L. Terry, and L.S. Beese

Department of Biochemistry, Duke University Medical Center

Protein geranylgeranyltransferase type-I (GGTase-I) is an essential enzyme in eukaryotes. GGTase-I catalyzes an essential reaction in which a specific lipid group, acting as a substrate, becomes covalently attached to proteins involved in cell growth and differentiation, allowing these proteins to associate with the cell membrane. We present the first structural information for mammalian GGTase-I, including a series of substrate and product complexes that delineate the path of the chemical reaction. These structures reveal that all protein prenyltransferases share a common reaction mechanism and identify specific amino acid residues that play a dominant role in selecting the correct lipid substrate. Protein prenyltransferase inhibitors are under evaluation in phase III clinical trials for the treatment of cancer and show promise for the treatment of parasitic infections, including malaria.

Over 100 proteins involved in cell growth and differentiation require the covalent attachment of an iosprenoid lipid, a process called prenylation, for membrane association and proper function. The three known enzymes that catalyze protein prenylation are GGTase-I, protein farnesyltransferase (FTase), and Rab GGTase. GGTase-I performs the bulk of cellular prenylation, and inhibiting its function has dramatic biological effects, such as blocking cell growth and promoting apoptosis, the natural death of a cell.

The structure of GGTase-I was determined by a method called single isomorphous replacement with anomalous scattering (SIRAS). There are six GGTase-I molecules (each is 91 kilo-Daltons in size), or approximately 33,000 non-hydrogen atoms, in each asymmetric unit. The overall structure of GGTase-I is shown in **Figure 1A**. The α subunit is composed of α-helical pairs, forming a crescent that wraps around the compact α-α barrel of the β subunit, and the active site opens into the central funnel-shaped cavity of the β subunit. At the rim of the active site is a catalytic zinc ion.

We have captured four crystal structures representative of the GGTase-I reaction cycle (**Figure 2**). The first step in the reaction cycle is the binding of the 20-carbon (20-C) lipid substrate geranylgeranyl diphosphate (GGPP, **Figure 1B**). GGPP binds in the GGTase-I active site with the first three isoprene units of the lipid group arranged along a straight line and the fourth isoprene unit turned approximately 90 degrees relative to this axis (**Figure 1C**). This structure permitted us to identify residues that are responsible for selecting the correct lipid substrate. To test this hypothesis, a single point mutation was constructed, which converted the lipid specificity of FTase (15-C lipid substrate) to that of GGTase-I (20-C lipid substrate) (**Figure 1C**). Following GGPP binding, the next step in the reaction cycle is substrate

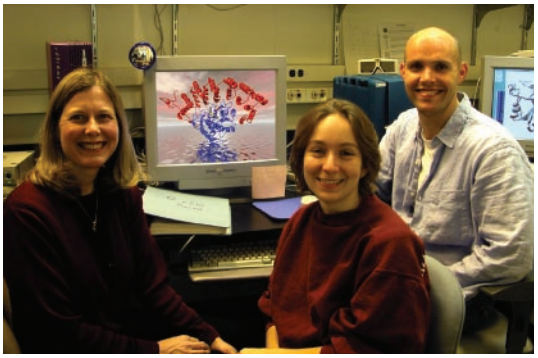

Authors (left to right)
Lorena Beese, Kimberly Terry, and Scott Reid

BEAMLINES
X12B, X25

Funding
National Institutes of Health; Postdoctoral Fellowship from the American Heart Association

Publication
J.S. Taylor, T.S. Reid, K.L. Terry, P.J. Casey, and L.S. Beese, "Structure of Mammalian Protein Geranylgeranyltransferase Type-I.," *EMBO J.*, **22**, 5963-5974 (2003).

Contact information
Lorena S. Beese
Department of Biochemistry, Duke University

Email: lsb@biochem.duke.edu

peptide binding (**Figure 2-2**). GGTase-I recognizes peptides that contain a C-terminal Ca_1a_2X box, defined by the cysteine (C), two aliphatic residues (a_1a_2), and a variable C-terminal residue (X), which determines whether the protein is a substrate for GGTase-I, FTase, or both. The Ca_1a_2X box binds in an extended conformation, with the cysteine coordinating the catalytic zinc and hydrogen bonds that anchor the carboxyl-terminus. After catalysis, the peptide-prenyl product is retained by the enzyme **(Figure 2-3)**. Comparing complexes 2 and 3 illustrates that the lipid substrate undergoes a conformational change during the transition state that brings it in-line for catalysis. GGPP binding partially displaces the product from the active site: The Ca_1a_2X peptide adopts an alternate conformation, and the product lipid group translocates (to make room for the incoming GGPP) into a shallow, solvent-accessible groove, called the "exit groove" (**Figure 2-4**). The dissociation of the product, which is accelerated by fresh substrate peptide, allows the reaction cycle to repeat.

The structural snapshots of the GGTase-I reaction cycle are consistent with the unusual reaction mechanism proposed for FTase, thereby indicating that this cycle is a common feature of the protein prenyltransferase family. Overall, these structures, when contrasted with FTase, reveal the dominant structural features responsible for substrate selectivity. Protein prenyltransferases are promising targets for chemotherapy drugs, but further development may require designing drugs that are highly selective for one enzyme. This work, along with our earlier work on FTase, provides a foundation for structure-based design and the optimization of drugs that are specific to a particular protein prenyltransferase.

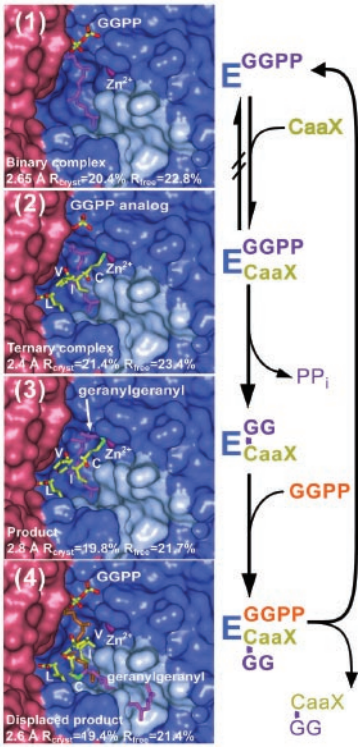

Figure 2. Structures of the GGTase-I reaction cycle. The GGTase-I active site is shown in stereo as a molecular surface, with the α subunit colored red, the β subunit blue, and the exit groove highlighted in cyan. Complex 1: The enzyme with bound GGPP. Complex 2: Ternary complex with 3'azaGGPP analog and Ca_1a_2X peptide substrate (only $CVIL_{COOH}$ shown). Complex 3: Prenylated peptide product complex. Complex 4: Displaced prenylated peptide product and GGPP.

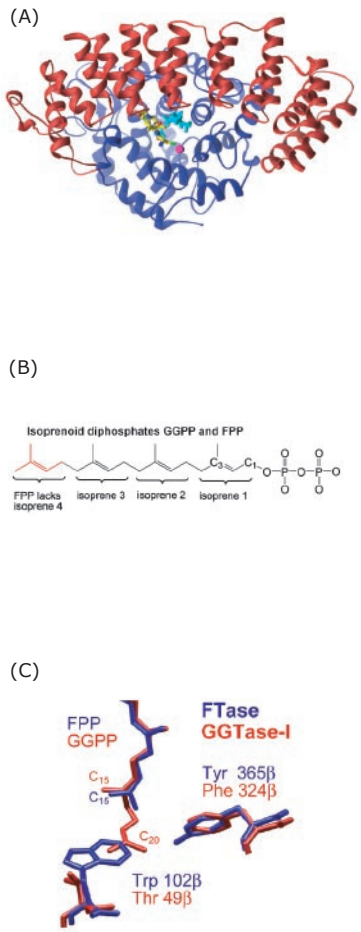

Figure 1. (A) GGTase-I ternary substrate complex. The GGTase-I consists of a 48 kilo-Dalton (kDa) α subunit (red) and a 43 kDa β subunit (blue). The non-reactive 3'azaGGPP (cyan) binds similarly to GGPP in the active site. The Ca_1a_2X portion of the KKKSKTKCVIL peptide substrate (yellow) binds against the isoprenoid, with the cysteine sulfur coordinating the catalytic zinc ion (magenta). (B) Geranylgeranyl diphosphate (GGPP) has four isoprene units; farnesyl diphosphate (FPP) has three. (C) Comparison of lipid substrate binding in FTase (blue) and GGTase-I (red). In FTase, the larger tryptophan residue fills the space where the additional five carbons of GGPP bind in GGTase-I and is one of the prime determinants of lipid substrate specificity. Mutation of the tryptophan residue to the equivalent GGTase-I threonine residue resulted in an FTase mutant that prefers the 20-C GGPP as a lipid substrate over the typical 15-C FPP lipid substrate.

Structural Effects of Radiation Damage and its Potential for Phasing

S. Banumathi[1], P.H. Zwart[2], M. Dauter[2], and Z. Dauter[1]

[1]Synchrotron Radiation Research Section, MCL, National Cancer Institute, Brookhaven National Laboratory; [2]SAIC Frederick, Inc., Basic Research Program, Brookhaven National Laboratory

We have carried out a detailed analysis on the structural effects of radiation damage on the model protein thaumatin. The most pronounced structural changes observed were disulfide bond breakage and the associated main and side chain movements, as well as the decarboxylation of the aspartate and glutamate residues. The structural changes induced on the sulfur atoms were used successfully to solve the structure via a Radiation-damage Induced Phasing (RIP) procedure.

Radiation damage has been a curse of macromolecular crystallography from its early days. Until the 1990s all diffraction data were collected from macromolecular crystals mounted in glass or quartz capillaries and kept at ambient temperature, in the range of 4-20°C. Initially, collecting data from protein crystals using precession cameras or multi-circle diffractometers took a very long time. The introduction of the screenless rotation method considerably sped up this process by recording more reflections simultaneously. Still, only the most robust crystals were able to deliver all the necessary data from one specimen, and very often a complete data set had to be combined from data measured on several crystals. Although the advent of cryo-cooling techniques, where diffraction data is obtained from crystals cooled down to approximately 100K, substantially alleviated the problem of radiation damage, the obvious deterioration of cryo-cooled crystals at bright undulator beamlines revived interest and prompted several investigations into the effects of radiation damage.

Whereas previous structural radiation damage studies have been carried out at third-generation synchrotron sources, the effects of radiation damage on protein crystals can be also observed after prolonged exposures at second-generation bending magnet synchrotron beamlines. We have analyzed the effects of radiation damage on crystals of thaumatin, a medium-sized protein containing 207 amino acids, including eight disulfide bridges. We collected twenty high-resolution data sets that allowed us to perform a detailed investigation of the structural changes induced by x-ray irradiation.

Authors (clockwise from top left)
Peter Zwart, Mirka Dauter, Zbigniew Dauter, and Banumathi Sankaran

The structural changes induced by radiation damage can be visualized using difference Fourier maps that reveal the appearance or disappearance of electrons on and around the molecular model. The most striking features our analyses revealed are the breakage of disulfide bonds and the associated main and side chain movements, as shown in **Figure 1**. Less prominent, but still significant, structural changes

BEAMLINE X9B

Funding
National Institutes of Health
National Cancer Institute

Publication
S. Banumathi, P.H. Zwart, U.A. Ramagopal, M. Dauter, and Z. Dauter, "Structural Effects of Radiation Damage and its Potential for Phasing," *Acta Cryst.*, **D60**, 1085-1093 (2004).

Contact information
Zbigniew Dauter
Argonne National Laboratory

Email: dauter@anl.gov

involve the decarboxylation of side chains and water molecule movements.

As can be seen from **Figure 1**, the amount of electrons relocated over the course of the experiment is quite large. This suggests that the observed changes in the diffraction intensities are dominated by this structural change and that the disulfide bridges can be located using the isomorphous difference only. When this so-called substructure is located, standard procedures can be used to obtain an image of the three-dimensional electron density of the protein, which finally results in an atomic model of the protein under investigation. Normal phasing techniques use chemical or biochemical methods in order to generate a so-called derivative. In this case, the interaction of the x-rays with the protein produces a derivative suitable for phasing, hence the name Radiation-damage Induced Phasing (RIP). In the investigated case, the electron density estimates that result from various standard crystallographic computations are of such a high quality that they can be easily interpreted, as indicated in **Figure 2**.

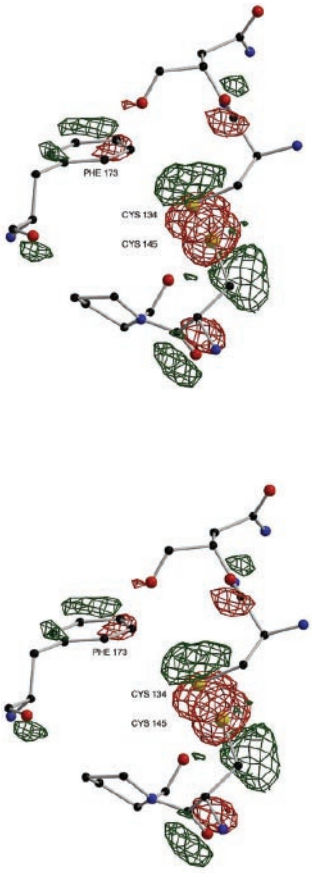

Figure 1. Positive and negative difference Fourier maps showing the disappearance of electrons in red and the appearance of electrons in green over the course of the data collection. The pattern of negative (red) and positive (green) peaks suggests that, upon the breakage of the disulfide bond CYS134-CYS145, the sulfur atoms 'swing out' while the surrounding main and side chain positions are affected.

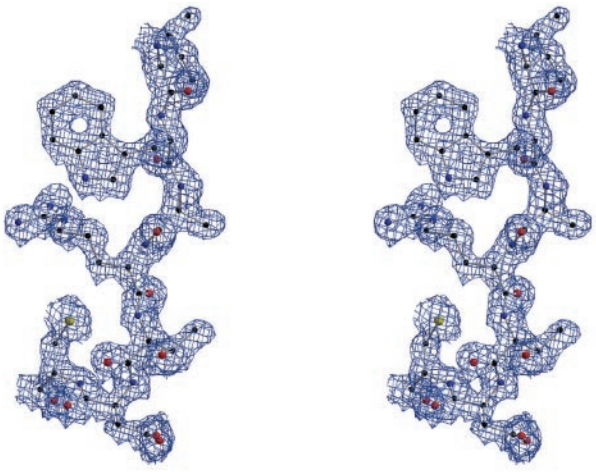

Figure 2. An electron density map calculated with solvent flattened RIP phases overlaid on the final model.

Amphiphilic 4-Helix Bundles Designed for BioMolecular Materials Applications

S. Ye, J.W. Strzalka, S. Zheng, T. Xu, J.K. Blasie, B.M. Discher, D. Noy, and P.L. Dutton

Department of Chemistry, University of Pennsylvania

Artificial peptides previously designed to possess α-helical bundle motifs have been either hydrophilic (soluble in polar media) or lipophilic (soluble in non-polar media) in their overall character. The realization of these bio-inspired bundles has led to the reproduction of a variety of biomimetic functions within the appropriate media. To translate this functionality into useful biomolecular devices, the bundles must be oriented in a macroscopic ensemble, e.g., at an interface. This goal has been achieved in a new family of α-helical bundle peptides that are amphiphilic, meaning they have well-defined hydrophilic and hydrophobic domains. This peptide family binds metallo-porphyrin prosthetic groups at selected locations within these domains to impart functionality.

Bundles of α-helices provide a robust scaffold for binding prosthetic groups (non-amino acid portions of proteins) at selected locations within the structure, which is necessary in order to mimic the functions exhibited by biological proteins. To be used in device applications, the peptide bundles must be vectorially oriented in an ensemble, e.g., at an interface. In order to generate vectorial function across an interface, we have investigated two approaches that are designed to render the 4-helix bundles themselves amphiphilic such that they possess both a hydrophilic and a hydrophobic domain along the length of each bundle.

In the first approach, each α-helix is designed to be amphipathic, i.e. having polar and non-polar faces. However, the amino acid sequence was oriented such that when the non-polar faces of each amphipathic helix were apposed in the 4-helix bundle over the first m-residues of each helix, the polar faces were apposed over the last n-residues. Thus, a 4-helix bundle with parallel (or syn) topology would possess a charged-polar exterior with a non-polar interior over the first m-residues, thereby forming the hydrophilic domain of the bundle, and a non-polar exterior with an uncharged-polar interior over the last n-residues, thereby forming the hydrophobic domain. The first of these amphiphilic 4-helix bundles was designated Amphiphilic Protein zero (AP0). AP0 can possess bis-histidyl metalloporphyrin binding sites at two positions of the sequence, which are separated by fourteen residues within the larger hydrophilic portion of the 4-helix bundle.

Alternatively, these amphiphilic peptides (the second case) can possess a hydrophobic domain that utilizes a sequence of exclusively non-polar amino acids. Like AP0, these amphiphilic peptides can possess bis-histidyl metalloporphyrin binding sites within the hydrophilic portion of the 4-helix bundle. Importantly, they can also possess bis-histidyl metalloporphyrin binding sites in the hydrophobic portion of the bundle. These two new types of amphiphilic 4-helix bundles now

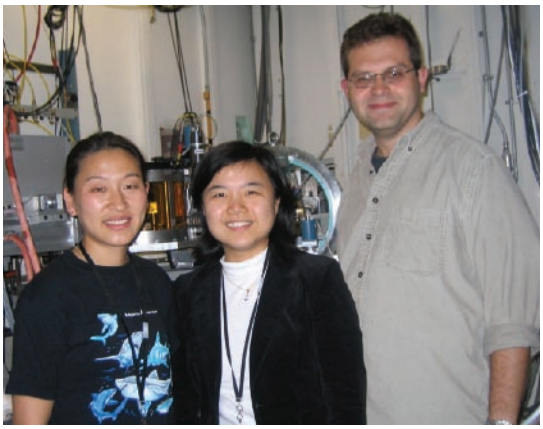

Authors (left to right)
Ting Xu, Shixin Ye, and Joseph Strzalka

BEAMLINE X22B

Funding
National Science Foundation
U.S. Department of Energy

Publication
S. Ye, B.M. Discher, J.W. Strzalka, D. Noy, S. Zheng, P.L. Dutton, and J.K. Blasie, "Amphiphilic 4-Helix Bundles Designed for BioMolecular Materials Applications," *Langmuir,* **20**(**14**), 5897-5904 (2004).

Contact information
Prof. J. Kent Blasie
Department of Chemistry,
University of Pennsylvania

Email: jkblasie@sas.upenn.edu

allow for the positioning of prosthetic groups on either side or both sides of the interface. This is essential for the vectorial electron transfer across the interface, which creates an electrochemical potential. This transforms a designed molecular property at the microscopic level into a material property of the interface at the macroscopic level.

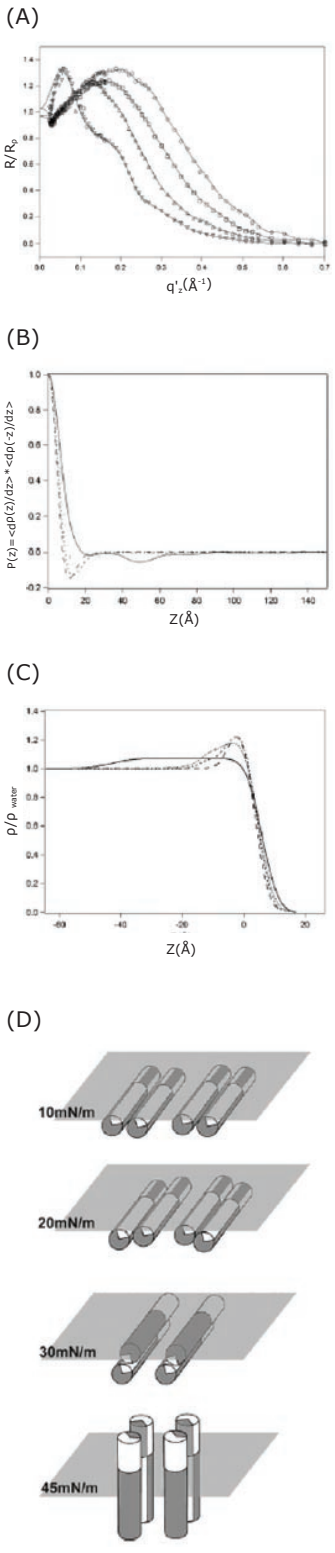

Figure 1. (A) Fresnel-normalized x-ray reflectivity data collected from a Langmuir monolayer of pure AP0 at surface pressures (π) of 10, 20, 30, and 45 mN/m. The data were collected on the liquid surface spectrometer on beamline X22B. The continuous curves are calculated from the box-refinement solution to the phase problem, thus providing the gradient electron density profiles (not shown). **(B)** The autocorrelation function of the monolayer gradient electron density profile (computed from the data in (A)) without phase information at π = 10 (long dash), 20 (short dash), 30 (dot), and 45 mN/m (solid). **(C)** The absolute electron density profiles for the monolayer at each pressure (same symbols as in (b)), computed by analytic integration of a sum of Gaussian functions that best fit the gradient profiles from box refinement. **(D)** A schematic illustration of the surface pressure-dependent orientational transition of AP0 at the air-water interface; the air-water interface is indicated by the plane. At lower surface pressures of 10, 20, and 30 mN/m, both the autocorrelation functions and the electron density profiles indicate that the long axis of the helices lies parallel to the interface, although the plane of the di-helices rotates from parallel to perpendicular to the interface with increasing pressure. When the pressure reaches 45 mN/m, both the autocorrelation function and the electron density profile indicate that all of the AP0 helices are oriented with their long axis normal to the plane of the air/water interface. However, the packing of the molecule along the surface cannot be derived from the electron density profile. An analysis of grazing-incidence x-ray diffraction from these monolayers, collected at Sector 09 at the Advanced Photon Source using a new version of the liquid surface spectrometer (developed by Ben Ocko and Scott Coburn, BNL Physics Department) and an undulator source, has shown that the bundles are indeed comprised of four helices and that the arrangement within the bundle cross-section is square rather than close-packed.

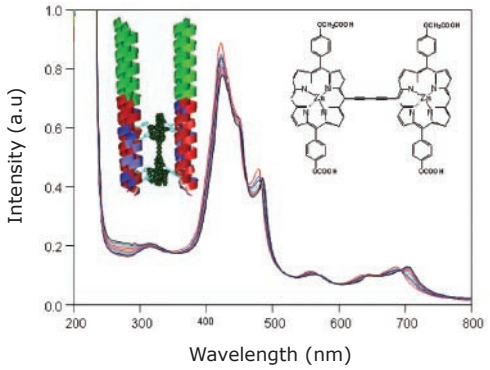

Figure 2: The amphiphilic 4-helix bundles can bind not only metallo porphyrin prosthetic groups, but also non-biological prosthetic groups possessing much more extended π-electron systems. These non-biological groups have the advantage of including the electron donor and the electron acceptor within the same prosthetic group, which is bound to the 4-helix bundle via only a single bis-histidyl site. An example of such a prosthetic group (synthesized and characterized by Prof. Michael Therien's research group in the Chemistry Department at the University of Pennsylvania) is shown, symmetric in this instance, with its anticipated location within AP0; the hydrophobic domain of the bundle is shown in green. The changes (red-shifts) in the rich electronic spectrum of this prosthetic group upon binding to the peptide are also shown. In addition, the vectorial incorporation of this symmetric prosthetic group into the amphiphilic 4-helix bundle via a single bis-histidyl site breaks the symmetry, which should result in an exceptionally large molecular hyperpolarizability, as exhibited by closely related asymmetric, extended π-electron systems. The vectorial orientation of the 4-helix bundles in a two-dimensional ensemble at an interface between polar and non-polar media should then allow large second-order non-linear optical phenomena to be generated at the interface.

The Crystal Structure of Activated Protein C-Inactivated Bovine Factor Va: Implications for Cofactor Function

T.E. Adams[1], M.F. Hockin[2], K.G. Mann[2], and S.J. Everse[1]

[1]Department of Biochemistry, University of Vermont; [2]Department of Human Genetics, Howard Hughes Medical Institute, University of Utah

Within the blood coagulation cascade, the process by which blood clots, factor Va serves as an essential protein cofactor for the efficient generation of thrombin, the primary blood-clotting enzyme. Upon the formation of the prothrombinase complex with factor Xa on a membrane surface, factor Va increases the catalytic efficiency of factor Xa 300,000-fold. The crystal structure of activated protein C (APC)-inactivated factor Va (Va_i) is the first view of this multi-domain cofactor and begins to address questions regarding its mechanism, including membrane binding, chain association, and complex assembly.

The majority of deaths throughout the world can be either directly or indirectly attributed to an imbalance in hemostasis, which leads to thrombosis – a blood clot. Under normal circumstances hemostasis is defined as the process that stops bleeding by activating the blood coagulation cascade. An action central to this cascade is the catalytic acceleration of each step through the assembly of the vitamin K-dependent enzyme complexes. This culminates in the conversion of prothrombin, an inactive zymogen in blood plasma, to its enzyme counterpart, thrombin, by the *prothrombinase* complex.

Factor V circulates in the plasma as a pro-cofactor comprised of six domains (A1-A2-B-A3-C1-C2). Thrombin activates factor V by excising the B domain, forming the heterodimer factor Va, composed of a heavy chain (A1-A2) and a light chain (A3-C1-C2) associated in a calcium-dependent manner. During the initial stages of coagulation, factor Va actively recruits the enzyme, factor Xa, and the substrate, prothrombin, to the membrane surface of activated platelets. Condensation of this enzyme-substrate pair on a surface contributes to the explosive generation of thrombin observed *in vivo*. The reaction is regulated through the inactivation of factor Va by APC, which removes the A2 domain, forming factor Va_i and shutting down thrombin production. A common polymorphism in which a single APC cleavage site is removed, factor V^{Leiden}, significantly increases the risk of thrombosis by sustaining factor Va activity.

We recently solved the crystal structure of bovine factor Va_i. This structure reveals a novel domain architecture that suggests a new mechanism for cofactor function (**Figure 1**). Our structure includes two A domains (A1 & A3), each encompassing two plastocyanin-like folds, and two C domains (C1 & C2) with weak homology to the discoidin family of lipid-binding proteins. In fact, historical

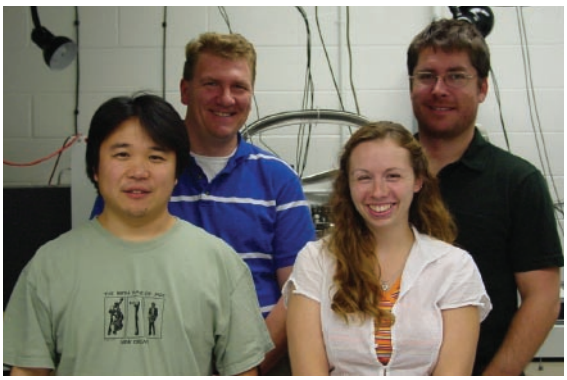

Authors (left to right)
Kihachiro Umezaki, Stephen J. Everse, Sara K. Briggs, and Ty E. Adams

BEAMLINES
X12C, X25

Funding
National Institutes of Health; American Society of Hematology Scholar Award; U.S. Department of Energy EPSCoR Fellowship; HHMI Support Program for Medical Schools

Publication
T.E. Adams, M.F. Hockin, K.G. Mann, and S.J. Everse, "The Crystal Structure of Activated Protein C-inactivated Bovine Factor Va: Implications for Cofactor Function," *Proc. Natl. Acad. Sci. USA*, **101**(**24**), 8918-23 (2004).

Contact information
Stephen J Everse
Department of Biochemistry, University of Vermont

Email: Stephen.Everse@uvm.edu

data concerning the membrane binding ability of factor V has been localized to the C domains, primarily the C2 domain, and previous hypothetical models have proposed that membrane interaction is mediated strictly by the C2 domain. However, we found that the C domains in factor Va_i are oriented in such a way that both domains may potentially interact with the membrane.

At the base of each C domain, several loops adopt an extended conformation and expose several hydrophobic residues at the apex of these loops (**Figure 2**). In the literature, these loops are referred to as "spikes" and have been postulated to be critical phospholipid-binding sites. Indeed, mutations of these loops within the C2 domain have been shown to reduce or knockout cofactor activity. Recent information has also shown that mutation of key hydrophobic residues within the spikes of the C1 domain decreases the membrane binding potential and activity of the cofactor. Along with our structure, this suggests that the C1 domain is important for membrane interaction and cofactor function.

Our structure provided the first glimpse into how this cofactor, as well as the homologous cofactor factor VIII, functions in coagulation. We can now use this information to develop improved methods of controlling coagulation *in vivo* for the treatment of thrombosis in such cases as factor V^{Leiden} and explain hemophilia in various factor VIII mutations.

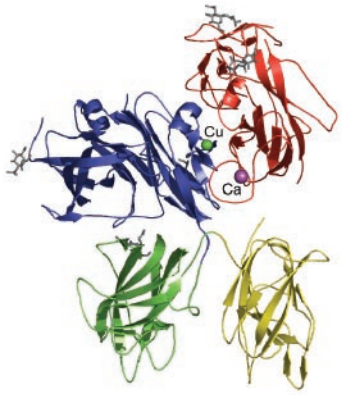

Figure 1. Ribbon diagram of the structure of bovine factor Va_i (PDB ID code 1SDD). The domains are colored as follows: A1 (red), A3 (blue), C1 (green), and C2 (yellow). The two metal ions, calcium and copper, are shown as magenta and green spheres, respectively. The five carbohydrates are shown in grey as ball-and-stick.

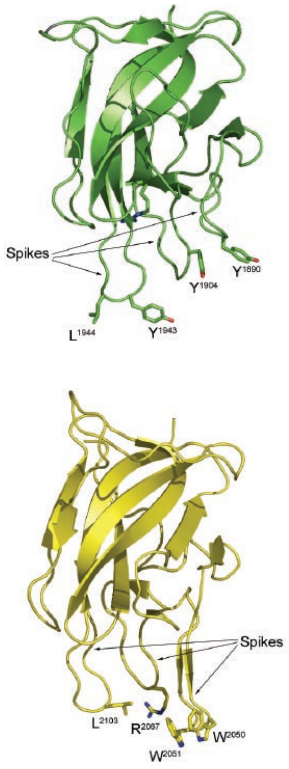

Figure 2. Membrane binding domains. The three loops that compose the "spikes" in each domain are marked with arrows. Residues important for membrane interaction are shown as ball-and-stick.

An Asymmetric Complex of Restriction Endonuclease MspI on its Palindromic DNA Recognition Site

Q.S. Xu[1], R.B. Kucera[2], R.J. Roberts[2], and H.-C. Guo[1]

[1]Department of Physiology and Biophysics, Boston University School of Medicine; [2]New England Biolabs

Most well-known restriction endonucleases recognize palindromic DNA sequences and are classified as Type IIP. Due to the recognition and cleavage symmetry, Type IIP enzymes are usually found to act as homodimers in forming two-fold symmetric enzyme-DNA complexes. Now we find an asymmetric complex of the Type IIP restriction enzyme MspI in complex with its cognate recognition sequence. Unlike any other type IIP enzyme reported to date, a MspI monomer and not a dimer binds to a palindromic DNA sequence. The enzyme makes specific contacts with all four base pairs in the recognition sequence. This MspI-DNA structure represents the first example of asymmetric recognition of a palindromic DNA sequence by two different structural motifs in one polypeptide.

Restriction endonucleases (REases) are enzymes that recognize specific DNA sequences and cleave at the sugar-phosphate backbone of DNA. They are components of restriction-modification systems that protect bacteria from invasive foreign DNA. However, REases are best known for their roles in recombinant DNA technology and genetic manipulation. More than 3,570 REases with 240 unique specificities have been biochemically characterized. Of the 588 commercially available REases, a great majority recognize double-strand DNA sequences of 4-8 base-pairs with a dyad axis of symmetry, called palindromes. In the presence of Mg^{2+}, these REases cleave both strands of the DNA at fixed symmetrical locations to generate cohesive or blunt ends suitable for molecular cloning. These symmetrically cleaving enzymes are grouped into a subtype, called Type IIP. Biochemical and structural evidence for several Type IIP prototype enzymes indicate that they form symmetric dimers or tetramers to recognize their palindromic recognition sequences. One of these Type IIP Reases, known as MspI, produces a different cleavage pattern from those of known structures. It recognizes the palindromic tetranucleotide sequence 5'-CCGG and cleaves between the first and second nucleotides, leaving two-base cohesive 5' overhangs.

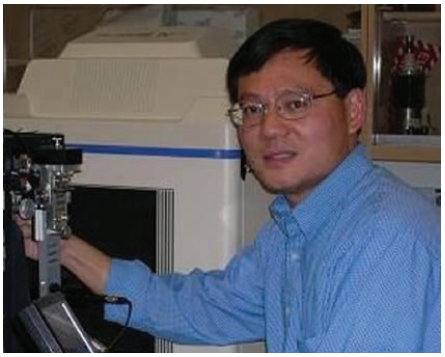

We recently reported the crystal structure of an MspI-DNA complex at 1.95 Å resolution, using a combination of multiple isomorphous replacement with anomalous scattering (MIRAS) and multiwavelength anomalous diffraction (MAD) methods. This represents the first crystal structure of a restriction enzyme that recognizes a tetranucleotide sequence. Unexpectedly, MspI interacts with the palindromic

Authors (from top)
Qian Steven Xu and Hwai-Chen Guo

BEAMLINES
X4A, X12C

Funding
National Institutes of Health

Publication
Q.S. Xu, R.B. Kucera, R.J. Roberts, and H.-C. Guo, "An Asymmetric Complex of Restriction Endonuclease MspI on its Palindromic DNA Recognition Site," *Structure,* **12**, 1741-1747 (2004).

Contact information
Hwai-Chen Guo
Department of Physiology and Biophysics, Boston University School of Medicine

Email: hcguo@bu.edu

recognition sequence as a monomer (**Figure 1**). As a result, two symmetric half-sites of DNA are recognized asymmetrically by the MspI monomer (**Figure 2**). Together, there are six direct and five water-mediated hydrogen bonds from the MspI monomer to the four base-pair recognition sequence, which nearly saturates the hydrogen-bonding potential in the major groove of the recognition site. In addition, the two dyad-related half-sites on DNA make asymmetric van der Waals contacts with different motifs in one MspI polypeptide. Although homodimers had been previously reported to bind pseudo-palindromic DNA sequences asymmetrically, the MspI-DNA complex represents the first structure of a palindromic DNA sequence bound by an asymmetric protein monomer.

The observation of a monomeric MspI-DNA complex in crystals (where MspI is in 18 mM concentration) suggests that such a unique DNA recognition by MspI is likely to occur in an optimal reaction solution where MspI concentrations are much lower (in the sub-μM range). Since there is only one catalytic site in an MspI monomer, some kind of enzyme dimerization or flipping is necessary to cleave both strands of DNA at the recognition site. It is thus plausible that MspI binds to its recognition sequence through the monomer-DNA intermediate captured in the crystals, and then proceeds to a final homodimer-DNA complex (**Figure 3**) responsible for symmetrical cleavage of both strands of DNA. Alternatively, MspI may achieve double-strand DNA cleavage by bringing together two monomers bound on two separate recognition sites, similar to the model proposed for the Type IIS REase FokI that recognizes a specific asymmetric DNA sequence. A third possibility is that MspI undergoes some conformational rearrangements to use a single active site to sequentially cut both DNA strands, similar to that proposed for BfiI, another Type IIS REase.

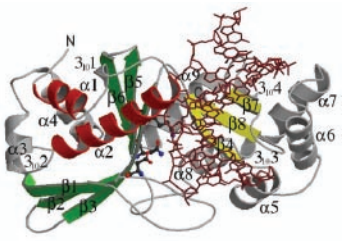

Figure 1. The tertiary structure of the MspI-DNA complex. The enzyme is represented as ribbons and the DNA as a brown stick model. Secondary structure elements of MspI are labeled and the conserved structural core is colored in red for N-terminal helices, green for the five-stranded central β-sheet, and yellow for the β-sheet involved in DNA recognition. Side chains of the catalytic site residues (Asp99, Asn117, and Lys119) are shown as ball-and-stick representations with carbons in black, nitrogens in blue, and oxygens in red.

Figure 3. The relationship between a putative MspI dimer and the crystallographic dimer in the MspI-DNA cocrystal. The enzymes are represented as ribbons and the DNAs as stick models. In the crystal, two MspI monomers (green and red) bind to two separate recognition sequences (brown and blue). To generate a putative dimer (gold and red), the red monomer was rotated 180° along the dyad axis (perpendicular to the paper plane) of the palindromic DNA (blue).

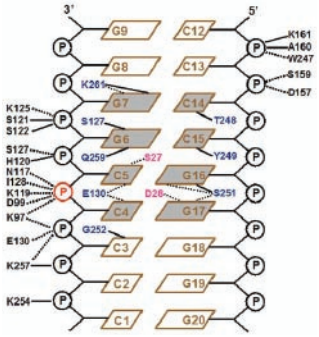

Figure 2. Schematic diagram of hydrogen bonding between MspI and DNA. The DNA recognition sequence is shaded in gray, with the scissile phosphate (C4-C5) circled in red. One DNA base pair (G10:C11) is omitted in the final model. Blue and pink represent amino acids that bind to DNA bases in the major and minor groove, respectively. Amino acids that bind to the phosphate backbone of DNA are colored in black. Solid and dotted lines represent direct and water-mediated hydrogen bonds, respectively.

Orientation and Crystallization of Natural Rubber Network as Revealed by WAXD Using Synchrotron Radiation

M. Tosaka[1], S. Murakami[1], S. Poompradub[1], S. Kohjiya[1], Y. Ikeda[2], S. Toki[3], I. Sics[3], and B.S. Hsiao[3]

[1]Institute for Chemical Research, Kyoto University, Japan; [2]Kyoto Institute of Technology, Matsugasaki, Japan; [3]Department of Chemistry, Stony Brook University

The tough elastic properties of natural rubber (NR) are thought to originate from its ability to crystallize rapidly upon stretching, which has been known since the 1920s. However, the growth mechanism of the strain-induced crystallites for cross-linked NR has only been revealed by our recent in-situ x-ray study of NR under uniaxial deformation. On the basis of these results, a new mechanism for strain-induced crystallization has been proposed.

Natural rubber (NR) is a biomass produced from *Hevea* trees. It is an indispensable material for many industrial and household applications, due to its outstanding tensile strength and crack growth resistance, which can be attributed to its ability to rapidly crystallize upon elongation. The main constituent of NR is cis-1,4-polyisoprene, which has a near-perfect sequence of cis structures – only one or two trans structures are found at both ends of a molecular chain (where cis and trans are the two types of polymer configurations). On the other hand, synthetic cis-1,4-polyisoprene (IR) always contains a few percent of trans structures, which are randomly positioned along the molecular chains. As a result, IR is not as strong as NR.

The x-ray diffraction pattern of stretched NR was reported in the1920s, prior to the acknowledgment of "macromolecules" or polymers. Though the knowledge of NR strain-induced crystallization was recognized long ago, the crystal growth mechanism in NR that is cross-linked (i.e. includes an additive that bridges the NR chains, giving the material the ability to retrieve its original shape after large deformation) has not been clear for the past eight decades.

In our study, the morphological features of strain-induced crystallites in NR were studied in real time. A series of NR samples with different crosslinking densities were continuously deformed using a custom-made stretching machine. We recorded two-dimensional wide-angle x-ray diffraction (WAXD) patterns during the deformation process with a MAR-CCD camera at beamline X27C.

By analyzing the WAXD patterns along with the tensile response of the NR samples, we recognized several interesting new features. First, even at the onset of crystallization, the NR crystallites were highly oriented. On the other hand, a strong isotropic amorphous halo persisted even when the sample was elongated up to eight times the initial

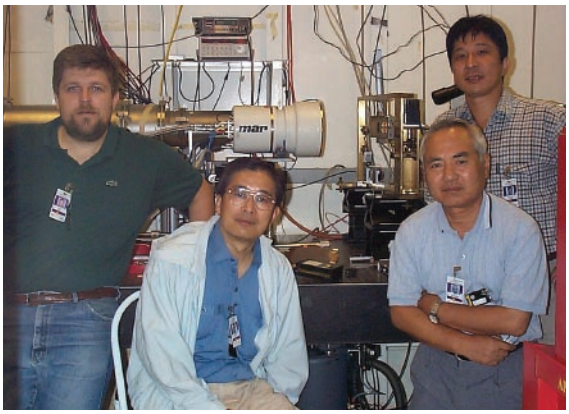

Authors (left to right)
Igors Sics, Shigeyuki Toki, Syozo Murakami, and Masatoshi Tosaka

BEAMLINE X27C

Funding
Japan Society for the Promotion of Science; National Science Foundation; U.S. Department of Energy

Publication
M. Tosaka, S. Murakami, S. Poompradub, S. Kohjiya, Y. Ikeda, S. Toki, I. Sics, and B. Hsiao, "Orientation and Crystallization of Natural Rubber Network as Revealed by WAXD using Synchrotron Radiation," *Macromolecules*, **37**(**9**), 3299-3309 (2004).

Contact information
Masatoshi Tosaka
Instructor, Institute for Chemical Research Kyoto University, Uji, Japan

Email: tosaka@scl.kyoto-u.ac.jp

length. The onset strain of crystallization upon elongation was almost independent of the cross-linking density. We also observed that the sample with the higher cross-linking density showed the smaller lateral crystallite size and that the crystal lattice was almost linearly deformed in response to nominal stress.

Based on these results, we proposed a model for the strain-induced crystallization (**Figure 1**). When the rubber sample is stretched, some molecular chains are highly extended, while most of the chains remain in the almost randomly coiled state. Upon further elongation, the melting temperature of the sample increases due to entropic changes, and is independent of the cross-linking density. When the melting temperature exceeds the ambient temperature, the system enters a supercooled state and oriented crystallites form immediately on the stretched chains. The molecular chains that are consumed by the crystal growth are supplied by the surrounding coiled chains. In this way, the higher the cross-linking density, which results in dense crystallites, the smaller the lateral crystallite size. As a result of crystallization, an elongated macromolecule coil would be converted into a series of crystalline portions comprised of straight chain segments, and an amorphous portion comprised of coiled chain segments. The entropy of the amorphous portion will increase, while the degree of supercooling (the difference between the ambient temperature and the melting temperature) will decrease. However, further crystallization would be hindered without increasing the supercooling by additionally elongating the sample. The persistence of an almost isotropic amorphous halo in the WAXD pattern of highly strained NR samples can be explained by this model.

The deformation of the crystal lattice indicates that the crystalline portion can bear the stress and act as a nanometer-sized reinforcing filler. As the crystallites appear in response to the mechanical load on NR, the strain-induced crystallization can be regarded as "smart *in-situ* nanocompounding."

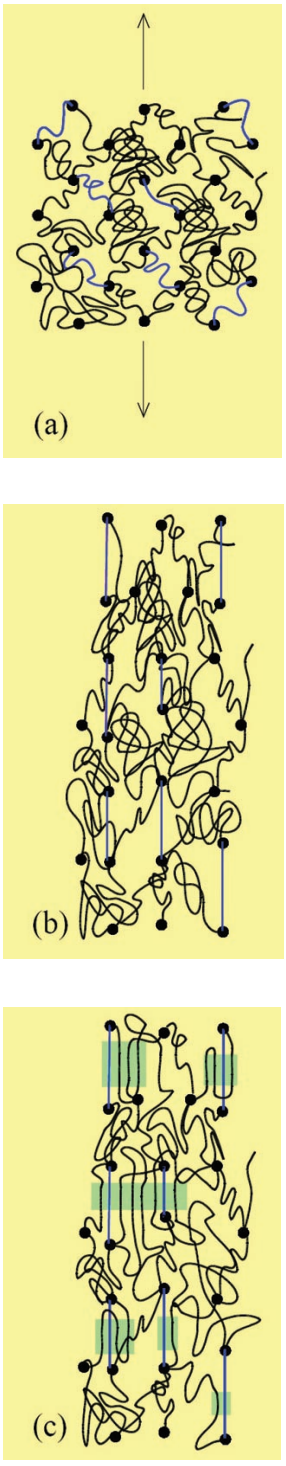

Figure 1. A model of the strain-induced crystallization in vulcanized NR. Relatively short chains are drawn as blue lines. Filled circles represent crosslinks. (a) Before deformation. (b) After deformation: Short chains are fully stretched. (c) Crystallites are grown from the stretched chains (green parts).

Tuning Substrate Surface Energies for Blends of Polystyrene and Poly (Methyl Methacrylate)

D.A. Winesett[1], S. Story[1], J. Luning[2], and H. Ade[1]

[1]Dept. of Physics, North Carolina State University; [2]Stanford Synchrotron Radiation Laboratory

We have developed and characterized three simple and inexpensive ways to make substrate surfaces that are neutral, i.e. that have the same interfacial energy, for polystyrene (PS), a common hard plastic, and poly (methyl methacrylate) (PMMA), a commercial plastic. In the first two of these surface treatment methods, two different high molecular-weight copolymers made of styrene and methyl methacrylate were absorbed onto hydroxylated silicon oxide. In another method, octyltrichlorosilane (OTS), a highly hydrophobic material, was covalently bonded onto hydroxylated silicon, a highly hydrophilic surface. A fourth method covalently attached hydroxyl-terminated, miscible, low molecular-weight homopolymers of PS and PMMA to the substrate. We found that the OTS treatment is advantageous because a gradient of continuous interaction can be created. Nonetheless, the principles of each method should be applicable to other polymer systems.

The ability to adjust the interactions between a material or a molecule and a substrate is desirable for a number of applications. This includes nano-patterning, sensing, and the dewetting and phase segregation in two-dimensional systems of polymer blends at elevated temperatures. In polymer blends, differences in interfacial energies, which reflect a preferential interaction, generally cause one polymer to segregate to the substrate or air interface. This segregation has to be avoided in a number of applications, and is prevented by tuning the polymer/substrate interfacial properties.

Homopolymer blends of polystyrene (PS) and poly (methyl methacrylate) (PMMA) of relatively low molecular weight (10,000 to 200,000 g/mol) make excellent model systems for a number of studies. Both polymers exhibit comparable glass transition temperatures (temperatures below which a polymer becomes hard and brittle) of approximately 102 to 120 degrees Celsius (°C) and are readily codissolved in a common solvent. Moreover, for typical annealing temperatures (140°C to 180°C), the interfacial tension between PS and PMMA is larger than the absolute value of the difference between the surface energies of PS and PMMA. Hence, neither polymer can spread onto the other at an air interface. A polymer-air interface might thus be one of two "neutral" interfaces that can be used to produce a two-dimensional system. A "neutral" substrate surface will provide the second defining interface.

Authors (clockwise from top left)
Harald Ade, Steve Story, Andy Winesett, and Jan Luning

Thin polymer films are often cast on silicon substrates. At elevated temperatures, it is well established that the PMMA in a PS/PMMA blend will quickly segregate to the

BEAMLINE X1A

Funding
National Science Foundation

Publication
D.A. Winesett, S. Story, J. Luning, and H. Ade,"Tuning Substrate Surface Energies for Blends of Polystyrene and Poly (Methyl Methacrylate)," *Langmuir*, **19**, 8526-8535 (2003).

Contact information
Harald Ade
Dept. of Physics, North Carolina State University

Email: harald_ade@ncsu.edu

native silicon oxide (SiO_x) interface to form a wetting layer. In order to avoid and/or control this segregation, the effectiveness of several simple surface energy tuning methods has been tested. Using a standard UV/O_3 process, in which ultraviolet light is used to produce ozone and oxygen radicals in the air that removes carbon from surfaces, silicon substrates were cleaned and simultaneously activated to produce –OH groups on their surfaces. They were subsequently treated with either a commercial random copolymer, P(S-*ran*-MMA), an alternation copolymer, P(S-*alt*-MMA), a partial or gradient n-octyltrichlorosilane (OTS) self-assembled monolayer, or a brush of a hydroxyl (–OH)-terminated low molecular-weight PS/PMMA blend with varying PS/PMMA composition. The relative effectiveness of all four methods was characterized using optical microscopy, Near Edge X-ray Absorption Fine Structure (NEXAFS) microscopy and spectroscopy, atomic force microscopy, and contact angle measurements.

The optical micrographs in **Figure 1** clearly show that very different morphologies develop, depending on the surface treatment. The P(S-*ran*-MMA)-treated surface shows a semi-bicontinuous morphology, wherein the two material phases are partially continuous across the whole sample. However, the untreated SiO_x surface and the P(S-*alt*-MMA)-treated surface show large droplets. Therefore, the P(S-*alt*-MMA) treatment clearly failed. To verify that the P(S-*ran*-MMA) treatment was successful, NEXAFS microscopy was used to quantitatively map the thickness of the PS and PMMA phases on P(S-*ran*-MMA)-treated silicon nitride (Si_3N_4) membranes (**Figure 2**). The results show that the morphology is essentially two-dimensional in nature, with a relatively uniform film thickness and domains of PS and PMMA that span the entire film thickness.

Our specific interests and studies on "neutral" surfaces were restricted to surfaces that would have the same interfacial energy for PS and PMMA. Hydroxy-terminated PS and PMMA is the most novel approach investigated. Except for the P(S-*alt*-MMA) treatment, all of the methods yielded neutral or near-neutral surfaces. The OTS treatment has the advantage that a gradient of continuous interaction ranging from preferential PMMA to preferential PS interactions can be created. However, the principles of all the methods developed should be applicable to other polymer systems.

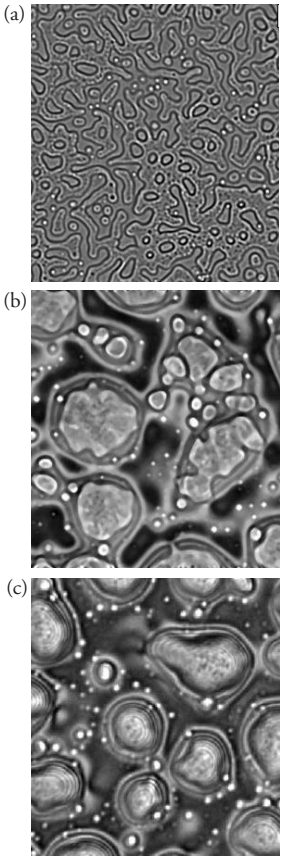

Figure 1. Optical micrographs of a PS_{21k}/$PMMA_{22k}$ blend film, spun to a thickness of 500 nm and annealed in vacuum at 170°C for 250 minutes on three types of surfaces: (a) SiO_x -OH surface treated with 270,000 g/mol P(S-ran-MMA), (b) SiO_x-OH surface treated with 108,000 g/mol P(S-alt-MMA), (c) Si-OH surface with no polymer treatment. The field of view in all three micrographs is 100 µm x 100 µm.

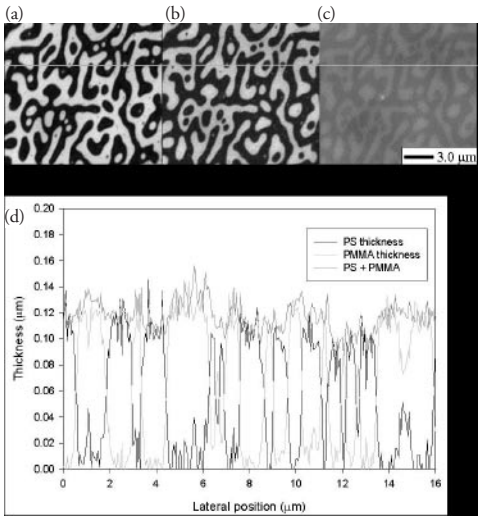

Figure 2. Quantitative STXM thickness maps of equal weight percent blend of PS_{21k}/$PMMA_{22k}$ annealed at 153°C for 1 hour on Si_3N_4 treated with 270,000 g/mol P(S-ran-MMA). (a) PS map (b) PMMA map (c) PS + PMMA map (d) The line profile of the thickness maps.

Block Copolymer Domain Reorientation in an Electric Field: An *In-Situ* Small-Angle X-ray Scattering Study

T. Xu[1], J. DeRouchey[1], T. Thurn-Albrecht[1], T.P. Russell[1], and R. Kolb[2]

[1]Department of Polymer Science and Engineering, University of Massachusetts; [2]Exxon Mobil Research

The electric field alignment of block copolymer thin films from an orientation nearly parallel to the substrate to an orientation normal to the substrate was investigated using in-situ small angle x-ray scattering (SAXS). An analysis of the scattering patterns indicated that, during alignment of the lamellar microdomains, the material goes through an intermediate state with substantially reduced order. After orientation, the sample consists of many small grains with the lamellae oriented parallel to the electric field and a random orientation in the plane perpendicular to the field.

Block copolymers, comprised of two chemically distinct polymers covalently linked at one end, self-assemble into well-ordered arrays of nanoscopic elements, ranging from spheres to cylinders to lamellae, depending on the volume fraction of the components. The size of the domains can be easily tuned by varying the molecular weight of the copolymer. However, it is imperative to control the orientation of these self-assembled morphologies, and the use of an external electric field has proven to be an effective method to achieve this. Nanoporous films with aspect ratios in excess of 300 have been successfully made by orienting the domains in thin block copolymer films and selectively removing one component. The subsequent electrodeposition of metal into these nanopores produces arrays of high-aspect ratio nanowires that are attracting substantial attention as candidates for high-density magnetic storage media. Understanding the mechanism by which the nanoscopic domains are aligned by an electric field is the key to optimizing their use.

Figure 1 shows the orientation of cylindrical domains of a diblock copolymer under an applied electric field. Starting from an ordered state with cylinders parallel to the surface, the applied electric field enhances fluctuations at the interfaces between the domains and at the matrix where the fluctuations have a wavelength comparable to L_o, the center-to-center distance between the cylindrical domains. The enhancement in the fluctuations leads to a disruption of cylindrical domains, the formation of spherical domains, the deformation of these spherical domains into ellipsoids, and the eventual reformation of nanoscopic cylinders highly oriented in the field direction. In-situ small angle x-ray scattering (SAXS) provides an ideal means of characterizing the orientation of the domains and elucidating the mechanism by which the orientation occurs. Two different copolymers were studied: one with cylindrical domains and the other with lamellar nanoscopic domains. Here, we discuss the orientation of lamellae due to geometric simplicity.

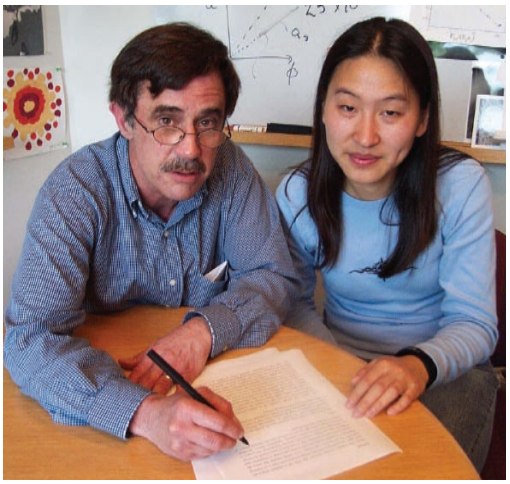

Authors (left to right)
Thomas Russell and Ting Xu

Figure 2 shows the azimuthal angular (Ω) dependence of the

BEAMLINE X10A

Funding
U.S. Department of Energy, Office of Basic Energy Sciences; Army Research Lab; National Science Foundation – Materials Research Science and Engineering Center

Publication
J. DeRouchey, T. Thurn-Albrecht, R. Kolb, and T.P. Russell, "Block Copolymer Domain Reorientation in an Electric Field: An *in-Situ* Small-Angle X-ray Scattering Study", *Macromolecules*, **37**(**7**), 2538 (2004).

Contact information
Thomas P. Russell
Department of Polymer Science and Engineering, University of Massachusetts

Email: russell@mail.pse.umass.edu

time-resolved SAXS pattern of an ordered, symmetric diblock copolymer, polystyrene-*b*-polyisoprene film (~ 80-120μm in thickness), that was heated above the glass transition temperature of both blocks under an applied electric field. Four distinct SAXS patterns were seen in the experiments that characterized different stages of the orientation. The sequence of patterns (**A-D**) arises from the re-orientation of the lamallar domains from nearly parallel to the substrate (**A, B**) to normal to the substrate (**D**). Curve **C**, however, revealed an unexpected result in which the azimuthal dependence of the SAXS was lost. This, coupled with a shift in the peak to higher scattering vectors (smaller spacing) and a broadening of the peak, suggests, contrary to the results from simulations, that the block copolymer domains disorder or are broken-up, and then reform in the presence of the field. These reformed domains are highly oriented in the direction of the applied field. Thus, the time-resolved SAXS pattern revealed an unexpected disordering of the copolymer.

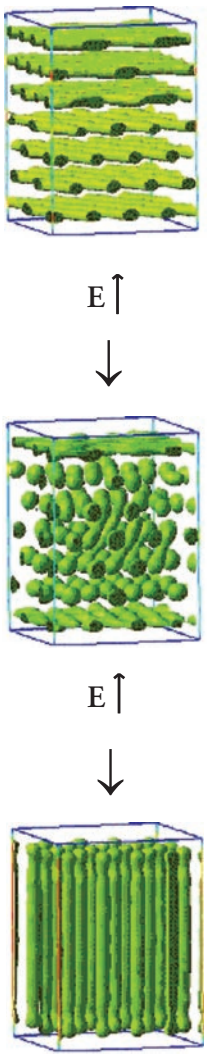

Figure 1. Simulation of the alignment of cylindrical microdomains under an electric field based on the dynamic self-consistent field (courtesy of A. Zvelindovsky).

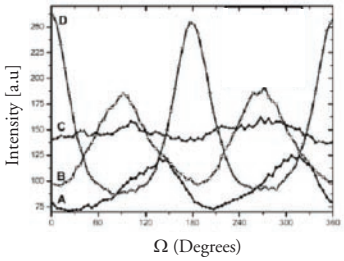

Figure 2. Azimuthal angular dependence of the scattering pattern integrated over the full width of the Bragg reflection of a lamellar PS-*b*-PI film under an 18 V/μm applied field. The film is tilted at a 45° angle. Four distinct SAXS patterns (A-D) are shown.

Time-Resolved Small-Angle X-ray Scattering Study of the Kinetics of Disorder-Order Transition in a Triblock Copolymer in a Selective Solvent for the Middle Block

H. Nie[1], R. Bansil[1], K. Ludwig[1], M. Steinhart[2], C. Konak[2], and J. Bang[3]

[1]Department of Physics, Boston University; [2]Institute of Macromoleculear Chemistry, Academy of Sciences of the Czech Republic; [3]Department of Chemical Engineering & Materials Science, University of Minnesota

Solutions of block copolymers in solvents that selectively dissolve one of the component polymers form micelles with the insoluble component in the cores. These complex fluid or gel states exhibit a rich phase diagram with many different ordered structures. Understanding the phase behavior and kinetics of these materials is of considerable importance to controlling their properties. We reported the first time-resolved small angle x-ray scattering (SAXS) study on the kinetics of the formation of a bcc ordered state from a disordered micellar fluid in solutions of Kraton, a commercial triblock copolymer. Our studies reveal a two-stage process that shows significant change of the micelle's size at the onset of ordering.

Solutions of multi-block copolymers exhibit rich phase diagrams and novel morphologies, and can form clusters, networks, and gels. These properties determine their numerous applications, such as detergents, adhesives, elastomers, bio-mimetic vesicles, and templates for nanomaterials. The phase behavior and properties of these materials can be tuned by varying the number of component polymers and blocks, the chemical composition and length of the blocks, and the blocks' interactions with solvents. For example, an ABA triblock copolymer solution in a solvent that is good for the outer (A) block forms isolated micelles with cores containing the B block. On the other hand, in a solvent that is good for the middle B block, loops or bridges will be formed and the middle block can tether two adjoining micelles, eventually forming a network. The micelles, which can be either spherical or cylindrical, either exist as a complex fluid or form ordered structures, such as cubic or hexagonal. Our focus is to understand the kinetics of the phase transitions between the different disordered and ordered states of the micellar phases of these solutions. Since the micellar cores are on nanometer-length scales and the phase transitions occur on the time scale of minutes, synchrotron based time-resolved small angle x-ray scattering (SAXS) is an ideal tool for examining their structure and kinetics.

A few SAXS studies of the kinetics of order-order and order-disorder transitions in melts of block copolymers have been reported. To the best of our knowledge, our recent publication is the first temperature jump study of isothermally evolving kinetics in solutions of triblocks. We examined the disorder-order transition kinetics of a styrene (S) ethylene-co-butylene (EB) triblock

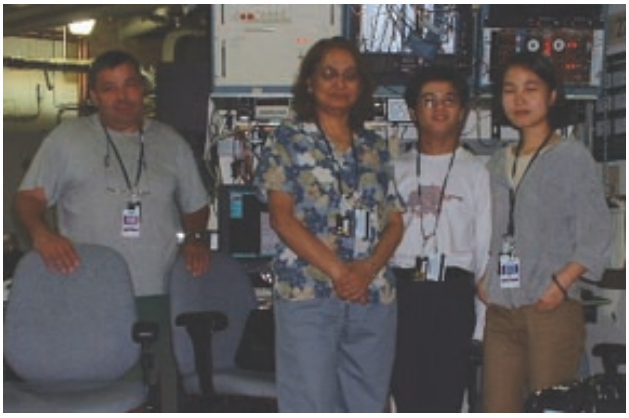

Authors (left to right)
Milos Steinhart, Rama Bansil, Minghai Li, and Huifen Nie

BEAMLINE X27C

Funding
National Science Foundation Division of Materials Research; National Science Foundation U.S.-Czech Collaborative Research Grants; Grant Agency of the Academy of Sciences of the Czech Republic; Grant Agency of the Czech Republic

Publication
H. Nie, R. Bansil, and K. Ludwig, "Time-Resolved Small-Angle X-ray Scattering Study of the Kinetics of Disorder-Order Transition in a Triblock Copolymer in a Selective Solvent for the Middle Block," *Macromolecules,* **36**, 8097-8106 (2003).

Contact information
Rama Bansil
Department of Physics, Boston University

Email: rb@bu.edu

copolymer, SEBS, in mineral oil, which preferentially dissolves the middle EB block. This commercial thermoplastic elastomer from Shell, known as Kraton®, is used in footwear, adhesive sealants and coatings, roofing, and packaging. Using the high flux monochromator at beamline X27C and a one-dimensional wire detector, we were able to measure the scattered intensity I(q) as a function of the wavenumber, q, with a time resolution of 10 seconds over the q-range 0.01 to 0.3 $Å^{-1}$, and thus follow the kinetics of the micellar fluid's ordering onto a bcc lattice. The transition was typically followed either by ramping the temperature over a wide range (**Figure 1**) or by rapidly quenching the sample temperature into the ordered phase (**Figure 2**). The temperature ramp experiment identifies the phase transition temperature, while the temperature quench experiment provides the isothermal kinetics. A model based on interacting hard spheres was used to analyze the data and provide detailed information about the time evolution of the micellar structural parameters during the ordering process. For example, the results showed that the core radius decreased sharply at the onset of the ordering process (**Figure 3a**). The kinetics exhibits two stages corresponding to temperature equilibration and supercooling of the micellar fluid, followed by the nucleation and growth of the ordered state **(Figure 3b**). The induction-time for the onset of the second stage shows a minimum around the glass transition temperature of the polystyrene cores.

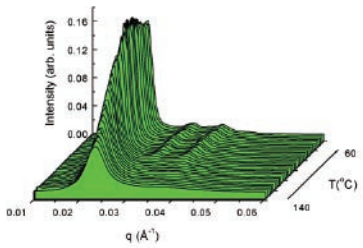

Figure 1. The development of Bragg peaks in the scattering intensity *I(q)* versus *q* during a cooling ramp from 140 to 60°C show a transition from a disordered micellar fluid at high temperatures to a bcc structure below about 120°C. The primary peak in the high-temperature data is due to the interacting micellar cores in the fluid phase.

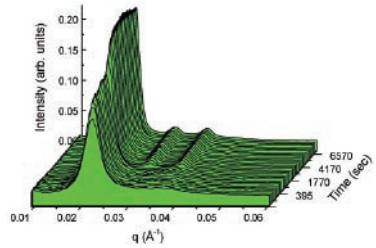

Figure 2. The time evolution of the scattering intensity *I(q)* versus *q* following a rapid jump from 140°C to 96°C shows the isothermal growth kinetics of the ordered bcc structure at the final temperature of 96°C. The delayed appearance of the higher Bragg peaks indicates a two-stage process. Note that the temperature of the sample equilibrates within 60 seconds following the jump.

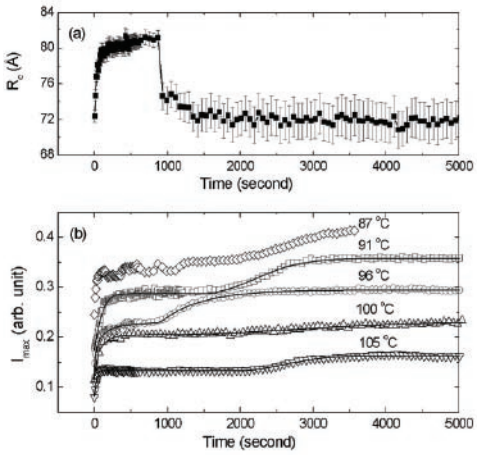

Figure 3. (a) The time evolution of the core radius R_c of the micelles following the quench from 140 °C to 96 °C shows a sudden decrease in the size of the micelle at the onset of ordering, at around 1000 seconds. (b) Temporal evolution of the primary peak's intensity following quenches from 140°C to different final temperatures, as indicated on the graph. The data reveal two stages in the ordering process. Note that the data are offset by different constants for visual clarity.

Low-Density Polymer Thin Film Formation in Supercritical Carbon Dioxide

T. Koga[1], Y.-S. Seo[1], J.L. Jerome[1], S. Ge[1], M.H. Rafailovich[1], J.C. Sokolov[1], B. Chu[1], O.H. Seeck[2], M. Tolan[3], and R. Kolb[4]

[1]Stony Brook University; [2]FZ Juelich GmbH, Institut fuer Festkoerperforschung, Germany; [3]Universitaet Dortmund, Experimentelle Physik I, Germany; [4]ExxonMobil Research and Engineering Company

We have developed a method for producing stable low-density polymer films using supercritical carbon dioxide ($scCO_2$). Two different molecular-weight polystyrene films with various thicknesses were exposed to $scCO_2$ along the density fluctuation ridge in a phase diagram. The swollen structures could be then frozen via the flash evaporation of CO_2 without forming additional large voids. X-ray reflectivity data clearly showed that exposure to $scCO_2$ could be used to produce uniform low-density films about $2R_g$ thick or less, where R_g is the radius of polymer gyration.

Increased miniaturization in the electronics industry has produced a need for highly uniform ultrathin polymer coatings with well-controlled optical and dielectric properties. Often the thickness of these films is commensurate with a few radii of gyration (R_g) of the polymer, and tight clearances impose very strict tolerances on surface roughness. This high degree of confinement therefore makes it difficult to satisfy the stringent uniformity requirements if we modify the electronic properties using standard gas foaming methods or blending it with other polymers or inorganic additives. Here we show a novel approach for producing stable, uniform, low-density polymer films using supercritical carbon dioxide ($scCO_2$).

$ScCO_2$ has long been known to be a "green" medium for polymer chemistry or material science. Unfortunately, its potential benefits have not been fully exploited since only a limited class of polymers can be dissolved in it. Recently, we have shown that a wide variety of polymer thin films can swell by as much as 30 to 60% when exposed to $scCO_2$ within a narrow temperature and pressure regime, known as the "density fluctuation ridge," even when the bulk miscibility of the films with $scCO_2$ is poor. In addition, we found that the *in situ* film quality, i.e. density, roughness, and film thickness, could be frozen via the flash evaporation of CO_2. We report x-ray reflectivity measurements in which the density profile of the vitrified films is measured directly and correlated with other properties, such as the dielectric constant, index of refraction, and surface glass transition.

Two kinds of polystyrene (PS), corresponding to molecular weights (M_w) of 2.0×10^5 and 6.5×10^5 g/mol, were used in this study. Thin films spun cast on cleaned Si substrates were placed in a high-pressure chamber containing $scCO_2$ at T = 36°C and P = 8.2 MPa, i.e. the ridge condition, for two hours and then quickly depressurized to atmospheric pressure within 10 seconds. The films were then characterized by x-ray reflectivity at beamline X10B. As shown in **Figure 1**, we found that the density of the films, which is obtained from a

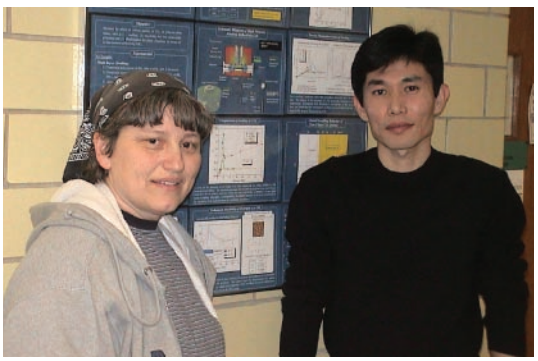

Authors (left to right)
Miriam Rafailovich and Tadanori Koga

BEAMLINE X10B

Funding
National Science Foundation

Publication
T. Koga, Y.-S. Seo, J.L. Jerome, S. Ge, M.H. Rafailovich, J.C. Sokolov, B. Chu, O.H. Seeck, M. Tolan, and R. Kolb, "Low-Density Polymer Thin Film Formation in Supercritical Carbon Dioxide," *Appl. Phys. Letts.*, **83**, 4309 (2003).

Contact information
Dr. Tadanori Koga
Department of Materials Science and Engineering, Stony Brook University

Email: tkoga@notes.cc.sunysb.edu

dispersion value in the x-ray refractive index, decreased from 23% to 13% by varying the thickness of both PS films. Furthermore, the data could be collapsed on a universal curve when the initial film thickness (L_0) was scaled by R_g (**Figure 1** inset). Hence, when confined as a thin film on a surface, thickness and molecular structure influence the density of the materials.

The reduction in density has several consequences affecting the material properties of the films. First, there is a decrease in its optical index of refraction (or dielectric constant). **Figure 2** shows the refractive indices (n_f) of the PS (M_w = 6.5×10^5 g/mol) films for the unexposed and two exposed films measured using spectroscopic ellipsometry. From the figure we can clearly see that the n_f values for the exposed films decreased with decreasing L_o values over the wide wavelength range. Second, there is a decrease in the glass transition temperature (T_g). In the **Figure 2** inset, we plot the modulation amplitude vs. T for unexposed and exposed PS thin films obtained using the Shear Modulation Force Microscopy technique. From the figure we can see that the discontinuity in the plot, which corresponds to T_g, occurs at T = 100°C for the unexposed film. The T_g value for the exposed film decreases by 10°C compared to that of the unexposed PS film.

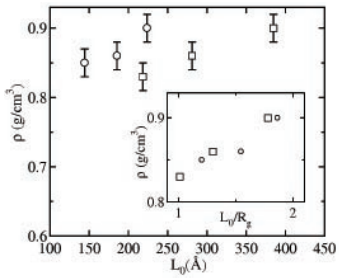

Figure 1. Density (ρ) vs. L_0 for the exposed films: PS (M_w = 2.0×10^5) (o), PS (M_w=6.5×10^5) (□). In the inset, L_0/R_g dependence of ρ is shown.

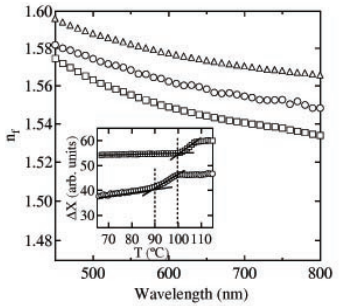

Figure 2. Index of refraction for PS (M_w = 6.5×10^5): before (Δ) and after (L_0 = $2R_g$ (o) and L_0 = $1.3R_g$ (□)). In the inset, X vs. T curves for PS films: exposed films L_0=$1.3R_g$ (o) and unexposed film (□).

Shear-Induced Crystallization Precursor Studies in Model Polyethylene Blends by *In-Situ* Rheo-SAXS and Rheo-WAXD

L. Yang[1], R.H. Somani[1], I. Sics[1], B.S. Hsiao[1], R. Kolb[2], H. Fruitwala[2], and C. Ong[3]

[1]Department of Chemistry, Stony Brook University; [2]ExxonMobil Research and Engineering Company; [3]ExxonMobil Chemical Company

The development of the shear-induced crystallization precursor structure of crystallizing, high molecular-weight binary polymer blends and non-crystallizing, low molecular-weight polyethylenes was investigated by in-situ rheo-small-angle x-ray scattering (SAXS) and wide-angle x-ray diffraction (WAXD) techniques. A "shish-kebab" structure, detected by both SAXS and WAXD, was observed in the blend containing the non-crystalline matrix of relatively higher viscosity, while only a twisted lamellar structure was seen in the rest of the blends. These results suggest that the matrix viscosity plays an important role in the formation of the crystallization precursor structure from the high molecular-weight chains under flow.

Prior to crystallization, the initially formed precursor structures, with a molecular orientation induced by flow during polymer processing – such as extrusion, injection molding, fiber spinning, and film blowing – can often dictate the subsequent morphology and, thus, the final properties of the polymer. Although extensive research on orientation-induced crystallization has been conducted, the nature of the earliest events during crystallization under flow is still not fully understood. In this study, a unique polymer blend system, inspired by studies of dilute polymer solutions under flow, was used to simulate the formation of precursor structures at the initial stage of flow-induced crystallization. In these blends, two low molecular-weight polyethylene copolymers, containing 2 mol % of hexene, with average molecular weights (M_w) of 50,000 (MB-50k) and 100,000 (MB-100k) and a polydispersity of 2, were used as the matrix material of different viscosity. A high molecular-weight polyethylene homopolymer with a Mw of 250,000 (MB-250k) and a polydispersity of 2, which is miscible with both low molecular-weight polyethylene matrices, was used as the crystallizing minor component. Two series of model blends, MB-50k/MB-250k and MB-100k/MB-250k, each containing weight ratios of 100/0, 97/3, 95/5, and 90/10, were prepared by solution blending to ensure thorough mixing at the molecular level. A Linkam CSS-450 high-temperature shear stage, modified for

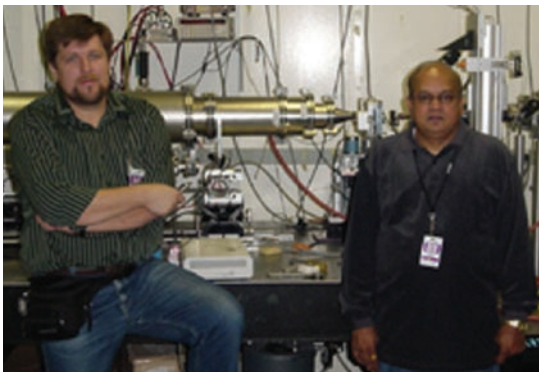

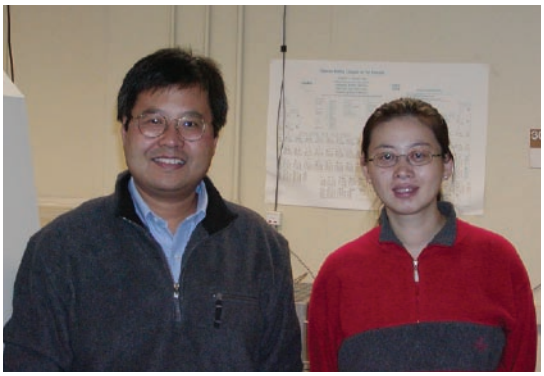

Authors (left to right)
(top) Igors Sics and Rajesh Somani,
(bottom) Benjamin S. Hsiao and Ling Yang

BEAMLINE X27C

Funding
National Science Foundation
ExxonMobil Company

Publication
L. Yang, R.H. Somani, I. Scis, B.S. Hsiao, R. Kolb, H. Fruitwala, and C. Ong, "Shear-Induced Crystallization Precursor Studies in Model Polyethylene Blends by *In Situ* Rheo-SAXS and Rheo-WAXD," *Macromolecules*, **37**(**13**), 4845-4859 (2004).

Contact information
Benjamin S. Hsiao
Stony Brook University

Email: bhsiao@notes.cc.sunysb.edu

in-situ x-ray scattering measurements, was used to control the shear conditions of the polymer samples. Two-dimensional WAXD and SAXS measurements (not measured simultaneously) were carried out at beamline X27C using a MAR CCD x-ray detector.

At the chosen shear conditions (rate = 60 s^{-1}, duration = 5 s, T = 120°C, which is greater than the melting point of the matrix), while no flow-induced structures were seen in pure MB-50k and MB-100k melts, the blends in both series showed distinct but different shear-induced structures. Our results indicate that the high molecular-weight MB-250k chains are responsible for the formation of crystallization precursor structures in the blend under shear, which can act as a template for further crystallization. A "shish-kebab" structure, detected by both WAXD (**Figure 1A**) and SAXS (**Figure 1B**), was observed in the MB-100k/MB-250k (90/10) blend, while only a twisted lamellar structure was seen in the rest of the blends under the same shear conditions. These findings suggest that the matrix viscosity plays an important role in influencing the formation of the crystallization precursor structure from the high molecular-weight chains under flow. The evolution of the shish-kebab structure from SAXS, consistent with the appearance of two equatorial (110) reflection peaks in WAXD, can be explained by the *coil-stretch* transition that is induced by flow. The observed "shish" is due to the extended chain crystallization of the stretched chains, whereas the kebabs are due to the folded chain crystallization of the coiled chains. In other blends, because the stretched chains could not aggregate rapidly, no detectable shish was observed. In the MB-100k/MB-250k (90/10) blend, the length of the shish was estimated from the equatorial streak in SAXS, and showed a noticeable decrease with time, possibly due to the relaxation of stress distribution or the overall crystal orientation.

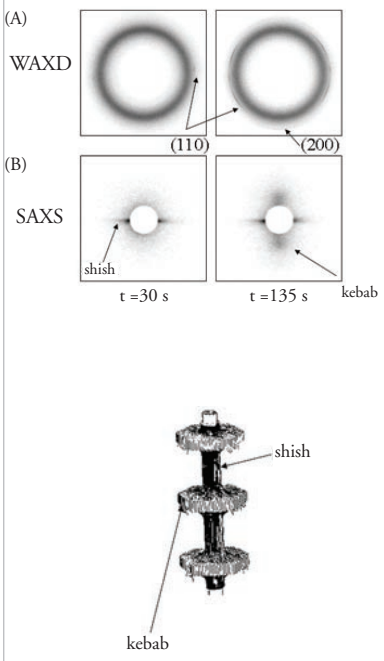

Figure 1. Selected two-dimensional (A) WAXD and (B) SAXS patterns, which illustrate the development of the "shish-kebab" morphology in the MB-100k/MB-250k (90/10) blend under shear (rate = 60 s^{-1}, duration = 5 s, T = 120 °C).

Influence of Crystallization Conditions on the Microstructure and Electromechanical Properties of Poly(Vinylidene Fluoride-Trifluoroethylene-Chlorofluoroethylene) Terpolymers

R.J. Klein[1], J. Runt[1,2], and Q.M. Zhang[1,2,3]

[1]Materials Research Institute; [2]Department of Materials Science and Engineering; and [3]Department of Electrical Engineering, The Pennsylvania State University

The crystallization process and its influence on the microstructure, ferroelectric, and electromechanical properties of a poly(vinylidene fluoride-trifluoroethylene-chlorofluoroethylene) (PVDF-TrFE-CFE) terpolymer were investigated. By varying the isothermal crystallization temperature T_x of this terpolymer, the ratio of ferroelectric crystal concentration to the concentration of relaxor ferroelectric crystal (a defect-modified class of ferroelectrics exhibiting strong electrostrictive behavior) can be determined. The higher T_x samples show an increased polarization hysteresis and reduced electric field-induced strain response. In addition, the experimental results, in combination with other reported results, indicate that CFE units are included in the crystalline lattice. Consequently, the influence of CFE on the ferroelectric behavior of the polymer is through the defects it induces in the crystal lattice.

Polymers for electromechanical applications offer many unique and inherent advantages when compared with other materials, being lightweight, flexible, and relatively easy to process and form into complicated shapes or large areas. We have examined one of these terpolymers, P(VDF-TrFE-CFE), and investigated how its ferroelectric and electromechanical responses are influenced by polymer crystallization processes in tandem with corresponding microstructure changes. We found that, by varying the crystallization temperature T_x, we can selectively vary the fraction of polar and non-polar crystallites in the crystalline phase. Crystallites formed during long periods of time at T_x exhibit less polar behavior. Crystallites formed during the rapid cooling process between T_x and room temperature exhibit stronger polar behavior. This is established most quantitatively by wide-angle x-ray diffraction (WAXD) and reinforced by Fourier transform infrared (FT-IR) spectroscopy, polarization loop, and electromechanical strain measurements. As will be shown, crystallizing the terpolymer at higher T_x values has an adverse effect on its electromechanical strain response.

X-ray data were collected in order to interrogate interchain spacing and, via x-ray peak width, the crystalline order perpendicular to the chain direction. For PVDF-TrFE copolymers in the ferroelectric phase, this peak corresponds to the (110, 200) reflection. The data were acquired at selected temperatures between room temperature and T_x (taken on heating) in order to follow the evolution of the microstructure. The x-ray data in the 2θ range of the (110, 200) reflection acquired at room temperature for ter-

Authors (left to right)
Kailiang Ren, Xuezhen Li, Yanyun Ma, Feng Xia, Sabrina Choudhury, Rob Klein, Qiming Zhang, and Cheng Huang

BEAMLINE X8A

Funding
The Office of Naval Research

Publication
R.J. Klein, J. Runt, and Q.M. Zhang, "Influence of Crystallization Conditions on the Microstructure and Electromechanical Properties of Poly(vinylidene fluoride-trifluoroethylene-chlorofluoroethylene) Terpolymers," *Macromolecules,* **36**, 7220-7226 (2003).

Contact information
Rob Klein
Penn State University

Email: rjk255@psu.edu

polymer films with different T_x are shown in **Figure 1a**.

For the terpolymer films with T_x at 112, 122, and 127°C, the x-ray data are relatively well characterized by a single peak at 14.7°, which represents the non-polar phase. The data fitting can be improved, however, by including a small peak at 15.3°, which is close to the position of the diffraction peak expected for the polar phase of the terpolymer's corresponding copolymer, PVDF-TrFE. As T_x is raised to 132 °C, this higher angle shoulder increases quite markedly, and the best fitting to the data is achieved by including two peaks, one near 15° and the other at 15.4°. **Figure 1b** summarizes the evolution of the x-ray peak positions as T_x is raised from 112 to 142°C. In comparison with the x-ray data for PVDF-TrFE, we deduced that the peak at the lower angle arises from the non-polar phase while the peaks at 15° and 15.4° indicate the presence of the polar phase component in the crystallites.

The importance of these x-ray peak assignments is seen in the electromechanical strain data for samples at the extremes of the T_x range. As shown in **Figure 2**, the terpolymer sample with a T_x of 112°C exhibits a field-induced strain of -5.9% at 133 MV/m (megavolts per meter), while for the sample with T_x of 142°C, the strain is reduced to -4.2% under the same field. The lower field-induced strain is due to existing ferroelectric domains that do not undergo the local conformation change upon application of the electric field. Thus, for better performance, a sample should be annealed near 112°C.

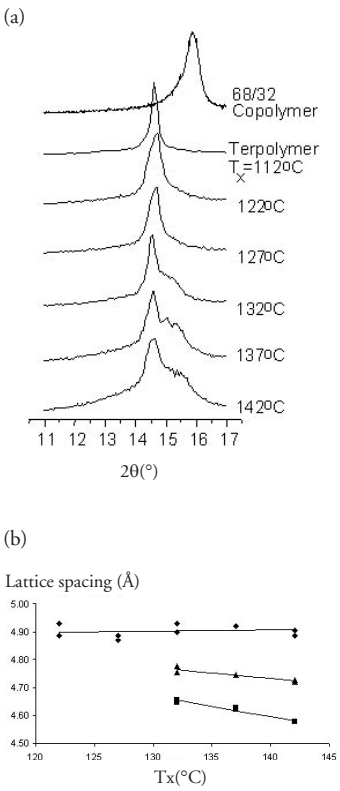

Figure 1. (a) X-ray data in the angular range of the (110, 200) reflection taken at room temperature for the terpolymers with different T_x, from which lattice constants are determined. (b) Lattice constants for the non-polar (4.9 Å) and polar (triangles and squares) components of the (110, 200) reflection measured at room temperature as a function of T_x. The data for the copolymer of similar composition are also shown. The x-ray wavelength is 1.2399 Å.

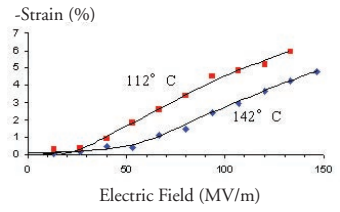

Figure 2. Thickness strain of the terpolymer as a function of the applied field for the terpolymer samples with T_x = 112 and 142 °C. The data were acquired at room temperature and 1 Hz AC field.

Year in Review

Brookhaven Town Supervisor John Jay LaValle Visits BNL

January 9, 2004

To learn more about research being done at BNL, which is one of Brookhaven Town's largest employers, Brookhaven Town Supervisor John Jay LaValle visited the Lab for the first time on December 15, 2003.

Laboratory Director Praveen Chaudhari welcomed LaValle and his office staffer Christopher Nuzzi, who both also met Michael Holland, DOE's Brookhaven Area Office Manager; Marge Lynch, Assistant Laboratory Director for Community, Education, Government & Public Affairs (CEGPA); and Jeanne D'Ascoli, CEGPA Community Relations Representative.

The visitors then toured part of the Lab, with a first stop at the National Synchrotron Light Source (NSLS). There, Associate Laboratory Director for Light Sources and NSLS Chair Steven Dierker gave an overview of how Lab scientists and some 2,500 researchers from across the nation and overseas who visit BNL annually use x-rays and ultraviolet and infrared light to make discoveries in biology and physics, chemistry and geophysics, materials science and medicine.

At beamline U10B at the National Synchrotron Light Source, researcher Lisa Miller explains to Brookhaven Town Supervisor John Jay LaValle how she uses infrared light to study bone composition in osteoporosis.

At the next stop, Bill Christie of the Physics Department talked about the massive STAR detector, where about 450 researchers are among the approximately 1,000 scientists, engineers, and technicians from the U.S. and abroad who work at the Relativistic Heavy Ion Collider to replicate conditions at the dawn of time to gain a better understanding of how the universe evolved.

Then, at the Positron Emission Tomography (PET) facility, the visitors learned from scientist David Schlyer of the Chemistry Department about BNL's work in probing the brain chemistry of addiction, mental illness, and aging, and recent work to find effective treatments.

—Liz Seubert

Brookhaven Lab Expects $30 Million to Support Life Sciences

February 12, 2004

The Biology Department at Brookhaven National Laboratory announced that it expects to receive more than $30 million over the next five years, which will renew financing to support structural biological research, including studies of disease and genomics.

The funding, administered by the Office of Biological and Environmental Research within the U.S. Department of Energy's (DOE) Office of Science and by the National Center for Research Resources within the National Institutes of Health, will support a group of six beamlines at the (NSLS).

"The large size of the grant is a tribute to the strong infrastructure within the NSLS and Brookhaven Lab," said Robert Sweet, a structural biologist in the Biology Department at Brookhaven and spokesperson for the research group that maintains the beamlines. "It also reflects how valuable we are to a large number of powerful Northeastern U.S. research groups that use our facility."

For example, researcher Roderick MacKinnon of The Rockefeller University received the 2003 Nobel Prize in Chemistry for his research, performed in part at the NSLS, on how nerve signals are propagated through the body.

"We're very proud of our ability to identify and support Nobel-quality projects like MacKinnon's work," Sweet said. "These funds will allow other important projects to move forward."

A research group from Yale University has used NSLS light to study the structure of ribosomes – cellular "machines" that assemble the proteins cells need to function. Also, scientists from Harvard University determined the structure of a type of tiny opening on the surface of cells that allows proteins to pass in and out of the cell. Their results may provide valuable insight into several basic cellular activities. The grants will also further the work of scientists from local Long Island institutions, such as Stony Brook University and Cold Spring Harbor Laboratory.

Ari Patrinos, Associate Director of Science for DOE's Office of Biological and Environmental Research within the Office of Science, welcomed the renewal of funding for the beamlines. "The Brookhaven scientists are addressing two major objectives of the Lab's structural biology program: developing state-of-the-art technologies for solving the most difficult molecular structure problems, and providing access to this major facility, which is used by more than 2,500 scientists each year," he stated.

This type of research is part of a field of biology called macromolecular crystallography, which uses x-rays to determine the structure of various proteins and nucleic acids, the molecular engines that control the functions of all living cells. Because abnormalities and malfunctions in macromolecules, especially proteins, are often the root of many diseases, an important step toward developing drug treatments is learning about these molecules' structures.

The funds will cover the expenses of improving and maintaining the beamlines, which is carried out by Sweet's research group – a team of nine scientists and fourteen engineers and technicians. It also will cover the costs of training and assisting researchers in performing their measurements.

One of the beamlines supported by the grants is brand-new, and will produce the brightest x-ray light at the NSLS. Another, the beamline where MacKinnon performed his research, will be upgraded to produce even brighter light. Lonny Berman, an NSLS physicist, will manage the upgrade.

Above are the staff of the Protein Crystallography Research Resource (PXRR), the Biology Department and National Synchrotron Light Source (NSLS) Department scientists, engineers, machinists, and technicians who operate six NSLS beamlines for macromolecular crystallography.

In addition, Sweet's group will use the funds to develop techniques that allow experimenters to work more quickly and efficiently. They have already pioneered a sophisticated service managed by Howard Robinson, a biophysicist, which allows crystal samples to be sent to NSLS researchers through the mail. In another project, managed by biophysicist Dieter Schneider, they are building a robot that will automatically change the specimens that are studied during NSLS experiments.

—Laura Mgrdichian

The DUV-FEL Workshop

February 19-20, 2004

The Deep Ultra Violet Free Electron Laser (DUV-FEL), a laser linac facility at Brookhaven National Laboratory, is the world's only facility dedicated to laser-seeded FEL research and development (R&D) and its applications. To explore opportunities for future experiments on free electron laser and beam physics at the DUV-FEL, the DUV-FEL Beam Physics and FEL Research and Development Workshop was held on February 19-20, 2004.

Representatives from seven countries and 14 institutions – including Lawrence Berkeley National Laboratory, the Massachusetts Institute of Technology, BESSY, and Pohang Accelerator Laboratory – participated in the workshop. More than 20 talks were presented, covering a broad spectrum of beam physics and FEL topics, such as cascaded high-gain harmonic generation (HGHG) FEL, ultra-short FEL generation techniques, electron-beam optimization, bunch compression, and femtosecond electron-beam instrumentation. The presentations revealed that the seeded FEL, especially the HGHG type, will play a critical role in the proposed x-ray FEL facility.

Brookhaven's Xijie Wang and Li Hua Yu began the workshop with presentations on the DUV-FEL facility and its current FEL R&D program. The facility's main components are a high-brightness electron accelerator, a HGHG FEL, a chemical science endstation, and sophisticated electron and photon beam instrumentation.

The DUV-FEL accelerator system consists of a 1.6 cell photo injector driven by a Ti:Sapphire laser system, and a four-section 2856 MHz SLAC-type traveling wave linac that is capable of producing a 200 MeV electron beam. The facility's magnetic chicane bunch compressor produces sub-picosecond-long electron bunches with a peak current of a few hundred amperes. The high-brightness electron beam travels down the 10 meter-long undulator to generate UV light with a fundamental wavelength of 266 nm.

Past DUV-FEL Activity

One of the most important milestones at the DUV-FEL last year is the initialization and completion of the first DUV-FEL user experiment by Arthur Suits and his collaborators from BNL's Chemistry Department.

This first chemical science experiment – on ion pair imaging – used the HGHG's third harmonic beam (89 nm) to study the super excited states of methyl fluoride, a highly flammable gas. Velocity-mapped ion images of the fluoride ion, obtained using intense, coherent, sub-picosecond pulses of 86-89 nm light, revealed a low translational energy, implying a very high internal excitation in the molecule's methyl cation cofragment [W. Li et al, PRL 92, 083002-1 (2004)].

An enthusiastic group of DUV-FEL workshop attendees, (from left) Xijie Wang (BNL), June-Rong Chen (NSRRC), Gwo-Huei Luo (NSRRC), Bill Weng (BNL), Li-Hua Yu (BNL), Rene Bakker (Trieste), and Jong Oh (PAL), enjoying dinner after a successful workshop.

In response to the requests of many users to study chemical science at the facility, the DUV-FEL linac is being upgraded from 200 to 300 MeV to enable the HGHG FEL to produce 100 μJ pulses of 100 nm light. This will help establish the DUV FEL as a premier user facility for ultraviolet radiation, and will enable state-of-the-art gas phase photochemistry research.

After successfully lasing at 266 nm with 800 nm laser seeding in late October 2002 [L.H. Yu et al, PRL 91, 074801-1 (2003)], experiments were carried out at the DUV-FEL to further characterize the properties of the HGHG FEL and to demonstrate its stability and controllability. The narrower spectrum and better stability of the HGHG, compared to a Self-Amplified Spontaneous Emission (SASE) FEL, were observed. Both the second and third harmonic HGHG FEL beams were experimentally characterized using a vacuum monochromator. The pulse energy for both harmonics (133 and 89 nm, respectively) was measured to be about 1 μJ, which is about one percent of the fundamental value at 266 nm.

A two-photon absorption auto-correlator with 100 femtosecond (fs) resolution was developed to characterize the HGHG output pulse length. It was experimentally demonstrated that the HGHG can produce output pulses with lengths from one picosecond down to 250 fs by varying the seed laser pulse length.

Experiments to investigate a chirped HGHG FEL were also initialized in 2003. The preliminary results are very promising, and the chirped FEL could lead to even shorter HGHS output pulses. The possibility of achieving HGHG output tuning via electron beam energy chirping was discussed by Timur Shaftan of BNL. Brian Sheehy, also of BNL, discussed various FEL output manipulation techniques and their limitations.

DUV-FEL in the Future

One of the main goals of FEL R&D at the DUV-FEL is to continue developing key technologies for a future x-ray FEL that will be based on the HGHG. For example, a cascaded HGHG and a higher harmonic (n>5) HGHG are critical for the realization of the HGHG x-ray FEL. Additionally, multi-laser electron beam synchronization and timing jitter reduction are very important technologies that will enable ultra-fast science at all future x-ray FEL facilities.

Paul Emma of SLAC discussed a technique that uses an emittance spoiler to achieve ultra-short FEL pulses. Computer simulations have shown that, by using a cleverly placed piece of slotted foil, the Linac Coherent Light Source (LCLS) at SLAC will be able to produce brilliant x-ray pulses that are extremely short – a few femtoseconds. This pulse length, which is more than 200 times shorter than the LCLS baseline design, will dramatically increase that facility's x-ray time resolution, giving scientists the ability to study the movement of matter at atomic scales and observe the structural changes that occur when chemical bonds are made or broken. To test the feasibility of an emittance spoiler at the DUV-FEL, Emma proposed a demonstration experiment. This could reduce the FEL output pulse length by a factor of four.

Beam physics during the electron-beam bunch compression was extensively discussed during the workshop. Zhirong Huang of SLAC gave an overview on microbunching instability during electron-beam compression and its impact on the future x-ray FEL. The LCLS proposes using a laser heater or superconducting undulator to mitigate microbunching instability. Michael Borland of the Advanced Photon Source discussed the latest developments in electron-beam bunch compression simulation. Experimental investigation of microbunching instability and validation of computer predictions will be the major part of beam physics R&D at the DUV-FEL.

To take advantage of the DUV-FEL's unique capabilities, other possibilities in beam physics and FEL R&D will continue to be explored, such as coherent terahertz generation and a femtosecond electro-optical bunch detector.

The workshop ended with a lively discussion on the possible future FEL and beam physics experiments at the DUV-FEL. The workshop participants ranked possible future experiments according to the following criteria:

1. What are likely critical beam physics and FEL experiments for future linac-based light sources? Can the DUV-FEL make an impact?
2. What is the best way to carry out those experiments? How can we take advantage of the unique features of the DUV-FEL?

—Xijie Wang and Laura Mgrdichian

NSLS-II Workshop Lights Brookhaven National Laboratory

March 15, 2004

On March 15, 2004, approximately four hundred registered attendees participated in the NSLS-II Workshop at Brookhaven National Laboratory to support the proposed facility, a world-leading synchrotron that will facilitate cutting-edge research in the biological, material, chemical, environmental, and physical sciences.

The current National Synchrotron Light Source (NSLS) is one of the world's most widely used scientific facilities. Each year, about 2,400 researchers from more than 400 universities, government laboratories, and companies use its x-rays, ultraviolet light, and infrared light for research. The scientific productivity of the NSLS user community is very high and has widespread impact, with approximately 800 publications per year, of which some 130 appear in so-called premier scientific journals.

Though the current NSLS has been continually updated since its commissioning in 1982, today the practical limits of machine performance have been reached. In order for the productivity of its user community to continue, and in order to tackle the 'grand challenge' scientific problems of tomorrow, plans to upgrade the NSLS are under way. The centerpiece of the proposed NSLS-II will be a state-of-the-art, medium-energy electron storage ring designed to deliver world-leading x-ray brightness and flux, more than 10,000 times brighter than the current NSLS. This facility, which will also include full-energy injection for constant intensity as well as a dedicated infrared ring, is expected to have profound impact on a wide range of scientific disciplines and initiatives and lead to many exciting discoveries in the coming decades.

Speakers at the NSLS-II Workshop at BNL included: (from left) BNL Director Praveen Chaudhari; Battelle President and CEO and current BSA Chair Carl Kohrt; Nobel Prize-winner Roderick MacKinnon of Rockefeller University; DOE Brookhaven Area Office Manager Michael Holland; DOE's Office of Basic Energy Sciences Associate Director Patricia Dehmer; Associate Laboratory Director for Light Sources and National Synchrotron Light Source Department Chair Steven Dierker; and IBM Senior Vice President and Director of Research Paul Horn.

Associate Laboratory Director for Light Sources and NSLS Chair Steve Dierker enthusiastically welcomed the workshop participants and speakers.

The NSLS-II workshop kicked off with opening remarks from Steve Dierker, the Associate Laboratory Director for Light Sources, Chair of the National Synchrotron Light Source (NSLS), and the workshop's host. "The design of NSLS-II has surpassed anything that has ever been built," said Dierker, setting the tone for the enthusiasm and interest that NSLS-II has generated. "The science that will come out of this will be very, very exciting."

Dierker then introduced the morning's first speakers: Brookhaven Lab Director Praveen Chaudhari and the Department of Energy's Brookhaven Area Office Manager, Michael Holland, who matched Dierker's enthusiasm for the days ahead. The stage was then turned over to the workshop's invited distinguished guests.

Addressing a packed auditorium, the morning speakers at the workshop – including NY Congressman Sherwood Boehlert, Chairman of the House Committee on Science, Patricia Dehmer, Associate Director of the DOE Office of Basic Energy Sciences, NY Congressman Tim Bishop, and Battelle President and CEO Carl Kohrt – praised and pledged their support for the proposed NSLS-II facility.

In addition, the two scientific speakers, the 2003 Nobel Prize in Chemistry recipient, Professor Roderick MacKinnon of Rockefeller University, and Dr. Paul Horn, the Vice President for Research and Development at IBM, gave stimulating talks that hinted at the new, exciting science NSLS-II will enable.

Their enthusiasm was shared by Boehlert, the keynote speaker, who said, "One doesn't need a degree in physics to understand the value of a scientific tool that furthers human understanding of matter while answering practical questions in materials science and biology; a tool that is of use to both academic and industrial researchers; a tool that attracts the best researchers from throughout the world."

"The U.S. simply must invest to upgrade its capabilities in this area, building on the expertise that Brookhaven and the researchers who use its facilities have developed over the last few decades," he continued.

"NSLS-II is something we need to do," Dehmer agreed in her talk. "I want you to know that I give you my commitment that NSLS-II will happen. Never doubt my resolve, never doubt your own power, never doubt the power of a great idea."

Bishop imparted a similar message. "We have such confi-

NY Congressman Sherwood Boehlert, Chairman of the House Committee on Science, the workshop's keynote speaker and distinguished guest.

dence in what this Lab can do and what the scientists in this Lab can do. And the best scientists in the world deserve the best equipment," he said.

Kohrt, who is also the Board Chair of Brookhaven Science Associates, the company formed by Battelle and Stony Brook University to manage Brookhaven Lab, also spoke enthusiastically about the new facility. "Thank you to the DOE and the visionaries that started this," he said of NSLS-II. "The journey has just begun."

But Boehlert also reminded the workshop participants of some very real issues, including the financial constraints that are involved. His main message: Nothing is certain in politics, and the realization of NSLS-II largely depends on the ability of its potential users to express why the facility is necessary. "I will do everything I can to help you, but I can't do it alone," he said. "Lawmakers need to hear from you, and especially from those of you in industry and your CEOs, why a light source, or any other piece of equipment or area of research, is important. They - we - need to learn from you what the nation will actually be giving up if you aren't able to succeed."

Patricia Dehmer, Associate Director of the Office of Basic Energy Sciences, gave an inspiring and positive speech in support of NSLS-II.

Seeming to answer this challenge, Horn gave examples of how his company would benefit from NSLS-II. In his presentation on nanoscience, Horn discussed why progress in improving the performance of silicon transistors has slowed, and how NSLS-II could open doors to new materials that may replace silicon transistors.

NY Congressman Tim Bishop spoke about the importance of NSLS-II to Brookhaven Lab and the scientific community.

The silicon transistor, Horn explained, has developed into a nanodevice. But any further miniaturization has all but halted because researchers can't solve the problem of transistor cooling. As a result, technology development companies have moved in a different direction, and are trying to gain better transistor performance without scaling them down. This involves researching new materials, which, Horn said, is where NSLS-II would step in as a valuable research tool.

"We are at a paradigm shift, where the physics that comes from synchrotrons like NSLS-II is absolutely critical," he said. "We can use x-rays to look at new materials and their features at an incredibly fine scale."

Carl Kohrt, the President and CEO of Battelle and the current chair of Brookhaven Science Associates, also offered his support for NSLS-II.

Horn hailed NSLS-II as a gateway into cutting-edge nanoscience research, a field that is expected to become a major engineering discipline that will integrate many fields – physics, materials science, chemistry, and biology – reduce the cost of manufacturing, ultimately reducing costs for the consumer, and generally revolutionize the information technology and electronics industries.

In his talk, MacKinnon also clearly explained how NSLS-II would further his work, which he said would be "impossible" with the current NSLS. He described his Nobel prize-winning research involving the structural determination of cell membrane proteins called ion channels, which was performed, in part, at the existing NSLS.

IBM Vice President for Research Paul Horn, who gave an excellent talk on how NSLS-II could help revive the silicon transistor industry.

In the meantime, however, there are still many other membrane proteins to study, which, according to MacKinnon, make up between 25 and 30 percent of all proteins. "We know almost nothing about this important class of proteins," he said, and emphasized the role that NSLS-II would play in changing that fact. "There is no other way to study these proteins at the level a synchrotron allows."

"We're behind," he added. "Our need is getting severe."

MacKinnon also stressed the importance of the facility's location in the northeastern United States. NSLS-II would service the many research institutions in the re-

Roderick MacKinnon, winner of the 2003 Nobel Prize in Chemistry, discussed how NSLS-II would enable further research on ion channels.

gion, he said, and it is essential for researchers whose work requires frequent visits to have local access to the facility.

During the afternoon, the workshop participants divided into seven breakout sessions, giving them a chance to provide input and feedback on the design and parameters of NSLS-II. The topics were spectroscopy, scattering, small angle x-ray scattering and x-ray photon correlation spectroscopy (SAXS/XPCS), nanoprobe/imaging, macromolecular crystallography, infrared, and inelastic x-ray scattering.

—Laura Mgrdichian

Cullie Sparks: In-Memoriam

March 19, 2004

Cullie Sparks, a charter member of the NSLS users group and one of the first Chairmen of the Users Executive Committee, died March 19, 2004. Dr. Sparks made major contributions to materials science, x-ray physics, and synchrotron science that continue to have a worldwide impact. He was a particularly enthusiastic supporter of synchrotron radiation and threw himself wholeheartedly into developing beamline X14 at the NSLS when the NSLS was still on the drawing board.

After earning a metallurgical Ph.D. from the University of Kentucky, Sparks joined Oak Ridge National Laboratory in 1957. In the mid 60's Sparks and his group leader, Bernard Borie, used symmetry to interpret variations in the weak so-called diffuse x-ray scattering from crystalline alloys. By quantitatively studying patterns in the diffuse x-ray scattering, they found that local structural fluctuations could be measured with unprecedented sensitivity. This early research explored the tendency for some materials to have a long-ranged average structure but with important nanoscale fluctuations about the average. Later this research led to elegant experiments at the NSLS that measured chemically specific bond distances to less than a tenth of a picometer (<0.001 Å).

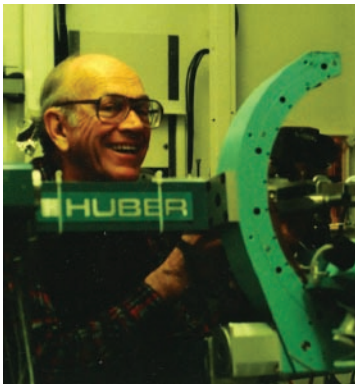

Cullie Sparks aligning a sample on beamline X14.

Their Borie-Sparks method for analyzing diffuse x-ray and neutron scattering is still used worldwide to interpret diffuse neutron scattering and forms the basis for modern diffuse x-ray techniques. Research based on their pioneering work continues at major Department of Energy facilities including the Advanced Photon Source, National Synchrotron Light Source, and ORNL's High Flux Isotope Reactor.

Also in the 60's, Dr. Sparks recognized the potential of artificial graphite crystals for high-performance x-ray and neutron monochromators. He worked with researchers at Union Carbide Corporation to perfect the manufacture and performance of graphite monochromators and became the world's expert on mosaic graphite optics. By combining the natural tendency of mosaic graphite crystals to focus in the plane-of-scatter with out-of-plane focusing based on curved surfaces, he created powerful doubly-focusing crystal optics. Carbide continues to make a range of graphite monochromators that are used worldwide both for x-rays and neutrons.

Armed with a vastly more powerful way to produce intense x-ray beams, Sparks began a systematic search for inelastic x-ray scattering contributions that might have contributed background in his diffuse scattering measurements. His careful research uncovered an unsuspected resonant-inelastic scattering mechanism. Although a respected reviewer from Bell Labs, who specialized in inelastic x-ray scattering, could find no fault in Sparks' 1974 Physical Review Letters paper, the reviewer personally performed definitive synchrotron experiments at Stanford Synchrotron Radiation Laboratory (SSRL) to check Sparks' results—and verified, much to his surprise, that Sparks was correct! Resonant raman x-ray scattering or "Sparks scattering" is still widely used to study the dynamics of x-ray-induced atomic transitions.

In 1976, proton microprobe measurements on monozite inclusions with anomalously large halos in micas from Madagascar indicated the presence of primordial superheavy elements. This "discovery" reverberated throughout the scientific community, as the presence of primordial superheavy elements suggested that the earth might be only a few thousand years old, a compact atomic weapon might be made of these unusual elements, and even the shape of the nucleus might differ from standard materials.

In a crash program to settle the issue, Sparks designed the first synchrotron-based x-ray fluorescence microprobe and led a team of distinguished scientists that installed and executed the critical test at the SSRL. Sparks and his team convincingly showed that primordial superheavy elements do not exist in these micas. As a result, the U.S. and other governments avoided the enormous resources that might

otherwise have been expended to understand something for which there is no evidence. This experiment clearly illustrated the critical need for intense synchrotron radiation sources.

In the summer of 1979, during a sabbatical at BNL, Sparks began studying how to focus x-rays with bent perfect crystals. He was motivated by the fact that crystals, with roughly a 20 times larger scattering angle than mirrors, can collect much larger divergences and focus them onto a sample. Although Sparks was greatly challenged by computer programming, he worked with scientists at BNL and ORNL to study ways to utilize the potential of crystal focusing. He discovered that in a nondispersive geometry, the Bragg angle of each ray reflected from a flat crystal is virtually the same off a crystal bent to focus at magnification=1/3. This discovery opened the possibility of dynamically bent sagittal focusing optics. Despite major technical challenges and a general consensus that the method could not work, sagittal focusing optics were demonstrated, paving the way

Cullie (left on banjo) and the Earsore Quartet playing at the 1985 NSLS Users' Meeting.

for beamline X14. Sagittal focusing optics are now installed in multimillion-dollar facilities around the world providing 20 times greater x-ray intensity than alternative focusing methods.

Not only were the sagittal focusing optics widely adopted by the worldwide synchrotron community, but the efficiency and flexibility of sagittal focusing optics on beamline X14 also led to numerous exciting collaborations. First or early measurements included fluorescence tomography, resonant magnetic scattering, multiple wavelength holography, anomalous powder and diffuse x-ray scattering, nuclear resonant scattering, glancing angle scattering from lipids, scattering from liquid crystals, quasi crystals, and other experiments.

In addition to his other contributions at the NSLS, in 1985 Sparks and three associates contributed the after-dinner show at the NSLS users meeting. This legendary performance of bluegrass songs with synchrotron themes was topped off with a round of authentic moonshine for those NSLS users and staff brave enough to try.

In short, Sparks was a gifted experimentalist and a good friend of the NSLS. His scientific legacy continues to this day through advanced x-ray optics, new fields of atomic physics, materials, and synchrotron science.

—Gene Ice, ORNL

New Technology Turns Dredged Material into Cement

April 7, 2004

In research performed in part at the NSLS, scientists at Brookhaven National Laboratory have helped develop a new technology that converts material dredged from the bottoms of harbors and waterways into a substance that can be made into construction-grade cement. The technology, called Cement-Lock, was developed in collaboration with the U.S. Environmental Protection Agency (EPA), the State of New Jersey, and other government and public groups.

"This technology will greatly help to increase the health of many U.S. harbors and waterways, such as the Port of New York and New Jersey," said Keith Jones, an environmental scientist at Brookhaven who took part in Cement-Lock's development. "These waterways are contaminated by metals and pollutants from many human activities, such as sewer overflow systems and discharges from industrial operations."

To ensure that the port can continue to service large container ships, which need deep water, it must be dredged regularly, Jones explained. But because the dredged material is contaminated, there are very strict restrictions on where and how it can be disposed of.

"This is one of several promising technologies that have the power to solve the problem of dredged material," said EPA Regional Administrator Jane M. Kenny at an event in Bayonne, New Jersey on November 24, 2003. "It enables us to treat contaminated material and use it

The kiln in Bayonne, New Jersey

A view into the kiln as it operates

beneficially, instead of adding tons of material to landfills that are already short on space."

According to Eric Stern, the EPA Regional Contaminated Sediment Program Manager, "Sediment decontamination is a component of an overall dredged material/contaminated sediment management strategy. What sets this program apart from typical remediation is that beneficial use products – cement, lightweight aggregates, bricks, and soils – are the end result. These products then serve as economic drivers for the restoration and revitalization of impacted waterways, ports, and harbors around the entire world."

Brookhaven Lab has been involved in the development of sediment decontamination strategies since 1994, when it began collaborating on a decontamination program for the Port of New York and New Jersey, called the New York/New Jersey Harbor Sediment Decontamination Project, led by Stern. The collaboration also includes the EPA, the U.S. Army Corps of Engineers, and the New Jersey Department of Transportation (NJDOT) Office of Maritime Resources, which joined the collaboration in 1998.

Many researchers at Brookhaven Lab participated in that project, and began by performing basic research on contamination chemistry. For example, using x-rays and infrared light at NSLS beamlines U2B, X1A, X26A, and X27A, the scientists closely studied how contaminants are bound to sediment particle grains.

Brookhaven researchers also determined which experimental treatment methods would be tested and selected several technology companies to perform bench and pilot-scale tests, which can treat a few gallons and several cubic yards of sediment, respectively.

Once those test results were completed, the Brookhaven group reviewed the results and selected several treatment methods for full-scale demonstrations. As a result, Brookhaven and the EPA awarded contracts for the construction and operation of two large-scale sediment treatment facilities that can treat thousands of cubic yards of material. The Gas Technology Institute (GTI) in Des Plaines, Illinois, which developed Cement-Lock during the initial testing phases, is one of the two winning companies. GTI is an independent company that develops energy and environmental technologies.

Grains of Ecomelt

"The GTI group developed a process that can treat all types of sediment, and highly contaminated ones, in particular," said Jones, who is also the project's technical manager. "The facility has potential for use on major problem spots in the region."

GTI is now carrying out a large-scale demonstration of the Cement-Lock process with a specially constructed 10-foot diameter by 30-foot long rotary kiln melter that they built for the demonstration in Bayonne. In the process, dredged material and modifying minerals are loaded into the kiln and heated to between 2,400 and 2,600 degrees Fahrenheit, creating a molten material. The high temperature causes some contaminants in the material to break down into environmentally safe components that are vented to the atmosphere, while the contaminants that do not break down are incorporated into the melt. The resulting treated material, called "Ecomelt," is then ground to a powder and blended with cement. The Ecomelt takes part in the hardening process of concrete, which is a mixture of cement, sand, gravel, and water. Further, Ecomelt reduces the quantity of other raw materials that are typically used in cement manufacturing, such as shale.

After the testing phase, which will treat 400 cubic yards of dredged material from New Jersey's upper Newark Bay, EPA and NJDOT will work with GTI to develop a commercial kiln that can treat up to 500,000 cubic yards of sediment per year.

The research is funded by EPA, the NJDOT Office of Maritime Resources, GTI, and Unitel Technologies.

—Laura Mgrdichian

NSLS Hosts More Than 100 Children on "Take Our Sons and Daughters to Work" Day

April 24, 2004

On April 24, more than 100 BNL daughters and sons learned about some of the scientific programs at the NSLS and even performed their own scientific experiments. The one-day visit was part of the national "Take our Sons and Daughters to Work Day."

At the NSLS, the children learned that the facility produces many types of light, from microwaves to x-rays, which have many applications in many fields, including computers,

Some of the participants at the NSLS "Take Our Sons and Daughters Work Day"

catalysis, microscopes, and medicine. Synchrotron light was contrasted with more familiar forms of light as the children played a game that tested their knowledge of everyday light sources, such as laser pointers, cell phones, radios, and TV remote controls.

The daughters and sons then toured the experimental floor, where NSLS Control Room Operator Gary Weiner explained how synchrotron light is made. NSLS scientists Marc Allaire, Lisa Miller, Cecilia Sanchez-Hanke, and Vivian Stojanoff then showed the students a few x-ray and infrared beamlines, where they discovered how synchrotron light is used to study the composition of rocks and minerals and, using protein crystallography, to develop new drugs.

After the tour, the daughters and sons had the chance to perform their own scientific experiments. Marc Allaire, NSLS student Tejas Telivala, and NSLS postdoc Adele Qi Wang demonstrated the refraction of light through a prism, and each child had the opportunity to test their skills with their own prism.

The children observed the effect of vacuum on a marshmallow Peep.

NSLS beamline scientist Randy Smith showed the students how a vacuum is created using a bell jar and vacuum pump. The children observed the effect of vacuum on balloons, a bell, a candle, and soda water. But perhaps the most memorable experiment was the effect of vacuum on marshmallow Peeps candies, which dramatically expanded under vacuum, but then shriveled to half their size when re-exposed to air. Regardless, the final product was still tasty.

—Lisa Miller

2004 RapiData Crystallography Course

April 25-30, 2004

From April 25 to 30, budding crystallographers from around the world gathered at Brookhaven Lab for RapiData 2004, a week-long course run by Brookhaven's Biology and National Synchrotron Light Source (NSLS) Departments. The course introduces students to the field of macromolecular x-ray crystallography by giving them access to advanced equipment, the latest crystallography techniques, and the instruction of experienced crystallographers.

2004 RapiData Crystallography course attendees

The course, "Rapid Data Collection and Structure Solving at the NSLS: A Practical Course in Macromolecular X-Ray Diffraction Measurement," consisted of two days of lectures and tutorials taught by scientists from BNL, industry, academia, and other national labs. This was followed by a marathon sixty-hour data-collection and analysis session at the NSLS, in which the same instructors and volunteers acted as hands-on advisors. Several of the course's 48 students left with solved structures, which will likely result in publications.

The course, which helps to train the next generation of NSLS users, is mostly organized by Bob Sweet and Denise Kranz of Biology, but they emphasize that its success depends on enthusiastic help from most of the twenty members of the PXRR (the Biology and NSLS Macromolecular Crystallography Research Resource), plus a dozen or so outside teachers.

Major funding for the course was provided by the National Institutes of Health through the National Center for Research Resources, and the Office of Biological & Environmental Research within the U.S. Department of Energy's Office of Science. Additional support comes from the NSLS, as well as equipment vendors and drug companies.

—Karen McNulty Walsh and Laura Mgrdichian

2004 NSLS Annual Users' Meeting Caps Off Another Successful Year

May 17-20, 2004

Almost 400 participants at the 2004 NSLS Annual Users' Meeting, held May 17-20 at Brookhaven National Laboratory (BNL), came together for a successful event full of interesting talks and important messages for the future. The meeting affirmed that the NSLS continues to be a facility that produces important science.

The new NSLS Users' Executive Committee Chair, Larry Shapiro, gave welcoming remarks at the main meeting.

In his welcoming remarks at the main meeting on May 18, the new Users' Executive Committee (UEC) Chair, Larry Shapiro, discussed the continuing excellence of NSLS research, such as the cellular ion channel structure determined by user Roderick MacKinnon, performed at the NSLS and the Cornell High Energy Synchrotron Source. This work earned MacKinnon the 2003 Nobel Prize in Chemistry.

Steve Dierker, NSLS Chairman and Associate Laboratory Director for Light Sources, described another important crystal structure, a cellular protein channel, recently determined here and featured on the cover of *Nature* in January 2004.

He also described other research highlights – a new liquid crystal phase in polar ordered materials, featured on the cover of *Science* in August 2003; a new material texture type, appearing in *Nature* in December 2003; and a new way to store hydrogen in molecular compounds, published in January 2004 in the *Proceedings of the National Academy of Sciences*.

Among the main meeting speakers at the Annual NSLS Users' Meeting were (from left): Bob Casey (BNL-NSLS), Pedro Montano (DOE), Mark Croft (Rutgers University), Steve Dierker (BNL-NSLS), John Hill (BNL-Physics), Lois Pollack (Cornell University), Simon Billinge (Michigan State University), and Chris Jacobsen (Stony Brook University).

"These give you a flavor of the diversity and quality of science that continues at this facility," he said. "The NSLS has a well-deserved reputation for outstanding productivity."

The main meeting's scientific talks focused on user research from a more in-depth perspective. Chris Jacobsen, of Stony Brook University (SBU), gave an overview of the many x-ray and infrared imaging techniques available to users at the NSLS. Mark Croft, from Rutgers University, described his research on strain fields in macroscopic materials, in which he uses an energy dispersive x-ray diffraction method.

Yvonne Akpalu (RPI) discussed the use of light and x-ray scattering on copolymers.

Simon Billinge, of Michigan State University, presented his work on the structures of complex materials that display order on the nanoscale, using the rapid acquisition pair distribution function technique he developed with his group. Brookhaven Lab's John Hill discussed how he uses soft x-ray scattering to probe the behavior of electrons in solids.

Another speaker, Cornell University's Lois Pollack, described an apparatus designed by her research group, which allows them to observe, using small angle x-ray scattering (SAXS), how an RNA chain molecule compacts and folds into a three-dimensional structure. Following this, Yvonne Akpalu, of Rensselaer Polytechnic Institute, presented her work, which investigates how to solve the crystal structure of a copolymer using SAXS.

On the days before and after the main meeting, users divided up to listen to additional talks on specific topics. These talks were organized into the following workshops: "Better Ways to See the Light: Advanced Detectors for Synchrotron Radiation," organized by Peter Siddons (BNL) and Gianluigi De Geronimo (BNL); "Anatomy of a Virus," organized by Marc Allaire (BNL) and Paul Freimuth (BNL); "Grazing Incidence Small Angle Scattering," organized by Ben Ocko (BNL) and Detlef Smilgies (Cornell University); "Pharmaceutical Applications of Synchrotron Radiation," organized by Evgenyi Shalaev (Pfizer Inc.), Raj G. Suryanarayanan (College of Pharmacy), and Peter Stephens (SBU); "Advanced Optical Systems and Metrology for High Power and Coherent Beamlines," organized by Peter Takacs (BNL) and Steve Hulbert (BNL); "Applications of Synchrotron Based Methods to Hydrogen Storage Materials," organized by Trevor Tyson (New Jersey Institute of Technology) and Wolfgang Caliebe (BNL); "Nanoprobes for Nanoscience,"

organized by Cecilia Sanchez-Hanke (BNL) and Peter Sutter (BNL); and "Crystallization, Membrane Proteins," organized by Naomi Chayen (Imperial College of Science, Technology & Medicine) and Vivian Stojanoff (BNL).

Now and Ahead

On the performance front, Dierker said the facility did well overall in the last year, with the VUV ring achieving 98 percent reliability and 108 percent availability. The x-ray ring didn't perform quite as well, operating at 89 percent reliability and 99 percent availability. He noted that more than 60% of the downtime on the x-ray ring was due to three unusual major events, including the Northeast electrical power blackout last August.

Brookhaven National Laboratory Director Praveen Chaudhari discussed his vision for the Laboratory in the next 20 years.

In a message users are very familiar with, he stressed that the NSLS, designed 30 years ago and the only remaining second-generation DOE light source, is now performing at the limits of its capabilities. Pedro Montano, manager of the X-ray and Neutron Scattering Facilities program within the Department of Energy's Office of Basic Energy Sciences, acknowledged this in his talk, referring to the NSLS as the "working horse" of the DOE light sources.

Dierker and Montano repeated the need and excitement for NSLS-II, the proposed third-generation light source that would replace the NSLS.

Members of the 2004 planning committee for the NSLS Users' Meeting include: (from left) Larry Shapiro (Columbia University), Liz Flynn (BNL-NSLS), Mary Anne Corwin (BNL-NSLS), Tony Lanzirotti (University of Chicago), Gretchen Cisco (BNL-NSLS), Lisa Miller (BNL-NSLS), Vivian Stojanoff (BNL-NSLS), Paul Stevens (Exxon Mobil Research & Engineering Company), and Dan Fischer (National Institute of Standards & Technology).

Currently, Montano said, an international panel of scientists is reviewing the proposal – the first step in the process. He urged the prospective users of NSLS-II to contact their representatives in Congress and tell them how vital the facility is.

"I think NSLS-II is necessary," Montano said. "There are a huge number of scientists in the Northeast that would benefit from it."

All of the day's speakers affirmed this idea – that NSLS-II is needed to broaden and enrich their research.

Center for Functional Nanomaterials (CFN) Director Robert Hwang gave the "CFN Update" at the main meeting.

BNL and the NSLS

In his "CFN Update" talk, Robert Hwang, director of the upcoming Center for Functional Nanomaterials (CFN) facility, discussed how the CFN will be "an interdisciplinary environment for nanoscience research," performed in conjunction with several BNL departments, including the current NSLS and NSLS-II.

In this way, the research the CFN will enable promises to be very exciting. "The Northeast is becoming a hotbed for nanoscience," said Dierker. "Brookhaven is becoming a focal point for much of that research."

The future of Brookhaven Lab was the subject of Lab Director Praveen Chaudhari's talk. In his vision for the Laboratory in the next 20 years, Chaudhari said NSLS-II plays a significant part in his desire to see more integration between departments, and the emergence of a new culture and way of thinking at the Lab.

"In a research lab, departmentalizing can be a hindrance," he said. "To reach the frontiers in the life, physical, and environmental sciences, we need to find the major challenges at these interfaces between disciplines, and begin to address them."

Another Lab-wide initiative – safety – was discussed by Bob Casey, the NSLS Associate Chair for Environment, Health, Safety, and Quality. While the NSLS safety record hovers around the DOE average, "We're being asked to really improve," Casey said. "We want to be best in class."

The types of accidents that occur at the NSLS are sometimes considered routine, such as slips and muscle strains, but, as Dierker said in his talk, "Accidents have consequences." Additionally, there have been near misses at BNL in the special-hazard category, which include more serious electrical, radiation, and laser accidents.

Poster prize winners at the 2004 NSLS Users' Meeting were (from left to right): Dario Arena (BNL-NSLS), Xianqin Wang (BNL-Chemistry), Marianna Kissell (SBU), Mehmet Aslantas (BNL-NSLS), and Alexei Grigoriev (Harvard University). Not pictured: Meghan Ruppel (SBU).

Casey made it clear that these must also be avoided, ending his talk with a series of photographs showing obvious safety violations in several areas of the NSLS. The pictures made it clear that safety really is an issue everybody must take seriously.

Tuesday night's Reggae Banquet was enjoyed by all including (from left to right): Gene Ice (ORNL), Pedro Montano (DOE), Peter Siddons (BNL-NSLS), Chi-Chang Kao (BNL-NSLS), and Chris Ryan (CSIRO, Australia).

Honorable Mentions

Numerous honors and awards were presented at the close of the meeting. Outgoing UEC chair Tony Lanzirotti presented the UEC Community Service Award to Sue Wirick of Stony Brook University. Additionally, Lisa Miller, the meeting's poster session and publicity chair, gave out awards for the best posters. The winners were Dario Arena (BNL-NSLS), Mehmet Aslantas (BNL-NSLS), Alexei Grigoriev (Harvard University), Marianna Kissel (SBU), Meghan Ruppel (SBU), and Xianqin Wang (BNL-Chemistry).

At the evening banquet, Shapiro presented the meeting's organizers – Mary Anne Corwin, Liz Flynn, Gretchen Cisco, and Melissa Abramowitz – with framed letters of appreciation. This year's banquet was reggae-themed, complete with a reggae band, colorful hats, and island fare.

—Laura Mgrdichian

Better Ways to See the Light: Advanced Detectors for Synchrotron Radiation Workshop

May 17, 2004

The workshop attracted 62 registrants, who enjoyed a wide range of talks about the latest in detector developments for synchrotron radiation (SR) applications. The following is a very brief resumé of the talks presented.

Many people think the center of this activity is in Europe these days, and to bring us up to date with what is happening over there, we heard Dr. Gareth Derbyshire (from the Rutherford-Appleton Laboratory in the UK) talk about "Detector Developments for Synchrotron Radiation in Europe." He described work underway at the Daresbury and Rutherford laboratories, as well as work being pursued by the Swiss Light Source in collaboration with the Centre Européenne pour la Recherche Nucléaire (CERN). In particular, he stressed the need to provide advanced detector systems to the UK's Diamond Light Source, currently under construction, ready for use on 'day 1.'

There are many interesting detector developments happening in fields other than SR. The next speaker, Dr. Oswald Siegmund, was from the Space Sciences Laboratory at the University of California Berkeley. In his talk, "Microlithographic Silicon-Based Microchannel Plates and Readout Techniques for Photon and Particle Detection," he told us of some interesting developments in microchannel electron multiplier device technology, in particular the use of micromachining techniques to make precision microchannels in silicon wafers. Such devices offer much improved uniformity and reduced noise over conventional drawn-glass structures. He also described readout electronics they are capable of providing good spatial resolution in one and two dimensions, for use with these new channel plates.

There is a real lack of detector technologies that are suitable for hard x-ray detection. Perhaps the most promising at the moment is cadmium-zinc telluride (CZT). This material is not ideal, but the use of special signal processing techniques can be helpful. Gabriella Carini (Brookhaven National Laboratory) spoke about "A New Integrated Circuit for Coplanar-grid Detector Readout." The coplanar grid detector has a special electrode structure which can mitigate the poor hole mobility in these room-temperature semiconductor detectors. The talk described a new microcircuit designed by the BNL microelectronics group, which provides enhanced capabilities for such devices.

A key part of any detector system is the software used to control the detector and analyze the data produced. Dr. Chris Ryan, from the Commonwealth Scientific & Industrial Research Organization (CSIRO) in Australia, has developed "A New Technique for Real-Time Spectral

Deconvolution of Energy-resolving Detector Data," which can generate quantitative elemental maps from fluorescence microprobe data, in real-time. Simple methods using pulse-height windows can lead to serious errors in elemental identification due to strong peak overlaps. Chris' technique is able to account for all these overlaps, together with other artifacts such as escape peaks, and build up an elemental map photon-by-photon.

An exciting development that is beginning to become more accessible is that of very high-resolution x-ray detectors based on cryogenic superconducting technology. Kent Irwin (National Institute of Standards and Technology, Boulder, CO) in his talk "Cryogenic Microbolometer X-ray Detectors," brought us up-to-date on these devices. They can reach single-digit eV resolution in the x-ray region, a remarkable achievement. The disadvantage of these detectors is that they are rather slow, and Kent described how his group is working to overcome this limitation by making large arrays of detectors, and how superconducting quantum interference device (SQUID) technology used to read them out can be integrated into such an array device.

Even the best detectors sometimes need help, and in the field of absorption spectroscopy this is particularly true. In his talk "Multilayer Optics for Fluorescence Detectors," Ke Zhang (BioCAT, Argonne National Laboratory) described the development and application of multi-element analyzer systems based on synthetic multilayer optical elements. The instrument he presented provides an efficient filter that only allows a particular spectral line to pass to the detector. The multiple elements provide enhanced solid angle and hence efficiency.

Perhaps the most powerful driver for advanced detector development in the synchrotron community has been the demands of macromolecular crystallography. The talk by Dr. Edwin Westbrook (Molecular Biology Consortium Inc.) titled "Silicon Pixel Array Detectors for Protein Crystallography," described some new ideas for fabricating detectors using non-traditional processing techniques. The result is a technology that can produce efficient arrays of detectors with excellent properties. One point that is unique to this technology is that the arrays do not have any dead area around the edges, so detectors can be easily tiled together to make large area systems without any lost image regions.

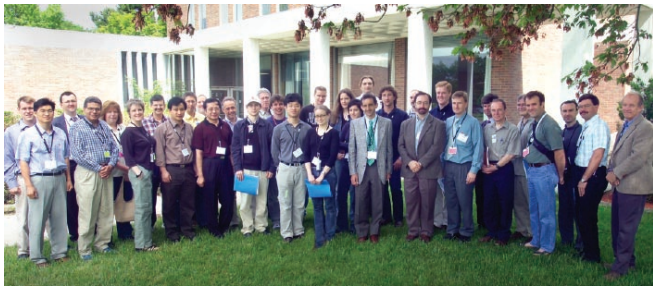

Better Ways to See the Light: Advanced Detectors for Synchrotron Radiation Workshop attendees

Tae Joo Shin (NSLS) then told us about his work using 2-D position-sensitive proportional counters (PSPCs) for x-ray speckle experiments. Present speckle experiments typically use either a single-point detector and photon-counting with high time resolution, or a CCD area detector, which has a readout time of, at best, tens of milliseconds. PSPCs have the potential to combine the advantages of a photon counting detector and an area detector. Preliminary experiments to characterize and improve the performance of such detectors to make them suitable for speckle were described.

The final talk was to have been given by Dr. Mark Rivers (University of Chicago). Although circumstances prevented him from giving the talk at that time, it was rescheduled for a few days later. It also concerned the software implications of advanced detector systems. This area of development is extremely important, and the difficulties and required effort are frequently underestimated. Mark told us about the software solutions he has developed for interfacing area detectors, in particular CCD devices, to data acquisition systems based on the EPICS framework.

The breadth and depth of these talks only scratch the surface of what we believe is the last remaining barrier to the full utilization of our powerful synchrotron facilities. We look forward to hearing much more of these developments at future meetings.

—D. Peter Siddons and Gianluigi De Geronimo

Anatomy of a Virus Workshop

May 17, 2004

It was a memorable day at the workshop, "Anatomy of a Virus," where prominent experts in the field got together to talk about their favorite subject. Sponsored by the User Executive Committee at the National Synchrotron Light Source, the National Institute of Health (National Institute of Allergy and Infectious Diseases, National Institute of General Medical Sciences, and National Center for Research Resources) and Area Detector System Corporation (Poway, CA), this full day workshop highlighted the frontiers in the study of viral structure and the future needs in structural virology. With the impressive list of speakers that were present on that day (front row of the picture), we all had the feeling that the future of structural virology was already there.

The workshop started with no less than a historical perspective given by Donald Caspar (Florida State University), which was elegantly introduced by Dieter Schneider. Don related the important factors that were required for the success and the birth of structural studies

Anatomy of a Virus Workshop attendees

of viral capsids. The next speaker was Denis Leclerc (Laval University), who reported on his progress on the assembly of nucleocapsid-like particles of hepatitis C virus. Their results suggest that the first N-terminal half of the core protein would be sufficient for the formation of viral particles. Michael Chapman (Florida State University) presented his work on structural studies of a gene therapy vector, the adeno-associated virus. From their atomic x-ray structure, it was possible to predict the viral site where it attaches to the cellular receptor. Huilin Li (Brookhaven National Laboratory) talked about genomic RNA packaging in the vesicular stomatitis virus. By single-particle cryo-electron microscopy, a ring of density was revealed on the inner surface, and the density is proposed to be the RNA. Stacy Benson (the Wistar Institute) followed and reported on structural studies of the lipid-containing bacteriophage PRD1. The x-ray crystal structure of its major coat protein has revealed a molecule that contains two viral jelly rolls and appears to link PRD1 evolutionarily with the human adenovirus. Michael Rossmann (Purdue University) talked about "Membranes and Motors: Where Electron Microscopy Meets Crystallography." He described a variety of examples in which crystallography and cryoEM were combined to construct detailed atomic models of large complexes. A striking example was the structure of the bacteriophage T4 base plate assembly in two different states. High-resolution structures of component proteins, combined with cryoEM reconstructions of the entire base plate complex in the extended and contracted states, revealed the extraordinary dynamic character of this complex and the large-scale motions of individual proteins.

The afternoon session started with Philip Dormitzer (Harvard Medical School) describing the structural rearrangements during rotavirus cell entry. His group's recent structure of the membrane penetration domain of VP4 reveals a fold-back rearrangement reminiscent of the enveloped virus fusion proteins that mediate enveloped virus cell entry. Wayne Hendrickson (Columbia University) gave his presentation on the structural biology of HIV attachment and entry into cells. His studies suggest that the flexibility of the glycoprotein GP120 of HIV is implicated in the escape to the immune response. The next talk, "Motors and Membranes: Where Crystallography Meets Electron Microscopy," was given by David Stuart (Oxford University). He presented his extensive work on the x-ray crystal structure analysis of the entire 66 MDa bacteriophage PRD1. These viral particles contain approximately 2000 protein subunits from 18 different protein species including integral membrane proteins associated with an internal lipid bilayer. Their crystal structure reveals, among other things, an ordered membrane structure that allows specific interactions with the genome and the coat proteins. John Johnson (The Scripps Research Institute) then closed the workshop with a lively talk about structure-based studies of auto-catalytic chemistry in virus particles. He described auto-catalytic cleavages that occur in the maturation of non-enveloped RNA insect viruses and proposed mechanisms based on atomic models from crystallography. The talk concluded with the description of a unique auto-catalytic ligation of a lysine side chain with an asparagine side chain to create catenated subunit rings that "chain-link" the capsid of HK97, a dsDNA bacteriophage.

—Marc Allaire

Grazing Incidence Small X-ray Scattering Workshop

May 17, 2004

A workshop on Grazing Incidence Small-Angle X-ray Scattering was held on May 17, 2004 as part of the 2004 National Synchrotron Light Source (NSLS) Users Meeting. This technique, commonly referred to by the acronym GISAXS, is the surface analogue of Small-Angle X-ray Scattering (SAXS). Scientific topics discussed included thin polymer films, nanoparticles at interfaces, and semiconductor nanostructures. GISAXS measurements are sensitive to both the surface morphology and the internal structure of films, and provide information both lateral and normal to the surface on length scales extending from 1-100 nm. As a result, GISAXS provides an excellent complement to more conventional nanoscale structural probes such as atomic force microscopy and transmission electron microscopy. Moreover, GISAXS lends itself to in-situ and real-time studies. Eleven speakers presented their results, followed by a discussion on ways to improve the technique and access to GISAXS facilities.

The first speaker was Detlef Smilgies from the Cornell High Energy Synchrotron Source (CHESS). Detlef presented a short introduction on the history and applications of GISAXS. He reviewed the rapid development of the technique, starting with the pioneering measurements of Levine and coworkers in the U.S. and Naudon and coworkers in France during the late 1980s. Detlef provided a perspective on how three different x-ray communities, SAXS, diffuse

reflectivity, and Grazing Incidence Diffraction (GID), were converging through GISAXS. In the following talk, a youthful Sunil Sinha from the University of California presented an intriguing and mesmerizing talk on the underlying scattering theory associated with GISAXS with a focus on the Distorted Wave Born Approximation (DWBA). Examples were presented in which wave-guiding effects, induced by the film interfaces, significantly enhanced the small-angle scattering from the particulate matter inside or on the surface of the film. In the third presentation, Ian Robinson from the University of Illinois presented a stimulating talk on coherent GISAXS investigations of granular micro-structures in thin metal films, performed at the Advanced Photon Source (APS). Speckled diffraction patterns were reported for gold nanoparticles prepared by the dewetting of a thin gold film on a solid support. The shapes of the speckle patterns were used to investigate the changing geometry associated with different parts of the diffraction pattern.

After a short break, Till Hartmut Metzger from the European Synchrotron Radiation Facility (ESRF) presented a captivating review on combined GISAXS and GID studies of semiconducting nanostructures, so-called quantum dots, performed at HASYLAB and the ESRF. Particular emphasis was placed on the role of strain, size, and chemical composition and their relationship to growth, which are the crucial input parameters for the understanding the electronic and optical properties of the quantum dots. Specific examples included InAs islands on GaAs and Ge pyramids on Si, for which detailed maps of strain and composition within the quantum dots were obtained. The following speaker, Alain Gibaud from the Université du Maine, presented a visually stimulating talk on *in-situ* studies of surfactant-templated silica thin films at the NSLS, which included the premier of several "reciprocal space" movies. In these studies, time resolved GISAXS measurements were carried out simultaneously with gravimetric studies during the slow evaporation of ethanol from a film containing surfactant (CTAB), silica precursor (TEOS), and water to obtain silica mesostructures. The time evolution was exploited to probe the mechanism of the self-assembly process. Prior to lunch, Thomas Russell from the University of Massachusetts gave a lively and animated presentation on the assembly of nanoparticles at the interface of two immiscible fluids. Tom noted that the nanoparticles mediate the interactions between the two fluids, thereby reducing the interfacial energy.

Grazing Incidence Small Angle Scattering Workshop attendees

After lunch, Christine Papadakis from the Technical University of Munich awoke the audience with an enlightening presentation on the inner structure of lamellar diblock copolymer thin films, as studied at CHESS and ESRF. Christine showed how poly(styrene-*b*-butadiene) films undergo a morphological transition from parallel lamellae for short chains to perpendicular lamellae for long chains. Complementary in-situ time-resolved GISAXS measurements were presented after the injection of toluene into the sample cell, which revealed both changes in the sample thickness and the lamella orientation on a timescale of minutes. Continuing the polymer theme, Matthew Misner from Prof. Russell's group at the University of Massachusetts presented an informative talk on real-time studies of block copolymer thin films at the NSLS. Results for two different systems were examined: polystyrene-block-poly(ethylene oxide) diblock copolymers, where the orientation of the micro domains was normal to the surface, and poly(ethylene-*alt*-propylene-*b*-lactic acid), where the orientation was parallel to the substrate. Analysis of the time-resolved GISAXS provided information on the size, morphology, and orientation of the films during solvent evaporation. In the final polymer talk, Phong Du, a student from Cornell University working with Prof. Ober and Prof. Wiesner, presented an intriguing overview of their GISAXS studies at the CHESS. Poly(styrene-*b*-ethylene oxide) structures were exploited to create silica nanostructures, making use of the silica precursor being readily concentrated in the poly(ethylene oxide) block and successive calcination. In a second project, nanosieves were prepared from cylindrical diblock copolymer films by selective photoreactions, in order to remove one block, while cross-linking the other for stability. To close out the session, Oleg Gang from Brookhaven National Laboratory presented a fascinating talk on liquid films on nano-sculptured surfaces. By varying the chemical potential difference between the liquid-vapor coexistence, small nanometer pits were filled with an organic liquid. By combining GISAXS and x-ray reflectivity at the NSLS, detailed information could be obtained on both the liquid in the pits and the thin wetting film above the surface.

After a short break, Gilles Renaud from the Commissariat à l'Energie Atomique (CEA) in Grenoble an inspiring whirl wind presentation of their work on real-time in-situ investigations of the morphology, organization, and internal structure of growing metal nanoparticles on oxide surfaces in ultra-high vacuum at ESRF. Results were presented for palladium, silver, and platinum on MgO(001) as well as for copper on alumina, gold on TiO_2, and copper and silver on ZnO. Combined GISAXS and wide-

angle x-ray scattering provided a wealth of information on the growth modes and particle morphology. Quantitative information could be extracted by theoretical modeling within the framework of DWBA. In the final presentation, Jin Wang from Argonne National Laboratory gave a thought-provoking talk on the kinetics of nanocomposites obtained from both SAXS and GISAXS measurements at the APS. Jin showed that the motion of the nanoparticles is highly anisotropic.

Following the talks there was an enthusiastic discussion on the future of GISAXS methods, including the needs of the emerging community. There was wide agreement that one of the key features of GISAXS is the ability to carry out real-time, in-situ measurements. While there are currently few dedicated GISAXS beamlines, GISAXS capabilities can often be implemented on existing SAXS or GID beamlines through the addition of a 2D detector. There was a lively discussion on CCD detectors including the need for faster readout times. For soft matter applications, it was noted that it is often desirable to combine GISAXS with reflectivity and SAXS measurements. Simultaneous optical measurements of the film thickness can be very useful for in-situ experiments. For hard-matter applications, it was noted that it is essential to combine GISAXS measurements with GID studies, in order to obtain shape and internal structural information. Finally, it was remarked that future GISAXS facilities should be user-friendly and well supported in order to open up the technique to non-specialists.

—Ben Ocko and Detlef Smilgies

Pharmaceutical Applications of Synchrotron Radiation Workshop

May 17, 2004

The workshop "Pharmaceutical Applications of Synchrotron Radiation" was held as part of the 2004 Annual Users' Meeting of the National Synchrotron Light Source (NSLS) on May 17th. The main goal was to bring together people working in the pharmaceutical industry with those familiar with synchrotron radiation techniques. The workshop focused on issues related to later stages of the drug development cycle, i.e., polymorphism, selection of salts and hydrates, quantification of crystallinity, partial states of crystallinity, etc. Research in drug discovery, such as protein crystallography, was not covered, although that has grown to a very large user base at synchrotron facilities worldwide.

One of the co-organizers, Evgenyi Shalaev of Pfizer, opened the discussion with an overview of the drug development cycle. Of several million candidates screened, only one or two will be reduced to a profitable new drug, after a development period of approximately fifteen years. X-ray techniques are crucial to many of the steps along the way, as well as the protection of intellectual property during the marketing lifetime of the drug.

Peter Stephens of Stony Brook University and the NSLS (also a workshop co-organizer) discussed the differences between laboratory and synchrotron x-ray sources, first from the standpoints of source properties and later in terms of access issues. He showed several comparisons of laboratory vs. synchrotron powder diffraction patterns and concluded that the additional information available was often dramatic in its ability to solve technical problems. He also emphasized that synchrotron sources are strongly motivated to attract new users, and while there may be some barriers to a new user getting a synchrotron research program started, they are generally fewer than popularly assumed, and the rewards are substantial.

Bill David and Kenneth Shankland, both of Rutherford Appleton Laboratory (UK), discussed many aspects of structure determination of small molecules from powder x-ray data. David emphasized the value of detailed structural crystallography, illustrated with the structure determination of a transient phase that existed for only one minute during the hydration of paracetamol (acetaminophen). He also showed the remarkable detail of information available, primarily through changes in diffraction peak shapes, of the transformation process in a dehydration reaction of the hypnotic zopiclone (see **figure below**). Shankland discussed the importance of various steps taken in experimental design and data collection to ensure the accurate solution of structures, emphasizing that these techniques, both experimental data collection and analysis through simulated annealing methods, are widely available to those who care to use them. His message is that you can solve, from powder diffraction, structures that represent the typical complexity

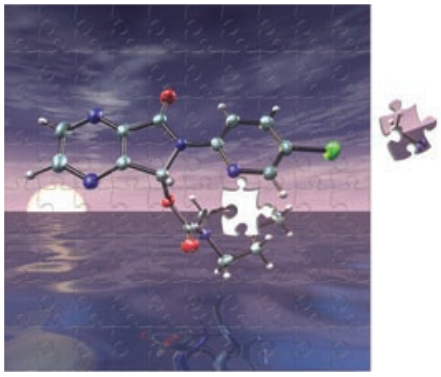

The molecular conformation of the hypnotic drug zopiclone in its monoclinic anhydrous form, solved from powder diffraction data taken at ESRF BM16. The puzzle alluded to in the illustration, that of significant batch-to-batch variation in the physical properties of commercially prepared zopiclone tablets, was solved only when XRPD was brought to bear. The experiments revealed the structural relationships between the previously unsolved monoclinic anhydrous form, the monoclinic dihydrate form, and the stable orthorhombic anhydrous form. Picture courtesy of Alastair Florence and Kenneth Shankland.

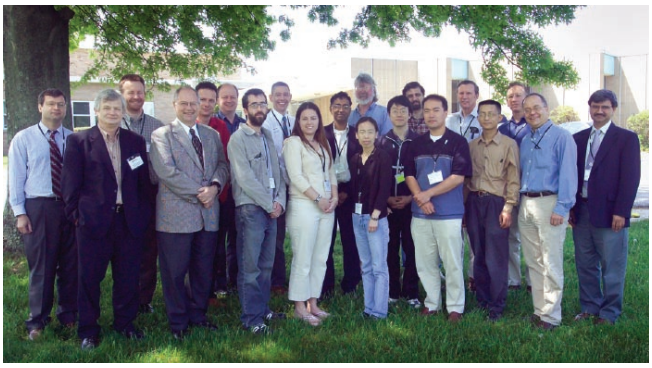

Pharmaceutical Applications of Synchrotron Radiation Workshop attendees

of most pharmaceutical compounds.

Mike Pikal of the University of Connecticut discussed the degradation of pharmaceutical compounds, such as freeze-dried proteins in the form of glassy solids. The stability of pharmaceutical solids can be extremely sensitive to formulation, and the relationship between thermodynamic measurements and structural relaxation is an important topic of research. The current state of understanding is largely empirical, and the development of other methods to characterize the state of glassy solids is an important challenge.

Shalaev discussed the nature of the disordered states, such as amorphous states, and crystalline mesophases, of pharmaceutically relevant solids. Amorphous solids can have advantages in solubility and bioavailability, but disadvantages in stability; amorphous phases can also arise during certain standard processing techniques such as milling, drying, and compaction. He challenged the audience to help to clarify the possible existence of more than one amorphous phase of a given system, so-called polyamorphism, and the extent to which nominally amorphous solids, e.g., protein/sugar mixtures, may be heterogeneous. Another important issue is the relationship between local structure of amorphous solids and the structure of crystalline phases of the same compounds.

The third co-organizer, Raj Suryanarayanan of the University of Minnesota, discussed x-ray measurements of the degree of crystallinity of pharmaceuticals, especially from the standpoint of monitoring the physical instability of products that are prepared as non-crystalline phases. He discussed *in situ* measurements of the crystallization of amorphous sucrose, performed with synchrotron radiation and an area detector. These experiments avoid the difficulties associated with the preparation of a large number of mixtures required for the traditional preparation of a calibration curve.

Satyendra Kumar, of Kent State University, discussed model systems related to the issue of delivering water-insoluble drugs. Such materials may be physically encapsulated in micelles or at the level of individual molecules, which then have interesting mesophases. He reported on synchrotron x-ray scattering studies of aqueous solutions of cyclodextrin and small molecule dyes, which have a variety of self-organized structures with varying degrees of orientational and structural order. He demonstrated how the use of external electric, magnetic, or mechanical (shear) fields can reveal important new structural details that otherwise cannot be obtained.

The final talk of the session was given by Heinz Amenitsch of the Austrian Institute of Biophysics and X-ray Structure Research outstation at the ELETTRA synchrotron source in Trieste. His topic was the use of simultaneous small- and wide-angle x-ray scattering to study nanostructural features of relevant solids. The size of domains of the different components of a pharmaceutical formulation, the nature of the internal surfaces, and the degree of dispersion are all accessible to these techniques. He showed that these measurements can be made with sub-millisecond time scales, allowing real-time study of the relevant structural changes during such processes as spray-drying.

At the end of the workshop, Bruno Hancock of Pfizer moderated a round-table discussion of collaboration between pharmaceutical scientists and facilities such as the NSLS. Some participants expressed concerns that the federal government might claim ownership of intellectual property derived from experiments at synchrotron sources, even if the user follows procedures for proprietary access. Obviously, this is a matter to be addressed by lawyers, not scientists, but the large investment in protein crystallography by major drug companies at synchrotron sources indicates that this might not be a serious impediment to the commercial use of these facilities. Participants who are not experienced with synchrotron radiation as a research tool probably came away thinking of synchrotron sources as valuable commodities, not heroic investments. And synchrotron experts should have seen that their expertise may be of real value to some important practical problems.

—Peter Stephens

Advanced Optical Systems and Metrology for High Power and Coherent Beamlines Workshop

May 19, 2004

Future light source beamline instrumentation will challenge users and instrument designers to take full advantage of the brightness and coherence of the x-rays delivered by the new sources. Since Brookhaven National

Laboratory has a strong tradition in the development of metrology instrumentation in support of synchrotron radiation optics, it is appropriate that this session on optical systems and metrology reviewed the current state-of-the-art in optical technology and metrology, and explored avenues that may lead to improved capabilities for the future.

Chris Jacobsen from Stony Brook University, who has extensive experience in the generation and use of coherent x-rays with existing sources, provided a summary of the capabilities of various groups around the world to produce small spot sizes from present sources of coherent x-rays. A Japanese group at SPring8 has demonstrated 90nm spot sizes with Kirkpatrick-Baez focusing optics, and 15nm line spacing in zone plates have been reported by workers at the Center for X-ray Optics at Berkeley.

Following Jacobsen's introduction to coherent imaging at x-ray wavelengths, the workshop heard from two speakers who are primarily involved with normal incidence UV and visible optics for large programs at Lawrence Livermore National Laboratory (LLNL) and at NASA Marshall Space Flight Center. The surface figure and finish requirements on normal incidence optics for DUV (Deep Ultraviolet) and EUV (Extreme Ultraviolet) lithography and for large space telescopes are nearly the same as those for grazing incidence optics, so it was appropriate to hear from John S. Taylor of LLNL and from Phil Stahl of NASA about mirror fabrication and metrology technologies that are being supported by these projects. Taylor discussed the development of diffraction-limited multilayer-coated optics for normal incidence EUV lithography systems that have been developed over the past several years by the Virtual National Laboratory consortium of three national laboratories and three companies involved in developing tools for the semiconductor manufacturing industry. Slope errors on these optical components are in the 200 nrad range, which is where synchrotron optics will need to be for effective utilization of the next generation of high-brightness x-ray sources. Stahl gave an overview of future NASA space telescope missions and the technology that will be required to build large, lightweight mirrors and structures. Over the past few years he has organized a symposium, "NASA Tech Days," for NASA contractors and university grant recipients to present progress in technology development programs funded by government agencies. Of interest to the Synchrotron Radiation (SR) community are the various materials-development projects investigating the use of Be, SiC, and other ceramic and composite materials as high power mirror substrates, and the fabrication technologies that accompany these new materials.

Advanced Optical Systems and Metrology for High Power and Coherent Beamlines Workshop attendees

Don Golini from QED Technologies in Rochester, NY, gave a presentation on a new surface finishing technique that looks quite promising as an alternative to conventional pitch polishing for the production of spherical and aspherical surfaces. His company has developed various polishing machines that use magnetorheological fluids as the polishing medium. These fluids change viscosity by orders of magnitude when a magnetic field is applied and can conform to exotic surface shapes not possible with hard laps, such as ellipsoids and toroids. A great deal of research has gone into characterizing the polishing process, which is highly deterministic. With the appropriate metrology, it is possible to quickly correct for figure errors and converge rapidly to the desired surface shape.

Refractive optics for focusing x-ray beams are a new addition to the techniques available to users for producing small spot sizes. Ken Evans-Lutterodt (National Synchrotron Light Source) gave an overview of the subject and discussed the production of the optimum elliptical hole shape with an e-beam writer and the use of diamond as a substrate for high heat load situations. Ali Khounsary, Argonne National Laboratory, followed with a discussion of high heat load optics. He emphasized the need for a systematic approach to the design of optical systems that incorporate knowledge of the source parameters, mirror substrate characteristics, mechanical design, and testing.

Following the lunch break, Peter Takacs (BNL/Instrumentation) discussed metrology issues related to the Long Trace Profiler (LTP). The LTP is widely used to measure the surface quality of large aspheric x-ray optics. In order to reach the 100 nrad measurement accuracy level, improvements are needed in the quality of the internal optical components in the system. Custom-made glass prisms with superpolished surfaces will be needed to reduce the systematic error to below the current 1 μrad level. Wayne McKinney (Advanced Light Source, Lawrence Berkeley National Laboratory) followed with a discussion of issues that are driving the direction of SR metrology. Although the LTP has served well in the past, other alternative metrology techniques need to be explored, such as stitching interferometry, Hartmann sensors, and multi-beam autocollimator techniques such as those proposed by Polack's group at SOLEIL in France and by Weingärtner's group at the

Physikalisch-Technische Bundesanstalt (PTB) in Braunschweig, Germany.

The final session of the day began with a description of Kirkpatrick-Baez (KB) mirror nanofocusing systems by Gene Ice from Oak Ridge National Laboratory. The practical limit to the focal spot size is in the range of 10 to 30 nm, which can be produced by highly demagnifying (~1000:1) elliptical cylinders. These mirrors need to have slope error tolerances of less than 200 nrad in order to perform correctly. The technique of differential deposition, which he has pioneered, appears to be a promising tool for converting cylindrical surfaces into accurate elliptical shapes.

The final two talks were presented jointly by Riccardo Signorato (ACCEL, France) and Daniel Hausermann (Advanced Photon Source, Argonne National Laboratory) as they related to the fabrication and use of modular piezoelectric bimorph mirrors as adaptive optics. The piezoelectric bimorph has been developed by Signorato and is currently in use at a number of sites, including beamlines at the APS. Hausermann uses a pair of bimorphs in a KB configuration to focus a 500µm x 500µm hard x-ray beam down to a 10 µm spot. The longest size currently available is 1050 mm in length with N=33 actuator segments. Signorato is looking into adding a Shack-Hartmann wavefront analyzer to the system to enable automated closed-loop focus control for the mirror.

Following the final talk, a quick tour of the Optical Metrology Laboratory in the NSLS Instrumentation Division was offered to those participants who remained. The workshop was successful in bringing together members of several different communities, including conventional optics fabricators, end users, and metrology specialists, to share thoughts and ideas on the current state of optical component technology, and to chart a course toward future capabilities.

—Peter Z. Takacs and Steven Hulbert

Applications of Synchrotron-Based Methods to Hydrogen Storage Materials Workshop

May 19, 2004

A workshop on "Applications of Synchrotron-based Methods to Hydrogen Storage Materials" was held in conjunction with the 2004 National Synchrotron Light Source (NSLS) Users' Meeting on May 19, 2004. The purpose of the workshop was to bring together scientists who synthesize materials with applications in hydrogen storage and scientists with expertise in the application of synchrotron radiation methods, who currently study these materials.

The workshop was opened by Doon Gibbs, the Associate Laboratory Director for Basic Energy Sciences at Brookhaven National Laboratory (BNL). He emphasized the importance of the Hydrogen Energy Project (production, storage, utilization) as one of the missions of the Department of Energy (DOE), and encouraged collaborations between scientists within BNL and with outside groups by utilizing facilities like the NSLS and the Center for Functional Nanomaterials (CFN) for research.

Applications of Synchrotron Based Methods to Hydrogen Storage Materials attendees

John Petrovic, from the Hydrogen Storage Team in the DOE Office of Hydrogen, Fuel Cells, and Infrastructure Technology, described in his talk titled "The DOE National Hydrogen Storage Project: Addressing Key Performance Targets for Materials-based Hydrogen Storage Systems" the targets for automotive research over the next 15 years, and the funding efforts by the DOE to reach these targets. He presented different projects and Centers of excellence that actively work in the field of hydrogen storage and that pursue different paths trying to create a successful system. Currently, none of the proposed hydrogen storage systems achieves the proposed targets for 2005!

James Reilly from the Department of Energy Science and Technology at BNL described in his talk "The Application of Hydrogen Driven Metallurgical Reactions to Prepare Reactive Nanoscale/Nanocomposite Materials" several ways to create nano-composite metal-hydrides, and discussed their properties. By doping some materials with fairly large amounts of different metals, the storage capacity can be increased, and the temperature for release is lowered.

Zafar Iqbal of the Department of Chemistry and Environmental Science at the New Jersey Institute of Technology talked about "Electrochemically-Induced Hydrogen Storage in Metal-Functionalized Carbon Nanotubes." He described different ways to synthesize single-wall nanotubes (SWNTs), ways to functionalize the SWNT with metals, and their properties. Experimental investigation with Raman and Fourier Transform Infrared (FTIR) spectroscopy indicate a chemisorption process in Co-

doped SWNT, while (weaker) physisorption is present in undoped nanotubes.

Tom Vogt of the CFN talked about "Hydrogen Storage and Nano-Structure." He emphasized the importance of clearly characterizing the materials to better understand their storage and release mechanisms. High-brightness synchrotron radiation sources like the proposed NSLS-II are ideal sources for real-space and dynamical imaging. Also, probes at the CFN, such as proximal probes, are well suited for studying SWNTs, for example.

Alexander Ignatov of the Department of Physics at the New Jersey Institute of Technology presented in his talk "X-ray Absorption Studies of Hydrogen Storage Materials – Strength and Limitations" experimental results of EXAFS and XANES experiments studying the Ti K-edge in Ti-doped $NaAlH_4$. The data indicate that Ti does not substitute Na in the lattice. Instead, amorphous $TiAl_3$ is formed, and H is found in the first coordination sphere about Ti. The EXAFS-analysis allows extraction of the position of H, but the H coordination numbers have large errors.

Yan Gao from the GE Global Research Center talked about "Characterization of $NaAlH_4$ by High-Pressure X-ray Diffraction and in-situ EXAFS." He presented the first powder-diffraction data of the re-hydrogenation process measured with high time resolution. The data clearly indicate that two steps in the dehydrogenation and re-hydrogenation process have to be completed individually before the next step can start. He also observed an increase in particle size, which slows down the reactions. His Ti XAS-data also indicate the formation of $TiAl_3$, and the growth of $TiAl_3$-crystals with the number of cycles.

The final speaker, Najeh Jisrawi from the Department of Physics and Astronomy at Rutgers University, discussed "Synchrotron XRD Studies of Hydrogen Absorption in Metallic Multilayers and Nano-Particles." He applied surface x-ray diffraction to study charge-discharge curves of Pd and Nb/Pd/Nb thin films, and of polyhedral clusters with magic-number sizes. Molecular dynamics calculations support his experimental results and demonstrate that a cluster with a size of 8 nm shows similar behavior to a thin film.

The workshop was concluded with a brief discussion of techniques and equipment that are required for further successful studies of hydrogen storage materials at the NSLS.

—Wolfgang Caliebe and Trevor Tyson

Nanoprobes for Nanosciences Workshop

May 19, 2004

A workshop on synchrotron-based nanoprobes was held on May 19th, 2004 as part of the National Synchrotron Light Source (NSLS) and Center for Functional Nanomaterials (CFN) annual users' meetings. The goal of the workshop was to explore the scientific opportunities offered by synchrotron-based nanoprobes, with emphasis on combined low-energy/photo-electron microscopy (LEEM/PEEM), soft x-ray microscopy, and x-ray micro-diffraction.

Nanoprobes for Nanosciences Workshop attendees

Bob Hwang, director of the CFN at Brookhaven National Laboratory (BNL), opened the workshop by giving an overview talk about the status of the CFN, current CFN capabilities that are open for users, including scanning probes, transmission electron microsocopy (TEM) and NSLS beamlines, and the plan to establish close collaborations with other BNL research departments. He also outlined the vision to provide the nanoscience user community 24/7 access to a broad range of "off the shelf" instruments, as well as develop new and novel characterization methods in conjunction with partner users to achieve a more efficient transfer of information and technology.

After the introduction, the workshop was divided into three dedicated sessions. In the soft x-ray microscopy session, Harald Ade from North Carolina State University presented an extensive review of his work on the characterization of polymers using soft x-ray transmission microscopy (XTM). The chemical sensitivity in near edge x-ray absorption fine structure (NEXAFS) and linear dichroism are exploited to provide a unique contrast mechanism to discriminate different components in the sample as well as characterize the crystallinity and morphology of the sample. The second speaker of the session was Chris Jacobsen from Stony Brook University. Chris first gave an excellent review of x-ray microscopy using zone-plates as well as the advances made in recent years in the fabrication of high-resolution x-ray zone-plates. In the second half of his talk, Chris talked about diffraction imaging, a new technique that has attracted a great deal of attention recently because the possibility of achieving higher spatial resolution than that of zone-plate-based x-ray microscopy. The key in diffraction imaging is, of course, recovering the phase information that is lost in the measurement. Chris gave a detailed account of a very efficient iterative algorithm recently developed.

After a short break, Cev Noyan from IBM and Columbia University started the session on hard x-ray micro-spectroscopy and micro-diffraction. Cev presented a study of strain in SiGe crystals grown on Si crystals. It was a very nice demonstration of the power of micro-diffraction. In this case, he was able to map out the strain in both the SiGe layer as well as that of the substrate. He also discussed in some length the challenges in finding and focusing on a single grain using x-ray microbeams. The second talk in the session was given by Barry Lai from the Advance Photon Source (APS) at Argonne National Laboratory. Barry talked about the applications of micro-fluoresence and x-ray absorption near edge spectroscopy (XANES) spectroscopy to life science problems, in particular the role of trace amounts of metals and metal oxides in immunology and intracellular processes. At the 2ID at the APS, x-rays down to 200 nm x 200 nm, with intensities up to 2 x 10^9 ph/sec, are achieved using a hard x-ray zone-plate. These hard x-ray zone-plates are extremely difficult to produce because of the narrow width and the height/width aspect ratio required. Barry also shared his experience in how to accurately align optics and position samples, a very challenging problem as the spatial resolution of the experiment improves to sub-micron level.

The third speaker of the session was Ken Evans-Lutterodt of NSLS. Ken gave an overview of the microdiffraction project at the X13B beamline at the NSLS. The project is funded by the Department of Energy to serve the increasing needs of nanoscience users. The instrument, taking advantage of the small source size at the X13 straight section of the ring, is designed to perform sub-micron x-ray micro-diffraction and imaging. It has the unique capability of allowing experimenters to choose the focusing optics to optimize their measurement. The beamline will also serve as a test bench for new emerging focusing optics and x-ray imaging techniques.

The third session, focused on LEEM/PEEM, began after lunch. Rudolph Tromp from IBM gave a broad overview of the history, current state-of-the-art, and future possibilities of this powerful technique. For example, structural information with 4 nm spatial resolution can be achieved with LEEM today. There are also a variety of contrast mechanisms that can be exploited in LEEM, for example, using bright and dark field imaging, as well as work function and electron energy dependence. A LEEM instrument can also be combined with a photon source to perform PEEM to obtain chemical contrast. The potential of combining the structural information from LEEM and chemical information from PEEM is extremely exciting. Finally, by using a spin-polarized electron source, LEEM can be used to study magnetic surfaces and interfaces (SPLEEM). Time-resolved study of magnetization dynamics has also been demonstrated. Stefan Heun from ELETTRA Trieste/Italy presented the capability and results from the X-PEEM instrument located at Synchrotrone Trieste. The unique feature of the instrument is the energy filtering of photoelectrons. It enhances the chemical sensitivity significantly. The session ended with a talk on the next generation of PEEM developed at the Advanced Light Source by Jun Feng from Lawrence Berkeley National Laboratory (LBNL). Jun talked about the design of the PEEM3 project at LBNL. The goal of PEEM3 is to achieve spatial resolution down to 5 nm, almost an order of magnitude better than the PEEMs currently operating at various synchrotron facilities. Jun discussed in detail the critically important aberration correction system, including an electron mirror aberration corrector and an aberration-free magnetic beam separator.

Following the three focused sessions, there was a lively discussion period, chaired by Peter Sutter of CFN/BNL, Ken Evans-Lutterodt, and Chris Jacobsen. These valuable ideas will be taken into consideration in the design of the new LEEM/PEEM end station and for the future upgrade of the x-ray microscopy programs at the NSLS.

—Cecilia Sanchez-Hanke

Crystallization: Focus on Membrane Proteins Workshop

May 19-20, 2004

The Crystallization workshop organized in conjunction with the 2004 National Synchrotron Light Source Annual Users' Meeting focused this year on crystallization techniques available to membrane proteins. This two-day workshop covered different crystallization methods from the most standard vapor diffusion to more advanced techniques. A morning of introductory talks was followed by five practical sessions, of two hours each, where participants had the opportunity to carry out different crystallization methods in the laboratory. The main purpose of this workshop was to bring the practical aspects of the crystallization methods to the participants, the exchange of experiences and ideas being its essence.

Naomi Chayen, Imperial College London, in her talk "Tackling the bottleneck of protein crystallization: Practi-

Crystallization: Focus on Membrane Proteins Workshop attendees

cal techniques with a difference," introduced the phase diagram and discussed the several different crystallization techniques developed for soluble proteins and the necessary modifications for crystallization of membrane proteins. The laboratory practical sessions included setting up microbatch and vapour diffusion trials using oils as a tool to aid crystal growth. Participants had the opportunity to try several different crystallization configurations.

Peter Nollert, deCODE Genetics, in his talk "Miniaturization of the cubic phase," introduced the cubic lipid phase method and discussed the difficulties of membrane protein crystallization. The cubic lipid phase method was demonstrated in the laboratory and participants were able to set up crystallization trials for bacteriorhodopsin. The application to soluble proteins was also introduced. A number of participants tried the method with their own proteins with success.

Petra Fromme, Arizona State University, talked about "Overcoming the Crystallization Problems of PSI and PSII." She discussed the importance of the phase diagram to the crystallization of PSI and PSII proteins. The contribution of the dialysis method was introduced and participants were able to assemble their own crystallization reactors. Most experiments lead to the crystallization of PSI within 24 hours and by the end of the workshop participants were able to harvest some of the crystals.

Marie Claude Marchand, NEXTAL Biotechnologies, in her presentation on "The Vapour Diffusion Method," discussed the vapour diffusion method, as well as seeding, derivatization, and optimization of the phase diagram. Some participants were able to screen for the best crystallization conditions of their own protein.

Ana Belen Moradela Merlo, University of Granada, discussed "Protein Crystallization by the Counter," diffusion, and introduced the counter diffusion method. Participants were able to set up crystallization trials of soluble proteins in the "Granada Box." Possible applications to membrane proteins were discussed.

The demand for the course was overwhelming. It was oversubscribed by over 100%. At the end of the workshop students were asked to evaluate the course and suggest changes and additions; two thirds responded to the survey. Overall the course was rated as extremely useful as reflected in one of the answers to the survey: "I learned a great deal about crystallization methods. Most importantly I now understand the more practical aspects of each method that I was not aware of. These ideas cannot be gained from other formats." All participants who answered the survey thought that the workshop should be offered again.

—Vivian Stojanoff and Naomi Chayen

UEC Community Service Award Presented to Sue Wirick

May 20, 2004

The National Synchrotron Light Source Users' Executive Committee (UEC) presented the 2004 UEC Community Service Award to Sue Wirick of Stony Brook University's Physics Department. Sue is a beamline scientist for the X1A insertion device beamline. This award is given for service, innovation, and dedication to users of the NSLS, and she is well deserving of that honor.

Members of the NSLS user community nominated Sue for this award. Here are some of the comments users made about her wonderful contributions:

UEC Chair Tony Lanzirotti presents the award to Sue Wirick.

- "Since joining the X1A effort more than a decade ago, Sue Wirick has played a central role in the development of the scientific program and in supporting user access to the spectromicroscopy facilities. Quite simply put, she is the key to outside users' ability to carry out experiments."
- "Our research team owes very much to the assistance that Sue Wirick was able to give us. She was available day and night, gave excellent advice, steered us through the experimental process with ease, and provided a positive and friendly environment that made it a pleasure to work at the beamline."
- "Sue Wirick actively participates in meetings of the user community to improve the user support at the NSLS. She contributed heavily in the past to making the annual user meeting a success by helping in the planning and chairing of sessions. Sue is known by users for helping with technical problems even for beamlines that are not her responsibility."
- "Sue Wirick has been a godsend to the NSLS community. She is one of the rare people who will help anyone, including the most difficult personalities, when they have

a problem. She will do this anytime, even on weekends and evenings. She is the person that I recommend first to outside users who want to find out more about NSLS and Brookhaven. She always provides detailed and concise advice on instrumental capabilities, and also on the more mundane aspects of how to get beam time, availability, etc."

Tony Lanzirotti, the Chair of the UEC, presented the award to Sue at the NSLS Users' Meeting banquet on the evening of Tuesday, May 18th. Sue receiveed a $250 gift certificate and her name was engraved on the plaque on display in the NSLS lobby. Congratulations Sue and well done!

—Tony Lanzirotti

The PASS System Arrives

June 23, 2004

We are very happy to announce the arrival of the new Proposal, Access, Safety and Scheduling (PASS) system, which debuted in May for the submission of general user proposals for the fall cycle.

PASS was developed to facilitate the submission and review of general user and proprietary proposals and the allocation and scheduling of beamtime at the NSLS. To meet DOE reporting requirements and to ensure safety compliance, the safety approval form is also incorporated into the system.

The first phase of development (proposal submission, safety approval, and the scheduling of general user proposals) is complete and online. Proposals (and Px Forms when appropriate) are submitted online in one system and routed for beamline review for feasibility and safety purposes. PASS then routes the form to proposal review panel (PRP) members for peer review and ratings, to allocation panel members for beamtime allocations, to NSLS safety staff for review and approval, and finally for beamtime scheduling. Each principal investigator and reviewer is granted individual access according to permissions assigned.

Instructions and frequently asked questions are provided throughout the system to ensure user friendliness and accessibility. The production version will soon include a link to send comments or report functionality issues or problems.

Further development will take place over the next few months to integrate proprietary proposals, safety approval for Participating Research Team (PRT) experiments, to further develop scheduling for all experiments, and to add more functionality and capabilities. The final phase will incorporate a reduced lead-time to provide for rapid access.

Some proposal process changes introduced in the PASS system are:

- PASS randomly assigns each proposal to three PRP reviewers who have reviewed the lowest number of proposals for the given cycle to date. This ensures that all reviewers review approximately the same number of proposals and that members are not overburdened with requests, and plans are in place to increase the pool of reviewers. PASS does not assign proposals to a PRP member whose institution is the same as the PI.
- PASS notifies PRP members by email immediately after submission of the proposal by the PI, allowing reviews to take place as soon as the PRP member is able.
- PRP reviews are completed independently of other PRP members and all ratings are averaged for a final rating.
- Lifetime days are no longer requested. The PI requests the number of days needed in a given cycle, and this is the information that is vital for review, allocation and scheduling.
- Penalties for canceling beamtime after allocation have been eliminated. Our goal is to re-assign canceled beam time to other users who were not allocated due to high demand.
- The one-half point credit given for one cycle to lower-rated proposals not allocated beam time is no longer given. Alternatives available are for the PI to submit a new proposal based on an existing one and to thereby address concerns or questions that were raised by reviewers in the previously submitted proposal. Another planned capability is to provide PRTs the ability to offer PRT beamtime to rated proposals that did not receive an allocation of beam time since higher-rated proposals filled up the general user obligation for that beamline.
- PIs must assign a lead experimenter to serve as lead person for the experimental team while present on the NSLS experimental floor, who will in turn receive an email with links to his/her roles and responsibilities.

—Mary Anne Corwin

NSLS EXAFS Data Collection and Analysis Short-Course "Graduates" 32 Students

June 22-25, 2004

A hands-on EXAFS Data Collection and Analysis Short-Course was held June 22-25, 2004 at the NSLS. The course was co-organized by Bruce Ravel (Naval Research Laboratory) and Simon Bare (UOP LLC), with excellent administrative support by Lisa Tranquada (SFA, Inc.) and Melissa Abramowitz from User Administration.

Thirty-two eager participants (graduate students, postdocs, and institution and industrial scientists), representing universities, national laboratories, research institutes, and industry, attended the four-day course.

Participants in the 2004 NSLS EXAFS course

Among the 32 participants, 15 were new users to the NSLS. The participants had diverse research interests across a broad spectrum of scientific fields, including materials science, geological and environmental sciences, catalysis, and biology.

The four-day course was divided into morning lectures, with two afternoons of hands-on data collection using seven different NSLS spectroscopy beamlines (X9B, X11A, X11B, X18B, X19A, X23B, and X26A), and two afternoons of data analysis. The instructors on the beamlines were Faisal Alamgir, Wolfgang Caliebe, Scott Calvin, Syed Khalid, Tony Lanzirotti, Nebojsa Marinkovic, and Kaumudi Pandya.

The eight morning lectures were: "Introduction to XAFS" and "Basics of sample preparation" by Matt Newville (CARS, University of Chicago), "XANES Measurements and Interpretation" by Simon Bare (UOP LLC), "Detectors and Synchrotron Radiation" by Peter Siddons (BNL), "Basics of Data Processing" by Scott Calvin (Sarah Lawrence College), "A Practical Introduction to Multiple Scattering Theory" by Bruce Ravel (Naval Research Laboratory), "Introduction to Data Analysis" by Shelly Kelly (Argonne National Laboratory), and "Incorporating XAFS into a Research Program" by Vince Harris (Northeastern University). The morning lectures included ample time for stimulating questions and discussion.

For the first two afternoons the participants were divided up into small groups in order to spend time on the NSLS floor at an EXAFS beamline. There, they learned first hand how to collect high quality EXAFS data. Each student became familiar with beamline operation and sample preparation while collecting EXAFS data on representative samples from their own individual research projects. It was fascinating to see the diverse array of samples and projects in which EXAFS was being used.

During the last two afternoons the participants learned EXAFS data analysis techniques using the data they had collected the prior two days. The participants enjoyed informal discussions during coffee breaks, lunches, and the dinners that were included in the course fee.

There was a tremendous amount of information disseminated over the four days. All the participants left the course with new friends and armed with the basic tools to apply x-ray absorption spectroscopy to their own research programs. The organizers thank all those who made the course the great success that it was!

We plan to offer the course again in 2005. Please check the NSLS website for updated information.

The course was sponsored by the NSLS, with support from the Center for Environmental Molecular Science at Stony Brook University.

—Simon Bare

NSLS Visiting Scientist Mehmet Aslantas Wins Prestigious Lecturer Award

July 18-22, 2004

National Synchrotron Light Source visiting scientist Mehmet Aslantas won the prestigious Margaret C. Etter Student Lecturer Award for a talk on his recent work: how to reduce the effects of radiation damage to protein crystals during synchrotron x-ray studies.

He received the award at the American Crystallographic Association national meeting, held in Chicago, Illinois, on July 18-22, 2004. The Etter award, given out just once a year, recognizes achievement and future potential for scientists at an early stage in their independent careers.

Aslantas, who initially came to the NSLS for six months through a U.S. Department of Energy Cooperative Research program, received an extension that allowed him to stay for over a year. "The NSLS is a great place to work, and I couldn't have completed my research or won this award without the research extension I received," said Aslantas. "I

would like to thank the NSLS Chairman, Steve Dierker, the Associate Chair for User Science, Chi-Chang Kao, Vivian Stojanoff, and the User Administration office for their support."

Aslantas worked under Stojanoff's supervision at NSLS beamlines X6A and X17B1. In his talk, titled "Radiation Effects on Biological Samples," he described his work at the beamlines. At X6A, he studied the effect of low-energy x-rays on 'Lyzozyme' crystals, which are standard test protein crystals. At X17B1, the sample was subjected to high-energy x-rays.

"My experimental results show that, with lower-energy x-rays, the sample absorbs more radiation than at higher energies, in which it absorbs less energy and sustains no significant damage," he said. "This is because the low-energy x-ray beam interacts with the inner shell electrons in the atoms of the protein, causing an overall higher dose to the sample. This leads to structural damage and limits the structural information we can learn about the sample. However the high energy x-rays interact with the outer shell electrons in the atom of the protein. This interaction, known as Compton scattering, plays a role in causing the overall dose deposited to the sample to be less significant. The sample will have a longer life time, too."

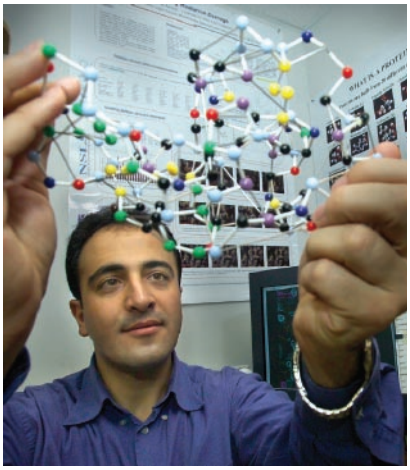

Mehmet Aslantas holds a ball-and-stick model of the test protein he used in his research.

Aslantas' work was funded by a U.S. Department of Energy Cooperative Research program, which allowed him to work at the NSLS as part of a scientific exchange program with another synchrotron, SESAME (Synchrotron-light for Experimental Science and Applications in the Middle East). SESAME is under construction.

Aslantas prepared three manuscripts describing his work at the NSLS. His experience will help him form a protein crystallography group at his home institution, Hacettepe University in Ankara, Turkey. In turn, this group will be working with SESAME to develop a protein crystallography beamline at the facility. After his return to Hacettepe University, Aslantas expects to keep in close contact with the NSLS and will continue his research.

—Laura Mgrdichian

Summer Sunday Visitors Battle the Weather for a Great Day at NSLS

August 1, 2004

Despite the rainy, humid weather, NSLS Summer Sunday, held August 1, still pulled in over 450 members of the community and was one of the most enjoyable Sundays yet.

For eight consecutive Sundays each summer, the Brookhaven National Laboratory Summer Sundays program welcomes the public to see the popular Whiz-Bang Science Show and several hands-on science exhibits. Each Sunday also showcases a different BNL facility.

Visitors wishing to see the NSLS began the tour in Berkner Room B, where there were NSLS-specific exhibits and posters, manned by NSLS staff volunteers Steve Ehrlich, Nick Gmur, Payman Mortazavi, Eva Rothman, and Marty Woodle, and student volunteers Meghan Ruppel and Jyoti Tibrewala. The visitors then saw a short "Introduction to the NSLS" overview film before boarding a bus for the facility.

Upon arrival, they went upstairs to see a presentation by an NSLS scientist, who welcomed them and gave more detailed information on the facility and the research performed here. They also discussed how they use synchrotron light to perform their individual research. Many guests were very curious about the NSLS, and the speakers answered several questions. This year's speakers were Marc Allaire, Elaine DiMasi, Tony Lanzirotti, Lisa Miller, Peter Siddons, and Vivian Stojanoff.

Visitors then filed down to the NSLS lobby and patio, where more activities awaited them, such as the "What am I looking at?" picture window that provides an impressive view of the VUV-IR experimental floor, a sight that is always fascinating for guests. NSLS staff members Steve Bennett, Mike Buckley, Susila Ramamoorthy, and Larry Fareria explained the view and answered questions, such as the common query, "What's the aluminum foil

Student volunteer Angela Padilla shows a group of young Sunday visitors how to build a protein crystal model from gumdrops.

for?" This year, for the first time, large neon numbers were placed on beamline components, which made it easier for guests to see the features described to them.

NSLS scientist Zhong Zhong (right) shows several Summer Sunday guests how a monochromator divides visible light into a rainbow of colors.

The lobby also contained several exhibits, such as "See the Light," in which volunteers Randy Smith and Ted Feldman showed how a fiber optic cable siphoned actual NSLS light into the lobby, and "Flowing Lasers," in which Tom Dickinson and Raji Sundaramoorthy made a laser beam "flow" down a stream of water. The children watched the laser light fill the water and sparkle when they put their hands under the stream. Other displays were hosted by additional NSLS scientists, staff, and students: Peter Abbamonte, Marc Allaire, Alec Bernston, Brandon Chapman, Ed Haas, Amubhav Jain, Payman Mortazavi, Angela Padilla, Vivian Stojanoff, Tejas Telivala, Adele Wang, and Zhong Zhong.

On the patio, the visitors saw how superconductivity can "levitate" a magnet and how boiling liquid nitrogen sends a sprinkler spinning. Scientists Wolfgang Caliebe and Cecilia Sanchez-Hanke kept watch over the outdoor activities.

A fun, new event this year was the quiz/raffle, which turned out to be quite successful. Each visitor received a yellow quiz card with questions, which could only be answered by visiting each exhibit. This encouraged them to stop at each one and also made the day more interactive. Every 20 minutes, the quiz cards were collected and Gerry Van Derlaske, the enthusiastic quiz/raffle MC, picked a winning name. Each winner received an NSLS flashlight.

Additionally, at several points during the day, Caliebe braved the rain to launch a giant water rocket in the parking lot across from the NSLS – a hit with all the guests.

The day was made possible by several additional volunteers, who served as tour guides, escorts, and support personnel: Melissa Abramowitz, Diane Hatton, Madeline Hughes, Laura Mgrdichian, Eileen Morello, Wendy Morrin, Gina Paveglio, Lydia Rogers, Nancye Wright, and Emil Zitvogel.

—Laura Mgrdichian

Summer Student Research at the NSLS

August 10, 2004

Each summer, many high school and college students perform summer research projects at Brookhaven National Laboratory. Many of the students work at the NSLS, teaming up with an NSLS scientist, as part of Laboratory-sponsored research internship programs.

The students work with scientists and engineers in a wide range of research fields, including medical sciences, geology and environmental sciences, chemistry, materials science, physics, and electrical and mechanical engineering. In addition to their research projects, students have the opportunity to attend scientific lectures, tour Brookhaven research facilities, and participate in numerous social activities.

The following are summaries of programs that NSLS summer students participated in, and short profiles of some of the students that performed research here this summer.

Community Summer Science Program (CSSP)

This program invites high school students who have completed their junior or senior year to come to BNL for a six-week period, where they attend morning lectures and demonstrations by BNL scientists, workshops, and afternoon internships. Volunteer BNL mentors guide the interns in individual research projects.

Michael Dibiccari, a junior at Hauppauge High School, worked at beamline X22B with Elaine DiMasi as part CSSP. After growing mineral crystals, he studied the x-ray diffraction patterns they created in order to determine how the crystals formed. This research will help scientists understand the process of biomineralization.

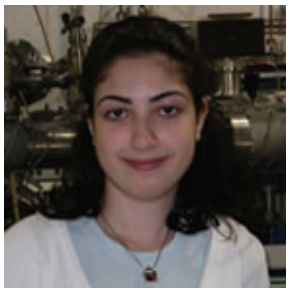

Dina Halajian is a senior a Half Hollow Hills High School East. Participating in CSSP, she also worked with NSLS scientist Elaine DiMasi. They investigated the growth process of minerals by growing calcium crystals and studying them at beamline X22B with a microscope. Their results will add to the field of biomineralization.

Science Undergraduate Laboratory Internships (SULI)

The SULI program is sponsored by the U.S. Department of Energy (DOE), and offers internships for college students in the spring, summer, and fall terms. Participants are paired with a member of the BNL staff to perform a research project in chemistry, physics, engineering, biology, nuclear medicine, applied mathematics, particle accelerators, or science writing.

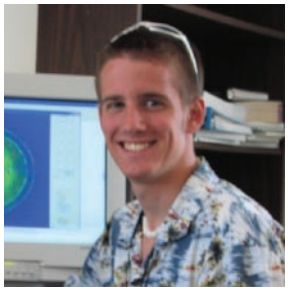

Alec Bernston is a sophomore at Cornell University, where he studies computer science. This summer, in the SULI program with NSLS mentor Vivian Stojanoff, he participated in the development of a software package for protein crystallography diffraction analysis. The software will help speed up the diffraction process.

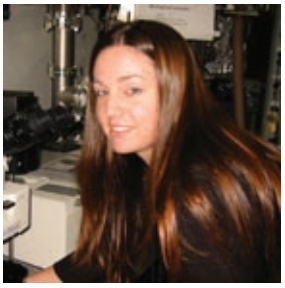

Meghan Ruppel is a senior at Stony Brook University, and will soon earn her degree in Materials Science and Engineering. In the SULI program, she worked with Lisa Miller at beamline U10B, using infrared light to study the chemical composition of bone and calcified cartilage in osteoarthritis. This work will help them understand how the makeup of bone in knee joints plays a role in cartilage breakdown.

Ted Feldman is a sophomore at Stony Brook University. As part of Stony Brook's Interdisciplinary Biomedical Research Program, Ted worked with Lisa Miller to study the chemical and mechanical properties of bone that has been mineralized. This work will help increase scientists' understanding of bone quality, which may help predict osteoarthritis.

Jyoti Tibrewala is a graduating senior at MIT and this summer she worked with Lisa Miller as a SULI participant. They studied the effects of pressure on the chemical composition of bone mineral using infrared spectroscopy at beamine U2A. Their results will help explain bone loss in post-flight astronauts and osteoporosis patients.

Anubhav Jain, a SULI participant, worked with Vivian Stojanoff, designing computer software that will automatically position crystal samples in the path of an x-ray beam for diffraction studies. This task is currently done manually by researchers – thus, this new software will decrease the time needed to collect data and allow the researchers to solve more crystal structures in less time.

Also involved in research at the NSLS this summer were SULI participants Patrick Lynch (Bucknell University) and Matthew Teng (Cornell University), who worked with NSLS mentors John Skaritka and Zhong Zhong, respectively. Lynch worked on a "Mechanical Design of a Five-Meter Superconducting Undulator" and Teng's project was titled "Use of Diffraction Enhanced Imaging to Determine Refractive Indices of Various Tissues at Select Energies."

Pre-Service Teacher program (PST)

In this program, a collaboration with the National Science Foundation and sponsored by the DOE Office of Science, teachers in training are paired with scientist mentors and a professional teacher, and immersed in a research environment. The pre-teachers perform scientific research, which helps them learn how to better explain scientific concepts in a classroom environment.

Participating in PST, Angela Padilla worked with Vivian Stojanoff to study samples from a native American 17th century artifact, using different spectroscopy and diffraction techniques. Their research may help anthropologists understand the social and economic relationships between native Americans.

Faculty and Student Teams (FaST)

The FaST program pairs a student/professor team from a university or college with limited research capabilities with a BNL scientist. For 10 weeks, the faculty/student team performs research they cannot do at their home institution, which not only helps the BNL researcher, but also gives the team experience while building a relationship between the institution and BNL.

At the NSLS, FaST program summer visitors from Southern University in Louisiana were faculty member Elhag Shaban and students Clifford Williams and Shayla Wilkinson. They worked with NSLS scientist Peter Siddons on new electron multiplier structures for synchrotron x-ray detector systems.

—Laura Mgrdichian

Parney Albright, DHS, Visits BNL

August 27, 2004

Parney Albright, Assistant Secretary of Homeland Security, Science & Technology Division of the Department of Homeland Security, came to BNL on August 27. After a welcome by BNL Director Praveen Chaudhari, Interim Deputy Director for Science & Technology Peter Bond, Brookhaven Site Office Manager Michael Holland, and Associate Laboratory Director for Energy, Environment & National Security Ralph James, Albright and his executive assistant Leslie Stone toured facilities and met with several scientists over lunch.

During a visit to the Radiation Detector Testing & Evaluation Center, James discussed portal monitors and hand-held monitoring devices and the results of BNL's

At BNL's Radiation Detector Testing & Evaluation Center are: (from left) Leslie Stone, Department of Homeland Security (DHS); Peter Bond, BNL; Ralph James, BNL; Parney Albright, DHS; and Joseph Indusi, BNL.

testing and evaluation of commercial, off-the-shelf radiation detectors for homeland security applications.

In touring the Instrumentation Division, the party learned about BNL's advanced detectors: Peter Vanier, Instrumentation, described the xenon gamma detector; Creighton Wirick, Department of Environmental Sciences (ES) Chair, spoke on the standoff detection capabilities of the Raman Mini-LIDAR chemical and biological sensor system; and Graham Smith, Instrumentation, explained how advanced neutron detectors and low-noise electronics for nuclear spectroscopy and imaging can be used to further national security.

A visit to the National Synchrotron Light Source (NSLS) was also on the agenda. NSLS scientist Peter Siddons gave an overview of the wide range of research in biology and physics, chemistry and geophysics, materials science and medicine, performed by Lab scientists and some 2,200 researchers from the U.S. and overseas at this facility. Aleksey Bolotnikov of the Nonproliferation & National Security Department discussed the expectations made possible by another kind of radiation detector utilizing cadmium zinc telluride crystals.

At the Lab's Relativistic Heavy Ion Collider (RHIC), the visitors saw another example of how basic research results in breakthrough detector capabilities. Tim Hallman of the Physics Department described the RHIC program and the giant STAR detector, conceived and developed with three other detectors to track instantaneously thousands of subatomic particles formed when two beams of heavy ions are crashed together at nearly the speed of light, to recreate and reveal what happened in the earliest stages of the universe.

In the environmental sciences area, Albright learned about BNL's contribution to the urban dispersion program and work on consequence management for radiological dispersal devices, topics discussed by Michael Reynolds, and Paul Kalb and Jeff Gillow, all of ES, respectively. The Lab's forefront research in areas involving biological security was represented by John Dunn of the Biology Department, who displayed real-time DNA sequencing for agricultural-biological terrorism counter measures, and Subramanyam Swaminathan, also of Biology, who described his work on ultra-sensitive assays for botulinum toxins.

— Liz Seubert

Awards and Good Times at the 2004 NSLS Barbeque

September 24, 2004

On September 24, a crowd of National Synchrotron Light Source staff members joined the recipients of the 2004 Spotlight and Service awards to celebrate the winners' careers and accomplishments, and to enjoy food, drinks, and the early autumn weather. NSLS Chairman Steve Dierker led the ceremony.

NSLS Chairman Steve Dierker

Service Awards

This year, the following staff members were honored with 25 years of service: Steve Bennett, Rich Biscardi, Conrad Foerster, Tony Lenhard, Bill Newburgh, Gary Ninztel, Stefan Palo, Sal Pjerov, Susila Ramamoorthy, Bob Scheuerer, and Jiunn-ming Wang.

Receiving the 20-year service awards were Bob Best, Pete Ratzke, Ray Raynis, and John Skaritka, and Qing-yi Dong received the 10-year award.

Spotlight Awards

The Spotlight awards, which commend deserving NSLS staff members for exceptional performance during the year, were presented to Laura Miller, recommended by Steve Dierker; Bob Best and Tony Santiago, both recommended by John Gallagher; and two groups (each group shares one award). The first group, nominated by Steve Hulbert, was Dennis Carlson, Michael Caruso, Shu Cheung, Rick Greene, Tony Lenhard, and Gary Nintzel. The second, nominated by Ed Haas, was Walter deBoer, Mike Radulescu, and Bob Scheuerer.

Bob Best: Bob received his award for building, testing, and

From left: Rodger Hubbard, Bob Best, Don Davis, Jim Newburgh, and Bob Scheuerer.

debugging the laser interlock/controllers system at beamline X17B3. This required extensive planning and coordination between the other electricians at the NSLS. If not for Bob's hard work, one of two costly alternatives to controlling the inner cavity shutter at the beamline would have been explored, resulting in long delays to the program at X17B3.

Tony Santiago: Tony was honored for modifying the Source Development Laboratory's (SDL) laser interlock system, a task that required extensive electrical work and rearrangment. With direction from Scott Buda and John Gallagher, he worked through breaks, lunches, and put in overtime to complete the project, and managed to do so without impacting the operations of the SDL.

Laura Miller: Presented as a surprise, Laura received this award for organizing and planning many of the details of the NSLS-II Workshop. Her hard work, involving extended hours and even weekends, helped to make the workshop incredibly successful. In turn, this success is vital to helping ensure that NSLS-II becomes a reality.

Dennis Carlson, Michael Caruso, Shu Cheung, Rick Greene, Tony Lenhard, and Gary Nintzel: This group was recognized for their exceptional service to the NSLS during the May 2004 shutdown. During this time, three major beamline upgrades were performed *in addition* to the increased beamline maintenance during that period. At X21, the largest of the upgrades, where two nested wiggler beamlines had to be fabricated and installed, the group performed much of this work during the shutdown, and faced several problems that popped up during the process. At the same time, they worked on the upgrades at X13A and X1A1, which both required unexpected work.

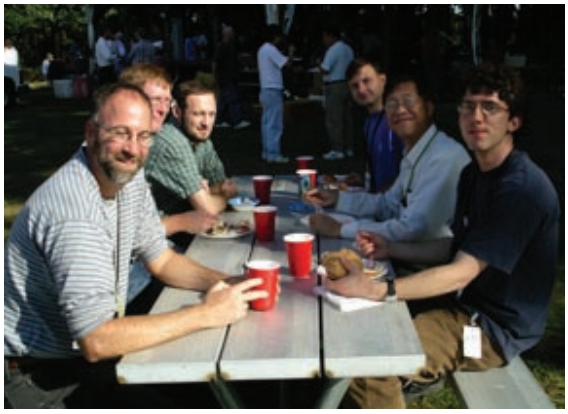

Clockwise, from left: Michael Appel, Jim Rose, Timur Shaftan, Alexei Blednykh, Li-Hua Yu, and Randy Smith.

Walter deBoer, Mike Radulescu, and Bob Scheuerer: Just before the NSLS May shutdown, a vacuum leak was found in the x-ray ring that worsened until x-ray operations were significantly affected. Walter, Mike, and Bob successful dealt with the problem and the intricate details surrounding it without impacting the x-ray schedule. Walter repeatedly came in after hours and on short notice to temporarily fix the leak. His repairs allowed operations to continue until he could properly fix the problem. From start to finish, Walter performed above and beyond the call of duty.

The leak forced the spring shutdown schedule to be changed, demanded that new work plans be reviewed and approved rapidly, required new hardware to be ordered, and necessitated the location, check, and approval of new fixtures. These details required coordinating many parties across varying time frames. Bob proved instrumental in making it happen.

Mike was the chief technician who performed the repair; he worked flawlessly and quickly, and put in long hours to complete it. His excellent, efficient work helped result in the quick-fix of a complex repair job – finished ahead of schedule with no significant errors.

—Laura Mgrdichian

The Hill Comes to the Lab

Energy & Water Development Appropriations Subcommittee personnel visit BNL

October 26, 2004

Visiting the Lab on Tuesday, October 26, were Kevin Cook, Majority Clerk of the Energy & Water Development Appropriations Subcommittee (EWDAS) and Dixon Butler, EWDAS Minority Professional Staff Member. Welcomed by BNL Director Praveen Chaudhari, DOE Brookhaven Site Office Manager Michael Holland, Deputy BNL Director for Operations Michael Bebon, and Assistant Lab Director for Community, Education, Government & Public Affairs Marge Lynch, the visitors, with Jack Bagley of Battelle's Washington Office, toured selected facilities to see more of BNL's research

Standing near the viewing window in the NSLS lobby are Brookhaven Lab Director Praveen Chaudhari; Steve Dierker, NSLS Chairman and Associate Laboratory Director for Light Sources; Kevin Cook, Majority Clerk of the Energy & Water Development Appropriations Subcommittee (EWDAS); and Dixon Butler, EWDAS Minority Professional Staff Member. Elaine Lowenstein, of Brookhaven's Community Relations group (foreground), led the group on a tour of the facility.

capabilities and learn about site infrastructure.

At the National Synchrotron Light Source (NSLS), which draws annually more than 2,200 researchers from the U.S. and overseas to join Lab scientists in studying physics, chemistry, materials science, biochemistry, geophysics, and medicine, Associate Laboratory Director for Light Sources and NSLS Chair Steve Dierker gave an overview of the facility and plans for its upgrade as well as for the proposed NSLS-II. Doon Gibbs, Associate Laboratory Director for Basic Energy Sciences, and Robert Hwang, Director of the Center for Functional Nanomaterials, discussed BNL's thriving nanoscience program.

The STAR detector at BNL's Relativistic Heavy Ion Collider (RHIC) provided another stop on the agenda. Derek Lowenstein, Collider-Accelerator Department Chair, and STAR spokesperson Timothy Hallman of the Physics Department described the RHIC facility and explained some of the physics being explored there. At RHIC, more than 1,000 researchers are working on four experimental teams to recreate and analyze conditions believed to have occurred during the earliest stages of the universe.

On a tour to look at site infrastructure, Bebon showed the visitors the recent improvements to the Materials Sciences Department in Building 480 and talked about near- and long-term plans being made for the needs of various areas of the Lab.

Lowenstein, with Betsy Sutherland of the Biology Department, outlined the National Aeronautics & Space Administration (NASA) and BNL research on the possible risks to humans exposed to space radiation. These studies, which use proton and ion beams that simulate the cosmic rays found in space, are done at the NASA Space Radiation Laboratory, known as the NSRL, operational at BNL since July 2003.

Another high-profile BNL initiative, medical imaging, was the focus of a stop at the Positron Emission Tomography (PET) facility. There, Helene Benveniste, who, at the time, was the Associate Laboratory Director for Life Sciences, and PET Program Director Joanna Fowler, Chemistry Department, described the Lab's pioneering work in probing the brain chemistry of addiction, mental illness, and aging, and other recent work to find effective treatments and on imaging awake animals.

—Liz Seubert

Remembering Dale Sayers

November 25, 2004

On November 25, 2004, Dale Sayers, a founder of the extended x-ray absorption fine structure (EXAFS) technique and a prominent NSLS user and advisor, passed away from complications due to a heart attack. He was 60 years old. He is remembered for his immense impact on NSLS science and operations, and his commitment to the field of synchrotron science.

Dale Sayers

Dale's part in developing EXAFS began in 1968 when he was a graduate student at the University of Washington. He was a student of Edward Stern, a UW faculty member and a consultant for the Boeing Scientific Research Laboratories (BSRL) in Seattle. Stern knew BSRL researcher Farrel Lytle and learned of his work on what would be the early theory of EXAFS. He decided that further work on the subject would be a good thesis project for Dale.

Dale began working with Lytle at his laboratory, measuring the EXAFS of various materials. By the end of the 1970 spring semester, the major parts of the theory were established, but one task was left: determining how to obtain structural information from the EXAFS equation they had formulated. The three decided that inverting the equation would be the way, and, in 1971, Dale tried applying the Fourier integral theorem to the equation. Success!

In a 1999 Journal of Synchrotron Radiation paper, Lytle wrote, "In a defining moment, I can still visualize Dale's excitement as he ran down the hall to greet me with the first plot of the first Fourier transform of the EXAFS function

From left, Edward Stern, Dale Sayers, and Farrel Lytle accept the American Crystallographic Association's Bertram Warren Award in 1979, for their development of EXAFS.

of germanium!" The EXAFS technique is now used at every synchrotron across the globe.

During his time as a NSLS user, beginning in the early days of the facility, Dale was a physicist with the North Carolina State University (NCSU) but spent a great deal of time here. He was the chair of the NSLS Users Executive Committee in the early 1980's, at a time when the NSLS was an "unrefined" scientific workplace, and often a difficult environment in which to perform research. Dale established trust between the NSLS and the user community, culminating in an excellent users' meeting in 1985 that included an especially memorable dinner event. He also chaired the UEC in 1987 and '88.

Dale's work at the NSLS led him to establish and operate beamline X11A. Under his leadership, X11A has been one of the most scientifically productive beamlines at the NSLS. He established a participating research team (PRT) at X11 (the longest-lived PRT beamline) and was its spokesperson from 1983 until 2001.

In the 1990's, Dale initiated a mammography project at the NSLS, working with former NSLS staff physicists Bill Thomlinson and Dean Chapman, and current NSLS physicist Zhong Zhong. The project led to the development of diffraction-enhanced imaging (DEI), a technique now used around the world to image bone and soft tissue in a way not possible using conventional x-rays. Dale became the co-spokesperson for beamline X15A after a dedicated DEI system was established there in 1998. He was leading efforts to apply DEI to a clinical setting and, for the past few years, had been working with graduate students Dean Connor and Miklos Kiss to characterize bone and reconstruct DEI images using computerized tomography (CT).

While Dale was renowned internationally for his research, his influence extended far beyond raw science. Astute and determined, he was committed to the successful operation of synchrotron facilities and the success of the field of synchrotron radiation research. This led him to become a trusted advisor to many facilities, and he sat on many scientific advisory committees.

Dale was known as a tough, yet fair, advisor, but his personal experiences were filled with laughter and frequent interactions with family, friends, and colleagues. He enjoyed traveling abroad with his wife, Anne, and did so often.

Dale earned his bachelor's degree from the University of California at Berkeley, his master's and Ph.D. degrees at the University of Washington, and then joined the NCSU physics department in 1976. He received many awards over the course of his career, including the American Crystallographic Association's Bertram Warren Award, Case Western Reserve University's Centennial Scholar Award, and the Outstanding Achievement Award of the International XAFS Society.

—Laura Mgrdichian

Contributors: Bill Thomlinson, Zhong Zhong, and Kumi Pandya

The Gregori Aminoff Prize Goes to Prominent NSLS User David Mao

December 1, 2004

David Mao, a frequent NSLS user, was awarded the 2005 Gregori Aminoff Prize in Crystallography by the Royal Swedish Academy of Sciences. Mao received this prestigious award "for pioneering research of materials at ultrahigh pressures and temperatures."

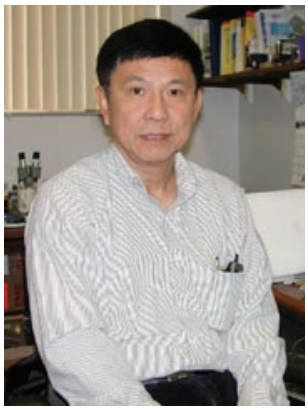

David Mao

"I am very honored to receive this award for my work using high-pressure diamond anvil cell devices," said Mao, a researcher with the Geophysical Laboratory at the Carnegie Institution of Washington. "We are at the exciting moment when high-pressure research may emerge as a major branch of modern science. Groundbreaking high-pressure experiments reveal numerous new phenomena of revolutionary importance for a wide range of problems in the physical sciences. Fortunately, with modern

synchrotron light sources, these phenomena can be directly probed and studied at extreme pressure conditions."

He continued, "There are so many colleagues at the Geophysical Laboratory to whom I am in debt for this development, particularly Larry Finger and Charlie Prewitt, from whom I learned structural crystallography; and Bill Bassett, Peter Bell, and Rus Hemley, who I joined in developing this new high-pressure field. I must also thank Chi-Chang Kao at the NSLS, who taught me how to study electron and phonon dynamics of crystals by inelastic x-ray scattering spectroscopy."

The Aminoff prize is given out annually to scientists or research groups (of three people or fewer) who have made a major contribution to the field of crystallography. It consists of a gold medal, a diploma, and a $10,000 cash award, and is named after Swedish crystallographer Gregori Aminoff, the first scientist to introduce crystallography to Sweden.

Mao will formally accept the prize from His Majesty King Carl XVI Gustaf, the king of Sweden, at the Royal Swedish Academy's annual meeting, to be held June 8, 2005. Following the ceremony, Mao will present a lecture on his work.

—Laura Mgrdichian

Zhong Zhong Explains Diffraction Enhanced Imaging at the 399th Brookhaven Lecture

December 15, 2004

To look below the surface of the human body in search of deep-seated injury or disease, today's radiologists use an alphabet-soup of imaging techniques: computerized tomography, or CT; magnetic resonance imaging, or MRI; positron emission tomography, or PET; single photon emission computed tomography, or SPECT; whole body scanners; and ultrasound.

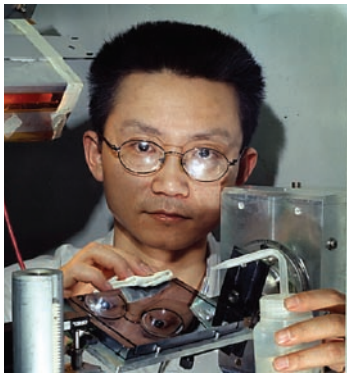

Zhong Zhong

Despite the advancements in non-invasive medical imaging, 80 percent of radiology still involves the well-known x-ray. But x-ray imaging technology has not changed very much over the past 100-plus years, mostly showing bone much more clearly than soft tissue, such as ligaments, cartilage, or blood vessels.

Now, thanks to researchers working at BNL, x-rays from the National Synchrotron Light Source (NSLS) are being employed in a new, low-dose experimental technique to visualize not only bone, but also soft tissue, in a way that is not possible using conventional x-rays. Called diffraction enhanced imaging (DEI), the technique provides all the information provided by conventional x-rays, plus additional data on soft tissues that were previously accessible only using alternative methods such as MRI or ultrasound.

Zhong Zhong, a physicist at the NSLS and the co-inventor of DEI, has been developing the technique for nine years. He discussed the imaging technique at the 399th Brookhaven Lecture, "Diffraction Enhanced Imaging: Seeing X-Rays as One Sees the Light," at 4 p.m. on Wednesday, December 15, 2004 in Berkner Hall. Zhong was introduced by Steve Dierker, NSLS Chair and Associate Laboratory Director for Light Sources.

Zhong is currently responsible for the DEI program and the high-energy x-ray scattering facility at NSLS beamlines X15A and X17B1, respectively.

Zhong earned his B.S. in physics from Beijing University, China, in 1990; received an M.S. in applied physics from Michigan Technological University in 1992; and, in 1996, received his Ph.D. in physics from Stony Brook University.

—Laura Mgrdichian

2004 NSLS Tours

1/13/2004	House Committee on Science
1/13/2004	New York Power Authority
2/26/2004	William Faulk, Suffolk County Legislature
2/27/2004	New Jersey Institute of Technology
3/9/2004	Stony Brook University - African Students
3/12/2004	CCNY of New York IEEE Chapter
3/15/2004	University of Louisville, Kentucky
3/19/2004	University of Connecticut, Storrs
3/25/2004	Charterhouse School
3/26/2004	New York University
3/29/2004	SUNY at Farmingdale
3/29/2004	Brian Davison, Director of Life Sciences Division at ORNL
3/30/2004	Defense Threat Reduction Agency
4/14/2004	Representatives from Historically Black Colleges and Universities
4/16/2004	Senator Charles Schumer Staff
4/16/2004	Nassau Community College
4/20/2004	Adult Program of the Great Neck Public Schools
4/20/2004	Johns Hopkins University
4/20/2004	Brookhaven Women In Science (BWIS) High School Career Day
4/22/2004	Take Our Daughters and Sons to Work Day
4/22/2004	Stony Brook University Research Executives
4/30/2004	Small Business Fair
5/5/2004	United Federation of Teachers
5/6/2004	The Roundtable at Stony Brook University
5/14/2004	SUNY at Farmingdale Information Club
6/4/2004	Stony Brook University Research Experience for Undergraduate (REU) Students
6/8/2004	Miller Place School District
6/9/2004	Nonproliferation and National Security (NNS) Workshop
6/25/2004	11th Advanced Accelerator Concepts Workshop
6/28/2004	Department of Homeland Security
7/16/2004	Stony Brook University Alliance for Graduate Education and the Professiorate (AGEP) Program
7/19/2004	Stony Brook University REU Students
7/21/2004	Columbia University REU Students
7/22/2004	Columbia University Summer Chemistry Program

2004 NSLS Tours

7/26/2004	BNL-Hofstra-Stony Brook University
7/28/2004	Stony Brook University Taiwanese Students
8/11/2004	Korean Institute of Science & Technology, KIST
8/19/2004	Property Management Association - Long Island Chapter
9/9/2004	Stony Brook University Foundation Trustees
9/13/2004	Congressman Tim Bishop's Staff
9/22/2004	Dr. Thomas Jourdan - FBI Liaison to the National Laboratories
9/23/2004	Retired Vice Admiral Grossenbacher
9/24/2004	Battelle NanoTechnology Alliance Group
9/29/2004	Stony Brook University - Biomedical Engineering Program
10/1/2004	United States Merchant Marine Academy
10/20/2004	English as a Second Language Program
10/22/2004	Stony Brook University Engineering Department
10/26/2004	House Appropriations Subcommittee on Energy and Water Development
10/27/2004	The Minister of the Science and Technology Ministry of the Republic of Korea
10/27/2004	Joint US-Japan Workshop
10/28/2004	Japanese Society for the Promotion of Science Group
11/5/2004	New York University
11/16/2004	Brookhaven Women In Science (BWIS) High School Career Day
11/17/2004	Adult Program of the Great Neck Public Schools
11/19/2004	Stony Brook University - Black Engineers Student Club
11/23/2004	Stony Brook University - Physics Department
11/30/2004	SUNY at Farmingdale - Institute of Retirement and Learning
12/7/2004	Columbia University Chemistry Department

Organization

National Synchrotron Light Source Organization

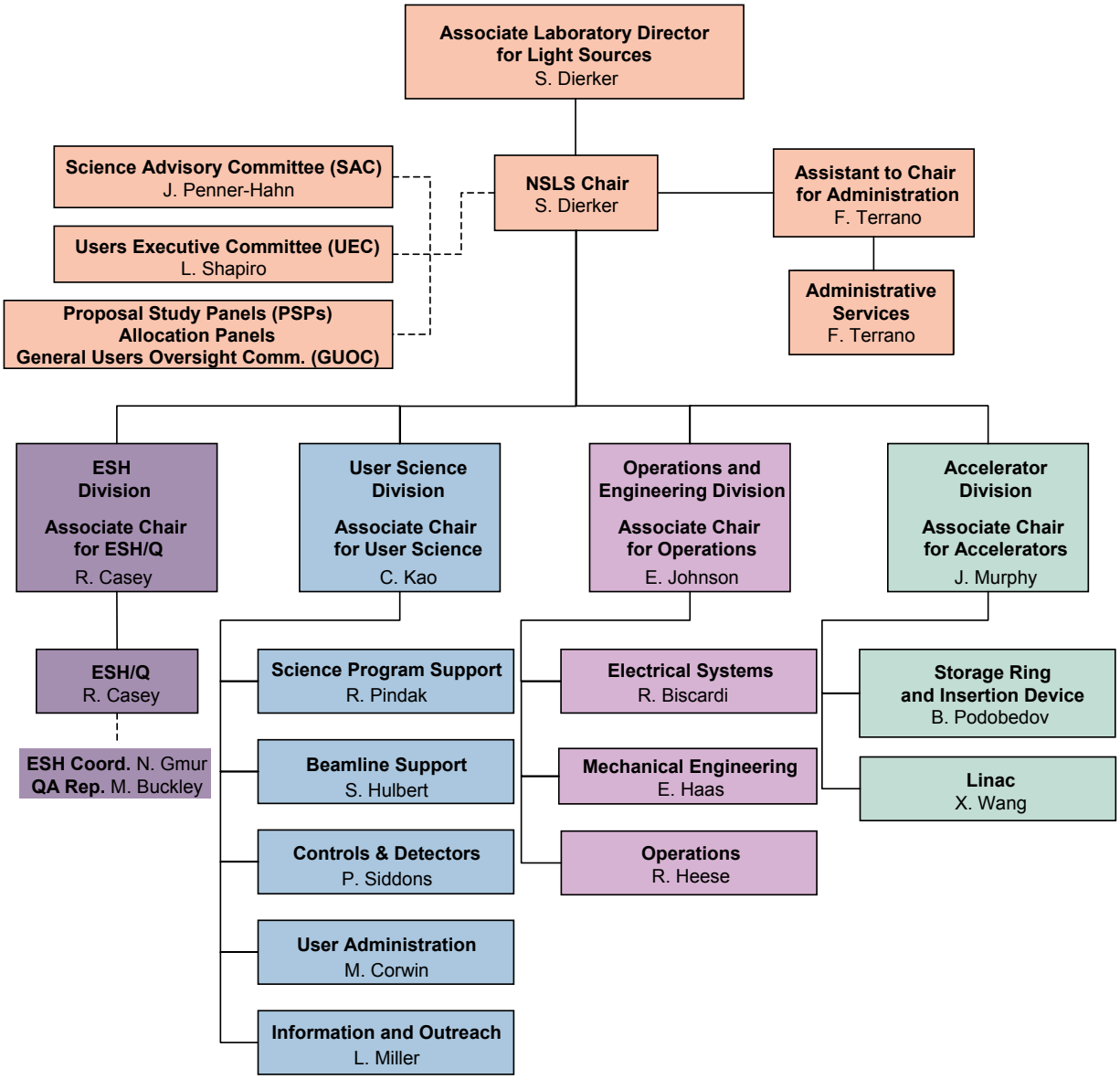

Members of the NSLS Staff

NSLS Advisory Committees

Users' Executive Committee
The Users Executive Committee (UEC) provides for organized discussions among the user community, NSLS administration, and laboratory directorate. It aims to communicate current and future needs, concerns, and trends within the user community to NSLS staff and management, and to disseminate to the users information about the NSLS and BNL plans.

Chair
Larry Shapiro, Columbia Univ.

Past Chair
Antonio Lanzirotti, Univ. of Chicago

Member
Daniel Fischer, NIST

Member
Dean Hesterberg, NCSU

Member
Trevor Tyson, NJIT

Member
Hao Wu, Cornell Univ.

Vice Chair
Peter Stephens, Stony Brook Univ.

Ex-Officio
Chi-Chang Kao, NSLS User Science Division

Ex-Officio
Mary Anne Corwin, User Administration Office

Ex-Officio
Lisa Miller, NSLS Information and Outreach Office

Special Interest Group Representatives
Special Interest Groups in areas of common concern communicate with NSLS management through the UEC

Bio. Scattering and Diffraction
Tom Hollis, Wake Forest Univ.

Industrial Users
Laura Silvian, Biogen Inc.

Imaging
Jeff Fitts, BNL-Environmental Sciences Department

Infrared Users
Randy Smith, BNL-NSLS

Nuclear Physics
Mahbub Khandaker, Thomas Jefferson National Lab.

Students and Post Docs
Meghan Ruppel, BNL-NSLS

XAFS
Simon Bare, UOP LLC

X-ray Scattering and Crystallography
Valery Kiryukhin, Rutgers Univ.

Time Resolved Spectroscopy
John Sutherland, BNL-Biology

Topography
Michael Dudley, Stony Brook Univ.

UV Photoemission and Surface Science
Elio Vescovo, BNL-NSLS

Science Advisory Committee
The Science Advisory committee (SAC) evaluates science programs at the NSLS and makes recommendations to the Chairman.

Mario Amzel, Johns Hopkins Medical School

Joel Brock, Cornell Univ.

Thomas Ellenberger, Harvard Medical School

Eric D. Isaacs, Argonne National Lab.

Edward Kramer, Univ. of California, Santa Barbara

Simon Mochrie, Yale Univ.

James Penner-Hahn, Univ. of Michigan

Larry Shapiro, Columbia Univ., Ex-Officio, UEC Chair

William Thomlinson, Canadian Light Source, Inc.

NSLS Advisory Committees

General User Proposal Review Panel

The Proposal Review Panel (PRP) reviews and rates General User Proposals. Members are drawn from the scientific community and generally serve a two-year term.

Imaging and Microprobes: Biological and Medical

Max Diem, City Univ. of New York
Paul Dumas, Centre National de La Recherche Scientifique
Kathleen Gough, Univ. of Manitoba
Lindsay Keller, NASA-Johnson Space Center
Irit Sagi, Weizmann Institute of Science

Imaging and Microprobes: Chemical and Materials Sciences

Harald Ade, NCSU
Barry Lai, Argonne National Lab.
I. Noyan, Columbia Univ.

Imaging and Microprobes: Environmental and Geosciences

Jeffrey Fitts, BNL-Environmental Sciences
George Flynn, SUNY @ Plattsburgh
Lindsay Keller, NASA-Johnson Space Center
Kenneth Kemner, Argonne National Lab.
David Wetzel, Kansas State Univ.

IR/UV/Soft X-ray Spectroscopy: Chemical Sciences/Soft Matter/Biophysics

Jingguang Chen, Univ. of Delaware
Daniel Fischer, NIST
Jan Genzer, North Carolina State Univ.
David Mullins, Oak Ridge National Lab.
Michael White, BNL-Chemistry

IR/UV/Soft X-ray Spectroscopy: Magnetism/Strongly Correlated Electrons/Surface

Robert Bartynski, Rutgers Univ.
Hong Ding, Boston College
Boris Sinkovic, Univ. of Connecticut
Jiufeng Tu, City Univ. of New York
Barrett Wells, Univ. of Connecticut

Methods and Instrumentation

Kenneth Finkelstein, Cornell Univ.
Albert Macrander, Argonne National Lab.
Ralf-Hendrik Menk, Univ. of Siegen
Peter Takacs, BNL-Instrumentation

Macromolecular Crystallography

Alex Bohm, Tufts Univ.
Brain Crane, Cornell Univ.
DaXiong Fu, BNL-Biology
Daniel Leahy, John Hopkins Univ.
Brenda Schulman, St. Jude Children's Research
Da Neng Wang, New York Univ.
Joshua Warren, Duke Univ.

Powder/Single Crystal Crystallography

Simon Billinge, Michigan State Univ.
Thomas Duffy, Princeton Univ.
John Parise, Stony Brook Univ.
Patrick Woodward, Ohio State Univ.

X-ray Scattering: Magnetism/Strongly Correlated Electrons/Surface

Sean Brennan, Stanford Linear Accelerator Center
Kenneth Finkelstein, Cornell Univ.
Valery Kiryukhin, Rutgers Univ.
Karl Ludwig, Boston Univ.
George Srajer, Argonne National Lab.

X-ray Scattering: Soft Matter and Biophysics

Paul Heiney, Univ. of Pennsylvania
Ben Hsiao, Stony Brook Univ.
Huey Huang, Rice Univ.
Robert Leheny, Johns Hopkins Univ.
H. Miriam Rafailovich, Stony Brook Univ.
Detlef Smilgies, Cornell Univ.
Helmut Strey, Stony Brook Univ.

X-ray Spectroscopy: Biological, Environmental, and Geoscience

Dean Hesterberg, North Carolina State Univ.
Douglas Hunter, Savannah River Technology Center
Kenneth Kemner, Argonne National Lab.
Satish Myneni, Princeton Univ.
James Penner-Hahn, Univ. of Michigan

X-ray Spectroscopy: Chemical and Material Sciences

Uwe Bergmann, Stanford Linear Accelerator Center
Simon Bare, UOP
Anatoly Frenkel, Yeshiva Univ.
Vincent Harris, Northeastern Univ.
Trevor Tyson, NJIT

Allocation Panel

The Allocation Panel allocates general user beam time to both new proposals and beam time requests based on ratings provided by the Proposal Study Panels. Members are drawn from the scientific community and generally serve a two-year term.

VUV

Laszlo Mihaly, Stony Brook Univ.
Elio Vescovo, BNL-NSLS

X-ray

Marc Allaire, BNL-NSLS
Annie Heroux, BNL-Biology
Jean Jordan-Sweet, IBM
Elaine DiMasi, BNL-Physics
Syed Khalid, BNL-NSLS
Wolfgang Caliebe, BNL-NSLS

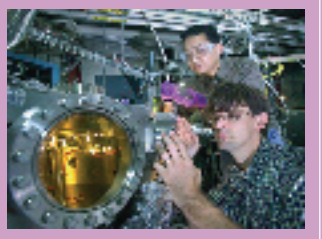

NSLS Accelerator Division

James B. Murphy
Associate Chair for Accelerators

Organization and Mission

The NSLS Accelerator Division (AD), headed by James B. Murphy, is organized into two sections: the Linear Accelerator (Linac) Section, headed by Xijie Wang, and the Storage Ring & Insertion Device Section (SR&ID), headed by Boris Podobedov. The AD staff consists of eleven accelerator physicists, two engineers, three technicians, and two postdocs.

The NSLS Accelerator Division has a four-part mission:

- To ensure the quality of the electron beam in the existing NSLS booster, linear accelerator, and x-ray & vacuum ultraviolet (VUV) storage rings
- To participate in the NSLS-II project, in particular the design of the storage ring and injection system
- To operate the Magnet Measurement Lab (MML) and the Deep Ultra Violet Free Electron Laser (DUV-FEL) Laboratory
- To perform fundamental research and development (R&D) in accelerator and free-electron laser physics

2004 Activities

Injection System & Storage Ring Improvements

In 2004, the activity with the most direct benefit to the NSLS user community was the restoration of the x-ray ring lattice symmetry, which resulted in a reduction of the horizontal emittance (**Figure 1**) and a more robust operational lattice.

The basic eight-fold symmetry of the x-ray ring magnet lattice can be broken due to gradient errors in the ring quadrupoles and changes in the reference closed orbit. The quadrupole errors can be partially mitigated by the installed trim coils available in the x-ray ring for one of the quad families. In studies that took place over the summer and fall of 2004, these gradient errors were determined through a series of orbit-response matrix measurements and an elaborate analysis that included fitting a ring model to a suitable set of parameters. The mathematical model was later confirmed by a direct measurement of the dispersion function of the eight-fold symmetric lattice. The optics system was commissioned before the winter shutdown and is now in routine operation.

Another important activity regarding the storage rings was the implementation of the so-called "middle layer" software interface on the NSLS control system. The middle layer was originally developed at the Advanced Light Source (ALS) to interface between the EPICS control system and the high-level MATLAB-based accelerator physics applications. It is currently used at a number of operating and future light sources, such as SPEAR-3, the Canadian Light Source, SOLEIL, and DIAMOND. The NSLS uses a real-time control system that is different from EPICS. However, due to the clever layered client-server architecture of the NSLS control system, the SR&ID staff, together with Operations and Engineering Division (OED) staff, were able to adapt the middle layer so that it could "hook into" the NSLS control system. This allowed us to port about five man-years worth of high-level accelerator physics and control tools development to the NSLS control system. One of the tools, a MATLAB-based version of the LOCO program, was used for the x-ray ring lattice symmetry restoration.

To ensure the smooth operation of the NSLS injection system, we per-

formed a thorough review of its operational principles and hardware systems. Aging electron and photon beam instrumentation was refurbished and new synchrotron-light monitors were added. This focused effort has led to a significant increase in the reliability of the injection system. An industrial partner was also identified to rejuvenate old klystrons for the linac injector.

A number of important contributions to the present facility came through the efforts of the magnet-measurement lab (MML) staff with support for the O&ED personnel. A vertical beam scraper assembly, built in the MML in 2003, was installed in the X13 straight section of the x-ray ring during the winter 2003/04 shutdown. Controls for the device were installed and calibrated during the May 2004 shutdown. The measurements of beam losses versus scraper position allow one to better understand the x-ray ring beam dynamics. In particular, it is possible to validate the minimum allowed vertical aperture, and hence the minimum magnetic gap, of future insertion devices planned for the x-ray ring, such as the X25 mini-gap undulator (MGU).

The magnetic design of the one-meter-long X25 MGU was finalized in 2004. The hybrid-permanent magnet design uses the newest high-field, high-temperature-capable magnets developed for hybrid/electric vehicle motors. The design is based on room temperature operation, but includes the option of cooling the magnet arrays to as low as -120° C to gain an additional 13% in field strength and a wider tuning range. Specifications for magnets and poles were developed, bids were received from three vendors, and NEOMAX America Inc. was selected. The mechanical support structure and vacuum chamber specifications were also developed and bids for construction were received from several U.S. and foreign vendors. The contract was awarded to Advanced Design Consultants Inc. A preliminary design review was held in December 2004. Delivery of the magnets, poles, and the mechanical structure are scheduled for summer 2005 and installation in the x-ray ring is planned for the winter 2005 shutdown.

It should be mentioned that the X29 MGU (designed and installed by the MML staff in collaboration with the O&E Division) and its new protein crystallography beamline were successfully commissioned in 2004 by NSLS user science and biology staff members. Optical measurements proved the X29 MGU to be performing "brilliantly" and this is currently the brightest insertion device in the NSLS complex.

NSLS-II Design Work

The NSLS-II storage ring will provide unprecedented high brightness to the NSLS user community. As such, the NSLS-II design presents challenges in the areas of lattice design, collective effects, superconducting insertion devices, and choice of injector.

Lattice: In Spring 2004 the NSLS-II lattice design team hosted visitors from the ALS, DIAMOND, the European Synchrotron Radiation Facility, KEK, and the Swiss Light Source, with the purpose of acquiring input from world-renowned experts on light source design. In the following summer, intensive effort was placed on developing improved lattice and tracking tools for addressing the higher-order nonlinear effects in the high-performance lattice. Work is continuing to optimize the baseline 24-cell triple-bend achromat lattice and we are considering the merits of other candidate lattices.

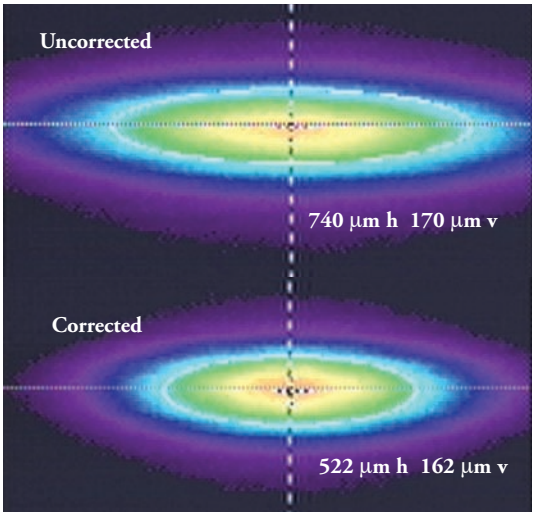

Figure 1. The x-ray ring photon beam spot size before and after the correction of the lattice symmetry.

Collective Effects: The combination of very low emittance (~ 1.5 nm), medium energy (3 GeV), and high single-bunch charge (I ~ 1 ma) makes the NSLS-II design challenging from the point of view of collective effects. To properly assess the impact of collective effects, an impedance budget is being developed, starting with the most critical components, such as MGUs, radio-frequency (RF) cavities, and beam position monitors. Much progress has been made in analyzing the impedance of vacuum chambers for the superconducting insertion devices, in particular the taper sections from the main ring vacuum chamber to the small-gap insertion devices.

Thresholds of various instabilities have been found and analyzed. In particular, the transverse mode coupling instability (TMCI) threshold driven by the resistive chamber of MGUs was estimated by compar-

ing the resistive wall tune shift to the synchrotron tune, and confirming the estimate with computer simulations. Other important findings were related to the beam-induced heat in the mini-gap undulators, which provided concrete estimates for the cryo-designers. It was also found that employing a third-harmonic RF system will lessen the problems associated with collective effects and significantly improve the beam lifetime.

Superconducting Undulator Development: Compared to conventional permanent-magnet MGUs, superconducting undulators (SCUs) can provide higher brightness and continuous photon coverage. However, one of the most significant challenges to building an SCU for NSLS-II is the ability to measure and correct the undulator field errors. Other challenges are heat management and removal. To address these challenges head-on, we are constructing a state-of-the-art cryogenic vertical test facility (VTF) for taking magnetic and calorimetric measurements of SCU test models (**Figure 2**). The VTF will allow precise magnetic field mapping of short SCU models up to 0.4 m long, using a motorized Hall probe field mapper. The mapper, which includes an NSLS-built six-element cryogenic Hall probe, has fast on-the-fly field mapping capabilities and has been bench-tested on an existing permanent magnet undulator. A superconducting Helmholz coil is under construction to provide an in-situ calibration check of the Hall sensors in liquid helium. A pulsed-wire insert, interchangeable with the Hall probe mapper, is also under construction, to provide a complementary magnetic measurement technique. Initial bench tests of the pulsed wire insert have been successfully completed. A cryogenic safety review of the VTF is planned for January 2005. The VTF will then be installed and commissioned at the BNL Superconducting Magnet Division's facilities in 2005.

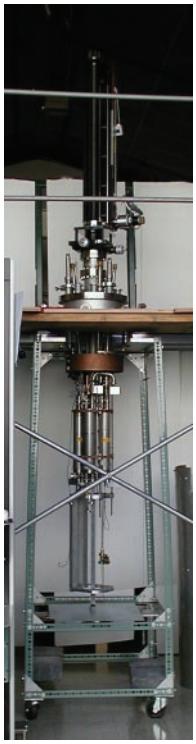

Figure 2. VTF

Both a booster synchrotron and full-energy linear accelerator were explored as possible injectors for the NSLS-II project.

The Deep Ultra Violet Free Electron Laser (DUV-FEL) Laboratory

The DUV-FEL is a dedicated platform for single-pass high-gain FEL R&D and applications. After successfully lasing at 266 nm with 800 nm laser seeding in late October 2002, experiments were carried out at the DUV-FEL last year to further explore laser-seeded high-gain harmonic generation (HGHG) FEL and improve its tunability. We also continued to provide significant support for users to explore the potential of the DUV-FEL for chemical science applications.

The chirped pulse amplification (CPA) experiments made significant progress in the last year with the development of a VUV SPIDER diagnostic apparatus and a pulse compressor. We demonstrated that by imposing a chirp on both the electron bean energy and the seed laser wavelength, a linear chirp could be detected on the HGHG FEL output. These results demonstrate the potential to generate short pulses through CPA. Another major achievement at the DUV-FEL was the successful characterization of half-cycle coherent THz pulses using an electro-optical technique.

The electron beam energy upgrade project was successfully completed with support from NSLS Engineering and Environment, Safety, and Health divisions in the last year. The DUV-FEL linac energy was upgraded from 200 to 300 MeV to enable the HGHG FEL to produce 100 μJ pulses of 100-nm light. This will establish the DUV-FEL as a premier source of ultraviolet radiation and will enable state-of-the-art gas phase photochemistry research. Furthermore, the upgraded facility will also enable future critical R&D experiments, such as multi-stage cascaded HGHG FELs and higher-harmonic HGHG ($n > 5$). The MML continued to support the DUV-FEL program in 2004 by rebuilding and recalibrating the modulator wiggler and adding a new dispersion magnet.

Operations and Engineering Division

Erik D. Johnson
Associate Chair for Operations and Engineering

Organization and Mission

The Operations and Engineering Division (OED) has three sections: Operations, which is led by Richard Heese; Electrical Systems, led by Richard Biscardi; and Mechanical Engineering, led by Ed Haas. To serve the NSLS user community, our mission falls into three main areas:

- Operating the NSLS 24 hours a day, seven days a week, and, on average, 44 weeks a year
- Designing, fabricating, and maintaining the NSLS accelerators, infrastructure, and instruments, including upgrades, modifications, and proposal development
- Providing engineering and technical support for other NSLS divisions and the NSLS user community

The OED staff includes one scientist, 21 engineers, and 57 technicians, making it the largest of the NSLS divisions. In addition to its own staff, the division coordinates the activities of seven skilled tradesmen from Brookhaven Lab. The breadth of our mission is such that we need to draw on the capabilities of the other NSLS divisions for support and, in turn, provide specialized support for their activities.

2004 Activities

Maintenance and upgrade activities continue to be important factors in achieving high performance for the NSLS, a facility that is now entering its third decade of operations. For fiscal year 2004, overall reliability was above 90% for the x-ray ring and 99% for the VUV ring. An overview of machine performance is provided in this report's "Facility Facts and Figures" section. The facility continued to operate well throughout most of the year, with a few rough patches in April/May and July/August on the x-ray ring, which accounted for much of the year's downtime.

On April 21, with the May shutdown already set and fully scheduled, the x-ray ring injection septum vacuum chamber began to fail. It quickly became evident that the most complex vacuum chamber on the x-ray ring would need to be replaced as part of the shutdown. Fortunately, the last time the septum was replaced, in 1987, a spare was built that was available for this emergency repair (see photos on next page). Nonetheless, the installation is extremely difficult because the chamber is deeply buried in shielding and is captured by two of the large quadrupole magnets. As the scope of the task became clear, we advised the user community to expect *at least* a week delay in operations. Through careful planning and execution, as well as some very long hours, the actual installation only took four days longer than the originally scheduled shutdown. An additional four days went into conditioning the machine, which was also not part of the original plan.

Routine operations were established on June 1, which was, overall, just eight days later than planned in January when the schedule was released. Without the hard work and dedication of the staff, as well as the existence of the spare chamber, this problem could well have stretched into the summer and beyond. The whole activity emphasizes the importance of preparing for surprises, no matter how improbable they seem.

The injection septum chamber replacement overshadowed a significant body of other shutdown work. The power distribution maintenance on May 8 revealed problems in each of the three substations, which were resolved. None of these issues would have resulted in unsafe conditions, but they could have led to failures that would have caused substantial operations downtime.

No less significant were several major activities by the Utilities Group, aimed at improving the reliability of the NSLS cooling systems. One involved the addition of a third pump to act as a rotating spare for the low-pressure cop-

per system that provides cooling for the machine power systems. Cleaning the high-pressure copper system heat exchangers was also required to bring the efficiency of that system back to specification.

Since 2003, when a failure on the site chilled-water system dislodged debris from the distribution piping, we have been experiencing significant difficulty keeping these systems clear and fully functional. This fine silt-like material has been migrating to the low point of the system (the NSLS) ever since, clogging equipment strainers (see photo below), and fouling the heat exchangers for the machines. To head off continuing fouling, full-flow strainers were installed on the 12" lines from the site central chilled-water supply to the machine cooling equipment.

Although the unanticipated replacement of the x-ray injection ceramic in May was the single largest contributor of downtime for the year, we also experienced a swarm of small system failures from late July into August that accrued more than 45 hours of downtime, almost twice the average for a whole month. These two types of failures illustrate several important points.

From the user's perspective, the summer episode of unrelated equipment failures was more disruptive than the single large failure in May. In the case of the injection ceramic, we knew the magnitude of the problem and were able to provide the user community with advance notice. The series of problems we encountered this summer resulted in downtime scattered throughout a three-week period of scheduled operations, impacting many more user experiments than the extension of the May shutdown (see table).

While a few large events can dominate the reliability statistics for any given year, the impact of small-duration but more frequent failures can be devastating for a single user's experimental run. Recognizing this problem, the NSLS has, for many years, run a preventive maintenance program to minimize equipment failures. Downtime faults and system failures that do occur are carefully monitored to look for trends and address problems where possible. The observed trends can result in significant investment by the NSLS in machine improvement efforts.

Both the Accelerator Division and the Operations and Engineering Division devoted a great deal of effort to NSLS machine improvements this year. Digital closed-orbit feedback has now been implemented in both planes on the x-ray ring, the culmination of several years work on orbit stabilization. New machine improvement activities have also been initiated. The injection system, including the linac, booster, and transport lines to the rings, has been the subject of an active study to characterize and improve the system's performance and reliability. Diagnos-

(A) Upstream before replacement: This photograph shows the injection point into the x-ray ring. It is a heavily shielded area because there can be significant losses on injection. The failing injection septum chamber is buried within this part of the ring. Replacing it required removing all of the shielding visible in the photograph, parting two large quadrupole magnets, removing the kicker magnet and supply, and removing the trims and all of the diagnostics attached to the injection septum. An activity of this magnitude would normally be reserved for a winter shutdown. (B) Upstream during replacement: This photo was taken during the installation process on May 11. The extent of the disruption of the machine is quite obvious. To protect against inadvertent damage as the machine components were reinstalled, the ceramic chamber was covered in bubblewrap. (C) Replacement Chamber: The spare Injection Septum Chamber is shown during preparations for the installation. The small port in the foreground is where the injected beam enters the machine. The ceramic chamber has a copper sleeve inside of it that surrounds the circulating beam to shield it from the field of the pulsed magnet that steers the injected beam into the ring. The replacement chamber dimensions were checked against the pulsed magnet (BXISH) and the ring girder to assure smooth installation. The entire assembly was prebaked before installation, which was a significant factor in the fast commissioning of the machine.

tics are being added to the transport lines and booster ring to monitor and improve the injection efficiency into the storage rings.

High-level accelerator modeling software developed over the last five years at the Advanced Light Source and SPEAR was successfully ported to the NSLS for use in machine studies of the storage rings. These MATLAB-based tools are linked to the NSLS control system and were used to restore the eight-fold symmetry of the x-ray ring lattice. Trim supplies on the 'D' family of quadrupoles are required to implement the lattice corrections. Significant effort was invested by the Electrical Systems Section to make sure the QD-trim supplies would be sufficiently robust to provide the required corrections and operate reliably. More about the lattice symmetrization work can be found in the Accelerator Division article in this report.

Group	Number of Faults			Downtime [hr]	
Area/System	Total	X- DT	U- DT	X-ray	UV
Total Charges to Down Time					
Controls and Diagnostics	103	38	14	29.3	9.5
Power Systems	218	109	15	106.9	22.0
Utilities	77	42	20	258.9	24.5
Miscellaneous	69	37	9	37.1	1.2
	467	226	58	432.2	57.2
Major Events					
Water Leak damaged Ion Pump feedthrough				24.0	
Persistent XRF1 Faults				17.3	
XRF1 Tube and Socket Replacement				13.4	
XQD trim failure				20.2	
BXESH1 failures				17.6	
BXISH Chamber Replacement				192.0	
				284.5	0.0
Balance to 'Routine' Faults					
				147.6	57.2

The winter 2004 shutdown schedule was originally planned with the goal of completing the radio frequency (RF) cavity upgrades on the x-ray ring. Unfortunately, we entered the fiscal year with a very austere budget under a continuing resolution. Although the new cavity is ready for installation, we deferred the task to mitigate the risk of damage to the machine that could draw on contingency funds. The shutdown was instead dedicated to routine maintenance and compelling installation tasks. One such task was the replacement of another injection ceramic for the BXIFB1 bump on the x-ray ring, which had begun to leak over the summer. Since this work required venting superperiod 8, the water-cooled 'speedbump' downstream of X1 was also removed. The water-cooling had been removed some time ago due to a leak, and with the advent of the active interlock system it was no longer required.

A number of activities to support initiatives from other divisions were also undertaken during the year. A major upgrade of the X25 wiggler to a one-meter-long mini-gap undulator (MGU) was initiated. The program's justification and coordination are provided by the User Science Division, the magnetic design is being undertaken by the Accelerator Division, and the mechanical and electrical design for the MGU, its controls, and the vacuum system is being performed by the Operations and Engineering Division. A bit further out, but following a similar path, is the development of a new insertion device program at beamline X9. Engineering design and analysis are also being provided to support several end station development projects, and significant support was provided for the energy upgrade of the Deep Ultra-Violet Free Electron Laser (DUV-FEL). The details of these activities can be found in the Accelerator Division article in this report.

Although not directly visible to the user community, substantial investment was made this year in safety programs. This included design reviews for new systems, documenting existing equipment, and developing procedures for maintenance and troubleshooting that address the heightened safety expectations of the Department of Energy. These activities are really investments for the future that keep our staff and users safe and, in the long run, will pay dividends in continued robust operations of the NSLS.

In fact, the vast majority of what the OED does is transparent to our user community, something we diligently strive to achieve. Through the hard work and dedication of the staff, most of the operational issues are headed off before they become problems. When problems do arise, we make every effort to minimize their impact on our users' research. In this way, we continue to work with the other NSLS divisions to ensure that our user community continues to be one of the most productive.

User Science Report

Chi-Chang Kao
Associate Chair for User Science

Organization and Mission

The User Science Division coordinates major facility activities related to users so that we can be more effective in communicating with the user community, strengthening existing scientific programs, fostering the growth of new scientific programs, and raising the visibility of the exciting science produced by our users. The division consists of five sections: User Administration (Mary Anne Corwin), Information and Outreach (Lisa Miller), Beamline Development and Support (Steve Hulbert), Scientific Program Support (Ron Pindak), and Detectors and Controls (Peter Siddons). The major initiatives and accomplishments of the User Science Division and the NSLS user community for 2004 are summarized below.

2004 Activities

With the help of a large number of users and staff, a major NSLS-II workshop was organized in March 2004 to summarize the outcome of more than a dozen focused workshops where the grand challenges in the individual fields of research, and the impact of NSLS-II on those challenges, as well as the technical challenges in the accelerator, insertion devices, optics, and detectors, were discussed. The workshop was well attended and provided additional support to the NSLS-II scientific case. Following the workshop, the NSLS-II proposal was officially submitted to the Department of Energy (DOE).

The general user proposal system was switched to the new online proposal system (PASS) in the May-August cycle of 2004, after extensive testing by the User Administration office and representative users. The transition has been very smooth, with only minor problems. Additional new features, in particular rapid access, will be implemented in 2005. As always, we welcome comments and input from users to continue improving the system.

This year was also a particularly busy year because, as part of the overall plan to enhance the experimental capabilities at the NSLS, we have completed a large number of beamline construction and upgrade projects, including beamline upgrades for the U12IR beamline, the X1A undulator beamline, the X13A elliptically polarizing wiggler beamline, and the X21 wiggler beamline, as well as the construction of the X27A x-ray microprobe beamline and the X29 undulator beamline. Some of the highlights are described below, and more detailed descriptions can be found in the pages following this article.

- **U12IR beamline upgrade:** The U12IR far-infrared beamline was upgraded to accommodate a Bruker IFS-125HR spectrometer with a resolution capability of 0.001 cm^{-1} (125 nV or 30 MHz), making U12IR the highest resolution IR beamline of any synchrotron facility. This new capability, in combination with the existing high-field magnet and Ti-sapphire laser, provides a unique facility for the study of THz spectroscopy, electron spin resonances, and time-resolved magneto-spectroscopy.

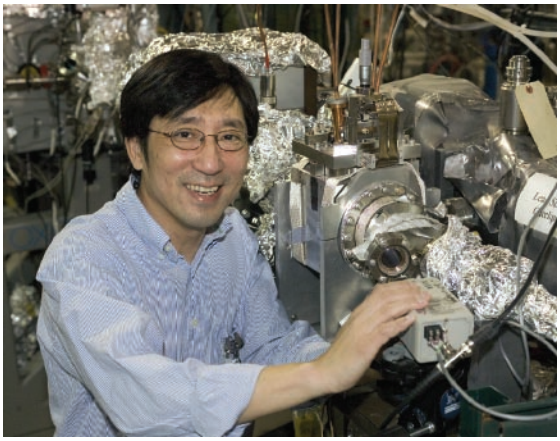

- **X1A beamline upgrade:** The X1A1 beamline is dedicated to scanning transmission soft x-ray spectromicroscopy in the 200-600 eV range, which includes the carbon, nitrogen, and oxygen K-edges. A new four-position interchangeable grating chamber with state-of-the-art soft x-ray laminar gratings optimized for specific portions of the X1A1 photon energy range was implemented to improve the throughput and energy resolution of the beamline.
- **X13A beamline upgrade:** A new motorized and water-cooled mirror system was installed in the X13A elliptically polarizing wiggler beamline. The larger collecting angle and improved mirror figure have resulted in an order of

magnitude increase in flux. The increased flux and temperature stability of the mirror will be particularly important for the detection of small magnetic circular dichroism signals.

- **X21 beamline upgrade:** The X21 wiggler beamline was upgraded for research programs in materials sciences, including x-ray scattering studies of materials under high magnetic fields, in-situ study of materials growth, and small angle x-ray scattering. An important feature of the new beamline is the non-dispersive double silicon crystal or multilayer monochromator, which contains selectable pairs of silicon crystals or multilayer elements that can be chosen in-situ to suit the experiment at hand.
- **X27A beamline construction:** A new hard x-ray microprobe beamline, X27A, has been completed to provide much-needed additional x-ray microprobe capacity and enhanced x-ray microspectroscopy capabilities to the NSLS. In particular, the beamline is optimized for the environmental science user community.
- **X29 beamline construction:** A new mini-gap in-vacuum undulator beamline, X29, dedicated for macromolecular crystallography, has been completed. The beamline was funded by various divisions of DOE (Offices of Basic Energy Sciences and Biological and Environmental Research within the Office of Science) and the National Institutes of Health (National Center for Research Resources, National Institute for Biomedical Imaging and Bioengineering, and National Institute of General Medical Sciences) in order to meet the increasing demand at the NSLS for high-brightness x-ray beamlines for the study of the most challenging problems in macromolecular crystallography.

In the areas of computer control and detector development, the major effort in the development of a multi-element Si detector was completed this year. Extensive testing of the detector with users has begun. Using the same technology, a linear array Si detector was constructed and used by users in real-time x-ray scattering experiments with great success. In addition, we have extended the fast avalanche photodiode (APD) detector-electronics unit to soft x-ray scattering experiments, and are working with outside vendors to make NSLS-designed APD-based detectors commercially available. We also continued the upgrade of EPICS-based beamline control system and PLC-based user interlock system on NSLS and PRT beamlines.

Finally, we continue to take more immediate steps to enhance user science, education, and outreach at NSLS. The annual short course on EXAFS "graduated" 32 students this summer. This hands-on workshop was organized by NSLS users Bruce Ravel (Naval Research Laboratory), Simon Bare (UOP LLC), and Lisa Tranquada (SFA, Inc.), and provided both new and experienced users with exposure to EXAFS theory, data collection, and analysis. A regular series of science highlight articles is now published on the NSLS website to help inform the NSLS user community and the broader scientific community of the exciting scientific results obtained at NSLS. The symposium series continues at the NSLS to give staff and users an opportunity to hear about cutting-edge synchrotron research that is performed worldwide. Upcoming seminars are listed on the NSLS homepage for easy access to the schedule. Finally, outreach events such as the NSLS Summer Sunday, "Take Our Sons and Daughters to Work" Day, and tours (more than 50 tours of the facility were conducted in 2004) continue to bring hundreds of members of the community to the NSLS to hear about the exciting science ongoing at the NSLS and how this research impacts their everyday lives.

X13A Magnetic Circular Dichroism Beamline Upgrade

Two insertion devices are installed in the X13 straight section: the mini gap undulator (MGU) and the fast-switching (22 Hz) elliptically polarizing wiggler (EPW). The X13A beamline, which utilizes the EPW source, is dedicated to the study of magnetic materials and their properties. The EPW provides alternately left- and right-handed elliptically polarized soft x-rays, which enables magnetic circular dichroism (MCD) measurements to be performed at a fixed magnetic field on the sample. The fast-switching capability simplifies the detection of small magnetic signals via the use of lock-in techniques.

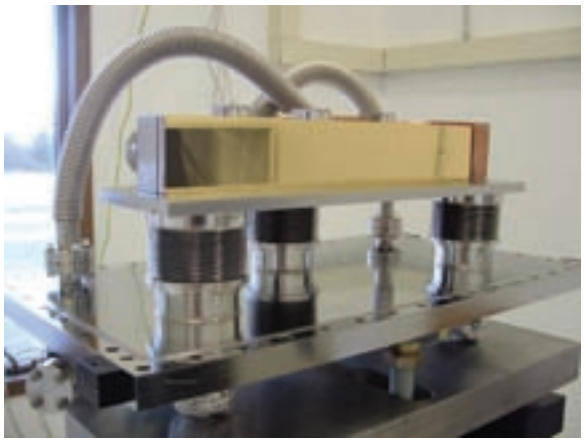

The new X13A M0 mirror before installation at the beamline. Only the bottom flange of the ultra-high vacuum chamber is shown in this photograph. The flexible bellows behind the mirror surrounds and vacuum-isolates the water-cooling plumbing. The mirror itself is gold-coated electroless nickel deposited on glidcop, which is explosion-bonded to a stainless steel substrate. The water-cooling channels are milled in the stainless steel/glidcop substrate, and then a stainless steel plate containing mechanical and plumbing fittings is welded to the mirror substrate. The three bellows underneath the mirror allow motor-driven adjustments of the mirror in the x and z translations and in rho and tilt rotations, while the surrounding chamber remains fixed.

The first optical element in the X13A beamline is a horizontally deflecting mirror (M0) that collects the central ~1 mrad of the EPW source, directs it to the X13A branch, and focuses it horizontally at the entrance slit of a horizontally dispersing spherical grating monochromator (SGM). The original (1980s) M0 mirror was too short, not well cooled, and suffered from mechanical stability problems and inadequate adjustment controls. We have replaced this mirror with a new one that remedies all of these problems. The new M0 mirror has twice the length of the old one, is integrally water-cooled, and is outfitted with a robust mounting and motor-driven mirror alignment system. These features have significantly improved the stability of the signal ratio between left and right elliptically polarized soft x-rays. Very often, the magnetic signals measured at X13A are quite small, such that an improvement in beam stability results in a significant improvement in data quality. In order to maximize beamline performance for demanding soft x-ray MCD measurements, the M0 mirror position for X13A operations has been centered on the EPW beam fan. This geometry necessarily blocks any output from the MGU, and results in a 50/50 scheduling split of X13 beamtime between X13A and X13B operations.

The new position of the X13A M0 mirror, both horizontally and along the beamline, required realigning the entire X13A beamline: the X13A SGM monochromator, I0 chamber, 22 Hz chopper, and diffractometer endstation. During initial commissioning of the newly rebuilt X13A beamline, it became clear that the EPW beam was not quite level, so we requested a vertical orbit correction for X13A. The new orbit bump was eventually made permanent, and contributed most of the factor-of-ten increase in intensity measured at the sample in the X13A endstation. (The doubled mirror length contributed only a factor of two.) The stability of the new mirror mounting system has also resulted in an improvement in stability of the left/right signal ratio. The flux and stability improvements combine to provide a significant increase in sensitivity, i.e. the ability to detect small magnetic signals. The newly renovated X13A beamline was tested by users during the fall 2004 scheduling cycle.

Principal thanks for the installation of this mirror, including the large amount of lead shielding required around the mirror chamber, go to the User Science Division technical group led by Tony Lenhard. In particular, Shu Cheung performed most of the mechanical assembly and installation work on this mirror chamber, once the vendor (Advanced Design Consulting, Lansing, NY) completed delivery. Thanks also go to the Operations and Engineering Division for mechanical survey work and control-room assistance during commissioning, as well as to the Accelerator Division for the X13 orbit bump work. —Cecilia Sanchez-Hanke, BNL-NSLS

A Unique Spectrometer for High-Resolution Inelastic X-ray Scattering

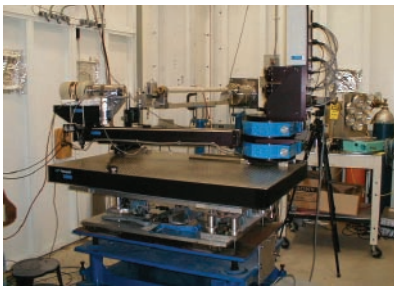

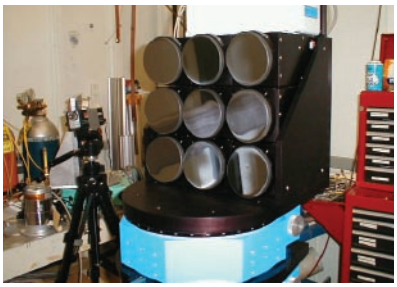

(Top) Picture of the IXS-spectrometer. The nine individual inverse joystick goniometers for each analyzer crystal are mounted on a two-circle goniometer, which in turn is mounted on a translation stage. The detector mounted on the two theta can move along the two-theta arm to stay on the Rowland circle. (Bottom) A close-up picture of the nine-crystal (10 cm each) analyzer array.

A nine-element, two-dimensional crystal array analyzer system for inelastic x-ray scattering (IXS) has been designed and built at the NSLS. Each individual crystal analyzer is aligned with an inverse joystick goniometer. The energy of the scattered photons is measured with a conventional double-circle goniometer mounted on a translation stage, which allows the maintenance of the sample, analyzers, and detector in a Rowland-circle geometry. The spherically bent crystal analyzers play the key role in this spectrometer. We chose a diameter of about 10 cm for a 500 μm thick Si(440) wafer, and bent it to radius of 1 m. We realized an adequate compromise between energy resolution (1.5 eV) and the solid angle (about 4% with nine analyzer crystals). At a Bragg-angle close to backscattering ($\theta = 88^{\circ}$), we obtained an energy resolution of 0.5 eV.

The instrument can be used to probe the metal site valence, spin polarized charge density, and local magnetic ordering in transition-metal systems. In addition, it can be used to obtain light-element x-ray absorption spectra by the use of inelastic scattering with bulk sensitivity without the need for vacuum conditions. The light-element sensitivity utilizing a hard x-ray incident beam makes the spectrometer useful for studying in-situ processes. The multi-element analyzer development was funded by a National Science Foundation Instrumentation for Materials Research (NSF-IMR) grant.

For more information on applications of this instrument see: Qian, Q., Tyson, T., Savrassov, S., Kao, C., and Croft, M., *Phys. Rev. B*, **68**, 014429 (2003). —Trevor Tyson, NJIT

A Renovated X-Ray Wiggler Beamline for Materials Science

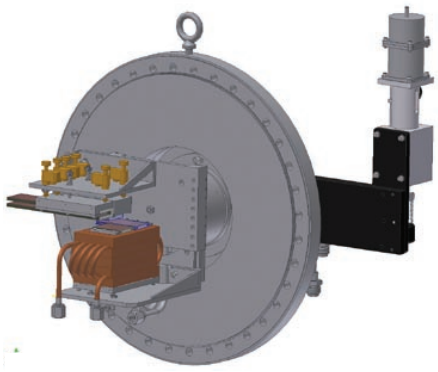

The new X21 monochromator internal assembly contains silicon crystal and multilayer pairs that can be selected in-situ via transverse alignment of the appropriate pair in the beam path. The first pair is mounted on a cryogenic copper support. The second silicon crystal and multilayer element are mounted on their own motor-driven kinematic supports. The entire assembly is mounted on a rotary vacuum feedthrough, which is driven by the motorized assembly shown behind the mounting flange.

The X21 hybrid wiggler x-ray beamline and its endstations are devoted to inelastic x-ray scattering for materials science research. To meet the increasing needs of these programs, the beamline optics and endstations have been upgraded.

The first optical component is a new non-dispersive double silicon crystal or multilayer monochromator, which contains selectable pairs of silicon crystals or multilayer elements that can be chosen in-situ to suit the experiment at hand. The first silicon crystal and multilayer element are mounted side-by-side on a helium-gas-cooled cryogenic support that suppresses thermal distortions of the crystal or multilayer when subjected to the 500 W wiggler beam.

The monochromatic beam that emanates can be used as is, or can be further conditioned by the original high-resolution four-reflection Si(220) monochromator, which remains installed in the beamline, if high energy resolution is desired.

Finally, the beam is then focused and delivered to the appropriate experimental setup by one of two bent cylindrical mirrors, each of which is shaped to focus the beam into one of the two experimental stations.

The X21 experimental endstations have been rebuilt to accommodate new experimental programs that address elastic x-ray scattering studies of materials under high magnetic fields, thin films grown *in-situ*, and materials studied with small angle x-ray scattering, with appropriate setups permanently installed in the endstations. The renovated beamline and both experimental endstations, including their dedicated instruments, are now in operation.

X1A Monochromator and Laser Interferometer Upgrades

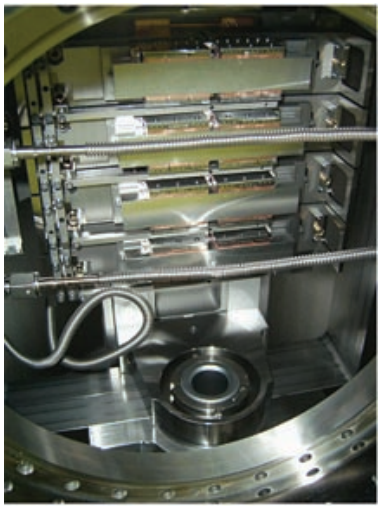

The new monochromator at beamline X1A1. It will provide for exchangeable gratings with higher diffraction efficiency, integrated water-cooling, and improved vacuum performance to minimize carbon contamination. It includes four selectable in-situ side-cooled grating holders, and provides for micro-radian angular precision and repeatability.

The X1A1 beamline received a new monochromator in May 2004. The purpose of this monochromator upgrade was to provide for exchangeable gratings with higher calculated diffraction efficiency, integrated water-cooling (such as will be required for NSLS-II), and improved vacuum performance to minimize carbon contamination. Due to constraints of the beamline length, the optical configuration could not be changed; it continues to be a spherical grating with a fixed exit arm and a resolving power of about 5000 at 290 eV. The monochromator was specified by Steve Hulbert of the NSLS, and manufactured by Physical Science Laboratories. It was installed by NSLS personnel during the May shutdown, and the electronic interfacing and alignment was done by the Stony Brook X1A group in late May and early June. The monochromator offers a significant improvement in ease of alignment, and the possibility of extending the operating energy range of X1A1. Two of the new gratings (Horiba Jobin-Yvon, Inc., Edison, NJ) are optimized for operation near the carbon K-edge (calculated diffraction efficiency 16% at 290 eV) and one is optimized for the oxygen K-edge (calculated diffraction efficiency 27% at 505 eV). At present it has been used primarily for carbon edge studies, and as the vacuum gradually improves we hope to see a reduction in the rate of carbon contamination. Thanks to Chi-Chang Kao, Steve Hulbert, Qing-Yi Dong, Gary Nintzel, and Dennis Carlson, along with many others from the NSLS, as well as Bjorg Larson, Mirna Lerotic, and Sue Wirick from Stony Brook, for their efforts with this system.

We are also in the middle of installing a laser interferometer upgrade to the scanning transmission x-ray microscope at X1A2, and then, at a later date, the one at X1A1. This will follow impressive developments at the Advanced Light Source by David Kilcoyne and others to use laser interferometer information on scanning stage position in a closed-loop feedback system to improve position stability in spectromicroscopy. The laser interferometer upgrade is also accompanied by a complete redesign of the control electronics and software, which will improve throughput of the microscope. This effort has included Holger Fleckenstein, Dan Flickinger, Benjamin Hornberger, and Mirna Lerotic from Stony Brook, and it is a key element to NASA-funded research performed by George Flynn of SUNY Plattsburgh in partnership with Stony Brook. —Chris Jacobsen, Stony Brook University

Ultrahigh Resolution Infrared Spectroscopy Moves In at Beamline U12IR

The ultrahigh resolution infrared spectrometer at beamline U12IR.

In a collaboration between Stony Brook and UCLA researchers and funded by the Defense Advanced Research Projects Agency (DARPA), a new high-resolution infrared spectrometer has been acquired for the U12IR beamline. It is hard to miss the long vacuum box next to the entrance to the NSLS VUV-IR floor, running approximately parallel to the walkway.

The key component of the instrument is a mirror that is mounted on a high precision motion stage and runs inside the box. The exceptionally long range of motion results in a high spectral resolution (on the order of 0.001 cm^{-1}); in fact, this Bruker Instruments spectrometer (Bruker IFS-125HR) has the highest possible resolution available today.

The spectrometer will be used to investigate low energy (<1 eV) vibrational and electronic excitations in gases, liquids, and solids. A particularly unique application is the study of electron spin resonance (ESR) with infrared light; this becomes possible when the light from the spectrometer is fed to the 16 Tesla superconducting magnet at the beamline, purchased earlier with support from the National Science Foundation. —Laszlo Mihaly, Stony Brook University

A New X-ray Undulator Beamline for Macromolecular Crystallography

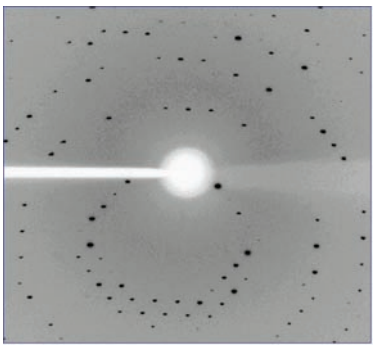

This is an example of the central region of a diffraction pattern recorded at X29. One can see that the undulator, the x-ray optics, and the detector provide excellent sensitivity and resolution. The system will work quite well for study of the largest and most difficult molecular systems.

A new experimental station dedicated to macromolecular crystallography has been completed and has commenced operation at beamline X29. The mini-gap in-vacuum undulator beamline was built in a collaboration between the BNL Biology Department, the Center for Synchrotron Biosciences at Albert Einstein College of Medicine, and the NSLS.

The funding for construction and operation comes from the Department of Energy's offices of Basic Energy Sciences and Biological & Environmental Research, and the National Institutes of Health (specifically, the National Center for Research Resources, the National Institute for Biomedical Imaging and Bioengineering, and the National Institute of General Medical Sciences).

The beamline was constructed especially to meet the increasing demand at the NSLS for a high-brightness x-ray beam for state-of-the-art macromolecular crystallography research, which had previously been served by a single beamline, X25.

The new diffractometer and detector system in the X29 x-ray hutch. This device is equipped with a high-speed and high-precision crystal axis suitable for operation with a robotic specimen changer.

The x-ray optics for the beamline consists of a Si(111) double crystal monochromator, with the first crystal being cryogenically cooled and second crystal bendable to provide sagittal focusing of the horizontal beam fan, followed by a vertically focusing mirror. The experimental station includes a Crystal Logic diffractometer, an ADSC Q315 CCD x-ray area detector, and an Oxford Instruments Cryojet sample conditioner. Already in heavy use by conventional means, the focus of this facility will be automation and high throughput operation. A fraction of this new beamline's use will be devoted to both "FedEx" (mail-in) crystallography and structural genomics.

Two New Facilities for High-Pressure Research

The X17 wiggler is the only high-energy x-ray insertion device at the NSLS. Over the years, user demand in high pressure, materials, and medical research has increased significantly. In order to meet the needs of these growing user communities, two new experimental hutches (X17B2 and X17B3), funded by the NSLS and NSF through COMPRES (Consortium for Materials Properties Research in Earth Sciences), were built and commissioned this year. In addition, a beam splitter/filter unit was installed in the upstream X17 transport hutch to allow x-ray beams to be relayed through the B1, B2, and B3 hutches in a manner that allows experiments to run in the three hutches simultaneously.

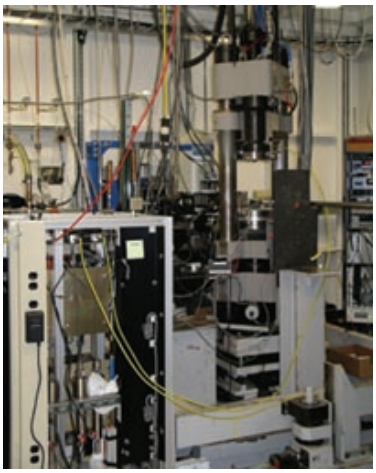

High-pressure, high-energy research occupies beamlines X17B2 and X17B3.

The new hutches are dedicated to high-pressure, earth, and mineral science research. The X17B2 hutch is utilized by the COMPRES consortium from Stony Brook University, led by Professor Don Weidner, to accommodate a multi-anvil large-volume press. White beam is currently used for experiments on this press. A multi-element Ge detector is used to collect energy-dispersive x-ray diffraction data. Radiographic imaging of the sample in the press can also be taken during all experiments. The development of a sagittal-focusing, side-diffracting Laue monochromator and a separate new large-volume press is underway for angle-dispersive diffraction. The X17B3 hutch, downstream of X17B2, is utilized by the diamond anvil cell group led by Dr. David Mao (Carnegie Institution of Washington, also a member of COMPRES). In this beamline, white beam is focused by Kirkpatrick-Baez mirrors onto the sample in the diamond anvil cell. Ongoing projects include the commissioning of an in-hutch, sagittal-focusing, 30 keV monochromator at X17B1 to provide monochromatic beam to X17B3, and safety and interlock approvals to include laser-heating capabilities.

—Zhong Zhong, BNL-NSLS

X27A: A New Hard X-Ray Microprobe Beamline for Environmental Research

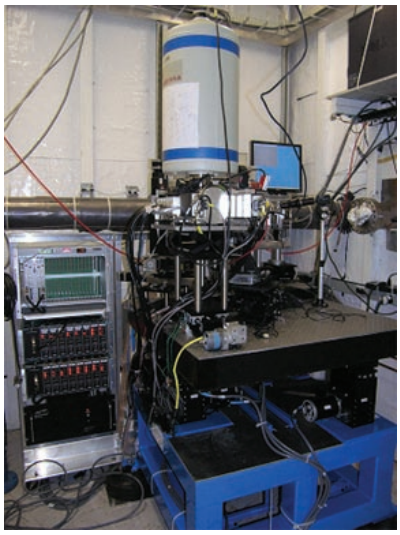

The new X27A hard x-ray microprobe shown within the experimental hutch.

A new and advanced hard x-ray microprobe facility has been installed at NSLS bending-magnet beamline X27A. This beamline was constructed to meet the increasing demand of environmental molecular science users for state-of-the-art x-ray microprobe research, only previously served by the highly productive X26A beamline. Operated as a microprobe since 1986 by the University of Chicago's Consortium for Advanced Radiation Sources, the Savannah River Ecology Laboratory, and BNL's Environmental Sciences Department, X26A's research mission has been to provide a national facility for micro-spectroscopy to the environmental sciences and geosciences community. However, as the only dedicated hard x-ray microprobe at the NSLS, beamline X26A has been consistently oversubscribed. X27A will allow the NSLS to meet the demand of this ever increasing and vibrant user base.

The new X27A microprobe facility consists of a newly designed monochromator and slit system, which is installed between the X27A & X27B hutches and enables both monochromatic and white-beam modes of operation. Si(111) and Si(311) channel-cut crystals are employed, enabling an energy accessible range from below 4 keV up to 32 keV. To micro-focus the incoming x-rays, a Kirkpatrick-Baez (K-B) bender system is used to form the required elliptical shapes from flat tapered rhodium-coated trapezoids. The x-ray beam is focused to a spot size of ~ 5 µm [vertical] x 15 µm [horizontal] at the sample location, which is ~ 9 cm from the end of the helium-filled mirror enclosure box. A 13-element, liquid-nitrogen cooled germanium detector is used to collect the fluorescence photons emitted from the sample. Transmission is collected with a photodiode. Spatially resolved information is obtained by raster-scanning the sample through the micro-focused x-ray beam with a high-resolution motorized sample stage.

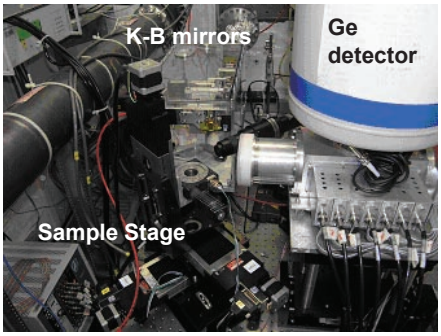

Close-up of the microprobe setup: The K-B mirror system is located towards the top center, the high-resolution sample stage is towards the bottom center, and the 13-element fluorescence detector is on the right of the photograph.

Beamline control is VME-based EPICS through the SPEC and IDL (using X26A IDL routines) software programs.

The X27A microprobe facility involves a collaboration between the NSLS, EnviroSuite, and CEMS. EnviroSuite is a strategic initiative within BNL's Environmental Sciences Department that facilitates environmental molecular science research at the NSLS, and CEMS is the Center for Environmental Molecular Science, based at Stony Brook University. The funding for construction of the X27A facility, the detector system, and operation comes from the Offices of Basic Energy Sciences and Biological & Environmental Research within the Department of Energy's Office of Science, and CEMS is supported by grants from the National Science Foundation and the Department of Energy. —James Ablett, BNL-NSLS

A New Micro-Focused Branch is Added to the U5UA Beamline

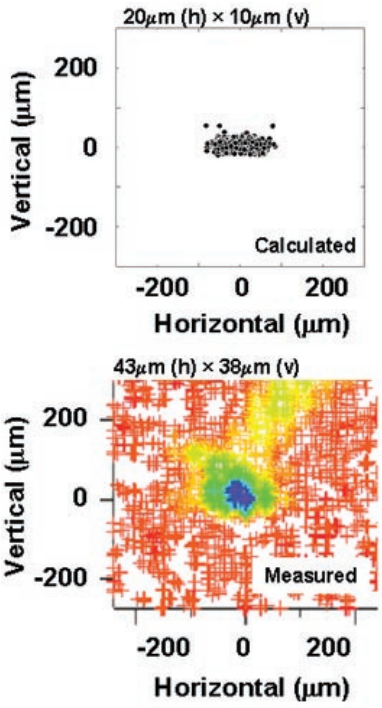

The new micro-focused branch at the U5UA undulator beamline meets the increasing demand of nanoscience users. The small spot will be of major importance in microscopy studies. In the figure the calculated spot-size is compared with direct measurements, obtained by scanning the light-beam with a 5 μm pinhole.

The U5UA beamline is an intense undulator beamline operating in the 15 to 200 eV photon energy range. It can excite valence bands electrons as well as shallow core levels from solid surfaces, and is also equipped with a four-reflection circular polarizer that operates in the 15 to 70 eV range.

U5UA has been upgraded with a new branch (#2) added downstream from the existing branch (#1). The new branch consists of a pair of ellipsoidal mirrors that demagnify the U5UA #1 sub-mm-sized beam by a factor of approximately 10, forming a micro-focused spot.

The new micro-focused branch is therefore particularly appropriate because it can be used as an intense excitation source in LEEM/PEEM experiments.

Furthermore, even conventional VUV spectroscopy techniques, such as angle-resolved photoemission, are currently spot-size limited in their quest for better and better energy resolution.

The U5UA beamline optics are capable of delivering very high photon energy resolution light. For example, a resolving power of 10,000 has been demonstrated at ~30 eV. However, in order to match this source ideally to a high-resolution electron spectrometer, a micro-focused light spot is required.

The new branch was constructed to meet the increasing demand of nanoscience users. The small spot will be of major importance in microscopy studies, such as LEEM/PEEM, where combining a small spot size with tunable synchrotron photon energy enables VUV spectromicroscopy experiments to be performed. The micro-spot will also benefit ultra-high resolution photoemission and emission experiments.

The new branch is now operational and available to users. Presently the performance of the new beamline is being characterized, and preliminary results indicate a spot-size of approximately 25 microns in diameter at fwhm.

A New Facility for Real-Time X-Ray Studies of Materials Processing

Formation of the advanced materials that are at the forefront of science and technology requires increasingly sophisticated thin film growth techniques and surface modification regimens. To better understand in real time the atomic-level changes occurring during such processing, a new facility is being developed at beamline X21 – the X-ray Studies of Materials with Analysis in Real Time (XSMART) facility. Funded with the National Science Foundation (NSF) Major Research Instrumentation (MRI), and Instrumentation for Materials Research (IMR) support to Boston University (K. Ludwig and T. Moustakas) and the University of Vermont (R. Headrick), the XSMART collaboration also includes C. Eddy of the Naval Research Laboratory. To promote flexibility, the x-ray spectrometer is designed so that modest-sized processing/vacuum chambers can be rolled onto a base diffractometer system. This design allows multiple specialized chambers to be constructed, optimized for processing, and then moved onto the diffractometer for x-ray experimentation. Thus, the base diffractometer system will be available for scientists in the community to design processing chambers to meet their individual needs.

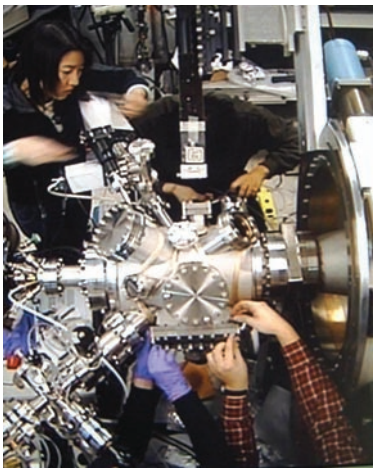

Real-time sample characterization is now available at beamline X21.

Initially, two UHV chambers have been constructed. First studies with these are focusing on surface evolution during several distinct processes: ion bombardment and plasma processing, growth of novel thin films by pulsed laser deposition (PLD), formation of ultra-thin silicide films, and growth of III-V nitrides by molecular beam epitaxy (MBE).
—Karl Ludwig, Boston University

User Administration Report

Mary Anne Corwin
User Administrator

Administrative Services

User Administration provides many services for our new and continuing users. Our primary goals are to facilitate site access, process user appointments, ensure safety training compliance, oversee the general user proposal process, organize the annual Users' Meeting, assist the Users' Executive Committee in its efforts, maintain beamline-specific information, and generate statistical reports.

PASS System
Proposal Allocation Safety Scheduling

Thanks to our applications developer Brian Bindert, the User Administration staff, and more than 30 NSLS staff and users, we proudly announced the debut of the new web-based Proposal, Allocation, Safety and Scheduling (PASS) system in May for general user proposals for the fall 2004 cycle.

PASS provides a single, web-based source for proposal submissions, feasibility and peer review, allocation and scheduling of beam time, safety review, and maintenance of beamline information. The proposal review panel (PRP) structure has changed and is now more closely associated with the synchrotron technique and field of research for the proposed experiment. A new safety measure incorporated into the system requires assignment of a lead experimenter during onsite experimental work.

Priorities for 2005 are to integrate proprietary proposals, provide rapid access to beamtime, and improve scheduling capabilities.

User Statistics

In FY04, 2,299 users from academia, government, industry, and other institutions performed experiments at the NSLS. More than a third were first-time users.

During the registration process, users select their primary field of science. In FY04, the majority of users came from the materials and life sciences arenas. Slight increases in applied science/engineering and in geosciences/ecology were noticed between FY03 and 04. At the same time, life sciences and non-specific areas decreased slightly. Other areas remained stable.

Education and employment levels vary. Over 44% of users are scientists, faculty members, or other professionals. Graduate students account for 36% and post-docs make up 13% of our population. Age levels vary, with 34% in the 20-29 age bracket and 33% in the 30-39 age bracket. In FY04, 383 unique academic, government, non-government laboratory, and industrial institutions sent users to the NSLS. Nearly 240 were academic institutions.

Experimental Statistics

During FY04, 1,374 experiments were performed, up from 1,145 in FY03. Just over 32% were materials science experiments; life sciences accounted for slightly under 32%. Funding comes primarily from the Office of Basic Energy Sciences within the DOE Office of Science, the National Science Foundation, and the National Institutes of Health.

Paperless Office

A milestone was achieved this year in converting User Administration into a paperless office. Over the last three years, as time and resources permitted, existing records were scanned. New records are now generated electronically. This accomplishment resulted in an $8K budget savings and eliminated the need for 280 cubic feet of office space. We exceeded DOE and BNL's

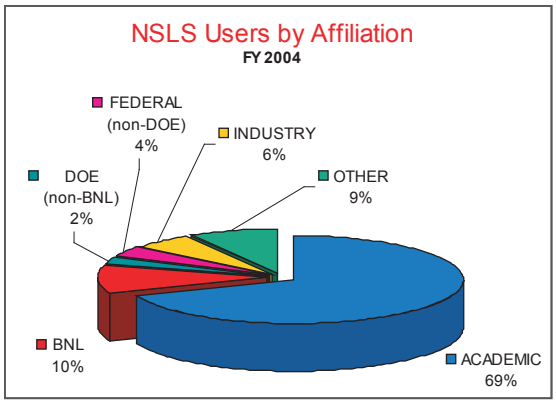

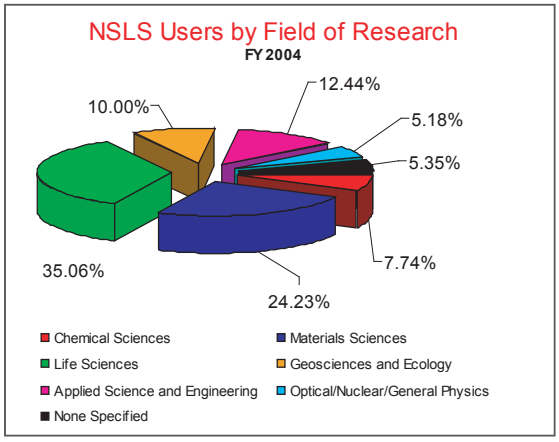

goals in reducing consumption and waste and are at the forefront in electronic records retention, significantly facilitating audits. Factors that helped us to achieve this goal include the web-based development of BNL's Guest Information System, the End of Run Form, and the PASS System.

Conferences & Workshops

Thanks to a tremendous effort by Gretchen Cisco, this year's Users' Meeting was as administratively successful as the last, with nearly 400 attendees and eight workshops. Limited funds for meals, entertainment, and other unallowable expenses come primarily from corporate vendor and sponsor support. To provide up-to-date information on allowable and unallowable funds to the Users' Executive Committee and for simplified maintenance and reporting, we entered all financial data into Microsoft Money. Though vendor space is very limited, User Administration staff worked diligently to accommodate six additional vendors, increasing revenue by $5.6K (our special thanks to Liz Flynn).

User Administration also handled the registration process for the NSLS-II Workshop in March. In May, we assisted with the coordination of and processed registrations for the CFN Users' Meeting, which occurred back-to-back with the NSLS Users' Meeting. With Liz's efforts, $30K was secured through vendor contributions to cover meals and related expenses.

Badge Scanning for Site Access

Site access policies require that users produce valid BNL identification badges or have active or pending appointments. A badge-scanning system notifies the officer at the gate of problems with a user's appointment or visa status. These users are asked to check in at User Administration and work cannot begin until the user has done so. However, though approved for site access, some users had difficulty on arrival. Our office was instrumental in providing feedback for improvements to several laboratory systems to ensure access. We have seen significant improvements since that time.

Check-In/Check-Out System

To minimize problems getting onsite, users are asked to complete BNL's check-in/check-out online form in advance. User Administration generates daily reports to verify users have arrived, have valid appointments, are in visa status, and to input user departure dates. Check-in at User Administration is only necessary when the report indicates a problem or the departure date is missing. In FY05, the check-in/check-out system will be upgraded to notify users of expiring appointments and visas.

Visas for Foreign Nationals

Foreign national users must possess work-type visas. Users who obtain B2 and WT visas are not permitted to perform experiments and are required to return to the port of entry within 24 hours to get corrected documents.Visa lengths vary from 90 days to several years. As a convenience, users are issued two-year appointments, sometimes extending beyond their visa expiration date, but must provide a new visa each time the documents we have on file expire. Users with short-term visas should schedule beam time during the workweek to ensure they will be permitted to work on arrival. We urge all foreign national users to bring valid passports, visas, and supporting documents during each visit. Several users have had to return home to retrieve their documents before starting their experiment.

Instances of non-compliance resulted from users who were out of visa status and began their experiments without checking in at User Administration, after being informed by BNL officers that they needed to do so. To minimize

The User Administration Group (from left): Mary Anne Corwin, Liz Flynn, Melissa Abramowitz, and Gretchen Cisco.

these problems, User Administration recommended modifications to the Guest Information System to inform foreign national guests of their expiration dates by email. Implementation is tasked for FY05.

In June, DOE issued a new Foreign Visits and Assignments order for which all laboratories must comply. Most requirements mimic those previously issued, but BNL is required to implement additional requirements in FY05.

Experimental Floor Access

We found instances of safety non-compliance where users accessed the experimental floor with expired or no training. To eliminate these problems, as well as non-compliances by foreign nationals, User Administration now provides "timed-access" to expire with the first expiration of training, ID badge, passport, or visa status dates. Modifications to the PASS system were made to ensure that experimenters are listed on safety approval forms and are in compliance. And, the laboratory's training record database (BTMS) now generates automatic emails to users whose training has expired.

On-Site Housing for Foreign Nationals

Last year's change in housing policies made it impossible for foreign national users with pending appointments to make reservations. User Administration worked with BNL Housing to correct a misconception that such users had not yet received approval to visit BNL. We have seen significant improvements since that time.

Vehicle Identification

New security policies require all users to obtain vehicle stickers or placards. To eliminate an unnecessary trip to Security for our users, User Administration received permission to acquire the stickers and placards in the same manner that we obtain identification badges.

Benefits to Compliance

With limited resources, we're very grateful to our users who help us maintain compliance with DOE directives. By eliminating non-compliances, we can focus more on user-related quality-of-life issues. We encourage our users to contact User Administration at (631) 344-USER (or nslsuser@bnl.gov) with any additional recommendations to eliminate non-compliances or with any questions.

Safety Report

Bob Casey
Associate Chair for ESH

Organization and Mission

Environmental, Safety, and Health (ESH) performance within the NSLS and at BNL in general remains an important issue for all NSLS staff, PRT members, and general users.

2004 Activities

There is a great emphasis at Brookhaven Lab on reducing the frequency of injuries and incidents, and this emphasis resulted in heightened visibility for all matters relating to safety during 2004. So how are we doing at the NSLS?

In many factors we are doing very well.

1. We had no injuries that met recording criteria or resulted in lost or restricted time during 2004. BNL and DOE weight this parameter heavily in judging safety performance — we can all take pride in that accomplishment.
2. Radiation exposure remains very low. The total recorded committed dose equivalent to NSLS staff and users for 2004 was less than 50 mRem. Fewer than 10 badges for the year had any recordable exposure.
3. Generation of hazardous and industrial wastes continues near all-time lows. Inspections of work sites indicate a high degree of compliance with hazardous waste and environmental requirements.
4. Responsiveness to inspection and audit findings was prompt and complete in general.
5. Compliance with safety and training requirements as evidenced through numerous audits is viewed as high.

These factors indicate a very satisfactory program. However, this year two events involving electrical safety raised concerns about that part of our program and have resulted in a considerable emphasis on improving electrical safety practices. For example, two significant incidents occurred this year: An NSLS technician received a high-voltage shock while working on a component at a beamline, and visiting researchers improperly modified a high-voltage power supply, leaving a shock hazard for subsequent groups. Detailed information on these incidents is available on the NSLS website.

Following Up with Concerns

In 2004, a key issue that emerged is ensuring that all electrical devices requiring lockout prior to maintenance or servicing have been identified. A major effort has been devoted to establishing this inventory and clearly labeling these devices. A second major effort has been on analyzing the adequacy of our work planning to ensure that hazards are identified and controlled prior to the start of work. Both of these efforts will continue to be a major focus in 2005.

Key Work-Planning Points for Electrical Safety for 2005

- Make sure that all work on electrical components is adequately screened for hazards by the supervisor or other knowledgeable person before the work begins — make no assumptions. If you are not knowledgeable of the equip ment and its potential hazards, find someone who is.
- All work involving exposed electrically energized surfaces, including troubleshooting measurements, must be planned and conducted in accordance with NSLS work planning requirements. In general, working with exposed energized circuits is not allowed unless explicitly authorized by the NSLS Electrical Safety Officer and the supervisor through a “working hot” permit.

- Unless specifically authorized by the responsible supervisor and the NSLS Electrical Safety Officer under the conditions of a "working hot" permit, all work that involves exposed electrical conductors less than 50 volts must be initiated by securing the electrical power source in accordance with the BNL lock-out/tag-out procedure.
- Proper protective clothing and gloves must be worn by all workers servicing or trouble-shooting electrical equipment until it has been verified that all electrical voltages have been secured and the equip ment is in a zero-energy state.

Adherence to these procedures will permit work with electrical components to be safely performed.

Conclusion

The NSLS Safety Program is based on the principles of safety that the U.S. Department of Energy refers to as Integrated Safety Management (ISM). The intent of this program is to ensure that all work is effectively performed by trained and qualified personnel and that hazards associated with the work have been fully identified and properly controlled. These concepts are embodied in the safety program requirements established for all users and staff.

We all take justifiable pride in the world-class research that is performed at the NSLS. We need a sharp focus on working safely and taking steps to ensure that our research programs fully capture the requirements of the NSLS safety program and the essence of ISM. It is clear that world-class research will not proceed without world-class safety.

NSLS User Training Programs

Eva Rothman
TRAINING COORDINATOR

NSLS user safety training has been available on the web for some time. Now, the vast majority of our users take advantage of this convenience to complete training before arrival. This year saw some further enhancements. The User Safety Module was converted from simple web pages to the format used by the other BNL web courses. During this conversion process, the course was edited page-by-page and pared down by about 30%, resulting in, hopefully, a more concise and memorable presentation. The new format allows the quiz to be automatically graded and the results returned to the trainee immediately. The safety module used for scientific and technical staff was also converted to this format.

The NSLS has discontinued using its own version of GERT, or General Employee Radiological Training, and has adopted the BNL version. Historically, GERT had only been available as a weekly classroom session that was inadequate for a 24-7 facility with around-the-clock arrivals. The NSLS used a videotape presentation of GERT as part of the safety training administered in the User Office and Control Room. Later, we implemented a web version, which, because we wanted to keep it short, was only applicable to the NSLS (not transferable to other BNL departments or other DOE facilities). In early 2004, BNL introduced GERT as a web course and the NSLS is now able to offer that to its users. The NSLS continues to have a reciprocal relationship with other DOE labs regarding GERT and now the GERT training obtained at BNL should be fully accepted by other DOE facilities.

Building Administration Report

Gerry Van Derlaske
NSLS Building Manager

Facing new safety initiatives, curtailed budgets, and a new emphasis on adhering to National Fire Protection Association electrical safety programs, the NSLS continued to be a vibrant beehive of activity in 2004. Scientists, technicians, support staff, and in-house service personnel worked together to establish a safe and healthy work environment for scientific research. Beamline X29 was fully commissioned and began data-taking runs, overhead projectors were installed in select conference rooms, maintenance programs in conjunction with the BNL Plant Engineering Division were undertaken, and several in-house workshops were held. These factors all contributed to another very active and productive year at the NSLS.

Safety

First and foremost on staff and users' minds these days is performing everyday duties in a manner that promotes a culture of safety and a safe working environment at the NSLS. Seasoned subject matter experts (SMEs) are available to answer questions relating to all aspects of industrial safety. Combined with a fully staffed Environment, Safety, Health, & Quality (ESH&Q) Division, these SMEs are conveniently located on the experimental floor, adjacent to the main control room. No one should feel that answers on how to proceed safely are far from hand. Stop-work orders may be invoked when observing operations that may place personnel in imminent danger. Numerous review avenues have been established that assist personnel with work being planned and carried out, such as hazard analyses, which are performed and reviewed by the appropriate SME. Everyone should take advantage of these services whenever a task is planned that may involve hazards, know or yet unknown.

During the past year, after a site-wide visit by the Occupational Safety and Health Administration (OSHA) inspection team in October 2003, the operative words for work performance within the laboratory continued to be "safety" and "compliance." Various NSLS and BNL support, safety, and technical groups corrected many findings of the various OSHA inspection teams. A small percentage of the findings were grouped with similar findings from other laboratory departments/divisions and will be tracked for future closeout by the BNL Plant Engineering Division. Tier 1 facility and beamline inspections by NSLS ESH&Q staff will continue to search for other possible safety concerns, and will record and forward these findings to the appropriate individuals or groups for remediation. Once notification is received, a data-based system will track the findings, which will either be repaired in a timely fashion or corrected immediately. After mitigation, the Tier 1 contact is notified to close out the finding.

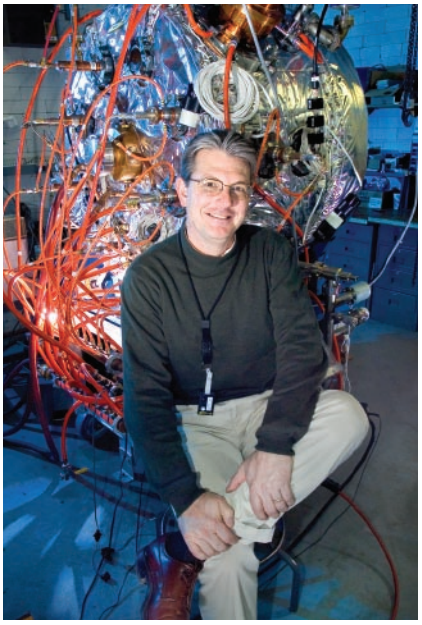

Simultaneously, we have reacted to other Lab-wide directives as they surfaced. One area of concern revolved around material-handling equipment and hoisting and lifting equipment. The NSLS point of contact for such issues is Bob Kiss. A new training program that Bob has been instrumental in developing is tailored to fit the requirements of the type and frequency of lifts performed within the NSLS facility. As a result of this directive, all cranes have been assigned a padlock, with limited key distribution to those individuals deemed "responsible" for the operations of a particular crane or overhead-lifting device. Feel free to contact Bob if you have any questions pertaining to lifts, hoists, cranes, and all of the "below the hook" lifting devices that you may encounter. An ongoing effort to capture all such devices in our inventory will assure that the proper inspections take place within the yearly time frame. If, at your workplace, you have any below-the-hook lifting devices, such as slings, shackles, strong backs, etc., that are not inspected on a yearly basis, please have Bob inspect these items. Any lifting device, such as portable lifters/engine hoists, hoists, chain falls, slings, shackles, etc., brought to BNL and used on-site must be inspected prior to use. This includes new and used items, even if the item will only be used once. All inspected items will carry a color-coded identification tag, alerting the user that a proper inspection took place and that the item

has been recorded in our inventory system. Of course, each below-the-hook item must be checked by the end user each time it is used, to assure that no damage has occurred to the device while in storage, or by the previous user.

A new worker qualification and training list for users and beamline staff was implemented and presented to the user community. The list outlines tasks considered to be "skill of the worker." Tasks were divided into three levels, with the rigor of training and enhanced work planning corresponding to the difficulty of the assigned tasks or systems being modified or impacted. In all cases, if the scope of the task has changed or new hazards have been introduced, stop, reassess, and get qualified assistance before returning to complete the task.

A new automated external defibrillator (AED) has been installed in the main lobby of Building 725 and another has been installed in Building 729 near the west doorway. A number of NSLS personnel have taken BNL's training course in CPR and AED use. Additional AEDs will be purchased and installed during FY05.

Maintenance/Upgrades

In a continuing program, the BNL Plant Engineering Division once more provided both material and manpower resources to address various roof leaks detected in areas above the experimental floor. Areas that received considerable attention were sections above the VUV ring, the vehicle ramp leading to the center of the x-ray ring, and the area above beamline X29. The proof testing of the repairs will be how well they survive the frost-thaw cycles of the winter season.

The main lobby stairwell leading to the User Administration reception area received a new coat of paint. New labeling schemes in the stairwell help direct visitors to the Chairman's office and conference rooms. New overhead digital projectors were installed in both the Seminar Room and Conference Room A.

A full inspection of the facility revealed some concerns with the interior seals and gaskets on several windows, installed during later phases of building construction. Those windows deemed to be in suspect condition were removed and replaced. The driver for this inspection was a pane of glass that separated itself from the vacuum seal on one of the double-pane insulating windows. When a vacuum seal deteriorates, moisture seeps between the panes of glass, causing the glue to weaken. Inspections will continue to look for windows with voided seals, and these units will be scheduled for replacement.

NSLS Administration Group

The annual stripping and waxing of the experimental floor was completed in mid-December. This coordinated effort requires much planning and logistical deployment of several custodial crews, working under the guidance of Plant Engineering Custodial Services supervisors and the NSLS alternate building manager to complete the tasks with as minimal an impact on beamline operations as possible. Two custodial supervisors, a lead custodian, and a crew of nearly 20 custodians refinished the beamline areas, hallways, and perimeter walkways on both the x-ray and VUV experimental floors.

In late December, the south elevator in the main lobby had to be shut down to repair leaky packing on the main lift cylinder. Concurrently, the flow valve, which allows the oil in the cylinder to return to the reservoir, was replaced. In the future, the Lab plans to fund a complete overhaul of the electrical drive components of this elevator, as the present logic system is driven by an outdated method using solenoids and relays. Installing solid state, up-to-date logic drive components will occur as funding becomes available.

Bicycles

The BNL Quality of Life Office has turned over bicycle management to department building managers. The NSLS maintains a fleet of seven bicycles that may be loaned out for both long and short terms. Once

signed out, the "owner" is responsible for maintaining the bicycle, keeping it protected from theft, and returning the bike in good condition at the end of the term. It is necessary to follow all applicable road-use rules when biking on- and off-site, and wearing a helmet is required when biking on-site.

Going Wireless

The x-ray and VUV floors now boast wireless capabilities, running at broadband speeds, with coverage extending to all areas within points of normal user access. Common areas, such as the library, conference rooms, and the main lobby are covered. This wireless connection is outside the BNL firewall, therefore, one would need to use virtual private network (VPN) software to enter the BNL intranet. Additional future planning includes installing wireless access points inside the firewall.

User Moves

A concerted effort between Plant Engineering, NSLS, Exxon, and the New York Structural Biology Center was undertaken during the summer, culminating in the relocation of machine tools and user shop equipment to Building 801. As a result, dedicated interior building space was allocated to the last user staff members being housed in portable structures in the NSLS trailer park, located east of Building 727.

Holiday Merrymaking

In our year-end event to celebrate the holiday season, the Budget group hosted a festive party. They transformed the main lobby with hanging snowflakes and created intimate bistro-style seating on the mezzanine overlooking the lobby. The decorations brightened the spirits of all in attendance. After feasting on a potluck buffet and tables of desserts, a staff "talent" show was held in the Seminar Room, hosted by Al "Donnie Osmond" Boerner, with accompaniment from Al Almasy on keyboard. There were singers, musical performers, a "hunters and reindeers" act, a tale of budget woes parodied to *The Night Before Christmas,* and an amusing show by the "Don Ho Hula Guys." All in all, it was a day to remember.

Conclusion

The multi-faceted NSLS facility, where each year thousands of users carry out their research, is alive and well. With assistance from many talented, behind-the-scene individuals, who work so diligently to make our time here a bit more pleasant, my thanks. We continue to pace ourselves, but we are moving forward steadily. There is brightness on the horizon, as the future holds plans for larger and more powerful tools to explore the mysteries of our surroundings.

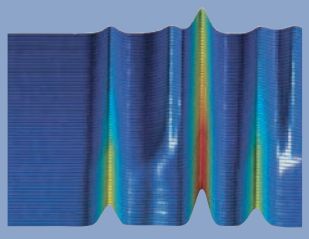

Facts & Figures

Facility Facts & Figures

The National Synchrotron Light Source (NSLS) is a national user research facility funded by the U.S. Department of Energy's Office of Basic Energy Science. The NSLS operates two electron storage rings: an x-ray ring (2.8 GeV, 280 mA) and a vacuum ultraviolet (VUV) ring (800 meV, 1.0 A), which provide intense light spanning the electromagnet spectrum from the infrared through x-rays. The properties of this light, and the specially designed experimental stations, called beamlines, allow scientists in many fields of research to perform experiments not otherwise possible at their own laboratories.

Over 2,200 scientists representing more than 350 institutions, more than 50 of them corporations, come to Brookhaven National Laboratory annually to conduct research at the NSLS. The facility operates seven days a week, 24 hours a day throughout the year, except during periods of maintenance and studies.

As a national user facility, the NSLS does not charge for its beamtime, providing that the research results are published in the open literature. Proprietary research is conducted on a full cost recovery basis.

There are two ways to obtain beamtime at the NSLS: either as a General User or as a member of a Participating Research Team (PRT). General Users are independent investigators interested in using the NSLS for their research. Access is gained through a peer-reviewed proposal system. All operational beamlines at the NSLS reserve at least 25% of their available beamtime for General Users. PRTs are groups of researchers with related interests from one or more institutions. Membership in a PRT is open to all members of the scientific community who can contribute significantly to the program of the PRT, (i.e., funding, contribution of equipment, scientific program, design and engineering, operations manpower, etc).

The NSLS currently has 54 x-ray and 16 VUV-IR operational beamlines for performing a wide range of experiments. The following pages list the operational beamlines at the NSLS and their unique characteristics.

Beamline Guide

Technique	Description
ARPES	UV photoelectron spectroscopy, angle-resolved
DAFS	X-ray diffraction anomalous fine structure
DEI	Diffraction-enhanced imaging
EXAFS	X-ray absorption spectroscopy, extended fine structure
IRMS	Infrared microspectroscopy
MAD	Multi-Wavelength anomolous dispersion
MCD	Magnetic circular dichroism
NEXAFS	Near edge x-ray absorption spectroscopy
SAXS	Small angle x-ray scattering
SPARPES	UV photoelectron spectroscopy, spin- and angle-resolved
STXM	Scanning transmission x-ray microscopy
UPS	UV photoelectron spectroscopy
UV-CD	Ultraviolet circular dichroism
WAXD	Wide-angle x-ray diffraction
WAXS	Wide-angle x-ray scattering
XAFS	X-ray absorption spectroscopy, fine structure
XANES	X-ray absorption spectroscopy, near edge structure
XAS	X-ray absorption spectroscopy
XPS	X-ray photoelectron spectroscopy
XRD	X-ray diffraction
XSW	X-ray standing waves

BEAMLINE	SOURCE	TYPE OF RESEARCH	ENERGY RANGE	ORGANIZATION
U1A	Bend	XAS XAFS NEXAFS XANES	270-900 eV	ExxonMobil Research and Engineering Co.
U2A	Bend	IRMS High pressure research IR spectroscopy	30-8000 cm-1	Carnegie Institution of Washington
U2B	Bend	IRMS IR spectroscopy	50-4000 cm-1	Albert Einstein College of Medicine
U3C	Bend	XPS	50-1000 eV	Bechtel Nevada Lawrence Livermore National Laboratory Los Alamos National Laboratory Sandia National Laboratory
U4A	Bend	UPS	10-250 eV	Army Research Laboratory Boston University BNL-NSLS North Carolina State University Rutgers University University of North Carolina
U4B	Bend	X-ray scattering, resonant MCD UPS X-ray fluorescence spectroscopy XPS	20-1200 eV	BNL-NSLS Montana State University
U4IR	Bend	IRMS	50-700 cm-1	BNL-Chemistry BNL-NSLS
U5UA	Insertion Device	Magnetospectroscopy UPS ARPES SPARPES	15-150 eV	BNL-NSLS
U7A	Bend	NEXAFS XANES XPS	180-1200 eV	BNL-Chemistry BNL-Physics Dow Chemical Company National Institute of Standards & Technology Rutgers University Texas A&M University University of Michigan
U9B	Bend	UV-CD UV fluorescence spectroscopy	0.8 - 8.0 eV	BNL-Biology BNL-NSLS
U10A	Bend	IR spectroscopy	30-20000 cm-1	BNL-NSLS BNL-Physics
U10B	Bend	IRMS IR spectroscopy	500-4000 cm-1	BNL-NSLS
U11	Bend	UV photoabsorption spectroscopy UPS UV photoionization spectroscopy	3-30 eV	BNL-Biology BNL-NSLS
U12A	Bend	XAS XPS	100-800 eV	BNL-NSLS Oak Ridge National Laboratory
U12IR	Bend	IR spectroscopy THz / millimeter wave spectroscopy Time-resolved spectroscopy	6-600 cm-1	BNL-NSLS Stony Brook University University of Florida
U13UB	Insertion Device	UPS ARPES	3-30 eV	Boston University BNL-NSLS BNL-Physics

BEAMLINE	SOURCE	TYPE OF RESEARCH	ENERGY RANGE	ORGANIZATION
X1A1	Insertion Device	STXM	.25-.50 keV	BNL-Environmental Science BNL-NSLS ExxonMobil Research and Engineering Co. SUNY @ Plattsburgh Stony Brook University University of Texas @ Houston
X1A2	Insertion Device	STXM	.25-1 keV	Stony Brook University
X1B	Insertion Device	X-ray scattering, coherent XAS X-ray fluorescence spectroscopy XPS	.2-1.6 keV	Boston University BNL-NSLS University of Groningen
X2B	Bend	X-ray microtomography	8-35 keV	ExxonMobil Research and Engineering Co.
X3B1	Bend	XRD, powder	6-30 keV	Stony Brook University
X4A	Bend	MAD Macromolecular crystallography	3.5-20 keV	Albert Einstein College of Medicine City University of New York (CUNY) Columbia University Cornell University Mount Sinai School of Medicine New York Structural Biology Center New York University SUNY @ Buffalo Sloan-Kettering Institute for Cancer Research Wadsworth Center
X4C	Bend	MAD Macromolecular crystallography	7-20 keV	Albert Einstein College of Medicine City University of New York (CUNY) Columbia University Cornell University Mount Sinai School of Medicine New York Structural Biology Center New York University Rockefeller University SUNY @ Buffalo Sloan-Kettering Institute for Cancer Research Wadsworth Center
X5A	Bend	Laser backscattering	150-420 MeV	BNL-Physics Forschungszentrum Juelich (KFA) James Madison University Norfolk State University Ohio University University of Paris University of Rome II University of South Carolina University of Virginia Virginia Polytechnic Institute and State University
X6A	Bend	MAD Macromolecular crystallography	6.0-23 keV	BNL-NSLS National Institutes of Health
X6B	Bend	MAD Macromolecular crystallography	7-19 keV	BNL-NSLS
X7A	Bend	XRD, powder	5-45 keV	BNL-Physics ChevronTexaco Energy Research and Technology Co. Ohio State University Stony Brook University University of Birmingham University of California @ Santa Barbara University of Pennsylvania
X7B	Bend	XRD, single crystal XRD, time resolved WAXD WAXS	5-21 keV	BNL-Chemistry

BEAMLINE	SOURCE	TYPE OF RESEARCH	ENERGY RANGE	ORGANIZATION
X8A	Bend	Metrology	1.0-5.9 keV	Bechtel Nevada Lawrence Livermore National Laboratory Los Alamos National Laboratory Sandia National Laboratory
X8C	Bend	MAD Macromolecular crystallography	5-19 keV	Biogen Incorporated BNL-Biology Hoffmann-La Roche National Research Council of Canada
X9A	Bend	MAD Macromolecular crystallography	5-15 keV	Albert Einstein College of Medicine Rockefeller University Sloan-Kettering Institute for Cancer Research
X9B	Bend	XAS EXAFS XAFS NEXAFS XANES	5-15 keV	Albert Einstein College of Medicine
X10A	Bend	XRD, powder XRD, time resolved WAXD X-ray reflectivity SAXS WAXS	6-15.2 keV	ExxonMobil Research and Engineering Co.
X10B	Bend	XRD, powder XRD, surface WAXD X-ray reflectivity X-ray scattering, surface WAXS	14 keV	ExxonMobil Research and Engineering Co.
X10C	Bend	XAS EXAFS XAFS NEXAFS XANES	4-24 keV	ExxonMobil Research and Engineering Co.
X11A	Bend	DAFS XAS EXAFS XAFS NEXAFS XANES	4.5-35 keV	BNL-Environmental Science Canadian Light Source Hunter College Naval Research Laboratory (NRL) Naval Surface Warfare Center New Jersey Institute of Technology North Carolina State University Northeastern University Paul Scherrer Institute U.S. Environmental Protection Agency Virginia Union University
X11B	Bend	DAFS XAS EXAFS XAFS NEXAFS XANES	5.0-23 keV	BNL-Environmental Science Canadian Light Source Hunter College Naval Research Laboratory (NRL) Naval Surface Warfare Center New Jersey Institute of Technology North Carolina State University Northeastern University Paul Scherrer Institute U.S. Environmental Protection Agency University of Connecticut Virginia Union University
X12B	Bend	MAD Macromolecular crystallography	5-20 keV	BNL-Biology
X12C	Bend	MAD Macromolecular crystallography	5.5-20.0 keV	BNL-Biology
X13A	Insertion Device	X-ray scattering, resonant MCD Magnetospectroscopy	.2-1.8 keV	BNL-NSLS

BEAMLINE	SOURCE	TYPE OF RESEARCH	ENERGY RANGE	ORGANIZATION
X13B	Insertion Device	Microdiffraction Imaging	4-16 KeV	BNL-NSLS
X14A	Bend	MAD XRD, powder XRD, single crystal XRD, time resolved WAXD X-ray reflectivity	5-26 keV	Oak Ridge National Laboratory Tennessee Technological University University of Tennessee
X15A	Bend	XSW DEI	3-25keV XSW 10-60keV DEI	Argonne National Laboratory BNL-NSLS Canadian Light Source Illinois Institute of Technology North Carolina State University Northwestern University University of North Carolina University of Saskatchewan
X15B	Bend	XAS EXAFS XAFS NEXAFS XANES	0.8-15 keV	BNL-Environmental Sceinces Lucent Technologies, Inc. Stony Brook University Temple University University of Texas @ Austin
X16C	Bend	XRD, powder XAS XAFS	4.5-25 keV	BNL-NSLS Yeshiva University
X17B1	Insertion Device	XRD, powder	White Beam 55-80 keV	BNL-Medical BNL-NSLS
X17B2	Insertion Device	XRD, powder	White Beam 55-80 keV	Stony Brook University
X17B3	Insertion Device	XRD, powder XRD, single crystal High pressure research	5-80 keV	BNL-NSLS Carnegie Institution of Washington
X17C	Insertion Device	XRD, powder XRD, single crystal High pressure research	5-80 keV	Carnegie Institution of Washington Lawrence Livermore National Laboratory Naval Research Laboratory (NRL) University of Chicago
X18A	Bend	XRD, powder XRD, single crystal XRD, surface WAXD X-ray reflectivity X-ray scattering, surface WAXS	4-19 keV	BNL-Department of Materials Sciences BNL-NSLS General Electric Indiana University @ Indianapolis Pennsylvania State University Purdue University University of Maryland University of Missouri @ Columbia
X18B	Bend	XAS EXAFS XAFS NEXAFS XANES	5.7-40 keV	BNL-Chemistry BNL-NSLS General Electric Natural Resources Canada North Carolina State University Rutgers University UOP University of Kentucky
X19A	Bend	XAS EXAFS XAFS NEXAFS XANES	2.1-17 keV	BNL-NSLS BNL-Chemistry Department General Electric Natural Resources Canada North Carolina State University Rutgers University UOP University of Kentucky

BEAMLINE	SOURCE	TYPE OF RESEARCH	ENERGY RANGE	ORGANIZATION
X19C	Bend	XRD, surface X-ray topography X-ray reflectivity X-ray scattering, liquid X-ray scattering, surface	6-17 keV	Army Research Laboratory Carnegie Mellon University Dartmouth College Johns Hopkins University Kansas State University National Aeronautics and Space Admin. (NASA) Stony Brook University University of Chicago University of Illinois @ Chicago University of Wisconsin
X20A	Bend	XRD, single crystal XRD, surface Microdiffraction Imaging X-ray reflectivity X-ray scattering, surface	4.5-13 keV	IBM Research Division
X20B	Bend	XRD, single crystal XRD, surface X-ray reflectivity X-ray scattering, surface	17.4 keV	IBM Research Division
X20C	Bend	XRD, single crystal XRD, surface XRD, time resolved X-ray reflectivity X-ray scattering, surface	4-11 keV	IBM Research Division
X21	Insertion Device	XRD, single crystal X-ray scattering, magnetic X-ray scattering, resonant SAXS	5-15 keV	BNL-NSLS
X22A	Bend	XRD, single crystal XRD, surface WAXD X-ray reflectivity X-ray scattering, surface WAXS	10 keV, 32 keV	BNL-Environmental Science BNL-Physics Rutgers University University of Maryland
X22B	Bend	XRD, surface X-ray scattering, liquid X-ray scattering, surface	6.5-10 keV	BNL-Physics Harvard University Rutgers University
X22C	Bend	XRD, single crystal XRD, surface X-ray reflectivity X-ray scattering, magnetic X-ray scattering, surface	3-12 keV	BNL-Physics Rutgers University University of Maryland
X23A2	Bend	XRD, powder DAFS XAS EXAFS XAFS NEXAFS XANES	4.7-30 keV	National Institute of Standards & Technology

BEAMLINE	SOURCE	TYPE OF RESEARCH	ENERGY RANGE	ORGANIZATION
X23B	Bend	XRD, powder XAS EXAFS XAFS NEXAFS XANES	3-10.5 keV	BNL-Environmental Science Canadian Light Source Hunter College Naval Research Laboratory (NRL) Naval Surface Warfare Center New Jersey Institute of Technology North Carolina State University Northeastern University Paul Scherrer Institute U.S. Environmental Protection Agency Virginia Union University
X24A	Bend	XSW Auger spectroscopy EXAFS X-ray fluorescence spectroscopy XPS	1.8-5 keV	National Institute of Standards & Technology
X24C	Bend	UV photoabsorption spectroscopy XAS	.006-1.8 keV	Naval Research Laboratory (NRL)
X25	Insertion Device	MAD Macromolecular crystallography	3-28 keV	BNL-Biology BNL-NSLS
X26A	Bend	Microdiffraction Imaging X-ray microprobe	3-30 keV	BNL-Environmental Science University of Chicago University of Georgia
X26C	Bend	MAD Macromolecular crystallography	5-20 keV	BNL-Biology Cold Spring Harbor Laboratory Stony Brook University
X27C	Bend	XRD, time resolved WAXD SAXS WAXS	9 keV	Basell USA, Inc. (formerly Montell) National Institute of Standards & Technology National Institutes of Health Naval Surface Warfare Center New Jersey Institute of Technology Stony Brook University U.S. Air Force
X28C	Bend	X-ray footprinting	White Beam	Albert Einstein College of Medicine
X29A	Insertion Device	MAD Macromolecular crystallography	6-15 keV	Albert Einstein College of Medicine BNL-Biology

NSLS Linac Parameters as of December 2004

Electron Gun Injection Energy	100 keV
Linac Final Energy	120 MeV
Number of Accelerating Sections	3
Number of Klystrons	3
Linac Frequency	2856 MHz
Horizontal Emittance into Booster (ε_x)	7.6 x 10^{-1} m-rad

NSLS Booster Parameters

Booster Injection Energy	120 MeV
Booster Extraction Energy	750 MeV
Circumference	28.35 m
Number of Superperiods (N_s)	4
Dipole Bend Radius (ρ)	1.91 m
Nominal Tunes (ν_x,ν_y)	2.42, 1.37
Betatron Function (βx,βy)	8.63 to 1.01, 5.26 to 1.73 m
Dispersion Function (η_x,η'_x)	1.21 to 0.41 m
Momentum Compaction (α)	0.106
RF Frequency (f_{rf})	52.88 MHz
RF Peak Voltage (V_{rf})	25 keV
Horizontal Acceptance	1.66 x 10^{-4} m-rad
Vertical Acceptance	6.11 x 10^{-5} m-rad
Momentum Acceptance	±0.0025
Horizontal Emittance at Extraction (ε_x)	7.6 x 10^{-7} to 1.0 x 10^{-7} m-rad
Energy Spread at Extraction (σE/E)	1.4 x 10^{-4}
Bunch Length at Extraction	110 mm

Booster Magnetic Elements (Fields at 750 MeV)

Name	Type	Quantity	B (kG)	B' (kG/m)	B" (kG/m)	Effective Length (m)
BB	Dipole	8	13.099	-7.97	-125	1.5
Q1	Quadrupole	4		68.82		0.3
Q2	Quadrupole	4		93.60		0.3
SF	Sextupole	4			1223.7	0.2

VUV STORAGE RING PARAMETERS AS OF DECEMBER 2004

Stored Electron Beam Energy	0.808 GeV
Injected Current	1.0 amp
Lifetime @ 200 mA unstretched (stretched)	~6 (9.8) hr
Circumference	51.0 meters

PHOTON CRITICAL WAVELENGTH (ENERGY)

Dipole Source 1.41 T $\lambda_c(E_c)$	19.9 Å (622 eV)

LATTICE STRUCTURE (CHASMAN-GREEN) SEPARATED FUNCTION, QUAD DOUBLETS

Number of Superperiods (N_s)	4
Magnet Complement	8 Bending Magnets (1.5 meters long each) 24 Quadrupole (0.3 meters long each) 12 Sextupole in two families (0.20 meters long each)

STORAGE RING CHARACTERISTICS

Number of Dipole Ports	18
Number of Insertion Device Straight Sections	2
Maximum Length of Insertion Devices	2.25 meters
Dipole Bend Radius	1.91 meters
Radiated Bending Magnet Power (I= 1A)	20.4 kW
Power per Horizontal Milliradian (I= 1A)	3.2 W
RF Frequency (f_{rf})	52.887 MHz
Electron Orbital Period	170.2 nanoseconds
Number of RF Buckets	9
Typical Bunch Mode (filled buckets)	7
Damping Times	$\tau_x=\tau_y$= 13 msec; τ_ε = 7 msec
Nominal Tunes (ν_x,ν_y)	3.14, 1.26
Momentum Compaction	0.0235
RF Peak Voltage with 52 MHz (with 211 MHz) (V_{rf})	80 keV (20 keV)
Design RF Power with 52 MHz (with 211 MHz)	50 kW (6 KW)
Synchrotron Tune (ν_s)	0.0018
Natural Energy Spread [I_b< 20 mA] ($\sigma E/E$)	5.0×10^{-4}
Natural Bunch Length[I_b< 20 mA]52 MHZ(211 MHZ)(2σ)	9.7 mm (360 mm)
Horizontal Damped Emittance (ε_x)	1.6×10^{-7} m-rad
Vertical Damped Emittance (ε_y)	3.5×10^{-10} m-rad (4×10^{-9} in normal ops.)*

ARC SOURCE PARAMETERS

Betatron Function (β_x,β_y)	1.18 to 2.25 m, 10.26 to 14.21 m
Dispersion Function (η_x,η'_x)	0.500 to 0.062 m, 0.743 to 0.093 m
$\alpha_{x,y} = -\beta'_{x,y}/2$	-0.046 to 1.087, 3.18 to -0.96
$\gamma_{x,y} = (1+\alpha^2_{x,y})/\beta_{x,y}$	0.738 to 0.970 m^{-1}, 1.083 to 0.135 m^{-1}
Source Size (σ_x,σ_y)	536 to 568 µm, >60 to >70 µm (170-200 µm in normal ops.)*
Source Divergence (σ'_x,σ'_y)	686 to 373 µrad, 19.5 to 6.9 µrad (55-20 µrad in normal ops.)*

INSERTION DEVICE PARAMETERS

Betatron Function (β_x,β_y)	11.1 m, 5.84 m
Source Size (σ_x,σ_y)	1240 µm, >45 µm (220 µm in normal ops.)*
Source Divergence (σ'_x, σ'_y)	112 µrad, >7.7 µrad (22 µrad in normal ops.)*

X-Ray Storage Ring Parameters as of December 2004

Stored Electron Beam Energy	2.800 GeV
Injected Current	0.3 A
Lifetime	~20 hours
Circumference	170.1 meters

Photon critical wavelength (energy)

Dipole Source 1.36 T $\lambda_c(E_c)$	1.75 Å (7.1 keV)
Wiggler Source 5.0 T $\lambda_c(E_c)$	0.48 Å (26.1 keV)

Lattice Structure (Chasman-Green) Separated Function, Quad Doublets

Number of Superperiods (N_s)	8
Magnet Complement	16 Bending (2.7 meters long each) 40 Quadrupole A,C and D type (0.45 meters each) 16 Quadrupole B type (0.8 meters long each) 32 Sextupole in two families (0.20 meters long each)

Storage Ring Characteristics

Number of Dipole Ports	30
Number of Insertion Device Straight Sections	6
Maximum Length of Insertion Devices	4.50 meters
Dipole Bend Radius	6.875 meters
Radiated Bending Magnet Power (1=0.25A)	198 kW
Power per Horizontal Milliradian (1=0.25A)	32 W
RF Frequency (f_{rf})	52.88 MHz
Electron Orbital Period	567.2 nanoseconds
Number of RF Buckets	30
Typical Bunch Mode (filled buckets)	25
Damping Times	$\tau_x=\tau_y=$ 4 msec; $\tau_\varepsilon=$ 2 msec
Nominal Tunes (ν_x,ν_y)	9.8, 5.7
Momentum Compaction	4.1×10^{-3}
RF Peak Voltage (V_{rf})	1120 keV
Design RF Power	450 kW
Synchrotron Tune (ν_s)	0.0023
Natural Energy Spread ($\sigma E/E$)	9.2×10^{-4}
Natural Bunch Length (2σ)	87 mm
Horizontal Damped Emittance (ε_x)	7.5×10^{-8} m-rad
Vertical Damped Emittance (ε_y)	1.5×10^{-10} m-rad

Arc Source Parameters

Betatron Function (β_x,β_y)	1.0 to 3.8 m, 7.9 to 26.5 m
Dispersion Function (η_x,η'_x)	0.47 to -0.11, -0.39 to 0.22
$\alpha_{x,y} = -\beta'_{x,y}/2$	-0.49 to 1.62, -3.4 to 4.5
$\gamma_{x,y} = (1+\alpha^2_{x,y})/\beta_{x,y}$	0.952 to 0.962 m^{-1}, 0.81 to 0.52 m^{-1}
Source Size (σ_x,σ_y)	371 to 612 µm, 27 to 53 µm
Source Divergence (σ_x',σ_y')	476 to 324 µrad, 9 to 7 µrad

Insertion Device Parameters

Betatron Function (β_x, β_y)	1.60 m, 0.35 m
Source Size (σ_x,σ_y)	300 µm, 6 µm
Source Divergence (σ_x', σ_y')	260 µrad, 35 µrad

FY 2004 NSLS Machine Activities

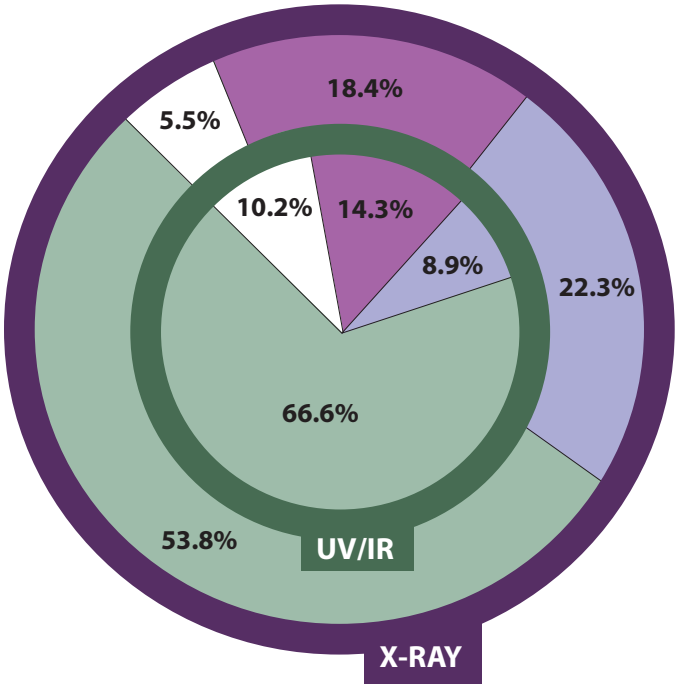

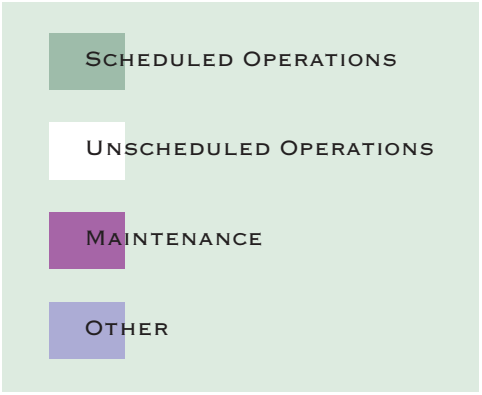

Other Activities	UV/IR	X-ray
Studies	2.3%	8.4%
Comm/Cond.	2.3%	3.5%
Holiday	2.4%	2.4%
Injection	1.2%	2.4%
Unscheduled Downtime	0.7%	4.9%
Interlock	0.0%	0.7%

Fiscal Year 2004

	VUV Actual FY 04			X-Ray Actual FY 04		
Month	Planned Hours	Reliability[1]	Availability[2]	Planned Hours	Reliability[1]	Availability[2]
October	605	99.5%	115.0%	561	92.3%	105.9%
November	499	99.0%	114.0%	403	91.1%	110.3%
December	0	-	-	0	-	-
January	409	97.7%	125.8%	335	93.0%	95.2%
February	570	98.8%	108.5%	511	98.1%	106.0%
March	620	99.7%	110.5%	510	98.2%	109.2%
April	592	99.9%	111.3%	583	97.3%	100.9%
May	348	98.6%	127.1%	238	22.5%	22.5%
June	551	98.9%	122.3%	528	98.5%	109.0%
July	500	99.8%	112.5%	448	94.9%	103.3%
August	615	98.6%	108.4%	509	89.2%	98.7%
September	597	98.4%	109.8%	525	96.5%	108.6%
	5906			5151		
Fiscal 2004 Delivered	5871	99.0%	114.2%	4725	91.7%	101.1%

Note: Delivered hours are only those accumulated during scheduled operations. Unscheduled operations do not contribute to this total.

[1] Operations during scheduled time
[2] Operations compared to total scheduled time

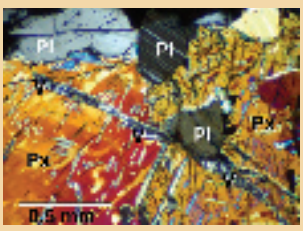
Pl
Pl
Px
Pl
Px
Px
0.5 mm

The following pages list all papers published in the 2004 calendar year as reported to the NSLS by February 28, 2005. Citations are listed in order of beamline number and then alphabetically by the last name of the first author. This list contains reported citations for journal articles, published conference proceedings, books, chapters in books, formal reports, informal reports, technical reports, theses, dissertations, and patents. For citation submissions where research was performed on more than one beamline, the citation is listed under each beamline. However, each citation was only counted once.

The first column in the table (right) lists the number of publications reported to the NSLS during the 2004 fiscal year (Oct. 1, 2003 – Sept. 30, 2004) and published between 2001 and 2004. Although some of these publications were published earlier than FY 2004, they were not reported to the NSLS until this fiscal year. Thus, they have not been counted in prior years' activity reports.

The second column in the table lists the number of publications published in the 2004 calendar year and reported to the NSLS as of Feb. 28, 2005. These numbers are slightly lower than the fiscal year values because they contain only publications from 2004 and it often takes many months or years to account for user and staff publications.

Several types of journal articles are reported in this list, including premier journals, peer-reviewed journals, and a few that are not peer-reviewed. Premier journals include: Physical Review Letters, Science, Nature, Cell, EMBO Journal, Nature Structural Biology, Proceedings of the National Academy of Sciences, Structure, and Applied Physics Letters.

	Reported in Fiscal Year 2004*	**Published in Calendar Year 2004****
Journals, peer-reviewed, premier	100	102
Journals, other peer-reviewed	506	487
Journals, non peer-reviewed	35	28
Total Journals and Magazines	**641**	**617**
Books/Chapters in Books	4	4
Published Conference Proceedings	40	40
Reports: Technical, Formal, Informal	3	3
Theses/Dissertations	15	15
Patents	0	0
Total Misc. Publications	**62**	**62**
Total Publications	**734**	**679**
NSLS VUV User Publications	**71**	**57**
NSLS X-Ray User Publications	**549**	**537**
NSLS Staff Publications	**114**	**85**
	734	**679**

** Publications reported to the NSLS from Oct 1, 2003 – Sept. 30, 2004 and published between 2001 – 2004.*
*** Publications published in 2004 as reported to the NSLS by Feb. 28, 2005.*

NSLS Users

Beamline U1A

H Hwu, B Fruhberger, J Chen. Different Modification Effects of Carbidic and Graphitic Carbon on Ni Surfaces. *J. Catal.*. **221** (1), 170-177 (2004).

J McCormick, B Zhao, S Rykov, H Wang, J Chen. Thermal Stability of Flame-Synthesized Anatase TiO2 Nanoparticles. *J. Phys. Chem. B*. **108**, 17398-17402 (2004).

S Xiao, S Brunner, M Wieland. Reactions of Surface Amines with Heterobifunctional Cross-Liners Bearing Both Succinimidyl Ester and Maleimide for Grafting Biomolecules. *J. Phys. Chem. B*. **108**, 16508-16517 (2004).

M Zellner, J Chen. Synthesis, Characterization and Surface Reactivity of Tungsten Carbide (WC) PVD Films. *Surf. Sci.*. **569**, 89-98 (2004).

Beamline U2A

D Klug, J Tse, Z Liu, X Gonze, R Hemley. Anomalous Transformations in Ice VIII. *Phys. Rev. B*. **70**, 144113 (2004).

J Kung, B Li, T Uchida, Y Wang, D Neuville, R Liebermann. In Situ Measurements of Sound Velocities and Densities Across the Orthopyroxene-High-Pressure Clinopyroxene Transition in MgSiO3 at High Pressure. *Phys. Earth Planet. Interiors*. **147**, 27-44 (2004).

H Liu, J Hu, J Xu, Z Liu, J Shu, H Mao, J Chen. Phase Transition and Compression Behavior of Gibbsite under High-Pressure. *Phys. Chem. Miner.*. **31**, 240-246 (2004).

C Slebodnick, J Zhao, R Angel, B Hanson, Y Song, Z Liu, R Hemley. High Pressure Study of Ru3(CO)12 by X-ray Diffraction, Raman, and Infrared Spectroscopy. *Inorg. Chem.*. **43** (17), 5245-5252 (2004).

D Wetzel. Recent Analytical Synchrotron Infrared Microspectroscopy and Imaging. *Microsc. Microanal.*. **10** (suppl 2), 1354-1355 (2004).

Beamline U2B

E Chouparova, A Lanzirotti, H Feng, K Jones, N Marinkovic, C Whitson, P Philp. Characterization of Petroleum Deposits Formed in a Producing Well by Synchrotron Radiation-Based Microanalyses. *Energ. Fuel*. **18** (4), 1199-1212 (2004).

S Lappi, S Franzen. Eigenvector Mapping: A Method for Discerning Solvent Effects on Vibrational Spectra. *Spectrochim. Acta A*. **60**, 357-370 (2004).

D Wetzel, J Striova, D Huggins, M Collinson. Synchrotron Infrared Microspectroscopy Reveals Localized Heterogeneities in an Organically Modified Silicate Film. *Vib. Spectrosc.*. **35** (1-2), 153-158 (2004).

P Yu, J McKinnon, C Christensen, D Christensen. Applications of Synchrotron Technology (SR_FTIR) to Feed Analysis and Utilization: A Novel Approach. *Proceeding of the 25th Western Nutrition Conference - Nutrient Requirement and Ingredient Evaluation in 21st Century*, Vol Sept 28-30, p. 98-112, sponsored by University of Saskatchewan. (2004).

P Yu, J McKinnon, C Christensen, D Christensen. Using Synchrotron Transmission FTIR Microspectroscopy as a Rapid, Direct and Nondestructive Analytical Technique to Reveal Molecular Microstructural-Chemical Features within Tissue in Grain Barley. *J. Agr. Food Chem.*. **52**, 1484-1494 (2004).

P Yu, J McKinnon, C Christensen, D Christensen. Using Synchrotron-Based FTIR Microspecscopy to Reveal Chemical Features of Feather Protein Secondary Structure: Comparison with Othe Feed Protein Sources. *J. Agr. Food Chem.*. **52**, 7353-7361 (2004).

Yu, J McKinnon, C Christensen, D Christensen. Imaging Molecular Chemistry of Pioneer Corn. *J. Agr. Food Chem.*. **52**, 7345-7352 (2004).

P Yu. Application of Advanced Synchrotron-Based Fourier Transform Infrared Microspectroscopy (SR-FTI) to Animal Nutrition and Feed Sciences: A Novel Approach. *Brit. J. Nutr.*. **92**, 869-885 (2004).

P Yu, J McKinnon, C Christensen, D Christensen, N Marinkovic. Chemical Imaging of Microstructures of Plant Tissues within Cellular Dimension using Synchrotron Infrared Microspectroscopy. *J. Agr. Food Chem.*. **51**, 6062-6067 (2004).

Beamline U4A

A Chan, W Chen, H Wang, J Rowe, T Madey. Methanol Reactions Over Oxygen-Modified Re Surfaces: Infleuence of Surface Structure and Oxidation. *J. Phys. Chem. B*. **108**, 14643-14651 (2004).

L Fleming, M Ulrich, K Efimenko, J Genzer, A Chan, T Madey, S Oh, O Zhou, J Rowe. NEXAFS and UPS Studies of Aligned Single-walled Carbon Nanotubes on Si(100). *J. Vac. Sci. Technol., B*. **22** (4), 2000-2005 (2004).

M Gladys, I Ermanoski, G Jackson, J Quinton, J Rowe, T Madey. A High Resolution Photoemission Study of Core-Level Shifts (SCLS) in Clean and Oxygen. *J. Electron. Spectrosc. Relat. Phenom.*. **135**, 105-112 (2004).

Beamline U4B

J Holroyd, Y Idzerda, S Stadler. Properties of thin film europium oxide by x-ray magnetic circular dichroism. *J. Appl. Phys.*. **95** (11), 6571 (2004).

A Lussier, J Dvorak, Y Idzerda, S Ogale, S Shinde, T Venkatesan. Comparative X-ray Absorption Spectroscopy Study of Co-Doped SnO2 and TiO2. *J. Appl. Phys.*. **95** (11), 7190-7191 (2004).

D Resnick, K Gilmore, Y Idzerda, M Klem, E Smith, T Douglas. Modeling of the Magnetic Behavior of Gamma-Fe[sub 2]O[sub 3] Nanoparticles Mineralized in Ferritin. *J. Appl. Phys.*. **95** (11), 7127 (2004).

S Stadler, Y Idzerda, J Dvorak, J Borchers. Using Circularly Polarized Soft X-rays to Probe antiferromagnetically correlated Co/Cu multilayers. *J. Appl. Phys.*. **95** (11), 6672 (2004).

P Wu, G Saraf, Y Lu, D Hill, R Bartinski, D Arena, R Mee-Yi, A Raley, K Yung. Ion-Beam-Induced Sharpening of ZnO Nanotips. *Appl. Phys. Lett.*. **85**, 1247 (2004).

Beamline U4IR

L Keller, S Messenger, G Flynn, S Clemett, S Wirick, C Jacobsen. The Nature of Molecular Cloud Material in Interplanetary Dust. *Geochim. Cosmochim. Acta*. **68** (11), 2577-2589 (2004).

Beamline U5UA

H Jeong, R Skomski, C Waldfried, T Komesu, P Dowben, E Vescovo. The Effective Spin Dependent Debye Temperature of Gd(0001). *Phys. Lett. A*. **324**, 242 (2004).

Beamline U7A

L Andruzzi, A Hexemer, X Li, C Ober, E Kramer, G Galli, E Chiellini, D Fischer. Control of Surface Properties Using Fluorinated Polymer Brushes Produced by Surface-Initiated Controlled Radical Polymerization. *Langmuir*. **20**, 10498-10506 (2004).

S Banerjee, T Hemraj-Benny, M Balasubramanian, D Fischer, J Misewich, S Wong. Ozonized Single-Walled Carbon Nanotubes Investigated using NEXAFS Spectroscopy. *Chem. Commun.*. **7** (7), 772-773 (2004).

S Banerjee, T Hemraj-Benny, M Balasubramanian, D Fischer, J Misewich, S Wong. Surface Chemistry and Structure of Purified, Ozonzied, Multiwalled Carbon Nanotubes Probed by NEXAFS and Vibrational Spectroscopies. *ChemPhysChem*. **5**, 1416-1422 (2004).

D Burnett, A Capitano, A Gabelnick, A Marsh, D Fischer, J Gland. In-situ Soft X-ray Studies of CO Oxidation on the Pt(111) Surface. *Surf. Sci.*. **564**, 29-37 (2004).

D Burnett, A Gabelnick, A Marsh, D Fischer, J Gland. Comparisons of Propylene and Propyne Catalytic Oxidation on a 100 Å Pt/Al2O3 Thin Film using in situ Soft X-ray Fluorescence Methods. *Surf. Sci.*. **553**, 1-12 (2004).

D Burnett, A Gabelnick, A Marsh, H Lewis, S Yalisove, D Fischer, J Gland. Defect Enhanced Carbon Monoxide Oxidation at Elevated Oxygen Pressures on a Pt/Al2O3. *J. Phys. Chem. B*. **108**, 5314-5323 (2004).

D Fischer, K Efimenko, R Bhat, S Sambasivan, J Genzer. Mapping Surface Chemistry and Molecular Orientation with Combinatorial Near-edge X-ray Absorption Fine Structure. *Macromol. Rapid Commun.*. **25**, 141-149 (2004).

E Jablonski, V Prabhu, S Sambasivan, D Fischer, E Lin, D Goldfarb, M Angelopoulos, H Ito. Surface and bulk chemistry of chemically amplified photoresists:. *Advances in Resist Technology and Processing*, Vol XXI, p. 31, sponsored by SPIE. (2004).

J Lenhart, S Fischer, D Sambasivan, E Lin, C Soles, R Jones, W Wu, W Goldfarb, M Angelopoulos. Utilizing Near Edge X-ray Absorption Fine Structure to Probe interfacial issues in Photolithography. *Polymers for Microelectronics and Nanoelectronics*, Vol 874, p. 98-117, sponsored by ACS. (2004).

G Liu, J Rodriguez, Z Chang, J Hrbek. Adsorption and Reaction of SO2 on Model Ce1-xZrxO2(111) Catalysts. *J. Phys. Chem. B*. **108**, 2931-2938 (2004).

A Marsh, D Burnett, D Fischer, J Gland. In-Situ Soft X-ray Studies of Toluene Catalytic Oxidation on the Pt(111) Surface. *J. Phys. Chem. B*. **108**, 605-611 (2004).

R Petrie, T Bailey, C Gorman, J Genzer. Fast Directed Motion of "Fakir" Droplets. *Langmuir*. **20**, 9893-9896 (2004).
J Rodriguez. Gold Nanoparticles on Titania: Activation and Behavior. *Dekker Encyclopedia of Nanoscience and Nanotechnology*, p. 1297-1304, Marcel Dekker, New York. (2004).
J Rodriguez, P Liu, J Dvorak, T Jirsak, J Gomes, Y Takahashi, K Nakamura. The Interaction of Oxygen with TiC(001): Photoemission and First-Principles Studies. *J. Chem. Phys.*. **121**, 465-474 (2004).
J Rodriguez, P Liu, J Dvorak, T Jirsak, J Gomes, Y Takahashi, K Nakamura. Adsorption of Sulfur on TiC(001): Photoemission and First-Principles Studies. *Phys. Rev. B*. **69**, 115414-1,10 (2004).
S Sambasivan, D Fischer, M Shen, S Hsu. Molecular Orientation of Ultrahigh Molecular Weight Polyethylene. *J. Biomed. Mater. Res. B*. **70B** (2), 278-285 (2004).
W Yoon, C Grey, M Balasubramanian, X Yang, D Fischer, J McBreen. A Combined NMR and XAS Study on the Local Environments and Electronic Structures of the Electrochemically Li-ion deintercalated LiCo1/3Ni1/3Mn1/3O2 electrode System. *J. Electrochem. Soc.*. **7** (3), A53 (2004).
W Yoon, M Balasubramanian, X Yang, Z Fu, D Fischer, J McBreen. Soft X-Ray Absorption Spectroscopic Study of a LiNi0.5Mn0.5O2 Cathode during Charge. *J. Electrochem. Soc.*. **151** (2), A246 (2004).
K Zhang, G Rosenbaum, C Liu, D Fischer. Development of Multilayer Analyzer Array Detectors for X-ray Fluorescence at the Third Generation Synchrotron Source. *Synchrotron Radiation Instrumentation: Eighth International*, Vol 8th, p. 957-960, sponsored by AIP. (2004).

Beamline U7B

M Fernandez-Garcia, A Martinez-Arias, J Hanson, J Rodriguez. Nanostructured Oxides in Chemistry: Characterization and Properties. *Chem. Rev.*. **104** (9), 4063-4104 (2004).

Beamline U8B

T Owens, B Ludwig, K Schneider, D Fosnacht, B Orr, M Banaszak Holl. Oxidation of Alkylsilane-Based Monolayers on Gold. *Langmuir*. **20** (22), 9636-9645 (2004).
T Owens, B Ludwig, D Fosnacht, J Bartolin, N Homann, N Wells, B Orr, M Banaszak Holl. Octylgermane on Gold: Synthesis, Oxidation, and Pattern Formation. *Langmuir*. **20**, 11422-11427 (2004).
T Owens. Formation and Reactivity of Alkylsilane-Based Monolayers on Gold. Ph.D. Thesis. University of Michigan, Ann Arbor. (2004).

Beamline U9B

J Lees, B Smith, F Wien, A Miles, B Wallace . CDtool - an Intergrated Software Package for Circular Dichroism Spectroscopic Data Processing, Analysis, and Archiving. *Anal. Biochem.*. **332**, 285-289 (2004).

Beamline U10A

C Homes, S Dordevic, M Strongin, D Bonn, R Liang, W Hardy, S Komiya, Y Ando, G Yu, et al.. A Universal Scaling Relation in High-Temperature Superconductors. *Nature*. **430**, 539-541 (2004).
A Zimmers, N Bontemps, R Lobo, C Hill, M Barr, R Greene, C Homes, A Millis. Infrared Signature of the Superconducting State in Pr(2-x)Ce(x)CuO(4). *Phys. Rev. B*. **70**, 132502 (2004).

Beamline U10B

D Chidambaram, G Halada, C Clayton. Synchrotron Radiation Based Grazing Angle Infrared Spectroscopy of Chromate Conversion Coatings Formed on Aluminum Alloys. *J. Electrochem. Soc.*. **151** (3), B160 (2004).
M Diem, M Romeo, C Matthaus, M Miljkovic, L Miller, P Lasch. Comparison of Fourier Transform Infrared (FTIR) Spectra of Individual Cells Acquired using Synchrotron and Conventional Sources. *Infrared Phys. Technol.*. **45**, 331-338 (2004).
P Dumas, N Jamin, J Teillaud, L Miller, B Beccard. Imaging Capabilities of Synchrotron Infrared Microspectroscopy. *Faraday Discuss*. **126**, 289-302 (2004).
G Flynn, L Keller, C Jacobsen, S Wirick. An Assessment of the Amount and Types of Organic Matter Contributed to the Earth by Interplanetary Dust. *Adv. Space Res.*. **33** (1), 57-66 (2004).
G Flynn, L Keller, C Jacobsen, S Wirick. The Origin of Organic Matter in the Solar System: Evidence from the Interplanetary Dust Particles . *Bioastronomy 2002: Life Among the Stars*, Vol 213, p. 275-280, sponsored by International Astronomical Union. (2004).
L Keller, S Messenger, G Flynn, S Clemett, S Wirick, C Jacobsen. The Nature of Molecular Cloud Material in Interplanetary Dust. *Geochim. Cosmochim. Acta*. **68** (11), 2577-2589 (2004).
J Kneipp, L Miller, S Spassov, F Sokolowski, P Lasch, M Beekes, D Naumann. Scrapie-infected Cells, Isolated Prions, and Recombinant Prion Protein: A Comparative Study. *Biopolymers*. **74** (1-2), 163-7 (2004).
L Miller, J Tetenbaum Novatt, D Hamerman, C Carlson. Alteractions in Mineral Composition Observed in Osteoarthritic Joints of Cynomologus Monkeys. *Bone*. **35** (2), 498-506 (2004).
D Wetzel, J Striova, D Huggins, M Collinson. Synchrotron Infrared Microspectroscopy Reveals Localized Heterogeneities in an Organically Modified Silicate Film. *Vib. Spectrosc.*. **35** (1-2), 153-158 (2004).
D Wetzel. Recent Analytical Synchrotron Infrared Microspectroscopy and Imaging. *Microsc. Microanal.*. **10** (suppl 2), 1354-1355 (2004).
P Yu. Application of Advanced Synchrotron-Based Fourier Transform Infrared Microspectroscopy (SR-FTI) to Animal Nutrition and Feed Sciences: A Novel Approach. *Brit. J. Nutr.*. **92**, 869-885 (2004).

Beamline U12A

S Linic, H Piao, K Adib, M Barteau. Ethylene Epoxidation on Ag: Identification of the Crucial Surface Intermediate by Experimental and Theoretical Investigation of its Electronic Structure. *Angew. Chem. Int. Ed.*. **43** (22), 2918-2921 (2004).
D Mullins. Adsorption of CO and C2H4 on Rh-Loaded Thin-Film Praseodymium Oxide. *Surf. Sci.*. **556** (2-3), 159-170 (2004).
H Piao, K Adib, M Barteau. A Temperature-Programmed X-ray Photoelectron Spectroscopy (TPXPS) Study of Chlorine Adsorption and Diffusion on Ag(111). *Surf. Sci.*. **557** (1-3), 13-20 (2004).

Beamline U12IR

L Mihaly, D Talbayev, L Kiss, J Zhou, T Feher, A Janossy. Field-frequency Mapping of the Electron Spin Resonance in the Paramagnetic and Antiferromagnetic States of LaMnO3. *Phys. Rev. B*. **69**, 024414 (2004).
D Talbayev, L Mihaly, J Zhou. Antiferromagnetic Resonance in LaMnO3 at Low Temperature. *Phys. Rev. Lett.*. **93** (1), 017202-1 (2004).

Beamline U13UB

T Valla, A Fedorov, P Johnson, P Glans, C McGuinness, K Smith, E Andrei, H Berger. Quasiparticle Spectra, Charge-Density Waves, Superconductivity, and Electron-Phonon Coupling in 2H-NbSe(2). *Phys. Rev. Lett.*. **92** (8), 086401 (2004).

S Wang, H Yang, A Sekharan, H Ding, J Engelbrecht, X Dai, Z Wang, A Kaminski, T Valla, et al.. The Quasiparticle Lineshape of Sr(2)RuO(4) and its Relation to Anisotropic Transport. *Phys. Rev. Lett.*. **92**, 137002 (2004).

Beamline X1A1

T Beetz. Soft X-ray Diffraction Imaging With and Without Lenses and Radiation Damage Studies. Ph.D. Thesis. SUNY at StonyBrook, StonyBrook. (2004).

C Boyce, M Zwieniecki, G Cody, C Jacobsen, S Wirick, A Knoll, N Holbrook. Evolution of Xylem Lignification and Hydrogel Transport Regulation. *Proc Natl Acad Sci USA*. **101** (50), 17555-17558 (2004).

A Braun, N Shah, F Huggins, G Huffman, S Wirick, C Jacobsen, K Kelly, A Sarofim. A Study of Diesel PM with X-ray Microspectroscopy. *Fuel*. **83**, 997-1000 (2004).

G Flynn, L Keller, C Jacobsen, S Wirick. An Assessment of the Amount and Types of Organic Matter Contributed to the Earth by Interplanetary Dust. *Adv. Space Res.*. **33** (1), 57-66 (2004).

G Flynn, L Keller, C Jacobsen, S Wirick. The Origin of Organic Matter in the Solar System: Evidence from the Interplanetary Dust Particles . *Bioastronomy 2002: Life Among the Stars*, Vol 213, p. 275-280, sponsored by International Astronomical Union. (2004).

H Geckeis, T Schäfer, W Hauser, T Rabung, T Missana, C Degueldre, A Möri, J Eikenberg, T Fierz, W Alexander. Results of the Colloid and Radionuclide Retention Experiment (CRR) at the Grimsel Test Site (GTS), Switzerland - Impact of Reaction Kinetics and Speciation on Radionuclide Migration. *Radiochim. Acta*. **92**, 765-774 (2004).

C Jacobsen, S Wang, W Yun, S Frigo. Calculation of X-ray Refraction from Near-Edge Absorption Data Only. *SPIE*, Vol 5583, p. 23-30, sponsored by SPIE. (2004).

L Keller, S Messenger, G Flynn, S Clemett, S Wirick. The Nature of Molecular Cloud Material in Interplanetary Dust. *Geochim. Cosmochim. Acta*. **68** (11), 2571-2589 (2004).

M Lerotic, C Jacobsen, T Schaefer, S Vogt. Cluster Analysis of soft X-ray spectromicroscopy Data. *Ultramicroscopy*. **100**, 35-57 (2004).

J Miao, H Chapman, J Kirz, D Sayre, K Hodgson. Taking X-ray Diffraction to the Limit: Macromolecular Structures from Femtosecond X-ray Pulses and Diffraction Microscopy of cells with Synchrotron Radiation. *Annu. Rev. Bioph. Biom.*. **33**, 157-176 (2004).

M Plaschke, J Rothe, M Denecke, T Fanghaenel. Soft X-ray Spectromicroscopy of Humic Acid Europium(III) Complexation by Comparison to Model Substances. *J. Electron. Spectrosc. Relat. Phenom.*. **135**, 55-64 (2004).

M Plaschke, J Rothe, M Denecke. Characterization of Gorleben groundwater colloids by scanning transmission X-ray microscope. *Prog. Coll. Pol. Sci. S.*. **126**, 130-133 (2004).

J Rothe, M Plaschke, M Denecke. Scanning Transmission X-ray Microscopy as Speciation Tool for Natural Organic Molecules. *Radiochim. Acta*. **92**, 711-715 (2004).

T Yoon, S Johnson, K Benzerara, C Doyle, T Tyliszczak, D Shuh, G Brown, Jr.. In Situ Characterization of Aluminum-Containing Mineral-Microorganism Aqueous Suspensions using Scanning Transmission x-Ray Microscopy. *Langmuir*. **20**, 10361-10366 (2004).

Beamline X1A2

M Lerotic, C Jacobsen, T Schaefer, S Vogt. Cluster Analysis of soft X-ray spectromicroscopy Data. *Ultramicroscopy*. **100**, 35-57 (2004).

T Yoon, S Johnson, K Benzerara, C Doyle, T Tyliszczak, D Shuh, G Brown, Jr.. In Situ Characterization of Aluminum-Containing Mineral-Microorganism Aqueous Suspensions using Scanning Transmission x-Ray Microscopy. *Langmuir*. **20**, 10361-10366 (2004).

Beamline X1B

P Abbamonte, G Blumberg, A Rusydi, A Gozar, P Evans, T Siegrist, L Venema, H Elsaki, E Isaacs, G Sawatzky. Crystallization of Charge Holes in The Spin Ladder of Sr14Cu24041. *Nature*. **431**, 1078 (2004).

J Downes, C McGuinness, P Glans, T Learmonth, D Fu, P Sheridan, K Smith. Electronic Structure Near the Fermi Level of the Organic Semiconductor Copper Phthalocyanine. *Chem. Phys. Lett.*. **390**, 203-207 (2004).

O Kugeler, E Rennie, A Ruedel, M Meyer, A Marquette, U Hergenhahn. N2 valence Photoionization Below and Above the 1s-1 Core IonizationThreshold. *J. Phys. B: At., Mol. Opt. Phys.*. **37**, 1353-1367 (2004).

K Thomas, J Hill, S Grenier, Y Kim, P Abbamonte, L Venema, A Rusydi, Y Tomioka, Y Tokura, et al.. Soft X-Ray Resonant Diffraction Study of Magnetic and Orbital Correlations in a Manganite Near Half Doping. *Phys. Rev. Lett.*. **92** (23), 237204-1 (2004).

Beamline X3A1

K Fiese, M Panthofer, G Wu, M Jansen. Strategies for the Structure Determination of Endohedral Fullerenes Applied to the Example of Ba@C74.Co(octaethylpophyrin).2C6H6. *Acta Cryst. B*. **60**, 520-527 (2004).

R Poulsen, A Bentien, T Graber, B Iverson. Synchrotron Charge-Density Studies in Materilas Chemistry: 16K X-ray Charge Density of a New Magnetic Metal-Organic Framework Material, [Mn2(C8H4O4)2(C3H7NO)2]. *Acta Cryst. A*. **60**, 382-389 (2004).

A Reich, M Panthofer, H Modrow, U Wedig, M Jansen. The Structure of Ba@C74. *J. Am. Chem. Soc.*. **126**, 14428-14434 (2004).

Beamline X3A2

A Nogales, G Broza, Z Roslaniec, K Schulte, I Sics, B Hsiao, A Sanz, M Garcia-Gutierrez, D Rueda, et al.. Low Percolation Threshold in Nanocomposites Based on Oxidized Single Wall Carbon Nanotubes and Poly(butylene terephthalate). *Macromolecules*. **37**, 7669-7672 (2004).

L Sun, L Zhu, Q Ge, R Quirk, C Xue, S Cheng, B Hsiao, C Avila-Orta, I Sics, M Cantino. Comparison of Crystallization Kinetics in Various Nanoconfined Geometries. *Polymer*. **45**, 2931 (2004).

L Sun, Y Liu, L Zhu, B Hsiao, C Avila-Orta. Path-dependent Melting in a Low Molecular Weight Polyethylene-block-poly(ethylene oxide) Diblock Copolymers. *Macromol. Rapid Commun.*. **25**, 853 (2004).

L Yang, R Somani, I Sics, B Hsiao, R Kolb, H Fruitwala, C Ong. Shear-Induced Crystallization Precursor Studies in Model Polyethylene Blends by In-Situ Rheo-SAXS and Reho-WAXD. *Macromolecules*. **37**, 4845-4859 (2004).

S Zhou, C Xu, J Wang, P Golas, J Batteas. Phase Behavior of Cationic Hydroxyethyl Cellulose-Sodium Dodecyl Sulfate Mixtures: Effects of Molecular Weight and Ethylene Oxide Side Chain Length of Polymers. *Langmuir*. **20**, 8482-8489 (2004).

S Zhou, C Xu, J Wang, W Gao, R Akhverdiyeva, V Shah, R Gross. Supramolecular Assemblies of a Naturally Derived Sophorolipid. *Langmuir*. **20**, 7926-7932 (2004).

Beamline X3B1

D Balzar, N Audebrand, M Draymond, A Fitch, A Hewat, I Langford, A Le Bail, D Louer, O Masson, N Popa. Size-Stain Line Broadening Analysis the Ceria Round-Robin Sample. *J. Appl. Cryst.*. **37**, 911-924 (2004).

C Botez, P Stephens, O Omotoso. Crystal Structure of Dicalcium Chromate Hydrate. *Powder Diffr.*. **19** (2), 133-136 (2004).

E Caspi, M Avdeev, S Short, J Jorgensen, M Lobanov, Z Zeng, M Greenblatt, P Thiyagarajan, C Botez, P Stephens. Structural and Magnetic Phase Diagram of the Two-Electron-Doped [Ca(1-x)Ce(x)]MnO3 System: Effects of Competition Among Charge, Orbital, and Spin Ordering. *Phys. Rev. B*. **69**, 104402 (2004).

A Hoennerscheid, L van Wuellen, R Dinnebier, M Jansen, J Rahmer, M Mehring. Evidence for C60 Dimerisation in the Fulleride [Cr(C9H12)2]+C60–. *Phys. Chem. Chem. Phys.*. **6**, 2454-2460 (2004).

M Lobanov, M Greenblatt, E Caspi, I Jorgensen, D Sheptyakov, B Toby, C Botez, P Stephens. Crystal and Magnetic Structure of the Ca3Mn2O7 Ruddlesden-Popper Phase: Neutron and Synchrotron X-ray Diffraction Study. *J. Phys.: Condens. Matter*. **16** (29), 5339-5348 (2004).

C Muehle, R Dinnebier, L van Wuellen, G Schwering, M Jansen. New Results in the Field of Lithiumhexaoxometallates Li7MO6 with M= Nb, Ta, Sb, Bi. *Inorg. Chem.*. **43** (3), 874-881 (2004).

C Nunes, R Suryanarayanan, C Botez, P Stephens. Characterization and Crystal Structure of D-Mannitol Hemihydrate. *J. Pharm. Sci.*. **93**, 2800-2809 (2004).

J Readman, P Barker, I Gameson, J Hriljac, W Zhong, P Edwards, P Anderson. An Ordered Array of Cadmium Clusters Assembled in Zeolite A. *Chem. Commun.*. **2004**, 736-737 (2004).

Y Soo, S Kim, Y Kao, A Blattner, B Wessels, S Khalid, C Sanchez-Hanke, C Kao. Local Structure Around Mn Atoms in Room-Temperature Ferromagnetic (In,Mn) As Thin Films Probed by Extended X-ray Absorption Fine Structure. *Appl. Phys. Lett.*. **84**, 481 (2004).

T Vos, Y Liao, W Shum, I Her, P Stephens, W Reiff, L Miller. Diruthenium Tetracarboxylate Monocation, [RuII/III2(O2CR)4]+, Building Blocks for 3-D Molecule-based Magnets. *J. Am. Chem. Soc.*. **126**, 11630-11639 (2004).

Beamline X4A

W Blankenfeldt, A Kuzin, T Skarina, Y Korniyenko, L Tong, P Bayer, P Janning, L Thomashow, D Mavrodi. Structure and Function of the Phenazine Biosynthetic Protein PhzF from Pseudomonas Fluorescens. *Proc Natl Acad Sci USA*. **101**, 16431-16436 (2004).

C Brautigam, Y Chelliah, J Deisenhofer. Tetramerization and ATP Binding by a Protein Comprising the A, B, and C Domains of Rat Synapsin I. *J. Biol. Chem.*. **279**, 11948–11956 (2004).

J Buglino, K Onwueme, J Ferreras, L Quadri, C Lima. Crystal Structure of PapA5, a Phthiocerol Dimycocerosyl Transferase from Mycobacterium Tuberculosis. *J. Biol. Chem.*. **279**, 30634-30642 (2004).

M Bukhtiyarova, K Northrop, X Chai, D Casper , M Karpusas, E Springman. Improved Expression, Purification, and Crystallization of p38alpha MAP Kinase. *Protein Expr. Purif.*. **37** (1), 154-161 (2004).

B Chakravarty, Z Gu, S Chirala, S Wakil, F Quicocho. Human Fatty Acid Synthase: Structure and Substrate Selectivity of the Thioesterase Domain. *Proc Natl Acad Sci USA*. **101**, 15567-15572 (2004).

Y Chen, M Li, Y Zhang, L He, Y Yamada, A Fitzmaurice, Y Shen, H Zhang, L Tong, J Yang. Structural Basis of the alpha 1-beta Subunit Interaction of Voltage-Gated Ca2+ Channels. *Nature*. **429**, 675 (2004).

Y Cheng, D Patel. Crystallographic Structure of the Nuclease Domain of 3'hExo, A DEDDh Family Member, Bound to rAMP. *J. Mol. Biol.*. **343**, 305-312 (2004).

J Dai, J Liu, Y Deng, T Smith, M Lu. Structure and Protein Design of a Human Platelet Function Inhibitor. *Cell*. **116**, 649-659 (2004).

H Dvir, M Harel, S Bon, W Liu, M Vidal, C Garbay, J Sussman, J Massoulie, I Silman. The Synaptic Acetylcholinesterase Tetramer Assembles Around a Polyproline II Helix. *EMBO J.*. **23**, 4394-4405 (2004).

C Fabrega, S Hausmann, V Shen, S Shuman, C Lima. Structure and Mechanism of the mRNA (guanine-N7) cap Methyltransferase. *Mol. Cell*. **13**, 77-89 (2004).

F Forouhar, I Lee, J Benach, K Kulkarni, R Xiao, T Acton, G Montelione, L Tong. A Novel Nad-Binding Protein Revealed by the Crystal Structure of 2,3-Diketo-L-Gulonate Reductase (YIAK). *J. Biol. Chem.*. **279**, 13148-13155 (2004).

S Galdiero, E Gouaux. High Resolution Crystallographic Studies of Alpha-Hemolysin–Phospholipid Complexes Define Heptamer–Lipid Head Group Interactions: Implication for Understanding Protein–Lipid Interactions. *Protein Sci.*. **13**, 1503-1511 (2004).

D Gebauer, J Li, G Jogl, Y Shen, D Myszka, L Tong. Crystal structure of the PH-BEACH domains of human LRBA/BGL. *Biochemistry*. **43**, 14873-14880 (2004).

S Goldsmith-Fischman, A Kuzin, A Edstrom, J Benach, R Shastry, R Xiao, T Acton, B Honig, G Montelione, J Hunt. The SufE Sulfur-Acceptor Protein Contains a Conserved Core Structure that Mediates Interdomain Interactions in a Variety of Redox Protein Complexes. *J. Mol. Biol.*. **344**, 549-565 (2004).

M Gu, C Fabrega, D Liu, H Liu, M Kiledjian, C Lima. Insights into the Structure , Mechanism and Regulation of Scavenger mRNA Decapping Activity. *Mol. Cell*. **14**, 67-80 (2004).

B Hamaoka, C Dann III, B Geisbrecht, D Leahy. Crystal Structure of Caenorhabditis elegans HER-1 and Characterization of the Interaction Between HER-1 and TRA-2A. *Proc Natl Acad Sci USA*. **101** (32), 11673-11678 (2004).

C Ho, L Wang, C Lima, S Shuman. Structure and Mechanism of RNA Ligase. *Structure*. **12**, 327-339 (2004).

Y Hsiao, G Jogl, L Tong. Structural and Biochemical Studies of the Substrate Selectivity of Carnitine Acetyltransferase. *J. Biol. Chem.*. **279**, 31584-31589 (2004).

C Huang, M Venturi, S Majeed, M Moore, S Phogat, M Zhang, D Dimitrov, W Hendrickson, J Robinson, et al.. Structural Basis of Tyrosine Sulfation and VH-gene Usage in Antibodies that Recognize the HIV Type 1 Coreceptor-Binding Site on gp120. *Proc Natl Acad Sci USA*. **101**, 2706-2711 (2004).

O Ibrahimi, F Zhang, A Eliseenkova, R Linhardt, M Mohammadi. Proline to Arginine Mutations in FGF Receptors 1 and 3 Result in Pfeiffer and Muenke Craniosynostosis Syndromes Through Enhancement of FGF Binding Affinity. *Hum. Mol. Genet.*. **13**, 69-78 (2004).

G Jogl, L Tong. Crystal Structure of Yeast Acetyl-Coenzyme A Synthetase in Complex with AMP. *Biochemistry*. **43**, 1425-1431 (2004).

J Khan, E Brint, L O'Neill, L Tong. Crystal Structure of the Toll/interleukin-1 Receptor (TIR) Domain of IL-1RAPL. *J. Biol. Chem.*. **279**, 31664-31670 (2004).

R Kovall, W Hendrickson. Crystal Structure of the Nuclear Effector of Notch Signaling, CSL, Bound to DNA. *EMBO J.*. **23**, 3441-3451 (2004).

J Liu, W Yong, Y Deng, N Kallenbach, M Lu. Atomic Structure of a Tryptophan-Zipper Pentamer. *Proc Natl Acad Sci USA*. **101**, 16156-16161 (2004).

S Olsen, O Ibrahimi, A Raucci, F Zhang, A Eliseenkova, A Yayon, C Basilico, R Linhardt, J Schlessinger, et al.. Insights into the Molecular Basis for Fibroblast Growth Factor Receptor Autoinhibition and Ligand-Binding Promiscuity. *Proc Natl Acad Sci USA*. **101**, 935-940 (2004).

S Patel, M Rajala, L Rossetti, P Scherer, L Shapiro. Disulfide-Dependent Multimeric Assembly of Resistin Family Hormones. *Science*. **304**, 1154-1158 (2004).
S Prigge, B Eipper, R Mains, L Amzel. Dioxygen Binds End-On to Mononuclear Copper in a Precatalytic Enzyme Complex. *Science*. **304**, 864 (2004).
D Reverter, C Lima. A Basis for SUMO Protease Specificity Provided by Analysis of Human Senp2 and a Senp2-SUMO Complex. *Structure*. **12**, 1519-1531 (2004).
Y Shen, S Volrath, S Weatherly, T Elich, L Tong. A Mechanism for the Potent inhibition of Eukaryotic Acetyl Coenzyme A Carboxylase by Soraphen A, a Macrocyclic Polyketide Natural Product. *Mol. Cell*. **16**, 881-891 (2004).
I Shumilin, R Bauerle, J Wu, R Woodard, R Kretsinger. Crystal Structure of the Reaction Complex of 3-Deoxy-D-arabino-heptulosonate-7-phosphate Synthase from Thermotoga maritima Refines the Catalytic Mechanism and Indicates a New Mechanism of Allosteric Regulation. *J. Mol. Biol.*. **341**, 455-466 (2004).
Y Wang, R Coulombe, D Cameron, L Thauvette, M Massariol, L Amon, D Fink, S Titolo, E Welchner, et al.. Crystal Structure of the E2 Transactivation Domain of Human Papillomavirus Type 11 Bound to a Protein Interaction Inhibitor. *J. Biol. Chem.*. **279** (8), 6976-6985 (2004).
H Ye, T Chen, X Xu, M Pennycooke, H Wu, C Steegborn. Crystal Structure of the Putative Adapter Protein MTH1859. *J. Struct. Biol.*. **148**, 251-256 (2004).
D Yernool, O Boudker, Y Jin, E Gouaux. Structure of a Glutamate Transporter Homologue From Pyrococcus Horikoshii. *Nature*. **431**, 811 (2004).
H Zhong, B Tweel, L Tong. Molecular Basis for the Inhibition of the Carboxyltransferase Domain of Acetyl-coenzyme-A Carboxylase by Haloxyfop and Diclofop. *Proc Natl Acad Sci USA*. **101**, 5910-5915 (2004).
H Zhong, B Tweel, J Li, L Tong. Crystal Structure of the Carboxyltransferase Domain of Acetyl-Coenzyme A Carboxylase in Complex with CP-640186. *Structure*. **12**, 1683-1691 (2004).

Beamline X5A

X Wei, C Bade, A Caracappa, T Dageya, F Lincoln, M Lowry, J Mahon, A Sandorfi, C Thorn, et al.. New Improvements Leading to Higher Polarization Frozen Spin HD targets at the LEGS Facility. *Nucl. Instrum. Meth. A*. **526**, 157 (2004).

Beamline X6A

S Gabelli, M Bianchet, H Azurmendi, Z Xia, V Sarawat, A Mildvan, L Amzel. Structure and Mechanism of GDP-Mannose Glycosyl Hydrolase, a Nudix Enzyme that Cleaves at Carbon Instead of Phosphorus. *Structure*. **12**, 927-935 (2004).
N Moiseeva, M Allaire. Crystals of Family 11 Xylanase II from Trichoderma Longibrachiatum that Diffract to Atomic Resolution. *Acta Cryst. D*. **60**, 1275-1277 (2004).

Beamline X6B

I Kim, E DiMasi, J Evans. Identification of Mineral Modulation Sequences within the Nacre-Associated Oyster Shell Protein, n16. *Cryst. Growth Des.*. **6** (6), 1113-1118 (2004).

Beamline X7A

G Bonilla, I Diaz, M Tsapatsis, H Jeong, Y Lee, D Vlachos. Zeolite (MFI) Crystal Morphology Control Using Organic Structure-Directing Agents. *Chem. Mater.*. **16**, 5697-5705 (2004).
M Colligan, P Forster, A Cheetham, Y Lee, T Vogt, J Hriljac. Synchrotron X-ray Powder Diffraction and Computational Investigation of Purely Siliceous Zeolite Y Under Pressure. *J. Am. Chem. Soc.*. **126**, 12015-12022 (2004).
M Hucker, K Chung, M Chand, T Vogt, J Tranquada, D Buttrey. Oxygen and Strontium Codoping of La2NiO4: Room Temperature Phase Diagrams. *Phys. Rev. B: Condens. Matter*. **70**, 064105 (2004).
I Jeong, T Darling, M Graf, T Proffen, R Heffner, Y Lee, T Vogt, J Jorgensen. Role of the Lattice in the gamma arrow alpha Phase Transition of Ce: A High-Pressure Neutron and X-ray Diffraction Study. *Phys. Rev. Lett.*. **92**, 105701-1 (2004).
P Juhas, I Grinberg, A Rappe, W Dmowski, T Egami, P Davies. Correlations between the Structure and Dielectric Properties of Pb(Sc2/3W1/3)O3-Pb(Ti/Zr)O3 Relaxors. *Phys. Rev. B*. **69** (21), 214101 (2004).
B Kennedy, L Li, Y Lee, T Vogt. Pressure Induced Valence and Structural Phase Transition in Ba2PrRu1-xIrxO6. *J. Phys.: Condens. Matter*. **16**, 3295-3301 (2004).
J Lai, K Shafi, A Ulman, K Loos, N Yang, M Cui, T Vogt, C Estournes, D Locke. Mixed Iron-Manganese Oxide Nanoparticles. *J. Phys. Chem. B*. **108**, 14876-14883 (2004).
Y Lee, C Martin, J Parise, J Hriljac, T Vogt. Formation and Manipulation of Confined Water Wires. *Nano Lett.*. **4**, 619-621 (2004).
Y Lee, J Hriljac, A Studer, T Vogt. Anisotropic Compression of Edingtonite and Thomsonite to 6 GPa at Room Temperature. *Phys. Chem. Miner.*. **31**, 22-27 (2004).
R Morris, A Burton, L Bull, S Zones. SSZ-51-A New Aluminophosphate Zeotype: Synthesis, Crystal Structure, NMR, and Dehydration Properties. *Chem. Mater.*. **16**, 2844 (2004).
H Xu, M Nyman, T Nenoff, A Navrotsky. Prototype Sandia Octahedral Molecular Sieve (SOMS) Na2Nb2O6.H2O: Synthesis, Structure and Thermodynamic Stability. *Chem. Mater.*. **16**, 2034-2040 (2004).
H Xu, A Navrotsky, M Nyman, T Nenoff. Crystal Chemistry and Energetics of Pharmacosiderite-Related Microporous Phases in the K2O-Cs2O-SiO2-TiO2-H2O System. *Microporous Mesoporous Mater.*. **72**, 209-218 (2004).
X Yang, M Camblor, Y Lee, H Liu, D Olson. Synthesis and Crystal Structure of As-Synthesized and Calcined Pure Silica Zeolite ITQ-12. *J. Am. Chem. Soc.*. **126**, 10403-10409 (2004).

Beamline X7B

S Antao, I Hassan, J Parise. Tugtupite: High-Temperature Structures Obtained from in situ Synchrotron Diffraction and Rietveld Refinements. *Am. Mineral.*. **89** (4), 492-497 (2004).
S Antao, I Hassan, J Parise. Chromate Aluminate Sodalite, Ca8[Al12O24](crO4)(2): Phase Transitions and High-Temperature Structural Evolution of the Cubic Phase. *Can. Mineral*. **42** (4), 1047-1056 (2004).
K Barkigia, M Renner, M Senge, J Fajer. Interplay of Axial Ligation, Hydrogen Bonding, Self-Assembly, and Conformational Landscapes in High-Spin Ni(II) Porphyrins. *J. Phys. Chem. B*. **108**, 2173-2180 (2004).
A Celestian, J Parise, C Goodell, A Tripathi, J Hanson. Time Resolved Diffraction Studies of Ion Exchange: K+ and Na+ Exchange into (Al, Ge) Gismondine (GIS) Na24Al24Ge24O96.40H2O and K8Al8Ge8O32&.8H2O. *Chem. Mater.*. **16** (11), 2244-2254 (2004).
A Christensen, T Jensen, N Scarlett, I Madsen, J Hanson. Hydrolysis of Pure Sodium Substituted Calcium Aluminates and Cement Clinker Compents Investigated by In Situ Synchrotron Powder Diffraction. *J. Am. Ceram. Soc.*. **87** (8), 1488-1493 (2004).
A Christensen, T Jensen, J Hanson. Formation of Ettringite, AFT and in Hydrothermal Hydration of Portland Cement Studied by in situ Synchrotron X-ray Powder Diffraction. *J. Solid State Chem.*. **177** (6), 1944-1951 (2004).

P Chupas, S Chaudhuri, J Hanson, X Qui, P Lee, S Shastri, S Billinge, C Grey. Probing Local and Long-Range Structure Simultaneously: An in situ Study of the High-Temperature Phase Transtion of Alpha-ALF3. *J. Am. Chem. Soc.*. **126**, 4756-4757 (2004).

M Fernandez-Garcia, A Martinez-Arias, J Hanson, J Rodriguez. Nanostructured Oxides in Chemistry: Characterization and Properties. *Chem. Rev.*. **104** (9), 4063-4104 (2004).

A Guiltieri, P Norby, C Grey, J Hanson. Sorbate Rearrangement and Cation Migration in HFC-134 Loaded NaY Zeolite; A Temperature Dependent Synchrotron Powder Diffraction Study. *Mater. Sci. Forum*. **443-4**, 295-298 (2004).

X Guo, P Devi, B Ravi, J Parise, S Sampath, J Hanson. Phase Evolution of Yttrium Aluminium Garnet (YAG) in a Citrate-nitrate Gel Combustion Process. *J Mater. Chem.*. **14** (8), 1288-1292 (2004).

I Hassan, S Antao, J Parise. Phase Transition and High-Temperature Structures Obtained from Synchrotron Radion and Rietveld Refinements. *Miner. Mag.*. **68** (4), 499-513 (2004).

I Hassan, S Antao, J Parise. HighTemperature Structures Obtained from Synchrotron Radition and Rietveld Refinements. *Am. Mineral.*. **89**, 359-364 (2004).

J Kim, J Hanson, A Frenkel, P Lee, J Rodriguez. Rduction of CuO with Hydrogen Studied by using Synchrotron-Based X-ray Diffraction. *J. Phys.: Condens. Matter*. **16**, s3459-s3472 (2004).

D Mahajan, C Marshall, N Castagnola, J Hanson. Sono Synthesis and Characterization of Nanophase Molybdenum-Based Materials for Catalytic Hydrodesulfurization. *Appl. Catal. A*. **258**, 83-91 (2004).

D Medvedev, A Tripathi, A Clearfield, A Celestian, J Parise, J Hanson. Crystallization of Sodium Titanium Silicate with Sitinakite Topology: Evolution from the Sodium Nonatitanate Phase. *Chem. Mater.*. **16** (19), 3659-3666 (2004).

O Rotthaus, L Le Roy, A Tomas, K Barkigia, I Artaud. Synthesis, Structure and Catalytic Activity of Low-Spin Dicyano iron(III) Complexes of N,N Œ-bis(quinolyl)malonamide Derivatives. *Inorg. Chim. Acta*. **357** (8), 2211 (2004).

Z Song, T Cai, J Grey, J Rodriguez, J Hrbek. Structure and Reactivity of Ru Nanoparticles Supported on Modified Graphite Surfaces: A Study of the Model Catalysts for Ammonia Synthesis. *J. Am. Chem. Soc.*. **126**, 8576-8584 (2004).

X Wang, J Hanson, A Frenkel, J Kim, J Rodriguez. Time-resolved Studies for the Mechanism of Reduction of Coper Oxides with Carbon Monoxide: Complex Behavior of Latice Oxygen and Formation of Suboxides. *J. Phys. Chem. B*. **108** (36), 13667-13673 (2004).

X Wang, J Hanson, G Liu, J Rodriguez, A Iglesias-Juez, M Fernandez-Garcia. the Behavior of Mixed-Metal Oxides: Physical and Chemical Properties of Bulk Ce(1-x)Tb(x)O(2) and Nanopatricles of Ce(1-x)Tb(x)O(y). *J. Chem. Phys.*. **121** (11), 5434-5444 (2004).

X Wang, J Hanson, J Szanyi, J Rodriguez. Interaction of H2O and NO2 with BaY Faujasite: Complex Contraction /Expansion Behavior of the Zeolite Unit Cell. *J. Phys. Chem. B*. **108**, 16613-16616 (2004).

Beamline X8C

K Backbro, A Roos, E Baker, V Arcus. Crystallization and Preliminary X-ray Analysis of a Conserved Hypothetical Protein PAE2754 from Pyrobaculum aerophilum and of a Double Leu arrow Met Mutant Engineered for MAD Phasing. *Acta Cryst. D*. **60**, 733-735 (2004).

M Bar, G Golan, M Nechama, G Zolotnitsky, Y Shoham, G Shoham. A New Crystal Form of XT6 Enables a Significant Improvement of its Diffraction Quality and Resolution. *Acta Cryst. D*. **60**, 545-549 (2004).

S Chan, B Segelke, T Lekin, H Krupka, U Cho, M Kim, M So, C Kim, C Naranjo, et al.. Crystal Structure of the Mycobacterium tuberculosis dUPTase: Insights into the Catalytic Mechanism. *J. Mol. Biol.*. **341**, 503-517 (2004).

J Cheeseman, A Tocilj, S Park, J Schrag, R Kazlauskas. Structure of an Aryl Esterase from Pseudomonas Fluorescens.. *Acta Cryst. D*. **60** (7), 1237-43 (2004).

C Chiu, A Watts, L Lairson, M Gilbert, D Lim, W Warkachuk, S Withers, N Strynadka. Structural Analysis of the Sialyltransferase CstII from Campylobacter jejuni in Complex with a Substrate Analog. *Nat. Struct. Mol. Biol.*. **11** (2), 163-170 (2004).

L Ejim, I Mirza, C Capone, I Nazi, S Jenkins, G Chee, A Berghuis, G Wright. New Phenolic Inhibitors of Yeast Homoserine Dehydrogenase. *BioOrg. Med. Chem.*. **12**, 3825-30 (2004).

T Fiedler, H Vincent, Y Zuo, O Gavrialov, A Malhotra. Purification and Crystallization of Escherichia coli Oligoribonulcease. *Acta Cryst. D*. **60**, 736-739 (2004).

D Fong, A Berghuis. Crystallization and Preliminary Crystallographic Analysis of 3'-Aminoglycoside Kinase Type IIIa Complexed with a Eukaryotic Protein Kinase Inhibitor, CKI-7. *Acta Cryst. D*. **60**, 1897-1899 (2004).

S Hauenstein, C Zhang, Y Hou, J Perona. Shape-Selective RNA Recognition by Cysteinyl-tRNA Synthetase. *Nat. Struct. Mol. Biol.*. **11**, 1134 (2004).

N Ishiyama, C Creuzenet, J Lam, A Berghuis. Crystal Structure of WbpP, a Genuine UDP-N-Acetylglucosamine 4-Epimerase from Pseudomonas Aeruginosa: Substrate Specificity in UDP-Hexose 4-Epimerases.. *J. Biol. Chem.*. **279**, 22635-42 (2004).

T Izard, J Sygusch. Induced Fit Movements and Metal Cofactor Selectivity of Class II Aldolases : Structure of Thermus Aquaticus Fructose-1,6-Bisphosphate Aldolase. *J. Biol. Chem.*. **279** (12), 11825–33 (2004).

L Jacquamet, J Ohana, J Joly, P Legrand, R Kahn, F Borel, M Pirocchi, P Charrault, J Ferrer. A New Highly Integrated Sample Environment for Protein Crystallography. *Acta Cryst. D*. **60**, 888-894 (2004).

N Koon, C Squire, E Baker. Crystal Structure of LeuA from Mycobacterium tuberculosis, a Key Enzyme in Leucine Biosynthesis. *Proc Natl Acad Sci USA*. **101** (22), 8295-8300 (2004).

S Ku, P Yip, K Cornell, M Riscoe, P Howell. Crystallization and Preliminary X-ray Analysis of 5'-methylthioribose Kinase from Bacillus subtilis and Arabidopis thaliana. *Acta Cryst. D*. **60**, 116-119 (2004).

B Liotard, J Sygusch. Purification, Crystallization and Preliminary X-ray Analysis of Native and Selenomethionine Class I Tagatose-1,6-biophosphate Aldolase from Streptococcus pyogenes. *Acta Cryst. D*. **60**, 528-530 (2004).

Y Lobsanov, P Romero, B Sleno, B Yu, P Yip, A Herscovics, P Howell. Structure of Kre2p/Mnt1p: A Yeast ƒÑ 1,2-mannosyltransferase Involved in Mannoprotein Biosynthesis. *J. Biol. Chem.*. **279** (17), 11672-82 (2004).

K Luk, M Simcox, A Schutt, K Rowan, T Thompson, Y Chen, U Kammlott, W DePinto, P Dunten, A Dermatakis. A New Series of Potent Oxindole Inhibitors of CDK2. *BioOrg. Med. Chem.*. **14** (4), 913-917 (2004).

V Lunin, Y Li, R Linhardt, H Miyazono, M Kyogashima, T Kaneko, A Bell, M Cygler. High-Resolution Crystal Structure of Arthrobacter Aurescens Chondroitin AC lyase: an Enzyme-Substrate Complex Defines the Catalytic Mechanism. *J. Mol. Biol.*. **337** (2), 367-386 (2004).

V Lunin, Y Li, J Schrag, P Iannuzzi, M Cygler, A Matte. Crystal Structures of Escherichia Coli ATP-Dependent Glucokinase and its Complex with Glucose. *J. Bacteriol.*. **186** (20), 6915-27 (2004).

V Lunin, C Munger, J Wagner, Z Ye, M Cygler, M Sacher. The Structure of the MAPK Scaffold, MP1, Bound to its Partner, p14. A Complex with a Critical Role in Endosomal Map Kinase Signaling. *J. Biol. Chem.*. **279** (22), 23422-23430 (2004).

G Michel, K Pojasek, Y Li, T Sulea, R Linhardt, R Raman, V Prabhakar, R Sasisekharan, M Cygler. The Structure of

Chondroitin B Lyase Complexed with Glycosaminoglycan Oligosaccharides Unravels a Calcium-Dependent Catalytic Machinery. *J. Biol. Chem.*. **279** (31), 32882-32896 (2004).
W Qiu, R Shi, M Lu, M Zhou, P Roy, J Lapointe, S Lin. Crystal Structure of Chloramphenicol Acetyltransferase B2 Encoded by the Multiresistance Transposon Tn2424.. *Proteins Str. Fun. Bioinformatics*. **57** (4), 858-61 (2004).
W Qiu, M Zhou, F Labrie, S Lin. Crystal Structures of the Multi-Specific 17b-Hydroxysteroid Dehydrogenase Type5: Critical Androgen Regulation in Human Peripheral Tissues. *Mol. Endocrinol.*. **7**, 1798-807 (2004).
E Rangarajan, Y Li, P Iannuzzi, A Tocilj, L Huang, A Matte, M Cygler. Crystal Structure of a Dodecameric FMN-Dependent UbiX-like Decarboxylase (Pad1) from Escherichia coli O157: H7.. *Protein Sci.*. **13** (11), 3006-16 (2004).
L Sampaleanu, P Codding, Y Lobsanov, M Tsai, G Smith, C Horvatin, P Howell. Structural Studies of Duck ƒÔ2 Crystallin Mutants Provide Insight into the Role of T161 and the 280i¦s Loop in Catalysis. *Biochem. J.*. **384** (Pt 2), 437-47 (2004).
J Schuermann, M Henzl, S Deutscher, J Tanner. Structure of an Anti-DNA Fab Complexed with a Non-DNA Ligand Provides Insights into Cross-Reactivity and Molecular Mimicry. *Proteins: Struc. Func. Genet.*. **57** (2), 269-278 (2004).
D Shaya, Y Li, M Cygler. Crystallization and Preliminary X-ray Analysis of Heparinase II from Pedobacter Heparinus. *Acta Cryst. D*. **60** (9), 1644-1646 (2004).
R Shi, S Lin. Cofactor Hydrogen Bonding onto the Protein Main Chain is Conserved in the Short-Chain Dehydrogenase/Reductase Family and Contributes to Nicotinamide Orientation. *J. Biol. Chem.*. **271** (16), 16778-85 (2004).
J Sivaraman, P Iannuzzi, M Cygler, A Matte. Crystal Structure of the RluD Pseudouridine Synthase Catalytic Module, an Enzyme that Modifies 23S rRNA and is Essential for Normal Cell Growth of Escherichia coli. *J. Mol. Biol.*. **335** (1), 87-101 (2004).
M Tsai, L Sampaleanu, C Greene, L Creagh, C Haynes, P Howell. A Duck delta1 Crystallin Double Loop Mutant Provides Insight into Residues Improtant for Argininosuccinate Lyase Activity. *Biochemistry*. **43**, 11672-11682 (2004).
L Vassilev, B Vu, B Graves, D Carvajal, F Podlaski, Z Filipovic, N Kong, U Kammlott, C Lukacs, et al.. In Vivo Activation of the p53 Pathway by Small-Molecule Antagonists of mdm2. *Science*. **303**, 844-848 (2004).
J Yeh, V Charrier, J Paulo, L Hou, E Darbon, A Claiborne, W Hol, J Deutscher. Structures of Enterococcal Glycerol Kinase in the Absense and Presence of Glycerol: Correlation of Conformation to Substrate Binding and a Mechanism of Activation of Phosphorylation. *Biochemistry*. **43**, 362-373 (2004).

Beamline X9A

L Bickford, E Mossessova, J Goldberg. A Structural View of the VOPII Vesicle Coat. *Curr. Opin. Struct. Biol.*. **14**, 147-153 (2004).
A Bobkov, A Muhlrad, A Shvetsov, S Benchaar, D Scoville, S Almo, E Reisler. Cofilin (ADF) Affects Lateral Contacts in F-Actin . *J. Mol. Biol.*. **337**, 93-104 (2004).
R Deo, E Schmidt, A Elhabazi, H Togashi, S Burley, S Strittmatter. Structural Bases for CRMP Function in Plexin-dependent Semaphorin3A Signaling. *EMBO J.*. **23**, 9-22 (2004).
A Gogos, J Gorman, L Shapiro. Structure of Escherichia coli YfdW, a type lll CoA Transferase. *Acta Cryst. D*. **60**, 507-511 (2004).
J Himanen, M Chumley, M Lackmann, C Li, W Barton, P Jeffrey, C Vearing, D Geleick, D Feldheim, et al.. Repelling Class Discrimination: EphrinA5 Binds to and Activates EphB2 Receptor Signaling. *Nat. Neurosci.*. **7**, 501-509 (2004).
P Iyer, S Lawrence, K Luther, K Rajashankar, H Yennawar, J Ferry, H Schindelin. Crystal Structure of Phosphotransacetylase from the Methanogenic Archaeon Methanosarcina thermophilia. *Structure*. **12**, 559-567 (2004).
L Jacquamet, J Ohana, J Joly, P Legrand, R Kahn, F Borel, M Pirocchi, P Charrault, J Ferrer. A New Highly Integrated Sample Environment for Protein Crystallography. *Acta Cryst. D*. **60**, 888-894 (2004).
D Jain, B Nickels, L Sun, A Hochschild, S Darst. Structure of a Ternary Transcription Activation Complex. *Mol. Cell*. **13**, 45-53 (2004).
S Masuda, K Murakami, S Wang, C Olson, J Donigian, F Leon, S Darst, E Campbell. Crystal structures of the ADP and ATP bound forms of the Bacillus anti-ssigma factor SpoIIAB in complex with the anti-anti-sigma SpoIIAA. *J. Mol. Biol.*. **340**, 941-956 (2004).
D Nesic, Y Hsu, E Stebbins. Assembly and Function of a Bacterial Genotoxin. *Nature*. **429**, 429-433 (2004).
L Olsen, B Huang, M Vetting, S Roderick. Structure of Serine Acetyltransferase in Complexes with CoA and Its Cysteine Feedback Inhibitor. *Biochemistry*. **43**, 6013-6019 (2004).
S Rudresh, S Ramakumar, U Ramagopal, Y Inai, S Goel, D Sahal, V Chauhan. De Novo Design and Characterization of a Helical Hairpin Eicosapeptide: Emergence of an Anion Receptor in the Linker Region. *Structure*. **12**, 389-396 (2004).
K Sekar, V Rajakannan, D Velmurugan, T Yamane, R Thirumurugan, M Dauter, Z Dauter. A Redetermnation of the Structure of the Triple Mutant (K53,56,120M) of Phosphiolipase A2 at 1.6 A Resolution using Sulfur-SAS at 1.54 A Wavelength. *Acta Cryst. D*. **60** (9), 1586-1590 (2004).
W Shi, L Ting, G Kicska, A Lewandowicz, P Tyler, G Evans, R Furneaux, K Kim, S Almo, V Schramm. Plasmodium Falciparum Purine Nucleoside Phosphorylase: Crystal Structures, Immucillin Inhibitors, and Dual Catalytic Function. *J. Biol. Chem.*. **279**, 18103 (2004).
F Smith, C Vearing, M Lackmann, H Treutlein, J Himanen, K Chen, A Saul, D Nikolov, A Boyd. Dissecting the EphA3/ephrin-A5 Interactions Using a Novel Functional Mutagenesis Screen . *J. Biol. Chem.*. **279**, 9522-9531 (2004).
J Thorson, W Barton, D Hoffmeister, C Albermann, D Nikolov. Structure-Based Enzyme Engineering and Its Impact on In Vito Glycorandomization. *ChemBioChem*. **5**, 16-25 (2004).
X Zhang, J Schwartz, X Guo, S Bhatia, E Cao, L Chen, Z Zhang, M Edidin, S Nathenson, S Almo. Structural and Functional Analysis of the Costimulatory Receptor Programmed Death-1. *Immunity*. **20**, 337-347 (2004).

Beamline X9B

S Banumathi, P Zwart, U Ramagopal, M Dauter, Z Dauter. Structural Effects of Radiation Damage and its Potential for Phasing. *Acta Cryst. D*. **60**, 1085-1093 (2004).
J Bayrer, Z Wan, B Li, M Weiss. Expression, Crystallization and Preliminary X-ray Characterization of the Drosophila Transcription Factor Doublesex. *Acta Cryst. D*. **60**, 1328-1330 (2004).
J Blaszczyk, Y Li, Y Wu, G Shi, X Ji, H Yan. Essential Roles of a Dynamic Loop in the Catalysis of 6-Hydroxymethyl-7,8-dihydropterin Pyrophosphokinase. *Biochemistry*. **43**, 1469-1477 (2004).
J Blaszczyk, G Shi, Y Li, H Yan, X Ji. Reaction Trajectory of Pyrophosphoryl Transfer Catalyzed by 6-hydroxymethyl-7,8-dihydropterin Pyrophosphokinase. *Structure*. **12**, 467-475 (2004).
J Blaszczyk, J Gan, J Tropea, D Court, D Waugh, X Ji. Noncatalytic Assembly of Ribonuclease III with Double-Stranded RNA. *Structure*. **12**, 457-466 (2004).

I Botos, E Melnikov, S Cherry, J Tropea, A Khalatova, F Rasulova, Z Dauter, M Maurizi, T Rotanova, et al.. The Catalytic Domain of E. coli Lon Protease has a Unique Fold and a Ser-Lys Dyad in the Active Site. *J. Biol. Chem.*. **279**, 8140-8148 (2004).

P Bryngelson, S Arobo, J Pinkham, D Cabelli, M Maroney. Expression, Reconstitution and Mutation of Recombinant Streptomyces Coelicolor NiSOD. *J. Am. Chem. Soc.*. **126**, 460-461 (2004).

M Bukowski, S Zhu, K Koehntop, W Brennessel, L Que. Characterization of an FeIII-OOH Species and its Decomposition Product in a Bleomycin Model System.. *J. Biol. Inorg. Chem.*. **9** (1), 39-48 (2004).

R Darbha, S Phogat, A Labrijin, Y Shu, Y Gu, M Andrykovitch, M Zhang, R Pantophlet, L Martin, et al.. Crystal Structure of the Broadly Cross-Reactive HIV-1-Neutralizing Fab X5 and Fine Mapping of its Epitope. *Biochemistry*. **43**, 1410-1417 (2004).

U Derewenda, A Oleksy, A Stevenson, J Korczynska, Z Dauter, A Somlyo, J Otlewski, A Somlyo, Z Derewenda. The Crystal Structure of RhoA in Complex with the DH/PH Fragment of PDZRhoGEF, an Activator of the Ca2+ Sensitization Pathway in Smooth Muscle. *Structure*. **12**, 1955-1965 (2004).

U Derewenda, A Mateja, Y Devedjiev, K Routzahn, A Evdokimov, Z Derewenda, D Waugh. The Structure of Yersinia Pestis V-Antigen, an Essential Virulence Factor and Mediator of Immunity Against Plague. *Structure*. **12**, 301-306 (2004).

T Dodatko, A Fedorov, M Grynberg, Y Patskovsky, D Rozwarski, L Jaroszewski, E Aronoff-Spencer, E Kondraskina, T Irving, et al.. Crystal Structure of the Actin Binding Domain of the Cyclase-Associated Protein. *Biochemistry*. **43**, 10628-10641 (2004).

L Esser, B Quinn, Y Li, M Zhanf, M Elberry, L Yu, C Yu, D Xia. Crystallographic Studies of Quinol Oxidation Site Inhibitors: A Modified Classification of Inhibitors for the Cytochrome bc1 Complex. *J. Mol. Biol.*. **341**, 281-302 (2004).

P Forrer, C Chang, D Ott, A Wlodawer, A Pluckthun. Kinetic Stability and Crystal Structure of the Viral Capsid Protein SHP. *J. Mol. Biol.*. **344**, 179-193 (2004).

A Guarne, S Ramon-Maiques, E Wolff, R Ghirlando, X Hu, J Miller, W Yang. Structure of the MutL C-Terminal Domain: A Model of Intact MutL and its Roles in Mismatch Repair. *EMBO J.*. **23**, 4134-4145 (2004).

T Gunter, L Miller, C Gavin, R Eliseev, J Salter, L Buntinas, A Alexandrov, S Hammond, K Gunter. Determination of the Oxidation States of Manganese in Brain, LIver, and Heart Mitochondria. *J. Neurochem.*. **88** (2), 266-280 (2004).

I Janda, Y Devedijiev, U Derewenda, Z Dauter, J Bielnicki, D Cooper, P Graf, A Joachimiak, U Jakob, Z Derewenda. The Crystal Structure of the Reduced, Zn2+ -Bound Form of the B. Subtilis Hsp33 Chaperone and Its Implications for the Activation Mechanism. *Structure*. **12**, 1901-1907 (2004).

I Janda, Y Devedijiev, U Derewenda, Z Dauter, J Bielnicki, D Cooper, P Graf, A Joachimiak, U Jakob, Z Derewenda. Effect of the Met344 His Mutatin on the Conformational Dynamis of Bovine bet-1,4-Galactosyltranserase: Crystal Structure of the Met344His Mutant in Complex with Chitobiose. *Biochemistry*. **43**, 12513-12522 (2004).

O Kleifeld, L Rulisek, O Bogin, A Frenkel, Z Havlas, Y Burstein, I Sagi. Higher Metal-Ligand Coordination in the Catalytic Site of Cobalt-Substituted Thermoanaerobacter brockii Alcohol Dehydrogenase Lowers the Barrier for Enzyme Catalysis. *Biochemistry*. **43**, 7151-7161 (2004).

L Masip, J Pan, S Haldar, J Penner-Hahn, M DeLisa, G Georgiou, J Bardwell, J Collet. An Engineered Pathway for the Formation of Protein Disulfide Bonds. *Science*. **303**, 1185-1189 (2004).

B Nolan, R Littlefield, T Pollard. Crystal Structures of Actin-Related Protein 2/3 Complex with Bound ATP and ADP. *Proc Natl Acad Sci USA*. **101**, 15627-15632 (2004).

A Petros, S Shaner, A Costello, D Tierney, B Gibney. Comparison of Cysteine and Penicillamine Ligands in a Co(II) Maquette. *Inorg. Chem.*. **43**, 4793-4795 (2004).

P Riggs-Gelasco, J Price, R Guyer, J Brehm, E Barr, J Bollinger, Jr., C Krebs. EXAFS Spectroscopic Evidence for an Fe=O Unit in the Fe(IV) Intermediate Observed During Oxygen Activation by Taurine:alpha-Ketoglutarate Dioxygenase. *J. Am. Chem. Soc.*. **126**, 8108-8109 (2004).

J Rohde, S Torelli, X shan, M Lim, E Kliner, J Kaizer, K Chen, W Nam, L Que, Jr.. Structural Insights into Nonheme Alkylperoxioiron(lll) and Oxoiron(IV) Intermediates by X-ray Absorption Spectroscopy. *J. Am. Chem. Soc.*. **126**, 16750-16761 (2004).

K Sasaki, J Wang, M Balasubramanian, J McBreen, F Uribe, R Adzic. Ultra-Low Platinum Content Fuel Cell Anode Electrocatalyst with a Long-Term Performance Stability. *Electrochim. Acta*. **49**, 3873-3877 (2004).

A Saxena, A Saul, D Garoboczi. Crystallization and Preliminary X-ray Analysis of the Plasmodium Vivax Sexual Stage 25 kDa Protein Pvs25, a Transmission-blocking Vaccine Candidate for Malaria. *Acta Cryst. D*. **60**, 706-708 (2004).

R Schwarzenbacher, F Stenner-Liewen, H Liewen, H Robinson, H Yuan, E Bossy-Wetzel, J Reed, R Liddington. Structure of the Chlamydia Protein CADD Reveals a Redox Enzyme that Odulates Host Cell Apoptosis. *J. Biol. Chem.*. **279** (28), 29320-4 (2004).

D Singh, K Saikrishnan, P Kumar, Z Dauter, K Sekar, A Surolia, M Vijayan. Purification, Crystalliztion and Preliminary X-ray Structure Analysis of the Banana Lectin from Musa Paradisiaca. *Acta Cryst. D*. **60**, 2104-2106 (2004).

V Singh, W Shi, G Evans, P Tyler, R Furnequx, S Almo, V Schramm. Picomolar Transition State Analogue Inhibitors of Human 5'-Methylthioadenosine Phosphorylase adn X-ray Structure with MT-Immucillin-A. *Biochemistry*. **43**, 9-18 (2004).

A Solomon, G Rosenblum, P Gonzales, J Leonard, S Mobashery, M Milla, I Sagi. Pronounced Diversity in Electronic and Chemical Properties Between the Catalytic Zinc Sites of TACE and MMP's Despite their High Structural Similarity. *J. Biol. Chem.*. **30**, 31646-31654 (2004).

S Taylor, A Ferguson, J Bergeron, D Thomas. The ER Protein Folding Sensor UDP-Glucose Glycoprotein-Glucosyltransferase Modifies Substrates Distant to Local Changes in Glycoprotein Conformation. *Nat. Struct. Mol. Biol.*. **11**, 128-134 (2004).

A Teplyakov, S Pullalarevu, G Obmolova, V Doseva, A Galkin, O Herzberg, M Dauter, Z Dauter, G Gilliland. Crystal Structure of the YffB Protein from Pseudomonas aeruginosa Suggests a Glutathione-Dependent Thiol Reductase Function. *BMC Struct. Bio.*. **4**, 5 (2004).

T Weng. X-Ray Absorption Spectroscopy Studies on Redox-Active Manganese. Ph.D. Thesis. University of Michigan, Ann Arbor. (2004).

A Wlodawer, M Li, A Gustchina, H Oyama, K Oda, B Beyer, J Clemente, B Dunn. Two Inhibitor Molecules Bound in the Active Site of Pseudomonas Sedolisin: A Model for the Bi-Product Complex Following Cleavage of a Peptide Substrate. *Biochem. Biophys. Res. Commun.*. **314**, 638-645 (2004).

K Zhang, R Liu, T Irving, D Auld. A Versatile Rapid-Mixing and Flow Device for X-ray Absorption Spectroscopy. *J. Synch. Rad.*. **11**, 204-208 (2004).

P Zwart, S Banumathi, M Dauter, Z Dauter. Radiation-Damage-Induced Phasing with Anomalous Scattering: Substructure Solution and Phasing. *Acta Cryst. D*. **60**, 1958-1963 (2004).

Beamline X10A

B Ash, R Siegel, L Schadler. Mechanical Behavior of Alumina/Poly(methyl methacrylate) Nanocomposites. *Macromolecules*. **37**, 1358-1369 (2004).

J DeRouchey, T Thurn-Albrecht, T Russell, R Kolb. Block Copolymer Domain Reorientation in an Electric Field: An In-Situ Small-Angle X-ray Scattering Study. *Macromolecules*. **37**, 2538-2543 (2004).

Y Li, Y Akpalu. Probing the Melting Behavior of a Homogeneous Ethylene/1-Hexene Copolymer by Small-Angle Light Scattering. *Macromolecules*. **37**, 7265-7277 (2004).

G Mazzanti, S Guthrie, E Sirota, A Marangoni, S Idziak. Novel Shear-Induced Phases in Cocoa Butter. *Cryst. Growth Des.*. **4**, 409-411 (2004).

G Mazzanti, S Guthrie, E Sirota, A Marangoni, S Idziak. Effect of Minor Components and Temperature Profiles on Polymorphism in Milk Fat. *Cryst. Growth Des.*. **4** (6), 1303-1309 (2004).

G Mazzanti. X-ray Diffraction Study on the Crystallization of Fats Under Shear. Ph.D. Thesis. University of Guelph, Guelph, ON. (2004).

E Minich, A Nowak, T Deming, D Pochan. Rod–Rod and Rod–Coil Self-Assembly and Phase Behavior of Polypeptide Diblock Copolymers. *Polymer*. **45** (6), 1951-1957 (2004).

B Ozbas, J Kretsinger, K Rajagopal, J Schneider, D Pochan. Salt-Triggered Peptide Folding and Consequent Self-Assembly into Hydrogels with Tunable Modulus. *Macromolecules*. **37**, 7331-7337 (2004).

Beamline X10B

G Mazzanti, S Guthrie, E Sirota, A Marangoni, S Idziak. Novel Shear-Induced Phases in Cocoa Butter. *Cryst. Growth Des.*. **4**, 409-411 (2004).

G Mazzanti. X-ray Diffraction Study on the Crystallization of Fats Under Shear. Ph.D. Thesis. University of Guelph, Guelph, ON. (2004).

Beamline X10C

D Chidambaram, G Halada, C Clayton. Spectroscopic Elucidation of the Repassivation of Active Sites on Aluminum by Chromate Conversion Coating. *Electrochem. Solid-State Lett.*. **7** (9), B31-B33 (2004).

T Prosek, D Thierry. A Model for the Release of Chromate from Organic Coatings. *Prog. Org. Coat.*. **49** (3), 209–217 (2004).

T Prosek, D Thierry. Corrosion Inhibition by Chromate at Defects of Organic Coatings. *Eurocorr 2004*, Vol 1, p. 1-9, sponsored by ISE. (2004).

Beamline X11A

Y Arai, D Sparks, J Davis. Effects of Dissolved Carbonate on Arsenate Adsorption and Surface Speciation at the Hematite-Water Interface. *Environ. Sci. Tech.*. **38**, 817-824 (2004).

J Bang, D Hesterberg. Dissolution of Trace Element Contaminants from Two Coastal Plain Soils as Affected by pH. *J. Environ. Qual.*. **33**, 891-901 (2004).

S Beauchemin, D Hesterberg, J Nadeau, J McGeer. Speciation of Hepatic Zn in Trout Exposed to Elevated Waterborne Zn Using X-ray Absorption Spectroscopy. *Environ. Sci. Tech.*. **38**, 1288-1295 (2004).

V Bhirud, J Goellner, A Argo, B Gates. Hexarhodium Clusters on Lanthana: Synthesis, Characterization, and Catalysis of Ethene Hydrogenation. *J. Phys. Chem. B*. **108**, 9752-9763 (2004).

M Daniel, D Pease, N Van Hung, J Budnick. Local Force Constants of Transition Metal Dopants in a Nickel Host: Comparison to Mossbauer Studies. *Phys. Rev. B*. **69**, 134414 - 134424 (2004).

I Drake, K Fujdala, S Baxamusa, A Bell, T Tilley. Effects of Percursor Compostion on the Local Structure of Cu Dispersed on Mesoporous Silica: A Detailed X-ray Absorption Spectroscopy Study. *J. Phys. Chem. B*. **108**, 18421-18484 (2004).

A Frenkel, D Pease, J Giniewicz, E Stern, D Brewe, M Daniel, J Budnick. Concentration-dependent Short-range Order in the Relaxor Ferroelectric (1-x)Pb(Sc,Ta))3-xPbTiO3. *Phys. Rev. B*. **70**, 014106 (2004).

K Fujdala, I Drake, A Bell, D Tilley. Atomic Level Control Over Surface Species via a Molecular Precursor Approach: Isolated Cu(I) Sites and Cu Nanoparticles Supported on Mesoporous Silica. *J. Am. Chem. Soc.*. **126**, 10864-10866 (2004).

M Grafe, M Nachtegaal, D Sparks. Formation of Metal-Arsenate Precipitates at the Geothite-Water Interface. *Environ. Sci. Tech.*. **38**, 6561-6570 (2004).

S Grenier, J Hill, D Gibbs, K Thomas, M v Zimmermann, C Nelson, V Kiryukhin, Y Tokura, Y Tomioka, et al.. Resonant X-ray Diffraction of the Magnetoresistant Perovskite Pr0.6Ca0.4MnO3. *Phys. Rev. B*. **69**, 134419 (2004).

J Guzman, B Gates. A Mononuclear Gold Complex Catalyst Supported on MgO: Spectroscopic Characterization During Ethylene Hydrogenation Catalysis. *J. Catal.*. **226**, 111-119 (2004).

J Guzman, S Kuba, J Fierro-Gonzales, B Gates. Formation of Gold Clusters on TiO2 from Adsorbed Au(CH3)2(C5H7O2): Characterization by X-ray Absorption Spectroscopy. *Catal. Lett.*. **95** (1-2), 77 (2004).

O Haas, R Struis, J McBreen. Synchrotron X-ray Absorption of LaCoO3 Perovskite. *J. Solid State Chem.*. **177** (3), 1000-1010 (2004).

H Khalil, D Mahajan, M Rafailovich, M Gelfer, K Pandya. Synthesis of Zerovalent Nanophase Metal Particles Stabilized with Poly(ethylene glycol). *Langmuir*. **20**, 6896-6903 (2004).

F Li, B Gates. Metal Carbonyl Cluster Synthesis in Nanocages: Spectroscopic Evidence of Intermediates in the Formation of Ir4(CO)12 in Zeolite NaY. *J. Phys. Chem. B*. **108**, 11259-11264 (2004).

D Mahajan, E Papish, K Pandya. Sonolysis Induced Decomposition of Metal Carbonyls: Kinetics and Product Characterization. *Ultrason. Sonochem.*. **11**, 385-392 (2004).

S Morrison, C Cahill, E Carpenter, S Calvin, R Swaminathan, M McHenry, V Harris. Magnetic and Structural Properties of Nickel Zinc Ferrite Nanoparticles Synthesized at Room Temperature. *J. Appl. Phys.*. **95** (11), 6392-6395 (2004).

S Mukerjee, X Yang, X Sun, S Lee, J McBreen, Y Ein-Eli. In Situ Synchrotron X-ray Studies on Copper-nickel 5 V Mn Oxide Spinel Cathodles for Li-Ion Batteries. *Electrochim. Acta*. **49**, 3373-3382 (2004).

M Naachtegaal, D Sparks. Effect of Iron Oxide Coatings on Zinc Sorption Mechanisms at the Clay-Mineral/Water Interface. *J. Colloid Interface Sci.*. **276**, 13-23 (2004).

M Teliska, W O'Grady, D Ramaker. Determination of H Adsorption Sites on Pt/C Electrodes in HC1O4 from Pt L23 X-ray Absorption Spectroscopy. *J. Phys. Chem. B*. **108**, 2333-2344 (2004).

P Trivedi, J Dyer, D Sparks, K Pandya. Mechanistic and Thermodynamic interpretation of Xinc Dorption onto Ferrihydrite. *J. Colloid Interface Sci.*. **270** (1), 77-85 (2004).

X Wang, S Sigmon, J Spivey, H Lamb. Support and Particle Size Effects on Direct NO Decomposition over Platinum. *Catal. Today*. **96**, 11-20 (2004).

J Zhang, Y Mo, M Vukmirovic, R Klie, K Sasaki, R Adzic. Platinum Monolayer Electrocatalysts for O2 Reduction: Pt Monolayer on Pd(111) and on Carbon-Supported Pd Nanoparticles. *J. Phys. Chem. B*. **108**, 10955-10964 (2004).

Y Zhang, M Toebes, A van der Eerden, W O'Grady, K de Jong, D Koningsberger. Metal Particle Size and Structure

of the Metal-Support Interface of Carbon-Supported Platinum Catalysts as Determined with EXAFS Spectroscopy. *J. Phys. Chem. B*. **108**, 18509-18519 (2004).

Beamline X11B

F Alamgir, J VanSluytman, D Carter, J Whitacre, C Kao, S Greenbaum, M denBoer. X-ray Absorption Spectroscopy Investigation of the Sub-Nanoscale Strain in Thin-Film Lithium Ion Battery Cathodes. *MRS Spring 2004*, Vol 822, p. S2.3, sponsored by MRS. (2004).

Beamline X12A

W Caliebe, S Cheung, A Lenhard, D Siddons. Fixed Exit Monochromator with Fixed Rotation Axis. *Synchrotron Radiation Instrumentation: Eighth International Conference on Synchrotron Radiation Instrumentation*, Vol 705, p. 643-646, sponsored by AIP Conference Proceedings. (2004).

Beamline X12B

B Canyuk, F Medrano, M Wenck, P Focia, A Eakin, S Craig, III. Interactions of the Dimer Interface Influence the Relative Efficiencies for Purine Nucleotide Synthesis and Pyrophosphorolysis in a Phosphoribosyltransferase. *J. Mol. Biol.*. **335**, 905 (2004).

A Delprato, E Merithew, D Lambright. Structure, Exchange Determinants, and Family-Wide Rab Specificity of the Tandem Helical Bundle and Vps9 Domains of Rabex-5. *Cell*. **118**, 607-617 (2004).

T Fiedler, H Vincent, Y Zuo, O Gavrialov, A Malhotra. Purification and Crystallization of Escherichia coli Oligoribonulcease. *Acta Cryst. D*. **60**, 736-739 (2004).

B Gibbons, T Hurley. Structure of Three Class I Human Alcohol Dehydrogenases Complexed with Isoenzyme Specific Formamide Inhibitors. *Biochemistry*. **43**, 12555-12562 (2004).

G Gopalan, Z He, Y Balmer, P Romano, R Gupta, A Heroux, B Buchanan, K Swaminathan, S Iuan. Structural analysis uncovers a role for redox in regulating FKBP13, an immunophilin of the chloroplast thylakoid lumen . *Proc Natl Acad Sci USA*. **101** (38), 13945-13950 (2004).

S Johnson, L Beese. Structures of Mismatch Replication Errors Observed in a DNA Polymerase. *Cell*. **116**, 803-816 (2004).

S Karthikeyan, Q Zhou, Z Zhao, C Kao, Z Tao, H Robinson, H Liu, H Zhang. Structural Analysis of Pseudomonas 1-Aminocyclopropane-1-carboxylate Deaminase Complexes: Insight into the Mechansim of a Unique Pyridoxal-5'-phosphate Dependent Cyclopropane Ring-Opening Reaction. *Biochemistry*. **43**, 13328-13339 (2004).

C Lawson, B Benoff, T Berger, H Berman, J Carey. E. Coli trp Repressor Forms a Domain-Swapped Array in Aqueous Alcohol. *Structure*. **12**, 1099-1108 (2004).

J Mao, Y Gao, S Odeh, H Robinson, A Montalvetti, R Docampo, E Oldfield. Crystallization and Preliminary X-ray Diffraction Study of the farnesyl diphosphate Synthase from Trypanosoma brucei. *Acta Cryst. D*. **60**, 1863-1866 (2004).

M Morais, G Zhang, W Zhang, D Olsen, D Dunaway-Mariano, K Allen. X-ray Crystallographic and Site-Directed Mutagenesis Analysis of the Mechanism of Schiff-Base Formation in Phosphonacetaldehyde Hydrolase Catalysis. *J. Biol. Chem.*. **279**, 9353 (2004).

T Reid, S Long, L Beese. Crystallographic Analysis Reveals that Anticancer Clinical Candidate L-778,123 Inhibits Protein Farnesyltransferase and Geranylgeranyltransferase-I by Different Binding Modes. *Biochemistry*. **43**, 9000-9008 (2004).

V Reiland, R Gilboa, A Spungin-Bialik, D Schomburg, Y Shoham, S Blumberg, G Shoham. Binding of Inhibitory Aromatic Amino Acids to Streptomyces griseus Aminopeptidase. *Acta Cryst. D*. **60**, 1738-1746 (2004).

S Saxena, P Yuan, S Dhar, T Senga, D Takeda, H Robinson, S Kornbluth, K Swaminathan, A Dutta. A Dimerized Coiled-Coil Domain and an Adjoining Part of Geminin Interact with Two Sites on Cdt1 for Replication Inhibition. *Mol. Cell*. **15**, 245-258 (2004).

R Schwarzenbacher, F Stenner-Liewen, H Liewen, H Robinson, H Yuan, E Bossy-Wetzel, J Reed, R Liddington. Structure of the Chlamydia Protein CADD Reveals a Redox Enzyme that Odulates Host Cell Apoptosis. *J. Biol. Chem.*. **279** (28), 29320-4 (2004).

J Truglio, D Croteau, M Skorvaga, M DellaVecchia, K Theis, B Mandavilli, B Van Houten, C Kisker. Interactions Between UvrA and UvrB - The Critical Role of UvrB's Domain 2 in Nucleotide Excision Repair. *EMBO J.*. **23**, 2498-2509 (2004).

E Vogan, C Bellamacina, X He, H Liu, D Ringe, G Petsko. Crystal Structure at 1.8 Angstrom Resolution of CDP-D-Glucose 4,6-Dehydratase from Yersinia pseudotuberculosis. *Biochemistry*. **43**, 3057-3067 (2004).

Z Zavala-Ruiz, I Strug, B Walker, P Norris, L Stern. A Hairpin Turn in a Class II MHC-Bound Peptide Orients Residues Outside the Binding Groove for T Cell Recognition. *Proc Natl Acad Sci USA*. **101** (36), 13279-13284 (2004).

G Zhang, M Morais, J Dai, w Zhang, D Duanway-Mariano, K Allen. Investigation of Metal Ion Binding in Phosphonoacetaldehyde Hydrolase Identifies Sequence Markers for Metal-Activated Enzymes of the HAD Enzyme Superfamily. *Biochemistry*. **43**, 4990-4997 (2004).

K Zhao, R Harshaw, X Chai, R Marmorstein. Structural Basis for Nicotinamide Cleavage and ADP-ribose Transfer by NAD+ -Dependent Sir2 Histone/Protein Deacetylases. *Proc Natl Acad Sci USA*. **101** (23), 8563-8568 (2004).

Beamline X12C

T Adams, M Hockin, K Mann, S Everse. The Crystal Structure of Activated Protein C-inactivated Bovine Factor Va: Implications for Cofactor Function. *Proc Natl Acad Sci USA*. **101** (24), 8918-8923 (2004).

R Agarwal, S Eswaramoorthy, D Kumaran, T Binz, S Swaminathan. Structural Analysis of Botulinum Neurotoxin Type E Catalytic Domain and Its Mutant Glu212 arrowGln Reveals the Pivotal Role of the Glu212 Carboxylate in the Catalytic Pathway. *Biochemistry*. **43**, 6637-6644 (2004).

N Alam, K Stieglitz, M Caban, S Gourinath, H Tsuruta, E Kantrowitz. 240S Loop Interactions Stabilize the T State of Escherichia Coli Aspartate Transcarbamoylase. *J. Biol. Chem.*. **279**, 23302 (2004).

M Ali, E Peisach, K Allen, B Imperiali. X-ray Structure Analysis of a Designed Oligomeric Miniprotein Reveals a Discrete Quaternary Architecture. *Proc Natl Acad Sci USA*. **101** (33), 12183-12188 (2004).

R Almog, F Maley, G Maley, R MacColl, P Van Roey. Three-Dimensional Structure of the R115E Mutant of T4-Bacteriophage 2'-Deoxycytidylate Deaminase. *Biochemistry*. **43**, 13715-13723 (2004).

J Anson James, A Aggarwal, R Linden, C Escalante. Structure of Adeno-Associated Virus Type 2 Rep40-ADP Complex: Insight into Nucleotide Recognition and Catalysis by Superfamily 3 Helicases. *Proc Natl Acad Sci USA*. **101** (34), 12455-12460 (2004).

B Appleton, A Loregian, D Filman, D Coen, J Hogle. The Cytomegalovirus DNA Polymerase Subunit UL44 Forms a C Clamp-Shaped Dimer. *Mol. Cell*. **15**, 233 (2004).

P Arjunan, K Chandrasekhar, M Sax, A Brunskill, N Nemeria, F Jordan, W Furey. Structural Determinants of Enzyme Binding Affinity: The E1 Component of Pyruvate Dehydrogenase from Escherichia Coli in Complex with the Inhibitor Thiamin Thizolone Diphosphate. *Biochemistry*. **43**, 2405 (2004).

K Barkigia, M Renner, M Senge, J Fajer. Interplay of Axial Ligation, Hydrogen Bonding, Self-Assembly, and Conformational Landscapes in High-Spin Ni(II) Porphyrins. *J. Phys. Chem. B*. **108**, 2173-2180 (2004).

J Calabrese, D Jordan, A Boodhoo, S Sariaslani, T Vannelli. Crystal Structure of Phenylalanine Ammonia Lyase: Multiple Helix Dipoles Implicated in Catalysis. *Biochemistry*. **43**, 11403-11416 (2004).

A Coros, L Swenson, W Wolodko, M Fraser. Structure of the CoA Transferase from Pig Heart to 1.7 Angstrom Resolution. *Acta Cryst. D*. **60**, 1717-1725 (2004).

K Das, T Acton, Y Chiang, L Shih, E Arnold, G Montelione. Crystal Structure of RlmA1: Implications for Understanding the 23S rRNA G745 / G748-methylation at the Macrolide Antibiotic-Binding Site. *Proc Natl Acad Sci USA*. **101**, 4041-4046 (2004).

M Del Campo, J Ofengand, A Malhotra. Crystal Structure of the Catalytic Domain of RluD, the Only Pseudouridine Synthases Required for Normal Growth of Escherichia coli. *RNA*. **10**, 231-239 (2004).

S Dhe-Paganon, E Werner, M Nishi, L Hansen, Y Chi, S Shoelson. A Phenylalanine Zipper Mediates APS Dimerization. *Nat. Struct. Mol. Biol.*. **11** (10), 968 (2004).

G Dong, G Chakshusmathi, S Wolin, K Reinisch. Structure of the LA Motif: A Winged Helix Domain Mediates RNA Binding Via a Conserved Aromatic Patch. *EMBO J.*. **23**, 1000 (2004).

A Dong, L Zhou, X Zhang, S Stickel, R Roberts, X Cheng. Structure of the Q237W Mutant of HHAI DNA Methyltransferase: An Insight Into Protein-Protein Interactions. *J. Biol. Chem.*. **385**, 373 (2004).

K Duda, Y Chi, S Shoelson. Structural Basis for HNF-4alpha Activation by Ligand and Coactivator Binding. *J. Biol. Chem.*. **279** (22), 23311-23316 (2004).

D Edgell, V Derbyshire, P Van Roey, S LaBonne, M Stanger, Z Li, T Boyd, D Shub, M Belfort. Intron-Encoded Homing Endonuclease I-TevI also Functions as a Transcriptional Autorepressor. *Nat. Struct. Mol. Biol.*. **11** (10), 936-944 (2004).

S Eswaramoorthy, D Kumaran, J Keller, S Swaminathan. Role of Metals in the Biological Activity of Clostridium botulinum Neurotoxins. *Biochemistry*. **43**, 2209-2216 (2004).

J Evans, D Huddler, M Hilgers, G Roamchuk, R Matthews, M Ludwig. Structures of the N-Terminal Modules Imply Large domain Motions During Catalysis by Methionine Synthase. *Proc Natl Acad Sci USA*. **101**, 3729-3736 (2004).

F Forouhar, I Lee, J Benach, K Kulkarni, R Xiao, T Acton, G Montelione, L Tong. A Novel Nad-Binding Protein Revealed by the Crystal Structure of 2,3-Diketo-L-Gulonate Reductase (YIAK). *J. Biol. Chem.*. **279**, 13148-13155 (2004).

J Goodman, S Wang, S Alam, F Ruzicka, P Frey, J Wedekind. Orithine Cyclodeaminase: Structure, Mechanism of Action, and Implications for the u-Crystallin Family. *Biochemistry*. **43** (44), 13883-13891 (2004).

A Gulick, X Lu, D Dunaway-Mariano. Crystal Structure of 4-Chlorobenzoate:CoA Ligase/Synthetase in the unliganded and aryl substrate-bound states. *Biochemistry*. **43** (27), 8670-8679 (2004).

M Hogg, S Wallace, S Doublie. Crystallographic Snapshots of a Replicative DNA Polymerase Encountering on Abasic Site. *EMBO J.*. **23**, 1483-1493 (2004).

Q Huai, H Wang, W Zhang, R Colman, H Robinson, H Ke. Crystal Structure of Phosphodiesterase 9 Shows Orientation Variation of Inhibitor 3-isobutyl-1-methylxanthine Binding. *Proc Natl Acad Sci USA*. **101** (26), 9624-9629 (2004).

J Jiang, R Sweet. Protein Data Bank Depositions from Synchrotron Sources. *J. Synch. Rad.*. **11**, 319-327 (2004).

S Karthikeyan, Z Zhao, C Kao, Q Zhou, Z Tao, H Zhang, H Liu. Structural Analysis of 1-Aminocyclopropane-1-Carboxylate Deaminase: Observation of an Aminyl Intermediate and Identification of TYR 294 as the Activie-Site Nucleophile. *Angew. Chem. Int. Ed.*. **43**, 3425 (2004).

Y Kaya, M Del Campo, J Ofengand, A Malhotra. Crystal Structure of TruD, a Novel Pseudouridine Synthase with a new Protein Fold. *J. Biol. Chem.*. **279**, 18107-18110 (2004).

K Kumaraswami, M Howe, H Park. Crystal Structure of the Mor Protein of Bacteriophage Mu, A Member of the Mor/C Family of Transcription Activators. *J. Biol. Chem.*. **279**, 16581 (2004).

J Kung, B Li, T Uchida, Y Wang, D Neuville, R Liebermann. In Situ Measurements of Sound Velocities and Densities Across the Orthopyroxene-High-Pressure Clinopyroxene Transition in MgSiO3 at High Pressure. *Phys. Earth Planet. Interiors*. **147**, 27-44 (2004).

G Martin, A Moeglich, W Keller, S Doublie. Biochemical and Structural Insights into Substrate Binding and Catalytic Mechanism of Mammalian Poly(A) Polymerase. *J. Mol. Biol.*. **341**, 911-925 (2004).

K Min, S Ha, P Hasegawa, R Bressan, D Jun, K Kim. Crystal Structure of Osmotin, A Plant Antifungal Protein. *Proteins: Struc. Func. Genet.*. **54**, 170 (2004).

T Moore, Y Zhang, M Fenley, H Li. Molecular Basis of Box C/D RNA-Protein Interactions: Cocrystal Structure of Archaela L7Ae and a Box C/D RNA. *Structure*. **12**, 807-818 (2004).

S Ni, H Robinson, G Marsing, D Bussiere, M Kennedy. Structure of 2C-methyl-D-erythritol-2,4-cyclodiphosphate Synthase from Shewanella Oneidensis at 1.6 Angstrom: Identification of Farnesyl Pyrophosphate Trapped in a Hydrophobic Cavity. *Acta Cryst. D*. **60**, 1949-1957 (2004).

C O'Neal, E Amaya, M Jobling, R Holmes, W Hol. Crystal Structures of an Intrinsically Active Cholera Toxin Mutant Yield Insight into the Toxin Activation Mechanism. *Biochemistry*. **43**, 3772-3782 (2004).

R O'Neil, R Lilien, B Stroud, A Anderson. Phylogenetic Classification of Protozoa Based on the Structure of the Linker Domain in the Bifunctional Enzyme, Dihydorfolate Reductase-Thymidylate Snythase. *J. Biol. Chem.*. **278**, 52980 (2004).

J Pascal, P O'Brien, A Tomkinson, T Ellenberger. Human DNA Ligase I Completely Encircles and Partially Unwinds Nicked DNA. *Nature*. **432**, 473 (2004).

E Peisach, J Selengut, D Dunaway-Mariano, K Allen. X-ray Crystal Structure of the Hypothetical Phosphotyrosine Phosphatase MDP-1 of the Haloacid Dehalogenase Superfamily. *Biochemistry*. **43**, 12770-12779 (2004).

N Silvaggi, K Kaur, S Adediran, R Pratt, J Kelly. Toward Better Antibiotics: Crystallographic Studies of a Novel Class of DD-Peptidase . *Biochemistry*. **43**, 7046-7053 (2004).

A Teplitsky, A Mechaly, V Stojanoff, G Sainz, G Golan, H Feinberg, R Gilboa, V Reiland, G Zolotnitsky, et al.. Structure Determination of the Extracellular Xylanase from Geobacillus stearothermophilus by Selenomethionyl MAD Phasing. *Acta Cryst. D*. **60**, 836-848 (2004).

B Turk, T Wong, R Schwarzenbacher, E Jarrell, S Leppla, R Collier, R Liddington, L Cantley. The Structural Basis for Substrate and Inhibitor Selectivity of the Anthrax Lethal Factor. *Nat. Struct. Biol.*. **11** (1), 60 (2004).

D Whittington, J Grubb, A Waheed, G Shah, W Sly, D Christianson. Expression, Assay, and Structure of the Extracellular Domain of Murine Carbonic Anhydrase XIV. *J. Biol. Chem.*. **279** (8), 7223-7228 (2004).

E Woo, Y Kim, M Kim, W Han, S Shin, H Robinson, S Park, B Oh. Structural Mechanism for Inactivation and Activation of CAD/DFF40 in the Apoptotic Pathway. *Mol. Cell*. **14**, 531-539 (2004).

Y Xiong, T Steitz. Mechanism of Transfer RNA Maturation by CCA-Adding Enzyme Without using an Oligonucleotide Template. *Nature*. **430**, 640 (2004).

Q Xu, R Kucera, R Roberts, H Guo. An Aysmmetric Complex of Restriction Endonuclease Mspl on Its Palindromic DNA Recognition Site. *Structure*. **12**, 1741-1747 (2004).

Y Zhao, Z Li, S Drozd, Y Guo, R Stack, C Hauer, H Li. Crystallization and Preliminary Crystallographic Analysis of Mycoplasma Arthritidis-derived Mitogen Complexed with Peptide/MHC Class II Antigen. *Acta Cryst. D*. **60**, 353-356 (2004).
Y Zhao, Z Li, S Drozd, Y Guo, W Mourad, H Li. Crystal Structure of Mycoplasma arthritidis Mitogen Complexed with HLA-DR1 Reveals a Novel Superantigen Fold and a Dimerized Superantigen-MHC Complex. *Structure*. **12**, 277-288 (2004).

Beamline X13B

J Ablett, L Berman, C Kao, G Rakowsky, D Lynch. Small-Gap Insertion-Device Development at the National Synchrotron Light Source - Performance of the New X13 Mini-Gap Undulator. *J. Synch. Rad.*. **11**, 129-131 (2004).
J Ablett, K Evans-Lutterodt, A Stein. Hard X-Ray Fresnel Prisms: Properties and Applications. *Design and Microfabrication of Novel X-Ray Optics II* , Vol 5539, p. 88-94, sponsored by The International Society for Optical Engineering. (2004).
J Ablett, L Berman, G Rakowsky, D Lynch. The NSLS X13 Mini-Gap Undulator: Design and Performance. *Synchrotron Radiation and Instrumentation: Eighth International Conference*, Vol 705, p. 271-273, sponsored by American Institute of Physics. (2004).
K Evans-Lutterodt, J Ablett, A Stein, D Tennant, F Klemens, A Taylor. Energy Dependent Focusing Properties of a Kinoform Fresnel Lens. *Design and Microfabrication of Novel X-Ray Optics II* , Vol 5539, p. 73-79, sponsored by The International Society for Optical Engineering. (2004).
A Stein, J Ablett, K Evans-Lutterodt, A Taylor, F Klemens, A Kornblit, S Polvino. Imaging with Single-Dimension Kinoform Lenses. *Design and Microfabrication of Novel X-Ray Optics II* , Vol 5539, p. 80-87, sponsored by The International Society for Optical Engineering. (2004).

Beamline X15A

M Kelly, E Schultke, C Beavis, D Fourney, R Griebel, Z Zhong, D Chapman. Synchrotron-supported Imaging of the Rat Spinal Column and Spinal Cord: a Feasibility Study in an Animal Model. *Canadian Congress of Neurological Sciences*, Vol 31, p. 11, sponsored by Canadian Congress of Neurological Sciences. (2004).
M Kiss, D Sayers, Z Zhong, C Parham, E Pisano. Improved Image Contrast of Calcifications in Breast Tissue Specimens using Diffraction Enhanced Imaging. *Phys. Med. Biol.*. **49** (15), 3427 - 3439 (2004).
J Li, Z Zhong, R Litdke, K Kuettner, C Peterfy, E Aleyeva, C Muehleman. Radiography of Soft Tissue of the Foot and Ankle with Diffraction Enhanced Imaging. *J. Am. Podiat. Med. Assn.*. **94**, 315-322 (2004).
J Li, Z Zhong, K Kuettner, M Aurich, J Williams, M Wimmer, C Muehleman. Detection of cartilage defects with diffraction enhanced x-ray imaging: accuracy and reliability. *Proc. 50th Ann. Mtg. Orthopaedic Res. Soc., Vol.29*, Vol 29, p. paper #1007, sponsored by Orthopaedic Research Society. (2004).
J Libera, R Gurney, S Nguyen, J Hupp, C Liu, R Conley, M Bedzyk. X-ray Nanoscale Profiling of Layer-by-Layer Assembled. *Langmuir*. **20**, 8022-8029 (2004).
P Lyman, D Walko, D Marasco, H Hutchason, M Keeffe, P Montano, M Bedzyk. Adsorption Sites of Te on Si(001). *Surf. Sci.*. **561**, 248-260 (2004).
C Muehleman, J Mollenhauer, M Aurich, K Kuettner, Z Zhong, A Cole, D Chapman. Diffraction Enhanced X-ray Imaging of Articular Cartilage. *The Many Faces of Osteoarthritis*, p. 351-354, Springer-Verlag, , Heidelberg . (2004).
C Muehleman, J Li, M Wernick, J Brankov, K Kuettner, Z Zhong. Yes, You Can See Cartilage with X-rays; Diffraction Enhanced X-ray Imaging for Soft and Hard Tissues. *J. Musculoskelet. Neuron. Int.*. **4**, 369-370 (2004).
C Muehleman, J Brankov, J Li, Z Zhong, K Kuettner, M Wernick. Multiple-Image Radiography for Soft Tissue. *Proc. 50 th Ann. Mtg. Orthopaedic Res. Soc.,*, Vol 29, p. #0104, sponsored by Orthopaedic Res. Soc.,. (2004).
C Muehleman, D Sumner, Z Zhong. Refraction Effects of Diffraction-Enhanced Radiographic Imaging. *J. Am. Podiat. Med. Assn.*. **94** (5), 453-455 (2004).
D Siddons, Z Zhong. A Flash Spectrograph for XANES Measurements at SPPS/LCLS. *Synchrotron Radiation Instrumentation: Eighth International Conference on Synchrotron Radiation Instrumentation*, Vol 705, p. 941, sponsored by AIP Conference Proceedings. (2004).
G Xu, Z Zhong, H Hiraka, G Shirane. Three Dimensional Mapping of Diffuse Scattering in PZN-xPT. *Phys. Rev. B: Condens. Matter*. **70**, 174109 (2004).
Z Zhang, P Fenter, L Cheng, N Sturchio, M Bedzyk, M Predota, A Bandura, J Kubicki, S Lvov, et al.. Ion Adsorption at the Rutile - Water Interface: Linking Molecular and Macroscopic Properties. *Langmuir*. **20**, 4954-4969 (2004).
Z Zhang, P Fenter, L Cheng, N Sturchio, M Bedzyk, M Machesky, D Wesolowski. Model-Independent X-ray Imaging of Adsorbed Cations at the Crystal-Water Interface. *Surf. Sci. Lett.*. **554**, 95-100 (2004).

Beamline X16A

C Kim, A Escuadro, M Bedzyk, L Liu, P Stair. X-ray Scattering Study of the Stoichiometric Recovery of the Alpha-Fe2O3(0001) Surface. *Surf. Sci.*. **572**, 239-246 (2004).
Y Zhong, C Bailat, R Averback, S Ghose, I Robinson. Damage Accumulation in Si During High-Dose Self-Ion Implantation. *J. Appl. Phys.*. **96** (3), 1328 (2004).

Beamline X16C

R Corriu, A Mehdi, C Reye, C Thieuleux, A Frenkel, A Gibaud. Unusual Eu(III) Coordination Mode Inside the Pore Channels of Ordered SBA-15 Mesoporous Silica Containing Chelating Groups. *New J. Chem.*. **1**, 156 (2004).
A Jokic, M Wang, C Liu, A Frenkel, P Huang. The polyphenol and Maillard Reactions as a Unified Pathway for Humic Substance Formation in Nature. *Org. Geoch.*. **35**, 747 (2004).
J Kim, J Hanson, A Frenkel, P Lee, J Rodriguez. Rduction of CuO with Hydrogen Studied by using Synchrotron-Based X-ray Diffraction. *J. Phys.: Condens. Matter*. **16**, s3459-s3472 (2004).
O Kleifeld, L Rulisek, O Bogin, A Frenkel, Z Havlas, Y Burstein, I Sagi. Higher Metal-Ligand Coordination in the Catalytic Site of Cobalt-Substituted Thermoanaerobacter brockii Alcohol Dehydrogenase Lowers the Barrier for Enzyme Catalysis. *Biochemistry*. **43**, 7151-7161 (2004).
D Schwarz, A Frenkel, R Nuzzo, T Rauchfuss, A Vairavamurthy. Electrosynthesis of ReS4. XAS Analysis of ReS2, Re2S7, and ReS4. *Chem. Mater.*. **16**, 151-158 (2004).
X Wang, J Hanson, A Frenkel, J Kim, J Rodriguez. Time-resolved Studies for the Mechanism of Reduction of Coper Oxides with Carbon Monoxide: Complex Behavior of Latice Oxygen and Formation of Suboxides. *J. Phys. Chem. B*. **108** (36), 13667-13673 (2004).

Beamline X17B1

T Chen, A Neville, M Yuan. Influence of Mg2+ on the Kinetics and Crystal Morphology of CaCO3 Scale Formation on the Metal Surface and in Bulk Solution. *Corrosion/04*, Vol NACE, p. #04393, sponsored by NACE. (2004).

T Chen, A Neville, M Yuan. Influence of Mg2+ on Initial Stages of CaCO3 Scale Formed on Metal Surface. *Chem. Res. Chinese U.*. **20** (4), 381-385 (2004).
T Chen, A Neville, M Yuan. Assessing the Effect of Mg2+ on CaCO3 Scale Formation Bulk Precipitation and Surface Deposition. *J. Cryst. Growth*. **273** (1-2), 1-7 (2004).
C Cui. High Pressure Effects on Electron Transport and Structure of Colossal . Ph.D. Thesis. New Jersey Institute of Technology, Newark. (2004).
C Cui, T Tyson. Pressure Effects on Charge, Spin, and Metal-Insulator Transitions in the Narrow Bandwidth Manganite Pr1-xCaxMnO3. *Phys. Rev. B: Condens. Matter*. **70**, 094409 (2004).
C Cui, T Tyson. Correlations Between Pressure and Bandwidth Effects in Metal-Insulator Transitions in Manganites. *Appl. Phys. Lett.*. **84**, 942 (2004).
K Darling, G Gwanmesia, J Kung, B Li, R Liebermann. Ultrasonic Measurements of the Sound Velocities in Polycrystalline San Carlos Olivine in Multi-Anvil, High-Pressure Apparatus. *Phys. Earth Planet. Interiors*. **143**, 19-31 (2004).
J Hu, Z Zhong, E Haas, S Hulbert, R Hubbard. Degradation of Magnet Epoxy at NSLS X-Ray Ring. *Mech. Engng. Design of Synch. Radiation Equipment & Inst. (MEDSI)*, Vol 2004, p. 9, sponsored by ESRF. (2004).
G Xu, H Hiraka, K Ohwada, G Shirane. Dual Structures in PZN-xPT Ferroelectric Relaxors. *Appl. Phys. Lett.*. **84**, 3975 (2004).
G Xu, Z Zhong, Y Bing, Z Ye, C Stock, G Shirane. An Anomalous Phase in the Relaxor Ferroelectric PZN. *Phys. Rev. B*. **70**, 064107 (2004).
G Xu, Z Zhong, H Hiraka, G Shirane. Three Dimensional Mapping of Diffuse Scattering in PZN-xPT. *Phys. Rev. B: Condens. Matter*. **70**, 174109 (2004).

Beamline X17B2

J Chen, L Li, D Weidner, M Vaughan. Deformation Experiments using Synchrotron X-rays: In situ stress and strain measurements at high pressure and temperature. *Phys. Earth Planet. Interiors*. **143-144**, 347-356 (2004).
L Li, D Weidner, P Raterron, J Chen, M Vaughan. Stress Measurements of Deforming Olivine at High Pressure. *Phys. Earth Planet. Interiors*. **143-144**, 357-367 (2004).
L Li, D Weidner, J Chen, M Vaughan, M Davis, W Durham. X-ray Strain Analysis of plasticity at High Pressure in Deforming MgO. *J. Appl. Phys.*. **95** (12), 8357 (2004).
B Li, J Kung, R Liebermann. Modern Techniques in Measuring elasticity of Earth Materials at High Pressure and High Temperature using Ultrasonic Interferometry in Conjunction with Synchrotron X-Radiation in Multi-Anvil Apparatus. *Phys. Earth Planet. Interiors*. **143-144**, 559-574 (2004).
P Raterron, Y Wu, D Weidner, J Chen. Low Temperature Olivine Rheology at High Pressure. *Phys. Earth Planet. Interiors*. **145**, 149-159 (2004).
D Weidner, L Li, M Davis, J Chen. Effect of Plasticity on Elastic Modulus Measurements. *Geophys. Res. Lett.*. **31**, L06621 (2004).
K Woody. Elastic Properties of MgO at High Pressure and Calibration of Pressure Scale. M.S Thesis. State University of New York Stony Brook, Stony Brook. (2004).
J Zhang, Y Zhao. Formation of Zirconium Metallic Glass. *Nature*. **430**, 332 (2004).

Beamline X17C

M Anand, A Taylor, M Nazanov, J Shu, H Mao, R Hemley. Space Weathering on Airless Planetary Bodies:Clues from the Lunar Mineral Hapkeite. *Proc Natl Acad Sci USA*. **101**, 14651 (2004).
B Chen, D Penwella, J Nguyenc, M Kruger. High Pressure X-ray Diffraction Study of Fe2B. *Solid State Commun.*. **129**, 573-575 (2004).
C Cui, T Tyson. Pressure Effects on Charge, Spin, and Metal-Insulator Transitions in the Narrow Bandwidth Manganite Pr1-xCaxMnO3. *Phys. Rev. B: Condens. Matter*. **70**, 094409 (2004).
C Cui, T Tyson. Correlations Between Pressure and Bandwidth Effects in Metal-Insulator Transitions in Manganites. *Appl. Phys. Lett.*. **84**, 942 (2004).
D Errandonea, F Manjon, M Somayazulu, D Hausermann. Effects of Pressure on the Local Atomic Structure of CaWO4 and YLiF4: Mechanism of the Scheelite-to-Wolframite and Scheelite-to-Fergusonite Transitions . *J. Solid State Chem.*. **177** (4-5), 1087-1097 (2004).
M Frank, Y Fei, J Hu. Constraining the Equation of State of Fluid H2O to 80 GPa using the Melting Curve, Bulk Modulus, and Thermal Expansivity of Ice VII. *Geochim. Cosmochim. Acta*. **68**, 2781-2790 (2004).
I Halevy, E Ustundag, S Salhov, A Yue, A Broide, J Hu. High Pressure Study of a Zr-Based Bulk Metallic Glass and its Composite. *Z. Kristallogr.*. **219**, 166-171 (2004).
H Liu, J Hu, J Xu, Z Liu, J Shu, H Mao, J Chen. Phase Transition and Compression Behavior of Gibbsite under High-Pressure. *Phys. Chem. Miner.*. **31**, 240-246 (2004).
Y Ma, M Somayazulu, G Shen, H Mao, J Shu, R Hemley. In Situ X-ray Diffraction Studies of Iron to Earth-Core Conditions. *Phys. Earth Planet. Interiors*. **143-144**, 453-467 (2004).
W Mao, H Mao. Hydrogen Storage in Molecular Compounds. *Proc Natl Acad Sci USA*. **101** (3), 708-710 (2004).
Y Meng, H Mao, P Eng, T Trainor, M Newville, M Hu, C Kao, J Shu, D Hausermann, R Hemley. BN Under Compression: The Formation of sp3 Bond. *Nat. Mater.*. **3**, 111 (2004).
R Patterson, K Cheng, J Akella. Static High-Pressure Structural Studies on Dy to 119 Gpa. *J. Appl. Phys.*. **95**, 5443-5446 (2004).
E Soignard, P McMillan, C Hejny, K Leinenweber. Pressure-Induced Transformations in - and -Ge3N4: in situ Studies by Synchrotron X-ray Diffraction. *J. Solid State Chem.*. **177** (1), 299-311 (2004).
N Velisavljevic, Y Vohra. Distortion of Alpha-Uranium Structure in Praseodymium Metal to 311 GPa. *High Pressure Res.*. **24**, 295 (2004).
Y Vohra, K Hope, J Patterson, J Akella. Crystallographic Anisotropy in Compression of Uranium Metal to 100 GPa. *Mater. Res. Soc. Symp. Proc*, Vol 802, p. DD 1.7.1, sponsored by Mater. Res. Soc. (2004).

Beamline X18A

J Jones, S Vogel, E Slamovich, K Bowman. Quantifying Texture in Ferroelectric Bismuth Titanate. *Scripta Mater.*. **51** (12), 1123-1127 (2004).
J Jones. Texture and Anisotropy in Ferroelectric Bismuth Titanate. Ph.D. Thesis. Purdue University, West Lafayette. (2004).
J Jones, E Slamovich, K Bowman. Critical Evaluation of the Lotgering Degree of Orientation Texture Indicator. *J. Mater. Res.*. **19** (11), 3414-3422 (2004).
H Lee, Z Ma, X Yang, X Sun, J McBreen. Synthesis of a New Series of Fluorinated Boronate Compounds as Anion Receptors and Studies of Their Use as Additives in Lithium Battery Electrolytes. *J. Electrochem. Soc.*. **151**, A1429 (2004).
L Liu, L Chen, X Huang, X Yang, W Yoon, H Lee, J McBreen. Electrochemical and In Situ Synchrotron XRD Studies on Al2O3-Coated LiCoO2 Cathode Material. *J. Electrochem. Soc.*. **151**, A1344 (2004).
H Mo. Neutron and X-ray Scattering Study of Intermediate-length Alkane Films. Ph.D. Thesis. University of Missouri-Columbia, Columbia. (2004).
H Mo, S Trogisch, H Taub, S Ehrlich, U Volkmann, F Hansen, M Pino. Structure and Growth of Dotriacontane films on SiO2 and Ag(111) Surfaces: Synchrotron X-ray Scattering and Molecular Dynamics Simulations. *Phys. Status Solidi (a)*. **201** (10), 2375-2380 (2004).

H Mo, S Trogisch, H taub, S Ehrlich, U Volkmann, F Hansen, M Pino. Studies of the Structure and Growth Mode of Dotriacontane Films by Synchroton X-ray Scattering and Molecular Dynamics Simulations. *J. Phys.: Condens. Matter*. **16**, S2905 (2004).

V Murthi, R Urian, S Mukerjee. Oxygen Reduction Kinetics in Low and Medium Temperature Acid Environment: Correlation of Water Activation and Surface Properties in Supported Pt and Pt Alloy Electrocatalysts. *J. Phys. Chem. B*. **108**, 11011-11023 (2004).

Beamline X18B

J Bang, D Hesterberg. Dissolution of Trace Element Contaminants from Two Coastal Plain Soils as Affected by pH. *J. Environ. Qual.*. **33**, 891-901 (2004).

S Beauchemin, J Fiset, T MacKinnon, D Hesterberg. Impact of a Water Cover on the Stability of Arsenic in a Neutralization Sludge. *Advances in Mineral Resources and Environmental Geotechnology*, Vol 1, p. 519-524, sponsored by Finobeton S. A.. (2004).

S Beauchemin, J Fiset, T Mackinnon. Stability of Arsenic in Neutralization Sludge Stored Under a Water Cover. CANMET Mining and Mineral Sciences Laboratories, Ottawa. Prepared for Natural Resources Canada. (2004).

J Guzman, B Gates. Catalysis by Supported Gold: Correlation Between Catalytic Activity for CO Oxidation and Oxidation States of Gold. *J. Am. Chem. Soc.*. **126**, 2672-2673 (2004).

J Guzman, S Kuba, J Fierro-Gonzales, B Gates. Formation of Gold Clusters on TiO2 from Adsorbed Au(CH3)2(C5H7O2): Characterization by X-ray Absorption Spectroscopy. *Catal. Lett.*. **95** (1-2), 77 (2004).

F Huggins, G Huffman. How do Lithophile Elements Occur in Organic Association in Bituminous Coals?. *Int. J. Coal Geol.*. **58** (3), 193-204 (2004).

F Huggins, G Huffman, W Linak, C Miller. Quantifying Hazardous Species in particulate Matter Derived from Fossil-Fuel Combustion. *Environ. Sci. Tech.*. **38**, 1836-1842 (2004).

G Jacobs, P Patterson, J Chaney, W Conner, T Das, M Luo, B Davis. Fischer-Tropsch synthesis: Influence of Reduction Promoters on Cluster Size and Stability of Co/Al2O3 Catalysts for GTL. *2004 Spring National Meeting*, Vol 49, p. 186, sponsored by ACS Div. Petr. Chem.. (2004).

G Jacobs, P Patterson, L Williams, E Chenu, D Sparks, G Thomas, B Davis. Water-gas Shift: In-situ Spectroscopic Studies of Noble Metal Promoted Ceria Catalysts for CO Removal in Fuel Cell Reformers and Mechanistic Implications. *Appl. Catal. A*. **262** (2), 177-187 (2004).

G Jacobs, J Chaney, P Patterson, T Das, B Davis. Fischer-Tropsch Synthesis: Study of the promotion of Re on the reduction property of Co/Al2O3 catalysts by in-situ EXAFS of Co K and Re LIII Edges. *Appl. Catal. A*. **264**, 203 (2004).

G Jacobs, T Das, P Patterson, M Luo, W Conner, B Davis. Fischer-Tropsch Synthesis: Effect of Water of Co/Al2O3 catalysts and XAFS characterization of reoxidation phenomena. *Appl. Catal. A*. **270**, 65 (2004).

G Jacobs, E Chenu, P Patterson, L Williams, D Sparks, G Thomas, B Davis. Water-Gas Shift: Comparative Screening of Metal Promoters for Metal-ceria Systems and Role of the Metal. *Appl. Catal. A*. **258**, 203 (2004).

G Jacobs, S Khalid, P Patterson, D Sparks, B Davis. Kinetic Isotope Effect Identifies Surface Formates in Rate Limiting Step for Pt/ceria Catalysts. *Appl. Catal. A*. **268**, 255-266 (2004).

G Jacobs, P Patterson, U Graham, D Sparks, B Davis. Low Temperature Water-Gas Shift: Kinetic Isotope Effect Observed for Decomposition of Surface Formates for Pt/ceria Catalysts. *Appl. Catal. A*. **269**, 63-73 (2004).

G Jacobs, J Chaney, P Patterson, T Das, J Maillot, B Davis. Fischer-Tropsch Synthesis: Study of the Promotion of Pt on the Reduction Property of Co/Al2O3 Catalysts by in situ EXAFS of Co K and Pt LIII Edges and XPS. *J. Synch. Rad.*. **11**, 414-422 (2004).

S Jongpatiwut, Z Li, D Resasco, W Alvarez, E Sughrue, G Dodwell. Competitive Hydrogenation of Poly-aromatic Hydrocarbons on Sulfur-Resistant Bimetallic Pt-Pd Catalysts. *Appl. Catal. A*. **262**, 241 (2004).

E Kim, J Shearer, S Lu, P Moenne-Loccoz, M Helton, S Kaderli, A Zuberbuhler, K Karlin. Heme/Cu/O2 Reactivity: Change in Fe^III-(O2^2-)-Cu^II Unit Peroxo Binding Geometry Effected by Tridentate Copper Chelation. *J. Am. Chem. Soc.*. **126**, 12716-12717 (2004).

K Mondal, N Sathitsuksanoh, M Croft, S Lalvani. X-ray Absorption Spectroscopic Analysis of Amorphous Cr-P Obtained Via Electrodeposition. *J. Mater. Sci. Lett.*. **22** (9), 655-657 (2004).

K Murthy, P Patterson, G Jacobs, B Davis, M Keane. An Exploration of Activity loss During Hydrodechlorination and Hydrodebromination over Ni/SiO2. *J. Catal.*. **223**, 74-85 (2004).

S Oyama, X Wang, Y Lee, W Chun. Active Phase of Ni2P/SiO2 in Hydroprocessing Reactions. *J. Catal.*. **221** (2), 263-273 (2004).

A Rouff, E Elzinga, R Reeder. X-ray Absorption Spectroscopic Evidence for the Formation of Pb(II) Inner-Sphere Adsorption Complexes and Precipitates at the Calcite-Water Interface. *Environ. Sci. Tech.*. **38**, 1700-1707 (2004).

V Schwartz, D Mullins, W Yan, B Chen, S Dai, S Overbury. XAS Study of Au Supported on TiO2: Influenece of Oxidation State and Particle Size on Catalytic Activity. *J. Phys. Chem. B*. **108**, 15782-15790 (2004).

Y Soo, S Kim, Y Kao, A Blattner, B Wessels, S Khalid, C Sanchez-Hanke, C Kao. Local Structure Around Mn Atoms in Room-Temperature Ferromagnetic (In,Mn) As Thin Films Probed by Extended X-ray Absorption Fine Structure. *Appl. Phys. Lett.*. **84**, 481 (2004).

G Veith, M Lobanov, T Emge, M Greenblatt, M Croft, F Stowasser, J Hadermann, G Van Tendelo. Synthesis and Characterization of the New Ln2FeMoO7 (Ln = Y, Dy, Ho) Compounds. *J Mater. Chem.*. **14**, 1623-1630 (2004).

W Yoon, C Grey, M Balasubramanian, X Yang, D Fischer, J McBreen. A Combined NMR and XAS Study on the Local Environments and Electronic Structures of the Electrochemically Li-ion deintercalated LiCo1/3Ni1/3Mn1/3O2 electrode System. *J. Electrochem. Soc.*. **7** (3), A53 (2004).

F Zhang, P Wang, J Koberstein, S Khalid, S Chan. Cerium Oxidation State in Ceria Nanoparticles Studied with X-ray Photoelectron Spectroscopy and Absorption Near Edge Spectroscopy. *Surf. Sci.*. **563**, 74-82 (2004).

Beamline X19A

S Beauchemin, J Fiset, T Mackinnon. Stability of Arsenic in Neutralization Sludge Stored Under a Water Cover. CANMET Mining and Mineral Sciences Laboratories, Ottawa. Prepared for Natural Resources Canada. (2004).

S Beauchemin, J Fiset, T MacKinnon, D Hesterberg. Impact of a Water Cover on the Stability of Arsenic in a Neutralization Sludge. *Advances in Mineral Resources and Environmental Geotechnology*, Vol 1, p. 519-524, sponsored by Finobeton S. A.. (2004).

S Beauchemin, D Hesterberg, J Nadeau, J McGeer. Speciation of Hepatic Zn in Trout Exposed to Elevated Waterborne Zn Using X-ray Absorption Spectroscopy. *Environ. Sci. Tech.*. **38**, 1288-1295 (2004).

W Caliebe, S Cheung, A Lenhard, D Siddons. Fixed Exit Monochromator with Fixed Rotation Axis. *Synchrotron Radiation Instrumentation: Eighth International Conference on Synchrotron Radiation Instrumentation*, Vol 705, p. 643-646, sponsored by AIP Conference Proceedings. (2004).

L Dieng. Understanding the Origin of the Recovery of Superconductivity in Halogenated YBCO Single Crystals:

Atromic Structure Study. Ph. D. Thesis. New Jersey Institute of Technology, Newark. (2004).
J Graetz, J Reilly, J Johnson, A Ignatov, T Tyson. X-ray Absorption Study of Ti-Activated Sodium Aluminum Hydride. *Appl. Phys. Lett.*. **85**, 500 (2004).
C Huang, Z Liu, A Cady, R Pindak, W Caliebe, P Barois, H Nguyen, K Ema, K Takekoshi, H Yao. Optical, Resonant X-ray Scattering, and Calorimetric Investigations of Two Liquid Crystal Compounds Exhibiting the SmA-SmC(alpha)*-SmC* Transitions. *Liq. Cryst.*. **31** (1), 127 (2004).
C Huang, S Wang, X Han, A Cady, R Pindak, W Caliebe, K Ema, K Takekoshi, H Yao. Experimental Investigations of one Liquid-Crystal Compound Exhibiting the No-Layer-Shrinkage Effect Near the SM-a-Sm-/sup*/Transition. *Phys. Rev. E*. **69** (4), 41702 (2004).
F Huggins, G Huffman. How do Lithophile Elements Occur in Organic Association in Bituminous Coals?. *Int. J. Coal Geol.*. **58** (3), 193-204 (2004).
F Huggins, G Huffman, W Linak, C Miller. Quantifying Hazardous Species in particulate Matter Derived from Fossil-Fuel Combustion. *Environ. Sci. Tech.*. **38**, 1836-1842 (2004).
K Hutchison, D Hesterberg. Dissolution of Phosphate in a Phosphorus-Enriched Ultisol as Affected by Microbial Reduction. *J. Environ. Qual.*. **33**, 1793-1802 (2004).
N Khare, D Hesterberg, S Beauchemin, S Wang. XANES Determination of Adsorbed Phosphate Distribution between Ferrihydrite and Boehmite in Mixtures. *Soil Sci. Soc. Am. J.*. **68**, 460-469 (2004).
K Mondal, N Sathitsuksanoh, M Croft, S Lalvani. X-ray Absorption Spectroscopic Analysis of Amorphous Cr-P Obtained Via Electrodeposition. *J. Mater. Sci. Lett.*. **22** (9), 655-657 (2004).
J Ramallo-Lopez, E Lede, F Requejo, J Rodriquez, J Kim, R Rosas-Salas, J Dominguez. XANES Characterization of Extremely Nanosized Metal-Carbonyl Subspecies (Me = Cr, Mn, Fe, and Co) Confined into the Mesopores of MCM-41 Materials. *J. Phys. Chem. B*. **108**, 20005-20010 (2004).
J Rodriguez. Gold Nanoparticles on Titania: Activation and Behavior. *Dekker Encyclopedia of Nanoscience and Nanotechnology*, p. 1297-1304, Marcel Dekker, New York. (2004).
J Rodriguez, P Liu, J Dvorak, T Jirsak, J Gomes, Y Takahashi, K Nakamura. Adsorption of Sulfur on TiC(001): Photoemission and First-Principles Studies. *Phys. Rev. B*. **69**, 115414-1,10 (2004).
A Sahiner, C Magee, D Downey, E Arevalo, J Woicik. The Role of Ge in Cluster Formation in B and BF2 Implanted Si Wafers after Ge Pre-Amorphization. *Materials Research Society Fall 2003 Meeting*, Vol 792, p. R7.3.1-7, sponsored by Materials Research Society. (2004).
A Sahiner, P Ansari, M Carroll, C Magee, S Novak, J Woicik. XAFS as a direct local structural probe in revealing the effects of C presence in B diffusion in SiGe layers. *Materials Research Society Spring 2004 Meeting*, Vol 810, p. C11.10.1-7, sponsored by Materials Research Society. (2004).
K Staats, Y Arai, D Sparks. Alum Amendment Effects on Phosphorus Release and Distribution in Poultry Litter-Amended Sandy Soil. *J. Environ. Qual.*. **33**, 1904-1911 (2004).
Y Suh, M Carroll, R Levy, A Sahiner, C King. Phophorus and Boron Implantation into (100) Germanium. *Materials Reseacrh Society Spring Meeting 2004*, Vol 809, p. B8.11.1-7, sponsored by Materials Research Society. (2004).
G Veith, M Lobanov, T Emge, M Greenblatt, M Croft, F Stowasser, J Hadermann, G Van Tendelo. Synthesis and Characterization of the New Ln2FeMoO7 (Ln = Y, Dy, Ho) Compounds. *J Mater. Chem.*. **14**, 1623-1630 (2004).
X Wang, J Hanson, G Liu, J Rodriguez, A Iglesias-Juez, M Fernandez-Garcia. the Behavior of Mixed-Metal Oxides: Physical and Chemical Properties of Bulk Ce(1-x)Tb(x)O(2) and Nanopatricles of Ce(1-x)Tb(x)O(y). *J. Chem. Phys.*. **121** (11), 5434-5444 (2004).
T Weng, W Hsieh, E Uffelman, S Gordon-Wylie, T Collins, V Pecoraro, J Penner-Hahn. XANES Evidence Against a Manganyl Species in the S3 State of the Oxygen-Evolving Complex. *J. Am. Chem. Soc.*. **126**, 8070-8071 (2004).

Beamline X19C

F Akin, I Jang, M Schlossman, S Sinnott, G Zajac, E Fuoco, M Wijesundara, M Li, A Tikhonov, et al.. Nanostructure of Fluorocarbon Films Deposited on Polystyrene from Hyperthermal C3F5+ Ions. *J. Phys. Chem. B*. **108**, 9656-9664 (2004).
J Bai, G Dhanaraj, P Gouma, M Dudley, M Mynbaeva. Porous SiC for HT Chemical Sensing Devices: An Assessment of its Thermal Stability. *International Conference on Silicon Carbide and Related Materials*, Vol 457-460, p. 1479-1482, sponsored by CNRS et al. (2004).
J Bai, M Dudley, B Raghotamachar, P Gouma, B Skromme, L Chen, P Hartlieb, E Michaels, J Kolis. Correlated Structural and Optical Characterization of Ammonothermally Grown Bulk GaN. *Appl. Phys. Lett.*. **84**, 3289-3291 (2004).
W Cho, X Huang, M Dudley. Exact Formulation for Pi-Polarization Waves of Dynamical X-ray Diffraction. *Acta Cryst. A*. **60**, 195-197 (2004).
X Huang, M Dudley, W Cho, R Okojie, P Neudeck. Characterization of SiC Epitaxial Structures using High-Resolution X-ray Diffraction Techniques. *International Conference on SiC and Related Materials 2003*, Vol 457-460, p. 157-162, sponsored by CNRS et al. (2004).
X Ma, M Dudley, T Sudarshan. Nondestructive Defect Characterization of SiC Epilayers and its Significance for SiC Device Research. *International Conference on Silicon Carbide and Related Materials 2003*, Vol 457-460, p. 601-604, sponsored by CNRS et al. (2004).
A Tikhonov, S Pingali, M Schlossman. Molecular Ordering and Phase Transitions in alkanol Monolayers at the Water–Hexane Interface. *J. Chem. Phys.*. **120** (24), 11822-11838 (2004).
W Vetter, M Dudley. The Contrast of Inclusions Compared with that of Micropipes in Back-Reflection Synchrotron White Beam Topographs of SiC. *J. Appl. Cryst.*. **37**, 200-2003 (2004).
W Vetter, R Nagarajan, J Edgar, M Dudley. Double Positioning Twinning in Icosohedral B12As2 Thin Films Grown by Chemical Vapor Deposition. *Mater. Lett.*. **58**, 1331-1335 (2004).

Beamline X20A

E Bernard, R Boltnev, V Khmelenko, V Kiryukhin, S Kiselev, D Lee. Impurity - Helium Solids: Chemistry and Physics at 1.5 K. *J. Low Temp. Phys.*. **134** (1/2), 133-143 (2004).
H Chen. Microscale Laser Shock Peening-- Experiment, Modeling and Spatially Resolved Material Characterization. Ph.D. Thesis. Columbia University, New York. (2004).
H Chen, Y Yao, J Kysar. Spatially Resolved Characterization of Residual Stress Induced by Micro Scale Laser Shock Peening. *J. Manuf. Sci. E*. **126** (2), 226-236 (2004).
H Chen, J Kysar, Y Yao. Characterization of Plastic Deformation Induced by Micro Scale Laser Shock Peening. *J Appl. Mech.*. **71**, 1-11 (2004).
C Detavernier, C Lavoie, J Jordan-Sweet. Texture of Tetragonal alpha-FeSi2 films on Si(001). *Phys. Rev. B*. **69**, 174106 (2004).
C Detavernier, C Lavoie. Influence of Pt Addition on the Texture of NiSi on Si(001). *Appl. Phys. Lett.*. **84** (18), 3549-3551 (2004).
E DiMasi, M Sarikaya. Synchrotron X-ray Microbeam Diffraction from Abalone Shell. *J. Mater. Res.*. **19**, 1471 (2004).
M Ramazanoglu, P Clegg, R Birgeneau, C Garland, M Neubert, J Kim. First Order Isotropic-Smectic-A transition

in Liquid-crystal-Aerosil Gels. *Phys. Rev. E*. **69**, 061706 (2004).

Beamline X20C

J Baglin, S Sun, A Kellock, T Thomson, M Toney, B Terris, C Murray. Ion Beam Stabilization of FePt Nanoparticle Arrays for Magnetic Storage. *Materials Research Symposium Proceedings*, Vol 777, p. 1, sponsored by Materials Research Society. (2004).

C Detavernier, C Lavoie, R Van Meirhaeghe. CoSi2 Formation in the Presence of Ti, Ta or W. *Thin Solid Films*. **468**, 174-182 (2004).

C Detavernier, C Lavoie, F d'Heurle, H Bender, R VanMeirhaeghe. Low-temperature Formation of CoSi2 in the Presence of Au. *J. Appl. Phys.*. **95** (10), 5340-5346 (2004).

S Fritz, S Martin, C Frisbie, M Ward, M Toney. Structural Characterization of a Pentacene Monolayer on an Amorphous SiO2 Substrate with Grazing Incidence X-ray Diffraction. *J. Am. Chem. Soc.*. **126**, 4084-4085 (2004).

H Kim, C Lavoie, M Copel, V Narayanan, D Park, S Rossnagel. The Physical Properties of Cubic Plasma-Enhanced Atomic Layer Deposition TaN Films. *J. Appl. Phys.*. **95** (10), 5848 (2004).

A Ozcan, K Ludwig, Jr., C Detavernier, C Lavoie, J Jordan-Sweet. Axiotaxy of CoSi2 Thin Films on Si(100) Substrates and the Effects of Ti Alloying. *J. Appl. Phys.*. **95** (12), 8376 (2004).

A Ozcan, K Ludwig, Jr., C Lavoie, S Basu, C Coia, C Cabral, Jr., K Rodbell, J Harper. Evolution of Microstructure in Ti-Ta Bilayer Thin Films on Polycrystalline-Si and Si(001). *Thin Solid Films*. **466**, 238-249 (2004).

W Prater, E Allen, W Lee, M Toney, J Daniels, J Hedstrom. Reduction of Resistivity in Cu Thin Films by Partial Oxidiation: Microstructural Mechanisms. *Appl. Phys. Lett.*. **84**, 2518 (2004).

T Thomson, M Toney, S Raoux, S Lee, S Sun, C Murray, B Terris. Structural and Magnetic Model of Self-assembled FePt Nanoparticle Arrays. *J. Appl. Phys.*. **96**, 1197 (2004).

T Thomson, B Terris, M Toney, S Raoux, J Baglin, S Lee, S Sun. Silicide Formation and Particle Size Growth in High Temperature Annealed, Self-assembled FePt Nanoparticles. *J. Appl. Phys.*. **95**, 6738 (2004).

B Yen, B Schwickert, M Toney. Origin of Low-Friction Behavior in Graphite Investigated by Surface X-ray Diffraction. *Appl. Phys. Lett.*. **84** (23), 4702 (2004).

Beamline X21

J Berret, B Vigolo, R Eng, P Herve, I Grillo, L Yang. Electrostatic Self-Assembly of Oppositely Charged Copolymers and Surfactants: A Light, Neutron, and X-ray Scattering Study. *Macromolecules*. **37**, 4922-4930 (2004).

W Caliebe, Q Qian, T Tyson, A Deyhim, B Blank, C Kao. Multi-Element Analyzer for Inelastic X-ray Scattering. *Synchrotron Radiation Instrumentation: Eighth International Conference on Synchrotron Radiation Instrumentation*, Vol 705, p. 893-896, sponsored by AIP Conference Proceedings. (2004).

M Deutsch, E Foerster, G Holzer, J Hartwig, K Hamalainen, C Kao, S Huotari, R Diamant. X-ray Spectrometry of Copper: New Results on an Old Subject. *J. Res - NIST*. **109**, 75-98 (2004).

D Farrell, Y Ding, S Majetich, C Sanchez-Hanke, C Kao. Structural Ordering Effects in Fe Nanoparticle Two- and Three-Dimensional Arrays. *J. Appl. Phys.*. **95**, 6636 (2004).

T Nicolai, F Lafleche, A Gibaud. Jamming and Crystallization of Polymeric Micelles. *Macromolecules*. **37**, 8066-8071 (2004).

Beamline X22A

Z Ban, S Alpay, F He, B Wells, X Xi. Multiple Relaxation Mechanisms in SrTiO3/SrRuO3 Heterostructures. *Appl. Phys. Lett.*. **84** (24), 4848 (2004).

A Baptiste, A Bulou, J Bardeau, J Nouet, A Gibaud, K Wen, S Hoeppener, R Maoz, J Sagiv. Substrate-Induced Modulation of the Raman Scattering Signals from Self-Assembled Organic Nanometric Films. *Langmuir*. **20**, 6232-6237 (2004).

F He, B Wells, Z Ban, S Alpay, S Grenier, S Shapiro, W Si, A Clark, X Xi. Structural Phase Transition in Epitaxial Perovskite Films. *Phys. Rev. B: Condens. Matter*. **70** (23), 235405 (2004).

H Katz, T Siegrist, M Lefenfeld, P Gopalan, M Mushbrush, B Ocko, O Gang, N Jisrawl. Mesophase Transitions, Surface Functionalization, and Growth Mechanism of Seminconducting 6PTTP6 Films of Solution. *J. Phys. Chem. B*. **108**, 8567-8571 (2004).

D Kim, S Kim, K Lavery, T Russell. Inorganic Nanodots from Thin Films of Block Copolymers. *Nano Lett.*. **4** (10), 1841-1844 (2004).

K Kim, L Lee, B Niece, J Wang, A Wewirth. Formation of Ordered Multilayers from Polyoxometalates and Ag on Electrode Surfaces. *J. Phys. Chem. B*. **108**, 7927 (2004).

D Liang, M Borthwick, R Leheny. Smectic liquid crystals in anisotropic colloidal silica gels. *J. Phys.: Condens. Matter*. **16**, S1989-S2002 (2004).

M Ramazanoglu, P Clegg, R Birgeneau, C Garland, M Neubert, J Kim. First Order Isotropic-Smectic-A transition in Liquid-crystal-Aerosil Gels. *Phys. Rev. E*. **69**, 061706 (2004).

R Ras, J Nemeth, C Johnston, E DiMasi, I Dekany, R Schoonheydt. Hybrid Langmuir-Blodgett monolayers contining clay minerals: effect of clay concentration and surface charge density on the film formation. *Phys. Chem. Chem. Phys.*. **6**, 4174 (2004).

K Tamura, J Wang, R Adzic, B Ocko. Kinetics of Monolayer Bi Electrodeposition on Au(111): Surface X-ray Scattering and Current Transients. *J. Phys. Chem. B*. **108**, 1992-1998 (2004).

G Tulevski, Q Miao, M Fukuto, R Abram, B Ocko, R Pindak, M Steigerwald, C Kagan, C Nuckolis. Attaching Organic Semiconductors to Gate Oxides: In Situ Assembly of Monolayer Field Effect Transitions. *J. Am. Chem. Soc.*. **126**, 15048-15050 (2004).

G Xu, H Hiraka, K Ohwada, G Shirane. Dual Structures in PZN-xPT Ferroelectric Relaxors. *Appl. Phys. Lett.*. **84**, 3975 (2004).

G Xu, Z Zhong, Y Bing, Z Ye, C Stock, G Shirane. An Anomalous Phase in the Relaxor Ferroelectric PZN. *Phys. Rev. B*. **70**, 064107 (2004).

Beamline X22B

E Bernard, R Boltnev, V Khmelenko, V Kiryukhin, S Kiselev, D Lee. ESR and X - ray Investigations of Deuterium Atoms and Molecules in Impurity - Helium Solids. *J. Low Temp. Phys.*. **134** (1/2), 169-174 (2004).

E Bernard, R Boltnev, V Khmelenko, V Kiryukhin, S Kiselev, D Lee. Deuterium atoms and molecules in nanoclusters of molecular deuterium. *Phys. Rev. B*. **69**, 104201 (2004).

M Fukuto, R Heilmann, P Pershan, A Badia, R Lennox. Monolayer/Bilayer Transition in Langmuir Films of Derivatized Gold Nanoparticles at the Gas/Water Interface: An X-ray Scattering Study. *J. Chem. Phys.*. **120**, 3446 (2004).

A Gibaud, S Dourdain, O Gang, B Ocko. In Situ Grazing Incidence Small-Angle X-ray Scattering Real Time Monitoring of the Role of Humidity During the Structural Formation of Templated Silica Thin Films. *Phys. Rev. B: Condens. Matter*. **70**, 161403R (2004).

S Kim, M Misner, M Kimura, T Xu, T Russell. Highly Oriented and Ordered Arrays from Block Copolymers Via Solvent

Evaporation. *Advanced Materials*. **16** (3), 226-231 (2004).
H Kraack, B Ocko, P Pershan, E Sloutskin, L Tamam, M Deutsch. Fatty Acid Langmuir Films on Liquid Mercury: X-ray and Surface Tension Studies. *Langmuir*. **20**, 5375-5385 (2004).
H Kraack, B Ocko, P Pershan, E Sloutskin, L Tamam, M Deutsch. The Structure and Phase Diagram of Langmuir Films of Alcohols on Mercury. *Langmuir*. **20**, 5386-5395 (2004).
H Kraack. Langmuir Films on Liquid Mercury. Ph.D. Thesis. Bar-Ilan University, Ramat-Gan. (2004).
H Kraack, B Ocko, P Pershan, E Sloutskin, L Tamam, M Deutsch. The Temperature Dependence of the Structure of Langmuir Films of Alkanes on Mercury. *J. Chem. Phys.*. **12**, 8003 (2004).
W Luo, H Sheng, F Alamgir, J Bai, J He, E Ma. Icosahedral Short-Range Order in Amorphous Alloys. *Phys. Rev. Lett.*. **92** (14), 145502-1 to 145502-4 (2004).
O Shpyrko. Experimental X-Ray Studies of Liquid Surfaces. Ph.D. Thesis. Harvard University, Cambridge. (2004).
E Sloutskin, E Sirota, O Gang, X Wu, B Ocko, M Deutsch. Surface and Bulk Interchange Energy in Binary Mixtures of Chain Molecules. *The Eur. Phys. J. E*. **13**, 109-112 (2004).
R Turgeman, O Gershevitz, O Palchik, M Deutsch, B Ocko, A Gendanken, C Sukenik. Oriented Growth of ZnO Crystals on Self-Assembled Monolayers of Functionalized Alkyl Silanes. *Cryst. Growth Des.*. **4** (1), 169-175 (2004).
T Xu, A Zvelindovsky, G Sevink, O Gang, B Ocko, Y Zhu, S Gido, T Russell. Electric Field Induced Sphere-to-Cylinder Transition in Diblock Copolymer Thin Films. *Macromolecules*. **37**, 6980 (2004).
T Xu. Electric Field Alignment of Diblock Copolymer Thin Films. Ph.D Thesis. University of Massachusetts, Amherst, Amherst. (2004).
T Xu, J Goldbach, M Misner, S Kim, A Gibaud, O Gang, B Ocko, K Guarini, C Black, et al.. Scattering study on the selective solvent swelling induced surface reconstruction. *Macromolecules*. **37**, 2972-2977 (2004).
S Ye, J Strzalka, I Churbanova, S Zheng, J Johansson, J Blasie. A Model Membrane Protein for Binding Volatile Anesthetics. *Biophys. J.*. **87**, 4065-4074 (2004).
S Ye. Design, Characterization of Amphiphilic Proteins and Potential Engineering Applications. Ph. D. Thesis. University of Pennsylvania, Philadelphia. (2004).
S Ye, J Strzalka, B Discher, D Noy, S Zheng, P Dutton, J Blasie. Amphiphilic 4-Helix Bundles Designed for Biomolecular Materials Applications. *Langmuir*. **20**, 5897-5904 (2004).

Beamline X22C

S Grenier, J Thomas, Y Kim, J Hill, D Gibbs, V Kiryukhin, Y Tokura, D Casa, T Gog, C Venkataraman. Resonant X-ray Scattering as a Probe of the Valence and Magnetic Ground State and Excitations in Pr(0.6)Ca(0.4)MnO(3). *Physica B*. **345**, 6-10 (2004).
S Grenier, J Hill, D Gibbs, K Thomas, M v Zimmermann, C Nelson, V Kiryukhin, Y Tokura, Y Tomioka, et al.. Resonant X-ray Diffraction of the Magnetoresistant Perovskite Pr0.6Ca0.4MnO3. *Phys. Rev. B*. **69**, 134419 (2004).
F He, B Wells, Z Ban, S Alpay, S Grenier, S Shapiro, W Si, A Clark, X Xi. Structural Phase Transition in Epitaxial Perovskite Films. *Phys. Rev. B: Condens. Matter*. **70** (23), 235405 (2004).
V Kiryukhin. Nanoscale Structural Correlations in Magnetoresistive Manganites. *New J. Phys.*. **6**, 155 (2004).
C Nelson, J Hill, D Gibbs, M Rajeswari, A Biswas, S Shinde, R Greene, T Venkatesan, A Millis, et al.. Substrate-induced Strain Effects on Pr_0.6Ca_0.4MnO_3 Films. *J. Phys.: Condens. Matter*. **16** (1), 13-27 (2004).
G Popov, M Lobanov, E Tsiper, M Greenblatt, E Caspi, A Borissov, V Kiryukhin, J Lynn. Crystallographic and Magnetic Structure of the Sr2MnReO6 Double Perovskite. *J. Phys.: Condens. Matter*. **16**, 135-145 (2004).

Beamline X23A2

F Aguirre-Tostado, A Herrera-Gomez, J Woicik, R Droopad, Z Yu, D Schlom, J Karapetrova, P Zschack, P Pianetta. Displacive Phase Transition in SrTiO3 Thin Films Grown on Si(001). *J. Vac. Sci. Technol., A*. **22**, 1356 (2004).
F Aguirre-Tostado, A Herrera-Gomez, J Woicik, R Droopad, Z Yu, D Schlom, P Zschack, E Karapetrova, P Pianetta, C Hellberg. Elastic Anomaly for SrTiO3 Thin Films Grown on Si(001). *Phys. Rev. B: Condens. Matter*. **70**, 201403(R) (2004).
Y Chen, D Ciuparu, S Lim, Y Yang, G Haller, L Pfefferle. Synthesis of Uniform Diameter Single Wall Carbon Nanotubes in Co-MCM-41: Effects of CO Pressure and Reaction Time. *J. Catal.*. **226**, 351-362 (2004).
Y Chen, D Ciuparu, S Lim, Y Yang, G Haller, L Pfefferle. Synthesis of Uniform Diameter Single-Wall Carbon Nanotubes in Co-MCM-41: Effects of the Catalyst Prereduction and Nanotube Growth Temperatures. *J. Catal.*. **225**, 453-465 (2004).
D Ciuparu, Y Chen, S Lim, Y Yang, G Haller, L Pfefferle. Mechanism of Cobalt Cluster Size Control in Co-MCM-41 during Single-Wall Carbon Nanotubes Synthesis by CO Disproportionation. *J. Phys. Chem. B*. **108** (40), 15565 (2004).
D Ciuparu, Y Chen, S Lim, G Haller, L Pfefferle. Uniform-Diameter Single-Walled Carbon Nanotubes Catalytically Grown in Cobalt-Incorporated MCM-41. *J. Phys. Chem. B*. **108** (2), 503-507 (2004).
M Duff, D Hunter, D Hobbs, S Fink, Z Dai, J Bradley. Mechanisms of Sr and U(VI) Removal from High-level Radioactive Waste Simulant Solutions by the Sorbent Monosodium Titanate. *Environ. Sci. Tech.*. **38**, 7 (2004).
W Luo, H Sheng, F Alamgir, J Bai, J He, E Ma. Icosahedral Short-Range Order in Amorphous Alloys. *Phys. Rev. Lett.*. **92** (14), 145502-1 to 145502-4 (2004).
A Rouff, E Elzinga, R Reeder. X-ray Absorption Spectroscopic Evidence for the Formation of Pb(II) Inner-Sphere Adsorption Complexes and Precipitates at the Calcite-Water Interface. *Environ. Sci. Tech.*. **38**, 1700-1707 (2004).
A Sahiner, P Ansari, M Carroll, C Magee, S Novak, J Woicik. XAFS as a direct local structural probe in revealing the effects of C presence in B diffusion in SiGe layers. *Materials Research Society Spring 2004 Meeting*, Vol 810, p. C11.10.1-7, sponsored by Materials Research Society. (2004).
A Sahiner, C Magee, D Downey, E Arevalo, J Woicik. The Role of Ge in Cluster Formation in B and BF2 Implanted Si Wafers after Ge Pre-Amorphization. *Materials Research Society Fall 2003 Meeting*, Vol 792, p. R7.3.1-7, sponsored by Materials Research Society. (2004).
D Siddons. An X-ray Michelson Interferometer with Low Intrinsic time Dispersion. *Synchrotron Radiation Instrumentation: Eighth International Conference on Synchrotron Radiation Instrumentation*, Vol 705, p. 997, sponsored by AIP Conference Proceedings. (2004).
Y Suh, M Carroll, R Levy, A Sahiner, C King. Phophorus and Boron Implantation into (100) Germanium. *Materials Reseacrh Society Spring Meeting 2004*, Vol 809, p. B8.11.1-7, sponsored by Materials Research Society. (2004).
T Tyson, M Deleon, M Croft, V Harris, C Kao, J Kirkland, S Cheong. Magnetic Field Melting of the Charge-Ordered State of La1/2Ca1/2MnO3: A Local Structure Perspective. *Phys. Rev. B*. **70**, 024410 (2004).

Beamline X23A3

D Schaefer, G Beaucage, D Loy, K Shea, J Lin. Structure of Arylene-Bridged Polysilsesquionxane Xerogels and Aerogels. *Chem. Mater.*. **16**, 1402-1410 (2004).

Beamline X23B

F Alamgir, J VanSluytman, D Carter, J Whitacre, C Kao, S Greenbaum, M denBoer. X-ray Absorption Spectroscopy Investigation of the Sub-Nanoscale Strain in Thin-Film Lithium Ion Battery Cathodes. *MRS Spring 2004*, Vol 822, p. S2.3, sponsored by MRS. (2004).

G Evmenenko, C Yu, S Kewalramani, P Dutta. Structural Reorganization in Films of Cellulose Derivatives in the Presence of Colloidal Particles. *Polymer*. **45**, 6269-6273 (2004).

G Evmenenko, C Yu, S Kewalramani, P Dutta. Structural Characterization of Thin Hydroxypropylcellulose Films. X-Ray Reflectivity Studies. *Langmuir*. **20**, 1698-1703 (2004).

H Kang, P Zhu, Y Yang, G Evmenenko, P Dutta, T Marks. Self-Assembled Electro-Optic Thin Films with Dramatically Blue-Shifted Optical Adsorption Based on Novel X-Shaped Two-Dimensional Charge-Transfer Chromophores. *Polym. Mater. Sci. Eng.*. **91**, 267-268 (2004).

S Morrison, C Cahill, E Carpenter, S Calvin, R Swaminathan, M McHenry, V Harris. Magnetic and Structural Properties of Nickel Zinc Ferrite Nanoparticles Synthesized at Room Temperature. *J. Appl. Phys.*. **95** (11), 6392-6395 (2004).

A Shukla, D Strawser, A Lucassen, D Freeman, H Cohen, D Jose, A Das, G Evmenenko, P Dutta, M van der Boom. Covalent Assembly of Stilbene-Based Monolayers: Factors Controlling Molecular Interactions. *J. Phys. Chem. B*. **108**, 17505-17511 (2004).

A Yang, V Harris, S Calvin, X Zuo, C Vittoria. x-ray Absorption Fine Structure Analysis of Cation Distribution in MnFe2O4 Single Crystal Films and Artificial Ferrite Structures. *IEEE Trans. Magn.*. **40** (4), 2802 (2004).

Beamline X24A

R Dunford, E Kanter, B Krassig, S Southworth, L Young. Higher Order Processes in X-ray Photoionization and Decay. *Radiat. Phys. Chem.*. **70**, 149 (2004).

T Jach, J Dura, N Nguyen, J Swider, G Cappello, C Righter. Comparative Thickness Measurements of SiO2/Si Films for Thicknesses Less than 10 nm. *Surf. Interface Anal.*. **36**, 23-29 (2004).

J Levin, B Armen. Studies of Gluorescence and Auger Decay Following Inner-Shell Photoionization. *Radiat. Phys. Chem.*. **70** (1-3), 105-121 (2004).

J Woicik. Site-Specific Valence X-ray Photoelectron Spectroscopy. *Synch. Rad. News*. **17**, 48 (2004).

Z Zhang, P Fenter, L Cheng, N Sturchio, M Bedzyk, M Machesky, D Wesolowski. Model-Independent X-ray Imaging of Adsorbed Cations at the Crystal-Water Interface. *Surf. Sci. Lett.*. **554**, 95-100 (2004).

Beamline X24C

B Kjornrattanawanich, S Bajt, J Seely. Mo/B4C/Si Multilayer-Coated Photodiode with Polarization Sensitivity at an Extreme Ultraviolet Wavelength of 13.5 nm. *Appl. Optics-OT*. **43**, 1082 (2004).

J Seely, C Brown, D Windt, S Donguy, B Kjornrattanawanich. Normal-Incidence Efficiencies of Multilayer-Coated Laminar Gratings for the Extreme-Ultraviolet Imaging Spectrometer (EIS) on the Solar-B Mission. *Appl. Optics-OT*. **43**, 1463 (2004).

Y Uspenskii, J Seely, N Popov, A Vinogradov, Y Pershin, V Kondratenko. Efficient Method for the Determination of Extreme-Ultraviolet Optical Constants in Reactive Materials: Application to Scandium and Titanium. *J. Opt. Soc. Am. A*. **21**, 298 (2004).

D Windt, S Donguy, J Seely, B Kjornrattanawanich. Experimental Comparison of Extreme-Ultraviolet Multilayers for Solar Physics. *Appl. Optics-OT*. **43**, 1835 (2004).

Beamline X25

P Adams, M Stahley, A Kosek, J Wang, S Strobel. Crystal Structure of a Self-Splicing Group I Intron with Both Exons. *Nature*. **430**, 45 (2004).

T Adams, M Hockin, K Mann, S Everse. The Crystal Structure of Activated Protein C-inactivated Bovine Factor Va: Implications for Cofactor Function. *Proc Natl Acad Sci USA*. **101** (24), 8918-8923 (2004).

J Anson James, A Aggarwal, R Linden, C Escalante. Structure of Adeno-Associated Virus Type 2 Rep40-ADP Complex: Insight into Nucleotide Recognition and Catalysis by Superfamily 3 Helicases. *Proc Natl Acad Sci USA*. **101** (34), 12455-12460 (2004).

J Avalos, J Boeke, C Wolberger. Structural Basis for the Mechanism and Regulation of Sir2 Enzymes. *Mol. Cell*. **13** (5), 639-648 (2004).

B Canagarajah, F Leskow, J Ho, H Mischak, L Saidi, M Kazanietz, J Hurley. Structural Mechanism for Lipid Activation of the Rac-Specific GAP, Beta2-Chimaerin.. *Cell*. **119** (3), 407-418 (2004).

C Chiu, A Watts, L Lairson, M Gilbert, D Lim, W Warkachuk, S Withers, N Strynadka. Structural Analysis of the Sialyltransferase CstII from Campylobacter jejuni in Complex with a Substrate Analog. *Nat. Struct. Mol. Biol.*. **11** (2), 163-170 (2004).

J Chrencik, B Staker, A Burgin, P Pourquier, Y Pommier, L Stewart, M Redinbo. Mechanisms of Camptothecin Resistance by Human Topoisomerase I Mutations. *J. Mol. Biol.*. **339**, 773 (2004).

G Clayton, W Silverman, L Heginbotham, J Morais-Cabral. Structural Basis of Ligand Activation in a Cyclic Nucleotide Regulated Potassium Channel. *Cell*. **119**, 615-627 (2004).

A Cordeiro, P Michels, L Delboni, O Thiemann. The Crystal Structure of Glucose-6-Phosphate Isomerase from Leishmania Mexicana Reveals Novel Active Site Features. *Eur. J. Biochem.*. **271**, 2765 (2004).

J Dai, J Liu, Y Deng, T Smith, M Lu. Structure and Protein Design of a Human Platelet Function Inhibitor. *Cell*. **116**, 649-659 (2004).

B Daniels, J Jiang, D Fu. Crystallization and Preliminary Crystallographic Analysis of the Escherichia coli Water Channel AqpZ. *Acta Cryst. D*. **60**, 561-563 (2004).

K Das, G Butler, V Kwiatkowski, A Clark, Jr., P Yadav, E Arnold. Crystal Structures of Arginine Deiminase with Covalent Reaction Intermediates: Implications for Catalytic Mechanism. *Structure*. **12**, 657-667 (2004).

D Das, M Georgiadis. The Crystal Structure of the Monomeric Reverse Transcriptase from Moloney Murine Leukemia Virus. *Structure*. **12**, 819-829 (2004).

K Das, A Clark, P Lewi, J Heeres, M De Jonge, L Koymans, H Vinkers, F Daeyaert, D Ludovici, et al.. Roles of Conformational and Positional Adaptability in Structure-Based Design of TMC125-R165335 (Etravirine)and Related Non-Nucleoside Reverse Transcriptase Inhibitors that are Highly Potent and Effective Against Wild-Type and Drug-Resistant HIV-1 Variant. *J. Med. Chem.*. **47**, 2550 (2004).

M Deutsch, E Foerster, G Holzer, J Hartwig, K Hamalainen, C Kao, S Huotari, R Diamant. X-ray Spectrometry of Copper: New Results on an Old Subject. *J. Res - NIST*. **109**, 75-98 (2004).

S Eswaramoorthy, D Kumaran, J Keller, S Swaminathan. Role of Metals in the Biological Activity of Clostridium botulinum Neurotoxins. *Biochemistry*. **43**, 2209-2216 (2004).

J Fromme, A Banerjee, S Huang, G Verdine. Structural Basis for Removal of Adenine Mispaired with 8-oxoguanine by

B van den berg, P Black, W Clemons, Jr., T Rapoport. Crystal Structure of the Long-Chain Fatty Acid Transporter FadL. *Science*. **304**, 1506 (2004).
Y Wang, Y Ha. The X-Ray Structure of an Antiparallel Dimer of the Human Amyloid Precursor Protein E2 Domain. *Mol. Cell*. **15**, 343-353 (2004).
Y Wang, R Coulombe, D Cameron, L Thauvette, M Massariol, L Amon, D Fink, S Titolo, E Welchner, et al.. Crystal Structure of the E2 Transactivation Domain of Human Papillomavirus Type 11 Bound to a Protein Interaction Inhibitor. *J. Biol. Chem.*. **279** (8), 6976-6985 (2004).
D Whittington, J Grubb, A Waheed, G Shah, W Sly, D Christianson. Expression, Assay, and Structure of the Extracellular Domain of Murine Carbonic Anhydrase XIV. *J. Biol. Chem.*. **279** (8), 7223-7228 (2004).
Y Xiong, T Steitz. Mechanism of Transfer RNA Maturation by CCA-Adding Enzyme Without using an Oligonucleotide Template. *Nature*. **430**, 640 (2004).
Z Yang, L Shipman, M Zhang, B Anton, R Roberts, X Cheng. Structural Characterization and Comparative Phylogenetic Analysis of Escherichia coli HemK, a Protein (N5)-Glutamine Methyltransferase. *J. Mol. Biol.*. **340**, 695-706 (2004).
J Ye, B van den Berg. Crystal Structure of the Bacterial Nucleoside Transporter Tsx. *EMBO J.*. **23**, 3187-3195 (2004).
D Yernool, O Boudker, Y Jin, E Gouaux. Structure of a Glutamate Transporter Homologue From Pyrococcus Horikoshii. *Nature*. **431**, 811 (2004).
K Zhao, R Harshaw, X Chai, R Marmorstein. Structural Basis for Nicotinamide Cleavage and ADP-ribose Transfer by NAD+ -Dependent Sir2 Histone/Protein Deacetylases. *Proc Natl Acad Sci USA*. **101** (23), 8563-8568 (2004).
Y Zhao, Z Li, S Drozd, Y Guo, W Mourad, H Li. Crystal Structure of Mycoplasma arthritidis Mitogen Complexed with HLA-DR1 Reveals a Novel Superantigen Fold and a Dimerized Superantigen-MHC Complex. *Structure*. **12**, 277-288 (2004).
K Zhao, X Chai, R Marmorstein. Structure and Substrate Binding Properties of Cobb, A SIR2 Homolog Protein Deacetylase from Eschericia Coli. *J. Mol. Biol.*. **337**, 731 (2004).
M Zhou, R MacKinnon. A Mutant KcsA K+ Channel with Altered Conduction Properties and Selectivity Filter Ion Distribution. *J. Mol. Biol.*. **338**, 830-846 (2004).
Y Zhou, R MacKinnon. Ion Binding Affinity in the Cavity of the KcsA Potassium Channel. *Biochemistry*. **43**, 4978-4982 (2004).

Beamline X26A

E Chouparova, A Lanzirotti, H Feng, K Jones, N Marinkovic, C Whitson, P Philp. Characterization of Petroleum Deposits Formed in a Producing Well by Synchrotron Radiation-Based Microanalyses. *Energ. Fuel*. **18** (4), 1199-1212 (2004).
J Cole, E Rasbury, I Montanez, V Pedone, A Lanzirotti, G Hanson. Petrographic and Trace Element Analysis of Uranium-rich Tufa Calcite, Middle Miocene Barstow Formation, California, USA. *Sedimentology*. **51**, 433-453 (2004).
J Cole, E Rasbury, I Montañez, V Pedone, A Lanzirotti, G Hanson. Uranium and Other Trace Element Incorporation into Tufa Calcite. *Geochim. Cosmochim. Acta*. **68** (11), A497 Suppl. (2004).
M Duff, D Hunter, D Hobbs, S Fink, Z Dai, J Bradley. Mechanisms of Sr and U(VI) Removal from High-level Radioactive Waste Simulant Solutions by the Sorbent Monosodium Titanate. *Environ. Sci. Tech.*. **38**, 7 (2004).
G Flynn, D Durda. Chemical and Mineralogical Size Segregation in the Impact Disruption of Inhomogeneous, Anhydrous Meteorites. *Planet Space Sci.*. **52** (12), 1129-1140 (2004).
H Jamieson, S Walker, C Andrade, M Parsons, A Lanzirotti. Using Synchrotron-Based Microanalysis to Predict Environmental Risk Associated with Mine Waste. *87th Canadian Chemistry Conference and Exhibition*, Vol Program with Abstracts, p. 775, sponsored by Canadian Society for Chemistry. (2004).
M McCanta, M Dyar, M Rutherford, J Delaney. Iron Partitioning Between Basaltic Melts and Clinopyroxene as a Function of Oxygen Fugacity. *Am. Mineral.*. **89**, 1685-1693 (2004).
A Treiman, A Lanzirotti, D Xirouchakis. Ancient Water on Asteroid 4 Vesta: Evidence from a Quartz Veinlet in the Serra de Magé Eucrite Meteorite. *Earth Planet Sci. Lett.*. **219**, 189-199 (2004).
S Walker, H Jamieson, C Andrade, A Lanzirotti. Solid-phase As Speciation in Roaster-derived Au Mine Tailings. *Eleventh International Symposium on Water-Rock Interaction, WRI-11*, Vol 1, p. 641-645, sponsored by Water-Rock Working Group of the IAGC. (2004).

Beamline X26C

A Auster, L Joshua-Tor. The DNA-binding Domain of Human Papillomavirus Type 18 E1. *J. Biol. Chem.*. **279** (5), 3733-3742 (2004).
L Brieba, B Eichman, R Kokoska, S Doublie, T Kunkel, T Ellenberger. Structural Basis for the Dual Coding Potential of 8-Oxoguanosine by a High-Fidelity DNA Polymerase. *EMBO J.*. **23**, 3452-3461 (2004).
T Caradoc-Davies, S Cutfiled, I Lamont, J Cutfield. Crystal Structures of Escherichia coli Uridine Phosphorylase in Two Natvie and Three Complexed Forms Reveal Basis of Substrate Specificity, Induced Conformational Changes and Influence of Potassium. *J. Mol. Biol.*. **337**, 337-354 (2004).
E Freisinger, A Grollman, H Miller, C Kisker. Lesion (in)tolerance Reveals Insights into DNA Replication Fidelity. *EMBO J.*. **23**, 1494-1505 (2004).
P Hanzelmann, H Schindelin. Crystal Structure of the S-adenosylmethionine-dependent Enzyme MoaA and its Implications for Molybdenum Cofactor Deficiency in Humans. *Proc Natl Acad Sci USA*. **101** (35), 12870-12875 (2004).
P Iyer, S Lawrence, K Luther, K Rajashankar, H Yennawar, J Ferry, H Schindelin. Crystal Structure of Phosphotransacetylase from the Methanogenic Archaeon Methanosarcina thermophilia. *Structure*. **12**, 559-567 (2004).
J Lovelace, A Soares, H Bellamy, R Sweet, E Snell, G Borgstahl. First Results of Digital Topography Applied to Macromolecular Crystals. *J. Appl. Cryst.*. **37**, 481-485 (2004).
A Nagpal, M Valley, P Fitzpatrick, A Orville, E Kramer, G Galli, E Chiellini, D Fischer. Crystallization and Preliminary Analysis of Active Nitroalkane Oxidase in Three Crystal Forms . *Acta Cryst. D*. **60**, 1456-1460 (2004).
V Reiland, R Gilboa, A Spungin-Bialik, D Schomburg, Y Shoham, S Blumberg, G Shoham. Binding of Inhibitory Aromatic Amino Acids to Streptomyces griseus Aminopeptidase. *Acta Cryst. D*. **60**, 1738-1746 (2004).
A Teplitsky, A Mechaly, V Stojanoff, G Sainz, G Golan, H Feinberg, R Gilboa, V Reiland, G Zolotnitsky, et al.. Structure Determination of the Extracellular Xylanase from Geobacillus stearothermophilus by Selenomethionyl MAD Phasing. *Acta Cryst. D*. **60**, 836-848 (2004).
J Truglio, D Croteau, M Skorvaga, M DellaVecchia, K Theis, B Mandavilli, B Van Houten, C Kisker. Interactions Between UvrA and UvrB - The Critical Role of UvrB's Domain 2 in Nucleotide Excision Repair. *EMBO J.*. **23**, 2498-2509 (2004).

Beamline X27A

K Jones, H Feng, A Lanzirotti, N Marinkovic, U Neuhaeusler, C Riekel, L Vincze, B Vekemans, I Szaloki, Z Song. Microanalysis of NY/NJ Harbor Sediments Using

Synchrotron X-Ray Beams. *Second International Conference on Remediation of Contaminated Sediments*, Vol CD-ROM, p. I-06, sponsored by Battelle Memorial Institute. (2004).

Beamline X27B

E Kossel, M Weber, R Kimmich. Visualization of Transport: NMR Microscopy Experiments with Model Objects for Porous Media with Pore Sizes Down to 50 µm. *Solid State Nucl. Mag.*. **25** (1-3), 28-34 (2004).

Beamline X27C

P Cebe, J Runt. P(VDF-TrFE)-Layered Silicate Nanocomposites: 1. X-ray Scattering Thermal Analysis Study. *Polymer*. **45** (6), 1923-1932 (2004).

Y Elabd, C Walker, F Beyer. Triblock Copolymer Ionomer Membranes: Part II. Structure Characterization and its Effects on Transport Properties and Direct Methanol Fuel Cell Performance. *J. Membr. Sci.*. **231** (1-2), 181-188 (2004).

M Gelfer, C Burger, A Fadeev, I Sics, B Chu, B Hsiao, A Heintz, K Kojo, S Hsu, et al.. Thermally Induced Phase Transitions and Morphological Changes in Organoclays. *Langmuir*. **20**, 3746-3758 (2004).

G Georgiev, N Gilfoy, P Cebe, M Capel. Phase Transitions and Structural Parameters of HIQ-40 Liquid Crystalline Co-Polyester. *Polymer*. **45** (10), 3429-3440 (2004).

J Gu, S Xu, B Belknap, H White , L Yu. Binding of Myosin. ADP Pi to Actin Improves the Regularity of the Thick Filament Helix. *Biophys. J.*. **86**, 567a (2004).

R Ho, F Lin, C Tsai, C Lin, B Ko, B Hsiao, I Sics. Crystallization-Induced Undulated Morphology in Polystyrene-b-Poly(L-lactide) Block Copolymer. *Macromolecules*. **37**, 5985-5994 (2004).

R Ho, Y Chiang, C Tsai, C Lin, B Ko, B Huang. Three-Dimensionally Packed Nanohelical Phase in Chiral Block Copolymers. *J. Am. Chem. Soc.*. **126**, 2704-2705 (2004).

P Huang, L Zhu, Y Guo, Q Ge, A Jing, W Chen, R Quirk, S Cheng, E Thomas, et al.. Confinement Size effect on Crystal Orientation Changes of Poly(ethylene oxide) Blocks in Poly(ethylene oxide) - b-polystyrene Diblock Copolymers. *Macromolecules*. **37**, 3689-3698 (2004).

H Jin, J Park, R Valluzzi, P Cebe, D Kaplan. Biomaterial Films of Bombyx Mori Solk Fibrion with Poly(ethylene Oxide). *Biomacromolecules*. **5** (3), 711-717 (2004).

D Kawakami, S Ran, C Burger, B Fu, I Sics, B Hsiao, T Kikutani. Structural Formation of Amorphous Poly (ethylene terephthalate) During Uniaxial Deformation Above the Glass Temperature. *Polymer*. **45** (3), 905-918 (2004).

K Kim, Y Luu, C Chang, D Fang, B Hsiao, B Chu, M Hadjiargyrou. Incorporation and Controlled Release of Hydrophilic Antibiotics Using Poly(lactide-co-glycolide) Based Electrospun Nanofibrous Membranes. *J. Controlled Release*. **98** (1), 47-56 (2004).

G Kumaraswamy, R Verma, J Kornfield, F Yeh, B Hsiao. Shear-Enhanced Crystallization in Isotactic Polypropylene. In-Situ Synchrotron SAXS and WAXD. *Macromolecules*. **37**, 9005-9017 (2004).

C Li, K Tenneti, D Zhang, H Zhang, X Wan, E Chen, Q Zhou, A Carlos, S Igos, B Hsiao. Hierarchical Assembly of a Series of Rod-Coil Block Copolymers: Supramolecular LC Phase in Nanoenviroment. *Macromolecules*. **37**, 2854-2860 (2004).

D Lincoln, R Vaia, R Krishnamoorti. Isothermal Crystallization of Nylon-6/Montmorillonite Nanocomposites. *Macromolecules*. **37**, 4553-4561 (2004).

S Lin-Gibson, G Schmidt, H Kim, C Han, E Hobbie. Shear-Induced Microstructural Orientation in Polymer-Clay Nanocomposite Solutions. *J. Colloid Interface Sci.*. **274**, 515-525 (2004).

Z Liu, S Chattopadhyay, M Shaw, B Hsiao. Anomalous Rheology in a Nanostructured Diblock Copolymer/Hydrocarbon System and Its Kinetic Origin. *J. Polym. Sci., Part B: Polym. Phys.*. **42** (8), 1496-1505 (2004).

Z Liu, M Shaw, B Hsiao. Ordering Kinetics of the BCC Morphology in Diblock Copolymer Solutions over a Wide Temperature Range. *Macromolecules*. **37**, 9880-9888 (2004).

D Martyn, B Adhikari, M Regnier, J Gu, S Xu, L Yu. Response of Equatorial X-Ray Reflections and Stiffness to Altered Sarcomere Length and Myofilament Lattice Spacing in Relaxed Skinned Cardiac Muscle. *Biophys. J.*. **86**, 1002-1011 (2004).

G Matsuba, K Shimizu, H Wang, Z Wang, C Han. The Effect of Phase Separation on Crystal Nucleation Density and Lamella Growth in Near-Critical Polyolefin Blends. *Polymer*. **45** (15), 5137-5144 (2004).

B Natesan, H Xu, B Ince, P Cebe. Molecular Relaxation of Isotactic Polystyrene: Real-Time Dielectric Spectroscopy and X-ray Scattering Studies. *J. Polym. Sci., Part B: Polym. Phys.*. **42** (5), 777-789 (2004).

A Norman, J Cabral, D Jo, E Amis, A Karim. Scattering Methods Applied to High Throughput Materials Science. *Polym. Mater. Sci. Eng.*. **90**, 339 (2004).

A Norman, J Cabral, A Karim, E Amis. Scattering Measurements for High Throughput Materials Science Research. *Macromol. Rapid Commun.*. **25** (1), 307-311 (2004).

J Ouyang, S Zhou, F Wang, S Goh. Structures of Properties of Supramolecular Assembled Fullerenol/Poly(dimethylsiloxane) Nanocomposites. *J. Phys. Chem. B*. **108**, 5937-5943 (2004).

S Park, H Koerner, S Putthanarat, R Ozisik, S Juhl, B Farmer, R Eby. Structure of poly (p-phenylenebenzobisoxazloe) (PBZO) and poly (p-phenylenebenzobisthiazole) (PBZT) for Proton Exchange Membranse (PEMs) in Fuel Cells. *Polymer*. **45** (1), 49-59 (2004).

S Poompradub, M Tosaka, S Kohjiya, Y Ikeda, S Toki, I Sics, B Hsiao. Lattice Deformation of Strain-Induced Crystallites in Carbon-filled Natural Rubber. *Chem. Lett.*. **33**, 220 (2004).

S Rao, C Burger, I Sics, K Yoon, D Fang, K Kim, C Avila-Orta, J Keum, B Chu, et al.. In-Situ Synchrotron SAXS/WAXD Studies During Melt Spinning of Modified Carbon Nanofiber and Isotactic Polypropylene Nanocomposite. *Colloid and Polymer Science*. **282** (8), 802-809 (2004).

K Sugiyama, T Tanabe, C Skinner, C Gentile. Measurement of Tritium Surface Distribution on TFTR Bumper Limiter Tiles. *Phys. Scr.*. **T108**, 68-71 (2004).

L Sun, Y Liu, L Zhu, B Hsiao, C Avila-Orta. Path-dependent Melting in a Low Molecular Weight Polyethylene-block-poly(ethylene oxide) Diblock Copolymers. *Macromol. Rapid Commun.*. **25**, 853 (2004).

L Sun, L Zhu, Q Ge, R Quirk, C Xue, S Cheng, B Hsiao, C Avila-Orta, I Sics, M Cantino. Comparison of Crystallization Kinetics in Various Nanoconfined Geometries. *Polymer*. **45**, 2931 (2004).

S Toki, I Sics, B Hsiao, S Murakami, M Tosaka, S Poompradub, S Kohjiya, Y Ikeda. Structural Developments in Synthetic Rubbers During Uniaxial Deformation by In Situ Synchrotron X-Ray Diffraction. *J. Polym. Sci., Part B: Polym. Phys.*. **42** (6), 956-964 (2004).

M Tosaka, S Murakami, S Poompradub, S Kohjiya, Y Ikeda, S Toki, I Sics, B Hsiao. Orientation and Crystallization of Natural Rubber Network as Revealed by WAXD Using Synchrotron Radiation. *Macromolecules*. **37**, 3299-3309 (2004).

R Vaia, W Liu, H Koerner. Analysis of Small-Angle Scattering of Suspensions of Organically Modified Montmorillonite: Implications to Phase Behavior of Polymer Nanocomposites. *J. Polym. Sci., Part B: Polym. Phys.*. **41** (24), 3214-3236 (2004).

Y Wang, S Ge, M Rafailovich, J Sokolov, Y Zou, H Ade, J Luning, A Lustiger, G Maron. Crystallization in the Thin and Ultrathin Films of Poly(ethylene-vinyl acetate) and Linear Low-Density Polyethylene. *Macromolecules*. **37**, 3319-3327 (2004).
S Xu, L Gu, L Yu, H White . BDM Promotes the Disorder to Order Transition in Thick Filaments. *Biophys. J.*. **86**, 213a (2004).
S Zhou, D Liang, C Burger, F Yeh, B Chu. Nanostructures of Complexed Formed by Calf Thymus DNA Interacting with Cationic Surfactants. *Biomacromolecules*. **5** (4), 1256-1261 (2004).
S Zhou, C Burger, B Chu. Supramolecular Structures of Polyethylenimine-Sodium Alkyl Sulfate Complexes. *J. Phys. Chem. B*. **108**, 10819-10824 (2004).

Beamline X28C

J Guan, M Chance. Footprinting Methods to Examine the Structure and Dynamics of Proteins. *Encyclopedia of Molecular Cell Biology and Molecular Medicine*, p. 549-568, Wiley, Inc., Weinheim. (2004).
J Guan, S Almo, M Chance. Synchrotron Radiolysis and Mass Spectrometry: A New Approach to Research on the Actin Cytoskeleton. *Acct. Chem. Res.*. **37**, 221-229 (2004).
S Gupta, W Mangel, W McGrath, J Perek, D Lee, K Takamoto, M Chance. DNA Binding Provides a Molecular Strap Activating the Adenovirus Proteinase. *Mol. Cell. Proteomics*. **3**, 950-959 (2004).
I Shcherbakova, S Gupta, M Chance , M Brenowitz. Monovalent Ion-Mediated Folding of the Tetrahymena thermophila Ribozyme. *J. Mol. Biol.*. **342**, 1431-1442 (2004).
K Takamoto, M Chance. Footprinting Methods to Examine the Structure and Dynamics of Nucleic Acids. *Encyclopedia of Molecular Cell Biology and Molecular Medicine*, p. 521-548, Wiley, Inc., Weinheim. (2004).
G Xu, M Chance. Radiolytic Modification of Acidic Amino Acids: New Probes of Protein Footprinting. *Anal. Chem.*. **76**, 1213-1221 (2004).

Beamline X29A

J Lu, D Ho, N Vogelaar, C Kraml, R Pascal, Jr.. A Pentacene with a 144 degree Twist. *J. Am. Chem. Soc.*. **126**, 11168-11169 (2004).

Y Wang, S Ge, M Rafailovich, J Sokolov, Y Zou, H Ade, J Luning, A Lustiger, G Maron. Crystallization in the Thin and Ultrathin Films of Poly(ethylene-vinyl acetate) and Linear Low-Density Polyethylene. *Macromolecules*. **37**, 3319-3327 (2004).

S Xu, L Gu, L Yu, H White . BDM Promotes the Disorder to Order Transition in Thick Filaments. *Biophys. J.*. **86**, 213a (2004).

S Zhou, D Liang, C Burger, F Yeh, B Chu. Nanostructures of Complexed Formed by Calf Thymus DNA Interacting with Cationic Surfactants. *Biomacromolecules*. **5** (4), 1256-1261 (2004).

S Zhou, C Burger, B Chu. Supramolecular Structures of Polyethylenimine-Sodium Alkyl Sulfate Complexes. *J. Phys. Chem. B*. **108**, 10819-10824 (2004).

Beamline X28C

J Guan, M Chance. Footprinting Methods to Examine the Structure and Dynamics of Proteins. *Encyclopedia of Molecular Cell Biology and Molecular Medicine*, p. 549-568, Wiley, Inc., Weinheim. (2004).

J Guan, S Almo, M Chance. Synchrotron Radiolysis and Mass Spectrometry: A New Approach to Research on the Actin Cytoskeleton. *Acct. Chem. Res.*. **37**, 221-229 (2004).

S Gupta, W Mangel, W McGrath, J Perek, D Lee, K Takamoto, M Chance. DNA Binding Provides a Molecular Strap Activating the Adenovirus Proteinase. *Mol. Cell. Proteomics*. **3**, 950-959 (2004).

I Shcherbakova, S Gupta, M Chance , M Brenowitz. Monovalent Ion-Mediated Folding of the Tetrahymena thermophila Ribozyme. *J. Mol. Biol.*. **342**, 1431-1442 (2004).

K Takamoto, M Chance. Footprinting Methods to Examine the Structure and Dynamics of Nucleic Acids. *Encyclopedia of Molecular Cell Biology and Molecular Medicine*, p. 521-548, Wiley, Inc., Weinheim. (2004).

G Xu, M Chance. Radiolytic Modification of Acidic Amino Acids: New Probes of Protein Footprinting. *Anal. Chem.*. **76**, 1213-1221 (2004).

Beamline X29A

J Lu, D Ho, N Vogelaar, C Kraml, R Pascal, Jr.. A Pentacene with a 144 degree Twist. *J. Am. Chem. Soc.*. **126**, 11168-11169 (2004).

NSLS Staff

P Abbamonte, G Blumberg, A Rusydi, A Gozar, P Evans, T Siegrist, L Venema, H Elsaki, E Isaacs, G Sawatzky. Crystallization of Charge Holes in The Spin Ladder of Sr14Cu24041. *Nature*. **431**, 1078 (2004).

P Abbamonte, K Finkelstein, M Collins, S Gruner. Imaging Density Disturbances in Water with a 41.3-Attosecond Time Resolution. *Phys. Rev. Lett.*. **92** (23), 237401-1 (2004).

J Ablett, K Evans-Lutterodt, A Stein. Hard X-Ray Fresnel Prisms: Properties and Applications. *Design and Microfabrication of Novel X-Ray Optics II* , Vol 5539, p. 88-94, sponsored by The International Society for Optical Engineering. (2004).

J Ablett, L Berman, C Kao, G Rakowsky, D Lynch. Small-Gap Insertion-Device Development at the National Synchrotron Light Source - Performance of the New X13 Mini-Gap Undulator. *J. Synch. Rad.*. **11**, 129-131 (2004).

J Ablett, L Berman, G Rakowsky, D Lynch. The NSLS X13 Mini-Gap Undulator: Design and Performance. *Synchrotron Radiation and Instrumentation: Eighth International Conference*, Vol 705, p. 271-273, sponsored by American Institute of Physics. (2004).

W Bailey, L Cheng, D Keavney, C Kao, E Vescovo, D Arena. Precessional Dynamics of Elemental Moments in a Ferromagnetic Alloy. *Phys. Rev. B*. **70**, 172403 (2004).

W Caliebe, Q Qian, T Tyson, A Deyhim, B Blank, C Kao. Multi-Element Analyzer for Inelastic X-ray Scattering. *Synchrotron Radiation Instrumentation: Eighth International Conference on Synchrotron Radiation Instrumentation*, Vol 705, p. 893-896, sponsored by AIP Conference Proceedings. (2004).

W Caliebe, S Cheung, A Lenhard, D Siddons. Fixed Exit Monochromator with Fixed Rotation Axis. *Synchrotron Radiation Instrumentation: Eighth International Conference on Synchrotron Radiation Instrumentation*, Vol 705, p. 643-646, sponsored by AIP Conference Proceedings. (2004).

B Capelle, Y Epelboin, J Hartwig, A Moraleda, F Otalora, V Stojanoff . Characterization of Dislocations in Protein Crystals by Means of Synchrotron Double Crystal Topography. *J. Appl. Cryst.*. **37**, 67-71 (2004).

E Caspi, M Avdeev, S Short, J Jorgensen, M Lobanov, Z Zeng, M Greenblatt, P Thiyagarajan, C Botez, P Stephens. Structural and Magnetic Phase Diagram of the Two-Electron-Doped [Ca(1-x)Ce(x)]MnO3 System: Effects of Competition Among Charge, Orbital, and Spin Ordering. *Phys. Rev. B*. **69**, 104402 (2004).

M Deutsch, E Foerster, G Holzer, J Hartwig, K Hamalainen, C Kao, S Huotari, R Diamant. X-ray Spectrometry of Copper: New Results on an Old Subject. *J. Res - NIST*. **109**, 75-98 (2004).

E DiMasi, M Sarikaya. Synchrotron X-ray Microbeam Diffraction from Abalone Shell. *J. Mater. Res.*. **19**, 1471 (2004).

A Doyuran, L DiMauro, W Graves, R Heese, E Johnson, S Krinsky, H Loos, J Murphy, G Rakowsky, et al.. Experimental Study of a High-Gain Harmonic-Generation Free-Electron Laser in the Ultraviolet. *Phys. Rev. ST AB*. **7**, 050701 (2004).

A Doyuran, L DiMauro, R Heese, E Johnson, S Krinsky, H Loos, J Murphy, G Rakowsky, J Rose, et al.. Chirped Pulse Amplification of HGHG-FEL Facility at BNL. *25th Annual Free Electron Laser Conference, Tsukuba, Japan*, Vol (05211) , p. 392-395, sponsored by IEEE. (2004).

A Doyuran, L DiMauro, W Graves, R Heese, E Johnson, S Krinsky, H Loos, J Murphy, G Rakowsky, et al.. Chirped Pulse Amplification of HGHG-FEL at DUV-FEL Facility at BNL. *Nucl. Instrum. Meth. A*. **528**, 467-470 (2004).

P Dumas, N Jamin, J Teillaud, L Miller, B Beccard. Imaging Capabilities of Synchrotron Infrared Microspectroscopy. *Faraday Discuss*. **126**, 289-302 (2004).

K Evans-Lutterodt, J Ablett, A Stein, D Tennant, F Klemens, A Taylor. Energy Dependent Focusing Properties of a Kinoform Fresnel Lens. *Design and Microfabrication of Novel X-Ray Optics II* , Vol 5539, p. 73-79, sponsored by The International Society for Optical Engineering. (2004).

D Farrell, Y Ding, S Majetich, C Sanchez-Hanke, C Kao. Structural Ordering Effects in Fe Nanoparticle Two- and Three-Dimensional Arrays. *J. Appl. Phys.*. **95**, 6636 (2004).

G Golan, D Shallom , A Teplitsky, G Zaide, S Shulami, T Bassov, V Stojanoff, A Thompson, Y Shoham, G Shoham. Crystal Structures of Geobacillus Stearothermophilus a-glucuronidase Complexed with its Substrate and Products: Mechanistic Implications. *J. Biol. Chem.*. **279** (4), 3014-24 (2004).

G Gopalan, Z He, Y Balmer, P Romano, R Gupta, A Heroux, B Buchanan, K Swaminathan, S Iuan. Structural analysis uncovers a role for redox in regulating FKBP13, an immunophilin of the chloroplast thylakoid lumen . *Proc Natl Acad Sci USA*. **101** (38), 13945-13950 (2004).

S Grenier, J Hill, D Gibbs, K Thomas, M v Zimmermann, C Nelson, V Kiryukhin, Y Tokura, Y Tomioka, et al.. Resonant X-ray Diffraction of the Magnetoresistant Perovskite Pr0.6Ca0.4MnO3. *Phys. Rev. B*. **69**, 134419 (2004).

T Gunter, L Miller, C Gavin, R Eliseev, J Salter, L Buntinas, A Alexandrov, S Hammond, K Gunter. Determination of the

Oxidation States of Manganese in Brain, LIver, and Heart Mitochondria. *J. Neurochem.*. **88** (2), 266-280 (2004).

H Hayashi, Y Udagawa, C Kao. Resonant and Near-Resonant Inelastic X-ray Scattering Spectroscopy and Lifetime-Broadening Removed XANES of CuO. *J. Electron. Spectrosc. Relat. Phenom.*. **137-140**, 277 (2004).

N Holden, R Reciniello, J Hu. Radiation Dosimetry of a Graphite Moderated Radium Beryllium Source. *Health Phys.*. **86** (2), S110-S112 (2004).

N Holden, R Reciniello, J Hu. 2003 Review of Neutron and Non-Neutron Nuclear Data. *Health Phys.*. **87** (4), 410-415 (2004).

J Hu, Z Zhong, E Haas, S Hulbert, R Hubbard. Degradation of Magnet Epoxy at NSLS X-Ray Ring. *Mech. Engng. Design of Synch. Radiation Equipment & Inst. (MEDSI)*, Vol 2004, p. 9, sponsored by ESRF. (2004).

J Hu, R Reciniello, N Holden. Optiminzation of the Epithermal Neutron Beam for Boron Neutron Capture Therapy at the Brookhaven Medical Research Reactor. *Health Phys.*. **86** (23), S103-S109 (2004).

Z Huang, S Krinsky. Femtosecond X-Ray Pulses From a Frequency Chirped SASE FEL. *Nucl. Instrum. Meth. A*. **528**, 28 (2004).

Z Huang, T Shaftan. Impact of Beam Energy Modulation of rf Zero-Phasing Microbunch Measurements. *Nucl. Instrum. Meth. A*. **528**, 345-349 (2004).

C Huang, S Wang, X Han, A Cady, R Pindak, W Caliebe, K Ema, K Takekoshi, H Yao. Experimental Investigations of one Liquid-Crystal Compound Exhibiting the No-Layer-Shrinkage Effect Near the SM-a-Sm-/sup*/Transition. *Phys. Rev. E*. **69** (4), 41702 (2004).

C Huang, Z Liu, A Cady, R Pindak, W Caliebe, P Barois, H Nguyen, K Ema, K Takekoshi, H Yao. Optical, Resonant X-ray Scattering, and Calorimetric Investigations of Two Liquid Crystal Compounds Exhibiting the SmA-SmC(alpha)*-SmC* Transitions. *Liq. Cryst.*. **31** (1), 127 (2004).

S Huotari, K Hamalainen, R Diamant, R Sharon, C Kao, M Deutsch. X-ray Hypersatellite Spectra of Hollow Atoms. *J. Electron. Spectrosc. Relat. Phenom.*. **137-140**, 293 (2004).

G Jacobs, S Khalid, P Patterson, D Sparks, B Davis. Kinetic Isotope Effect Identifies Surface Formates in Rate Limiting Step for Pt/ceria Catalysts. *Appl. Catal. A*. **268**, 255-266 (2004).

H Jamieson, S Walker, C Andrade, M Parsons, A Lanzirotti. Using Synchrotron-Based Microanalysis to Predict Environmental Risk Associated with Mine Waste. *87th Canadian Chemistry Conference and Exhibition*, Vol Program with Abstracts, p. 775, sponsored by Canadian Society for Chemistry. (2004).

H Jeong, R Skomski, C Waldfried, T Komesu, P Dowben, E Vescovo. The Effective Spin Dependent Debye Temperature of Gd(0001). *Phys. Lett. A*. **324**, 242 (2004).

E Kakuno, G Camarda, D Siddons. Cadmium-Zinc Telluride Detector Arrays for Synchrotron Radiation Applications. *Hard X-Ray and Gamma Ray Detector Physics V*, Vol 5198, p. 19, sponsored by SPIE. (2004).

I Kim, E DiMasi, J Evans. Identification of Mineral Modulation Sequences within the Nacre-Associated Oyster Shell Protein, n16. *Cryst. Growth Des.*. **6** (6), 1113-1118 (2004).

J Kneipp, L Miller, S Spassov, F Sokolowski, P Lasch, M Beekes, D Naumann. Scrapie-infected Cells, Isolated Prions, and Recombinant Prion Protein: A Comparative Study. *Biopolymers*. **74** (1-2), 163-7 (2004).

S Krinsky, B Podobedov, R Gluckstern. Impedance of Finite Length Resistive Cylinder. *Phys. Rev. ST AB*. **7**, 114401 (2004).

S Krinsky. Saturation of a High-Gain Single-Pass FEL. *Nucl. Instrum. Meth. A*. **528**, 52 (2004).

S Krinsky. Model for Nonlinear Behavior in the Self-Amplified Spontaneous-Emission Free-Electron Laser. *Phys. Rev. E*. **69**, 066503 (2004).

J Li, Z Zhong, R Litdke, K Kuettner, C Peterfy, E Aleyeva, C Muehleman. Radiography of Soft Tissue of the Foot and Ankle with Diffraction Enhanced Imaging. *J. Am. Podiat. Med. Assn.*. **94**, 315-322 (2004).

J Li, Z Zhong, K Kuettner, M Aurich, J Williams, M Wimmer, C Muehleman. Detection of cartilage defects with diffraction enhanced x-ray imaging: accuracy and reliability. *Proc. 50th Ann. Mtg. Orthopaedic Res. Soc., Vol.29*, Vol 29, p. paper #1007, sponsored by Orthopaedic Research Society. (2004).

Y Li, S Krinsky, J Lewellen, V Sajaev. Frequency-Domain Statistics of the Chaotic Optical Field of a High-Gain, Self-Amplified Free-Electron Laser and its Correlation to the Time-Domain Statistics. *Appl Phys B*. **80**, 31 (2004).

W Li, R Lucchese, A Doyuran, Z Wu, H Loos, G Hall, A Suits . Superexcited State Dynamics Probed with an Extreme-Ultraviolet Free Electron Laser. *Phys. Rev. Lett.*. **92**, 083002-1 (2004).

D Lynch, L Berman. Superconducting Undulator and Beamline Evaluation Report. Brookhaven National Laboratory, Upton. Prepared for BNL/DOE. (2004).

D Lynch. Engineering Design Analyses: Thermal Protection for Micro Gap Undulator Insertion Devices for Beamlines X9, X13, and X29. Brookhaven National Laboratory, Upton. Prepared for BNL/DOE. (2004).

Y Meng, H Mao, P Eng, T Trainor, M Newville, M Hu, C Kao, J Shu, D Hausermann, R Hemley. BN Under Compression: The Formation of sp3 Bond. *Nat. Mater.*. **3**, 111 (2004).

L Miller, J Tetenbaum Novatt, D Hamerman, C Carlson. Alteractions in Mineral Composition Observed in Osteoarthritic Joints of Cynomologus Monkeys. *Bone*. **35** (2), 498-506 (2004).

H Mo, S Trogisch, H taub, S Ehrlich, U Volkmann, F Hansen, M Pino. Studies of the Structure and Growth Mode of Dotriacontane Films by Synchroton X-ray Scattering and Molecular Dynamics Simulations. *J. Phys.: Condens. Matter*. **16**, S2905 (2004).

H Mo, S Trogisch, H Taub, S Ehrlich, U Volkmann, F Hansen, M Pino. Structure and Growth of Dotriacontane films on SiO2 and Ag(111) Surfaces: Synchrotron X-ray Scattering and Molecular Dynamics Simulations. *Phys. Status Solidi (a)*. **201** (10), 2375-2380 (2004).

N Moiseeva, M Allaire. Crystals of Family 11 Xylanase II from Trichoderma Longibrachiatum that Diffract to Atomic Resolution. *Acta Cryst. D*. **60**, 1275-1277 (2004).

K Mondal, N Sathitsuksanoh, M Croft, S Lalvani. X-ray Absorption Spectroscopic Analysis of Amorphous Cr-P Obtained Via Electrodeposition. *J. Mater. Sci. Lett.*. **22** (9), 655-657 (2004).

C Muehleman, D Sumner, Z Zhong. Refraction Effects of Diffraction-Enhanced Radiographic Imaging. *J. Am. Podiat. Med. Assn.*. **94** (5), 453-455 (2004).

C Muehleman, J Li, M Wernick, J Brankov, K Kuettner, Z Zhong. Yes, You Can See Cartilage with X-rays; Diffraction Enhanced X-ray Imaging for Soft and Hard Tissues. *J. Musculoskelet. Neuron. Int.*. **4**, 369-370 (2004).

C Muehleman, J Brankov, J Li, Z Zhong, K Kuettner, M Wernick. Multiple-Image Radiography for Soft Tissue. *Proc. 50 th Ann. Mtg. Orthopaedic Res. Soc.,*, Vol 29, p. #0104, sponsored by Orthopaedic Res. Soc.,. (2004).

C Muehleman, J Mollenhauer, M Aurich, K Kuettner, Z Zhong, A Cole, D Chapman. Diffraction Enhanced X-ray Imaging of Articular Cartilage. *The Many Faces of Osteoarthritis*, p. 351-354, Springer-Verlag, , Heidelberg . (2004).

C Nelson, J Hill, D Gibbs, M Rajeswari, A Biswas, S Shinde, R Greene, T Venkatesan, A Millis, et al.. Substrate-induced Strain Effects on Pr_0.6Ca_0.4MnO_3 Films. *J. Phys.: Condens. Matter*. **16** (1), 13-27 (2004).

R Ras, J Nemeth, C Johnston, E DiMasi, I Dekany, R Schoonheydt. Hybrid Langmuir-Blodgett monolayers contining clay minerals: effect of clay concentration and surface charge density on the film formation. *Phys. Chem. Chem. Phys.*. **6**, 4174 (2004).

T Shaftan, Z Huang, L Carr, A Doyuran, W Graves, C Limborg, H Loos, J Rose, B Sheehy, et al.. Experiments with Electron Beam Modulation at the DUVFEL Accelerator. *Nucl. Instrum. Meth. A*. **528**, 397-401 (2004).

D Siddons, Z Zhong. A Flash Spectrograph for XANES Measurements at SPPS/LCLS. *Synchrotron Radiation Instrumentation: Eighth International Conference on Synchrotron Radiation Instrumentation*, Vol 705, p. 941, sponsored by AIP Conference Proceedings. (2004).

D Siddons. An X-ray Michelson Interferometer with Low Intrinsic time Dispersion. *Synchrotron Radiation Instrumentation: Eighth International Conference on Synchrotron Radiation Instrumentation*, Vol 705, p. 997, sponsored by AIP Conference Proceedings. (2004).

D Siddons, G Camarda, E Kakuno. A Cadmium-Zinc-Telluride Strip Detector for High-Energy Diffraction Applications. *Synchrotron Radiation Instrumentation: Eighth International Conference on Synchrotron Radiation Instrumentation*, Vol 705, p. 965, sponsored by AIP Conference Proceedings. (2004).

D Siddons, R Beuttenmuller, P O'Connor , A Kuczewski, Z Li. The BNL Silicon Multi-Element Detector System for Dilute EXAFS Experiments. *Synchrotron Radiation Instrumentation: Eighth International Conference on Synchrotron Radiation Instrumentation*, Vol 705, p. 953, sponsored by AIP Conference Proceedings. (2004).

Y Soo, S Kim, Y Kao, A Blattner, B Wessels, S Khalid, C Sanchez-Hanke, C Kao. Local Structure Around Mn Atoms in Room-Temperature Ferromagnetic (In,Mn) As Thin Films Probed by Extended X-ray Absorption Fine Structure. *Appl. Phys. Lett.*. **84**, 481 (2004).

A Stein, J Ablett, K Evans-Lutterodt, A Taylor, F Klemens, A Kornblit, S Polvino. Imaging with Single-Dimension Kinoform Lenses. *Design and Microfabrication of Novel X-Ray Optics II* , Vol 5539, p. 80-87, sponsored by The International Society for Optical Engineering. (2004).

V Stojanoff. A Novel Approach to High-Throughput Screening: A Solution for Structural Genomics?. *Structure*. **12**, 1127 (2004).

J Strzalka, E DiMasi, I Kuzmenko, T Gog, J Blasie. Resonant X-ray Reflectivity from a Bromine-Labeled Fatty Acid Langmuir Monolayer. *Phys. Rev. E*. **70**, 051603 (2004).

A Teplitsky, A Mechaly, V Stojanoff, G Sainz, G Golan, H Feinberg, R Gilboa, V Reiland, G Zolotnitsky, et al.. Structure Determination of the Extracellular Xylanase from Geobacillus stearothermophilus by Selenomethionyl MAD Phasing. *Acta Cryst. D*. **60**, 836-848 (2004).

K Thomas, J Hill, S Grenier, Y Kim, P Abbamonte, L Venema, A Rusydi, Y Tomioka, Y Tokura, et al.. Soft X-Ray Resonant Diffraction Study of Magnetic and Orbital Correlations in a Manganite Near Half Doping. *Phys. Rev. Lett.*. **92** (23), 237204-1 (2004).

T Tyson, M Deleon, M Croft, V Harris, C Kao, J Kirkland, S Cheong. Magnetic Field Melting of the Charge-Ordered State of La1/2Ca1/2MnO3: A Local Structure Perspective. *Phys. Rev. B*. **70**, 024410 (2004).

G Veith, M Lobanov, T Emge, M Greenblatt, M Croft, F Stowasser, J Hadermann, G Van Tendelo. Synthesis and Characterization of the New Ln2FeMoO7 (Ln = Y, Dy, Ho) Compounds. *J Mater. Chem.*. **14**, 1623-1630 (2004).

S Walker, H Jamieson, C Andrade, A Lanzirotti. Solid-phase As Speciation in Roaster-derived Au Mine Tailings. *Eleventh International Symposium on Water-Rock Interaction, WRI-11*, Vol 1, p. 641-645, sponsored by Water-Rock Working Group of the IAGC. (2004).

J Wang, J Wu. Cumulatvie Beam Breakup Due to Resistive-Wall Wake. *Phys. Rev. ST AB*. **7**, 34402 (2004).

E Woo, Y Kim, M Kim, W Han, S Shin, H Robinson, S Park, B Oh. Structural Mechanism for Inactivation and Activation of CAD/DFF40 in the Apoptotic Pathway. *Mol. Cell*. **14**, 531-539 (2004).

G Wright, G Camarda, E Kakuno, L Li, F Lu, C Lee, A Burger, J Trombka, D Siddons, R James. Effects of Surface Roughness on Large-Volume CdZnTe Nuclear Radiation Detectors and Removal of Surface Damage by Chemical Etching. *Hard X-Ray and Gamma Ray Detector Physics V*, Vol 5198, p. 306, sponsored by Proceedings of SPIE. (2004).

P Wu, G Saraf, Y Lu, D Hill, R Bartinski, D Arena, R Mee-Yi, A Raley, K Yung. Ion-Beam-Induced Sharpening of ZnO Nanotips. *Appl. Phys. Lett.*. **85**, 1247 (2004).

G Xu, Z Zhong, Y Bing, Z Ye, C Stock, G Shirane. An Anomalous Phase in the Relaxor Ferroelectric PZN. *Phys. Rev. B*. **70**, 064107 (2004).

T Xu, A Zvelindovsky, G Sevink, O Gang, B Ocko, Y Zhu, S Gido, T Russell. Electric Field Induced Sphere-to-Cylinder Transition in Diblock Copolymer Thin Films. *Macromolecules*. **37**, 6980 (2004).

G Xu, Z Zhong, H Hiraka, G Shirane. Three Dimensional Mapping of Diffuse Scattering in PZN-xPT. *Phys. Rev. B: Condens. Matter*. **70**, 174109 (2004).

Y Yacoby, D Walko, D Brewe, M Bretshcneider, M Sowwan, R Clarke, R Pindak, E Stern. Diffractometer-Control Software for Bragg-Rod Measurements. *Synchrotron Radiation Instrumentation: Eighth International Conference on Synchrotron Radiation Instrumentation*, Vol 705, p. 1221-1222, sponsored by AIP Conference Proceedings. (2004).

L Yu, A Doyuran, L DiMauro, W Graves, E Johnson, R Heese, S Krinsky, H Loos, J Murphy, et al.. Ultraviolet High-Gain Harmonic-Generation Free-Electron Laser at BNL. *Nucl. Instrum. Meth. A*. **528**, 436-442 (2004).

L Yu, H Yi. Accurate Synchronization Between Short Laser Pulse and Electron Bunch using HGHG Output at 266 nm as Photo-Cathode Laser for RF-Gun. *Nucl. Instrum. Meth. A*. **528**, 481-485 (2004).

F Zhang, P Wang, J Koberstein, S Khalid, S Chan. Cerium Oxidation State in Ceria Nanoparticles Studied with X-ray Photoelectron Spectroscopy and Absorption Near Edge Spectroscopy. *Surf. Sci.*. **563**, 74-82 (2004).

Z Zhang, P Fenter, L Cheng, N Sturchio, M Bedzyk, M Machesky, D Wesolowski. Model-Independent X-ray Imaging of Adsorbed Cations at the Crystal-Water Interface. *Surf. Sci. Lett.*. **554**, 95-100 (2004).